

# **Vascular and cardiac effects of endothelium-specific bradykinin type-II receptor overexpression**

Inaugural dissertation

for the attainment of the title of doctor  
in the Faculty of Mathematics and Natural Sciences  
at the Heinrich Heine University Düsseldorf

presented by

**Sara Refaat Azab Metry**

from Egypt

Düsseldorf, November 2024

from the institute for Pharmacology  
at the Heinrich Heine University Düsseldorf

Published by permission of the  
Faculty of Mathematics and Natural Sciences at  
Heinrich Heine University Düsseldorf

Supervisor: Prof. Dr. Georg Kojda  
Co-supervisor: Prof. Dr. Stephanie Lärer

Date of the oral examination: 07.11.2024

Printed with the support of the German Academic Exchange Service (DAAD)

*To my parents and brother for their unconditional care and love*

## Table of Contents

List of abbreviations .....	I
1. Introduction .....	1
1.1. Cardiovascular diseases epidemiology and hypertension .....	1
1.2. Bradykinin .....	2
1.2.1. Production, metabolism, and receptors .....	2
1.2.2. Bradykinin downstream signalling .....	3
1.2.3. Bradykinin functions .....	6
1.2.4. Regulation of bradykinin type-II receptors expression .....	8
1.3. Drugs that interfere with bradykinin signalling .....	9
1.3.1. Drugs increasing bradykinin effects .....	9
1.3.2. Drugs decreasing bradykinin effects .....	10
1.4. Interaction of bradykinin pathway and renin-angiotensin system .....	11
1.5. Polymorphism studies of bradykinin type-II receptor gene .....	11
1.6. Genetically modified models of kallikrein-kinin system .....	12
1.7. Aim of the work .....	13
2. Materials and Methods .....	14
2.1. Buffers and reagents .....	14
2.2. Laboratory mice .....	17
2.2.1. Description of mice .....	17
2.2.2. Organ harvesting .....	18
2.3. Genotyping .....	18
2.3.1. DNA isolation and purification .....	18
2.3.2. Polymerase Chain Reaction .....	18
2.4. Preparation and analysis of RNA .....	20
2.4.1. RNA isolation and purification .....	20
2.4.2. RNA Quantification .....	21
2.4.3. Complementary DNA (cDNA) synthesis .....	21
2.4.4. Real-time quantitative polymerase chain reaction .....	21
2.5. Preparation and analysis of proteins .....	24
2.5.1. Protein isolation .....	24
2.5.2. Protein quantification .....	24
2.5.3. Sodium Dodecyl Sulfate Polyacrylamide Gel Electrophoresis .....	25
2.5.4. Western Blot .....	26
2.6. Proteome analysis .....	28
2.6.1. Background/theory .....	28
2.6.2. Tissue harvesting and lysis .....	28
2.6.3. Mass spectrometry sample preparation .....	29
2.6.4. Liquid chromatography-mass spectrometry analysis .....	29

2.6.5. Data analysis.....	30
2.7. Vascular reactivity studies .....	30
2.7.1. Preparation of aorta .....	30
2.7.2. Organ bath experiments.....	31
2.8. Aortic incubation experiments .....	32
2.9. Blood pressure and heart rate measurements .....	32
2.9.1. Theoretical background of tail-cuff method .....	32
2.9.2. Protocol of measurements.....	33
2.10. Transthoracic echocardiography .....	34
2.11. Flow-mediated dilation.....	35
2.12. Statistical analysis.....	35
3. Results.....	37
3.1. Gene expression levels .....	37
3.1.1. Gene expression levels of human and murine bradykinin type-II receptors in B <sub>2</sub> <sup>tg</sup> mice.....	37
3.1.2. Gene expression levels of angiotensin II type-1 receptors in B <sub>2</sub> <sup>tg</sup> mice.....	38
3.2. Bradykinin type-II receptors protein expression .....	39
3.2.1. Mouse monoclonal anti-bradykinin type-II receptors antibody .....	39
3.2.2. Bradykinin type-II receptors protein expression using rabbit monoclonal antibody .....	40
3.3. Effect of endothelium-specific bradykinin type-II receptors overexpression on bradykinin signalling .....	43
3.3.1. Protein expression of endothelial nitric oxide synthase in B <sub>2</sub> <sup>tg</sup> mice.....	43
3.3.2. Protein expression of phosphorylated ERK1/2 in aorta .....	44
3.4. Vascular reactivity studies .....	46
3.4.1. Effect of endothelium-specific bradykinin type-II receptors overexpression on endothelium-dependent relaxation .....	46
3.4.2. Mediators of endothelium-dependent relaxation in B <sub>2</sub> <sup>tg</sup> mice .....	47
3.4.3. Effect of endothelium-specific bradykinin type-II receptors overexpression on phenylephrine-induced vasoconstriction .....	48
3.4.4. Effect of endothelium-specific bradykinin type-II receptors overexpression on endothelium-independent relaxation .....	49
3.4.5. Effect of endothelium-specific bradykinin type-II receptors overexpression on bradykinin mediated vasoconstriction .....	50
3.5. Systolic blood pressure and heart rate measurements .....	51
3.5.1. Effect of endothelium-specific bradykinin type-II receptors overexpression on systolic blood pressure and heart rate.....	51
3.5.2. Effect of cyclooxygenase inhibitor on blood pressure and heart rate in B <sub>2</sub> <sup>tg</sup> mice .....	54
3.5.3. Effect of bradykinin type-II receptor antagonist on blood pressure and heart rate in B <sub>2</sub> <sup>tg</sup> mice .....	56
3.5.4. Effect of nitric oxide synthase inhibitor on blood pressure and heart rate in B <sub>2</sub> <sup>tg</sup> mice .....	59
3.6. Assessment of flow-mediated dilation in B <sub>2</sub> <sup>tg</sup> mice .....	61
3.7. Effect of endothelium-specific bradykinin type-II receptors overexpression on cardiac function .....	64
3.8. Effect of endothelium-specific bradykinin type-II receptors overexpression on expression of different proteins: Proteomic analysis .....	68

3.9. Sex-specific effects of bradykinin signalling.....	81
3.9.1. Vascular reactivity studies.....	81
3.9.2. Bradykinin type-II receptors and endothelial nitric oxide synthase gene expression levels in aorta of B <sub>2</sub> <sup>tg</sup> mice.....	82
4. Discussion.....	84
4.1. Quantification of bradykinin type-II receptors .....	84
4.2. Vascular effects of endothelium-specific bradykinin type-II receptors overexpression.....	85
4.2.1. Aortic reactivity studies in B <sub>2</sub> <sup>tg</sup> mice.....	85
4.2.2. Systolic blood pressure measurements.....	86
4.2.3. Flow-mediated dilation .....	89
4.3. Cardiac effects of endothelium-specific bradykinin type-II receptors overexpression .....	90
4.3.1. Heart rate .....	90
4.3.2. Echocardiography .....	91
4.4. Expression of proteins relevant to bradykinin type-II receptors signalling .....	93
4.4.1. Proteomics data .....	93
4.4.2. Protein expression of endothelial nitric oxide synthase .....	96
4.4.3. Protein expression of p-ERK1/2/ERK1/2 .....	97
4.5. Sex-specific difference in response to bradykinin .....	98
4.6. Limitations and future recommendations .....	98
Summary and Conclusions.....	100
Summary .....	101
References .....	103
Appendix .....	132
Publications.....	137
Acknowledgments.....	138
Declaration of authorship .....	139

## List of abbreviations

°C: degree Celsius

μl: microliter

μM: micromolar

AA: arachidonic acid

AC: adenylate cyclase

ACE: angiotensin-converting enzyme

ACEI: angiotensin-converting enzyme inhibitors

AET: aortic ejection time

Akt: protein kinase B

ApoE: apolipoprotein E

APP: aminopeptidases

APS: ammonium persulfate

ARBs: angiotensin receptor blockers

Arg: arginine

ARNi: angiotensin receptor-neprilysin inhibitor

AT<sub>1</sub>R: angiotensin II type-1 receptors

AT<sub>2</sub>R: angiotensin II type-2 receptors

ATP: adenosine triphosphate

B<sub>1</sub>R: bradykinin type-I receptors

B<sub>2</sub><sup>n</sup>: negative littermates of transgenic mice of endothelium-specific human bradykinin type-II receptors overexpression

B<sub>2</sub>R: bradykinin type-II receptors

B<sub>2</sub>R-KO: bradykinin type-II receptor knockout

B<sub>2</sub><sup>tg</sup>: transgenic mice of endothelium-specific human bradykinin type-II receptors overexpression

BDKRB2: bradykinin type-II receptor gene

BK: bradykinin

BKCa: large-conductance Ca<sup>2+</sup> sensitive potassium channels

BMFZ: Biologisch-Medizinisches Forschungszentrum

bp: base pair

bpm: beats per minute

BSA: bovine serum albumin

C: cytosine

C1-INH: C1 esterase Inhibitor

Ca<sup>2+</sup>: calcium ions

CaCl<sub>2</sub>: calcium chloride

cAMP: cyclic adenosine monophosphate

cDNA: complementary DNA

CDS: coding sequence  
cGMP: cyclic guanosine monophosphate  
CO: cardiac output  
CO<sub>2</sub>: carbon dioxide  
COVID-19 Coronavirus disease of the year 2019  
COX: cyclooxygenase enzymes  
CPN: carboxypeptidases  
CPT2: Carnitine O-palmitoyltransferase 2  
C<sub>t</sub>: Cycle threshold  
CVDs: Cardiovascular diseases  
DAG: diacylglycerol  
dBp: diastolic blood pressure  
DEA NONOate: [Diethylammonium (Z)-1-(N,N-diethylamino)diazen-1-ium-1,2-diolate  
DNA: deoxyribonucleic acid  
DPP-IV: dipeptidyl peptidase IV  
DTT: Dithiothreitol  
E/A: early to late diastolic transmitral flow velocity  
ECG: electrocardiogram  
EDHF: endothelium derived hyperpolarizing factor  
EDTA: ethylenediaminetetraacetic acid  
EET: epoxyeicosatrienoic acids  
EF: ejection fraction  
EGF-R: epidermal growth factor receptor  
EndMT: endothelial-to-mesenchymal-transition  
eNOS: endothelial nitric oxide synthase  
ERK1/2: extracellular signal-regulated kinases1/2  
*et al: et alia*, and others.  
FAM: fluorescent dye 5-(and-6)-Carboxyfluorescein  
FGF-2: fibroblast growth factor-2  
FMD: flow-mediated dilation  
FS: fractional shortening  
g: gram  
G: gauge  
GAPDH: glyceraldehyde 3-phosphate dehydrogenase  
gDNA: genomic deoxyribonucleic acid  
Gly: glycine  
GPCRs: G-protein-coupled receptors  
GRKs: G-protein-coupled receptor kinases  
GTP: guanosine triphosphate

H<sub>2</sub>O: water, monohydrate  
HCl: hydrochloride  
HEPES: 2-[4-(2-hydroxyethyl)piperazin-1-yl]ethanesulfonic acid  
HMWK: high molecular weight kininogen  
HPLC: high performance liquid chromatography  
Hprt1: Hypoxanthine Guanine Phosphoribosyltransferase  
HR: heart rate  
Hyal1: hyaluronidase 1.  
i.p.: intraperitoneal  
IK<sub>Ca</sub>: intermediate-conductance Ca<sup>2+</sup> sensitive potassium channels  
IL-1: interleukin-1  
iNOS: inducible nitric oxide synthase  
IP<sub>3</sub>: inositol 1,4,5-trisphosphate  
IP<sub>3</sub>R: inositol 1,4,5-trisphosphate receptor  
IVCT: isovolumic contraction time  
IVRT: isovolumic relaxation time  
K<sup>+</sup>: potassium ions  
kb: kilobase  
KCl: potassium chloride  
kDa: kilo dalton  
KH<sub>2</sub>PO<sub>4</sub>: potassium dihydrogen phosphate  
KKS: kallikrein-Kinin system  
LANUV: ethics committee of the district government Düsseldorf  
LC-MS: Liquid chromatography-mass spectrometry  
LMWK: low molecular weight kininogen  
L-NAME: N<sup>ω</sup>-Nitro-L-arginine methyl ester hydrochloride  
LV: left ventricle  
LVPW;d: left ventricular posterior wall thickness in diastole  
LVPW;s: left ventricular posterior wall thickness in systole,  
Lys: lysine  
MAP: mean arterial pressure  
MAPK: mitogen-activated protein kinases  
MEK: Mitogen-activated protein kinase/ERK kinase  
mg: milligram  
MGB: minor groove binder  
MgSO<sub>4</sub>: magnesium sulfate  
MHz: megahertz  
MI: myocardial infarction  
ml: millilitre

mm: millimeter  
mM: millimolar  
MPI: myocardial performance index  
mRNA: messenger ribonucleic acid  
MS: mass spectrometry  
ms: millisecond  
MV DT: deceleration time of the E wave  
Na<sub>2</sub>HPO<sub>4</sub>: disodium hydrophosphate  
NaCl: sodium chloride  
NADPH: nicotinamide adenine dinucleotide phosphate  
NaHCO<sub>3</sub>: sodium bicarbonate  
NaOH: sodium hydroxide  
NEP: neutral endopeptidase  
NFQ: nonfluorescent quencher  
ng: nanogram  
nM nanomolar  
nm: nanometer  
NO: nitric oxide  
NOS: nitric oxide synthase,  
O<sub>2</sub>: oxygen  
OD: optical density  
PBS: phosphate-buffered saline  
PBST: phosphate-buffered saline with tween  
PCR: polymerase chain reaction  
pD<sub>2</sub>: negative decadic logarithm of effector concentration producing the half-maximal effect  
PECAM-1: platelet endothelial cell adhesion molecule  
PG: prostaglandins  
pH: negative of the logarithm of the concentration of hydrogen ions  
Phe: phenylalanine  
PI<sub>3</sub>K: phosphatidylinositol 3-kinase  
PIP<sub>2</sub>: phosphatidylinositol (4,5) bisphosphate  
PKC: protein kinase C  
PLA<sub>2</sub>: phospholipase A<sub>2</sub>  
PLC: phospholipase C  
PRCP: prolyl carboxypeptidase.  
PREP: prolyl endopeptidase  
Pro: proline  
qs: *quantum satis*, the sufficient amount  
RAAS: renin-angiotensin-aldosterone system

RAS: renin-angiotensin-system  
RIPA: Radioimmunoprecipitation assay  
RNA: ribonucleic acid  
ROS: reactive oxygen species  
rpm: round per minute  
RT-qPCR: real-time quantitative polymerase chain reaction  
sBP: systolic blood pressure  
SDS: sodium dodecyl sulfate  
SDS-PAGE: sodium dodecyl sulfate Polyacrylamide Gel Electrophoresis  
SEM: standard error of the mean  
Ser: serine  
sGC: soluble guanylate cyclase  
SHP-1: protein tyrosine phosphatase  
SK<sub>Ca</sub>: small-conductance Ca<sup>2+</sup> sensitive potassium channels  
SNS: sympathetic nervous system  
SOD2: superoxide dismutase [Mn]  
STAT3: signal transducer and activator of transcription 3  
SV: stroke volume  
T: thymidine  
TAE: tris-acetic acid-ethylenediaminetetraacetic acid  
TBS: tris-buffered saline  
TBST: tris-buffered saline with tween  
TEAB: Triethylammonium bicarbonate  
TEMED: tetramethylethylenediamine  
Thr: threonine  
TNF- $\alpha$ : tumour necrosis factor alpha  
t-PA: tissue plasminogen activator  
Tris: tris(hydroxymethyl)aminomethane  
Tris-HCl: tris hydrochloride  
Tyr: tyrosine  
UCP-1: uncoupling protein 1  
UV: ultraviolet  
v/v: volume/volume  
VEGF: vascular endothelial growth factor  
VIC: fluorescent dye 2'-chloro-7'-phenyl-1,4-dichloro-6-carboxyfluorescein  
Volume;d: left ventricular volume during diastole  
Volume;s: left ventricular volume during systole  
vWF: von Willebrand factor  
WT: wild-type

# 1. Introduction

## 1.1. Cardiovascular diseases epidemiology and hypertension

Cardiovascular diseases (CVDs) are classified among the top 10 leading causes of death globally according to the statistics reported by the World Health Organization (WHO), despite tremendous research and advances in medications developed over decades (1). This creates a continuous need to explore new signalling pathways related to the pathogenesis of heart and vessels. The new pathways will help improve therapeutic modalities to maximize efficacy and minimizing side effects, which can further burden patients with CVDs.

Hypertension is a prevalent cardiovascular disease and a major risk factor for other diseases like heart failure, myocardial infarction, stroke, and chronic kidney disease (2). Hypertension is classified into primary hypertension if there is no underlying cause or secondary hypertension if there is a specific cause induce the hypertension. Primary hypertension is a heterogeneous disorder caused by genetic components and other factors such as obesity, high salt intake, smoking, excess alcohol consumption and sedentary lifestyle. Pathogenesis of hypertension is complex and involves endocrine, neural, and paracrine systems, in which renin-angiotensin-aldosterone system (RAAS) and sympathetic nervous system (SNS) are the two major causal systems. Activation of RAAS and SNS leads to an increase in vascular resistance, as well as sodium and water retention, which collectively contribute to elevated blood pressure. (3). Additionally, inflammation, oxidative stress, and immunity trigger vascular dysfunction and are thought to contribute to hypertension pathogenesis (4, 5). Management of hypertension includes both lifestyle modifications and antihypertensive drugs. The well-established lifestyle modifications are weight loss, regular physical activity, decrease sodium intake, and smoking cessation. The main pharmacological therapies for hypertension are angiotensin-converting-enzyme inhibitors, angiotensin receptor blockers, calcium channel blockers, thiazide/thiazide-like diuretics and beta-blockers (2, 6).

The two major determinants controlling blood pressure are cardiac output and total peripheral resistance. The peripheral resistance is dependent on the vasodilatory capacity of blood vessels (3, 7). Blood vessels are composed of three layers: intima, media, and adventitia. The intima mainly composed of endothelial cells that acts as sensors of various stimuli and control the degree of vascular relaxation and contraction. The media contains vascular smooth muscle cells that regulate vascular tone. The adventitia contains fibroblasts, extracellular matrix, adipocytes, lymphocytes, nerves, progenitor cells, and immune cells (4). Healthy endothelium is accountable for several biological processes including regulation of vascular tone, repairing of vascular injury, mechanotransduction, and serves as a semipermeable barrier (8). Endothelium dysfunction is a hallmark for hypertension, where the balance between vasoconstrictors [angiotensin II, endothelin, prostanoids] and vasodilators [nitric oxide (NO), prostacyclin, bradykinin, endothelium derived hyperpolarizing factor (EDHF)] is impaired (9, 10).

There is a constant need for gaining new insights about the signalling pathways that are regulating vasculature functions. One of these pathways which is anticipated to play a beneficial role in blood pressure regulation, yet overlooked, is the bradykinin pathway.

## 1.2. Bradykinin

Bradykinin was first discovered by a Brazilian group in 1949, they gave the name bradykinin (brady: slow, kinin: movement) based on their observation of slow smooth muscle contractions upon stimulation with bradykinin in gut of guinea pigs (11). Bradykinin is a nine amino acids peptide that is physiologically active (12).

### 1.2.1. Production, metabolism, and receptors

Bradykinin is formed from high molecular weight kininogen by plasma kallikrein that is produced from prekallikrein by activated factor XII (13). Bradykinin can be also transformed via aminopeptidase from kallidin which is formed from high and low molecular weight kininogen by tissue kallikrein. Carboxypeptidases convert bradykinin and kallidin into des-Arg9-bradykinin and des-Arg10-kallidin respectively (14) (Figure 1). Bradykinin, kallidin, des-Arg9-bradykinin, and des-Arg10-kallidin are called kinins (15).

Bradykinin has a very short half-life in plasma (about 20-30 seconds) (15, 16). Thirteen plasma and tissue peptidases were recognized to degrade bradykinin such as: angiotensin-converting enzyme (ACE), neutral endopeptidase (Nepriylisin, NEP), dipeptidyl peptidase IV, aminopeptidases, carboxypeptidases, prolyl endopeptidase, and prolyl carboxypeptidase (17). Increasing knowledge about bradykinin degrading enzymes helped to improve plasma collection handling and methods used for measuring bradykinin levels in plasma which represents an analytical dilemma since the bradykinin discovery. Bradykinin and other active and inactive peptides were identified in human blood and urine (18). Kinins, kallikreins, kininogens and kininases collectively constitute the components of Kallikrein-Kinin system (KKS) (14). The production of bradykinin is mainly controlled by C1 esterase Inhibitor (C1-INH). Bradykinin levels are approximately 3 fmol/mL and are higher in tissues compared to plasma (12).

The actions of kinins are mediated through two G-protein-coupled receptors (GPCRs): bradykinin type-I receptors ( $B_1R$ ) and bradykinin type-II receptors ( $B_2R$ ). The main actions of KKS occur via  $B_2R$  which are constitutively found in tissues, whereas  $B_1R$  is inducible in certain conditions like injury, inflammation, and myocardial infarction (15, 19-22). Bradykinin and kallidin are agonists on  $B_2R$ , while des-Arg9-bradykinin and des-Arg10-kallidin are agonists on  $B_1R$  (Figure 1).

$B_2R$  is a seven-helix transmembrane receptor and composed of 391 amino acids; the gene encoding for  $B_2R$  (BDKRB2) in the human genome is located on chromosome 14q32 (23-25).  $B_2R$  has been identified in most cell types such as endothelial cells, smooth muscle cells, immune cells, epithelial cells, fibroblast, sensory neurons, monocytes, and cardiomyocytes (26-30). The  $B_2R$  can be phosphorylated or glycosylated (25).  $B_2R$  undergo desensitization upon agonist stimulation, which means that attenuation of the response occurs with continuous or repeated agonist stimulation (31). Desensitization occurs through phosphorylation of  $B_2R$  by GPCR kinases (GRKs) followed by binding to  $\beta$ -arrestin. GRK-2 is one of the GPCR kinases which phosphorylates  $B_2R$ , and its inhibition enhances response to bradykinin (32). The  $B_2R$  signalling is considered transient in nature due to the rapid desensitization and internalization of  $B_2R$ . Interestingly it takes 1-3 hours for  $B_2R$  to be recycled and returned to the cell surface after being endocytosed. In contrast,  $B_1R$  is resistant to desensitization and

their degradation is agonist independent. Since B<sub>1</sub>R are inducible, the half-life is 2-4 hours, and they are not recycled (26).

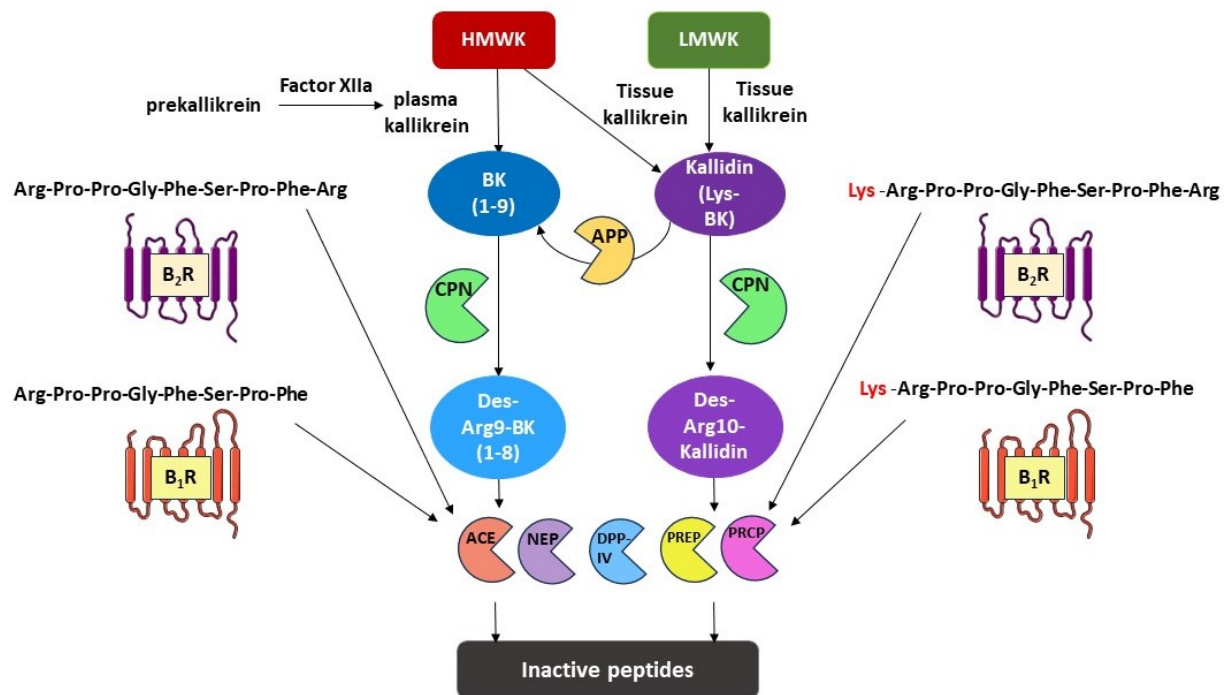


**Figure 1:** Schematic diagram showing production and breakdown of agonists of bradykinin type-II receptors and bradykinin type-I receptors (B<sub>2</sub>R and B<sub>1</sub>R). Bradykinin (BK) is produced from cleavage of high molecular weight kininogen (HMWK) by plasma kallikrein. Kallidin (Lys-bradykinin) is another B<sub>2</sub>R agonist which is produced from cleavage of HMWK or low molecular weight kininogen (LMWK) by tissue kallikrein. Kallidin can be transformed into BK via aminopeptidases (APP). Des-Arg<sup>9</sup>-BK and Des-Arg<sup>10</sup>-kallidin are B<sub>1</sub>R agonists that are produced via carboxypeptidases (CPN) from BK and KD, respectively. BK, kallidin, Des-Arg<sup>9</sup>-BK and Des-Arg<sup>10</sup>-kallidin are degraded into inactive peptides via angiotensin-converting enzyme (ACE), neutral endopeptidase (NEP), dipeptidyl peptidase IV (DPP-IV), prolyl endopeptidase (PREP), and prolyl carboxypeptidase (PRCP). Arg: arginine, Pro: proline, Gly: glycine, Phe: phenylalanine, Ser: serine, Lys: lysine.

### 1.2.2. Bradykinin downstream signalling

B<sub>2</sub>R are coupled to G<sub>i</sub>, G<sub>q</sub>, G<sub>12/13</sub>, and G<sub>s</sub> proteins but the main actions of B<sub>2</sub>R occurred through G<sub>q</sub>. Upon binding of bradykinin to B<sub>2</sub>R, G<sub>αq</sub> subunit dissociates from G<sub>q</sub> protein. G<sub>αq</sub> activates phospholipase C (PLC) which cleaves phosphatidylinositol (4,5) biphosphate (PIP<sub>2</sub>) into inositol 1,4,5-trisphosphate (IP<sub>3</sub>) and diacylglycerol (DAG). DAG activates protein kinase C (PKC) which in turn activates phosphorylation steps that eventually phosphorylates phospholipase A<sub>2</sub> (PLA<sub>2</sub>). IP<sub>3</sub> binds to receptors on endoplasmic reticulum and induces the release of calcium ions (Ca<sup>2+</sup>), the increase in intracellular calcium concentration leads eventually to the release of mediators of vasodilation: NO, prostaglandins and EDHF (15, 19, 26, 33). Ca<sup>2+</sup> binds to calmodulin and activates endothelial nitric oxide synthase (eNOS) which catalyzes the production of NO, where NO moves into vascular smooth muscle cells and activates soluble guanylate cyclase (sGC) that converts guanosine triphosphate (GTP) to cyclic guanosine monophosphate (cGMP) (34). Ca<sup>2+</sup> can also directly activate small- and

intermediate-conductance  $\text{Ca}^{2+}$  sensitive potassium channels ( $\text{SK}_{\text{Ca}}$  and  $\text{IK}_{\text{Ca}}$ ), the increase of potassium ions ( $\text{K}^+$ ) in the myo-endothelial space induces smooth muscle hyperpolarization and relaxation (35). Arachidonic acid is produced from membrane phospholipids by the activated  $\text{PLA}_2$  (activated by  $\text{Ca}^{2+}$  and PKC) and acts as a substrate for cyclooxygenase enzymes (COX) and cytochrome P450 epoxygenases to produce prostaglandins and epoxyeicosatrienoic acids (EETs) respectively (36). Prostaglandins activate adenylate cyclase (AC) that converts adenosine triphosphate (ATP) to cyclic adenosine monophosphate (cAMP) (37). cAMP and cGMP are intracellular second messengers that trigger vascular smooth muscle cell relaxation (38). EETs are considered EDHF as they open large-conductance  $\text{Ca}^{2+}$  sensitive  $\text{K}^+$  channels ( $\text{BK}_{\text{Ca}}$ ) channels and increase  $\text{K}^+$  levels. The increase in  $\text{K}^+$  levels by opening  $\text{SK}_{\text{Ca}}$ ,  $\text{IK}_{\text{Ca}}$  and  $\text{BK}_{\text{Ca}}$  leads to hyperpolarization which cause smooth muscle relaxation and this pathway is termed EDHF (35) (Figure 2). Worth mentioning, the abovementioned described downstream signalling is the one reported for the vasodilatory effect of bradykinin, for other bradykinin-induced effects the underlying mediators should be thoroughly studied. For instance, the bradykinin-induced tissue plasminogen activator (t-PA) release is independent of NOS and COX pathways (39) but rather mediated by EDHF pathway (40, 41).

Some differences were reported between  $\text{B}_2\text{R}$  and  $\text{B}_1\text{R}$  signalling. For instance, in endothelial cells  $\text{B}_2\text{R}$  stimulation resulted in transient NO release (approximately 5 minutes) while in cytokine-treated endothelial cells  $\text{B}_1\text{R}$  activation led to a prolonged NO release (approximately 90 minutes). The  $\text{B}_1\text{R}$  induced NO release is mediated via Ras/Raf/MEK/ERK/iNOS pathway (42).

Several biological processes beyond vasodilation have been identified for the  $\text{B}_2\text{R}$  signalling such as angiogenesis, cell migration, pain, inflammation, autophagy, and apoptosis. Knowledge about  $\text{B}_2\text{R}$  signalling downstream mediators evolved over years and still under study, recently Rex et al. developed a pathway map to summarize the proteins which are known to be involved in  $\text{B}_2\text{R}$  signalling (43).  $\text{B}_2\text{R}$  downstream signalling and the involved mediators in angiogenesis were explored over years. A combination of increase in vascular endothelial growth factor (VEGF) expression, and epidermal growth factor receptor (EGF-R) stimulation through S-nitrosylation by NO were proposed to be involved in  $\text{B}_2\text{R}$  induced angiogenesis (44). Further intercellular mediators were explored, where it was found that NO nitrosylated the protein tyrosine phosphatase SHP-1 and p21Ras. SHP-1 activates the EGF-R and p21Ras activates signal-regulated kinases1/2 (ERK1/2) that further activates EGF-R and increases VEGF levels. Another study showed an upregulation of fibroblast growth factor-2 (FGF-2) by bradykinin in human endothelial cells, FGF-2 promotes vascular permeability and cell migration as a part of the angiogenic process. Bradykinin transactivates FGF receptor-1 by phosphorylation of FGF receptor substrate, ERK1/2, and signal transducer and activator of transcription 3 (STAT3) (45).

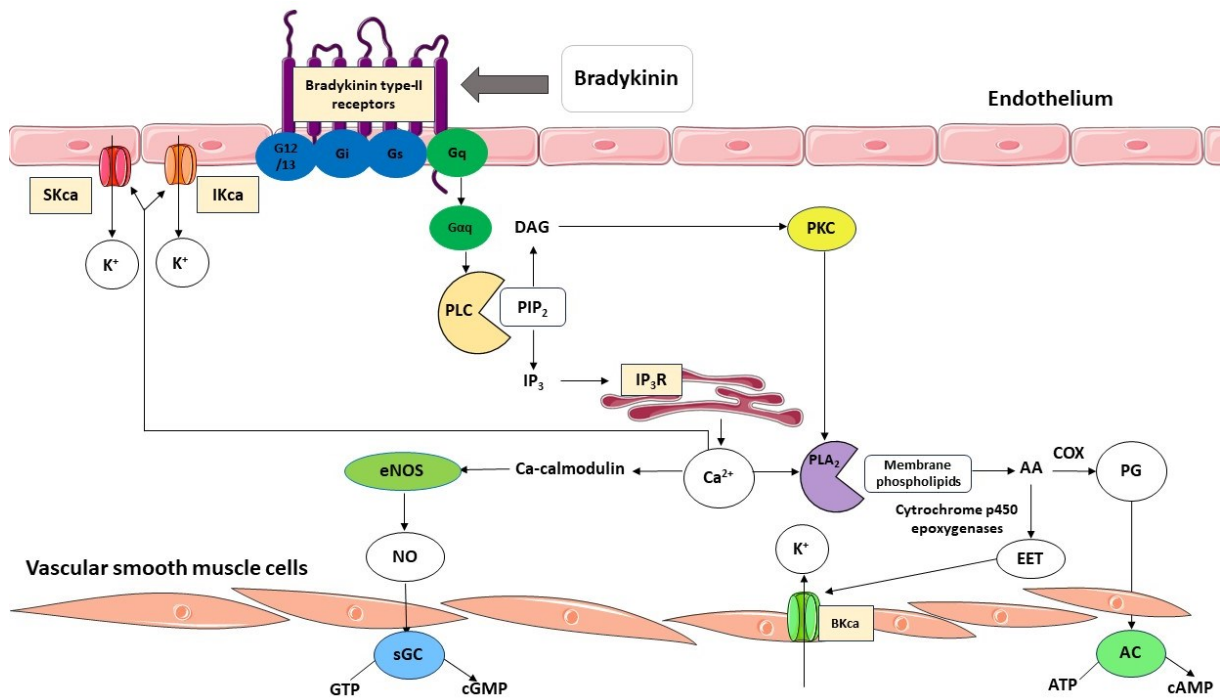


**Figure 2:** Schematic diagram showing downstream signalling and mediators of bradykinin-induced vasodilation. Activation of bradykinin type-II receptors with bradykinin leads to  $G_{\alpha q}$  subunit dissociation from  $G_q$  coupled protein.  $G_{\alpha q}$  subunit activates phospholipase C (PLC) that cleaves phosphatidylinositol (4,5) bisphosphate ( $PIP_2$ ) into inositol 1,4,5-trisphosphate ( $IP_3$ ) and diacylglycerol (DAG).  $IP_3$  bind to their receptors ( $IP_3R$ ) on endoplasmic reticulum triggering calcium ions ( $Ca^{2+}$ ) release. The increase in  $Ca^{2+}$  concentration stimulates cascades that end with the production of vasodilation mediators: nitric oxide (NO), prostaglandins (PG), and endothelium-derived hyperpolarizing factor (EDHF). NO is produced from L-arginine by nitric oxide synthase (eNOS) that is activated by calcium calmodulin. NO passes across vascular smooth muscle cells and activates soluble guanylate cyclase (sGC) that catalyses the cyclic guanosine monophosphate (cGMP) release from guanosine triphosphate (GTP). Additionally, phospholipase  $A_2$  ( $PLA_2$ ) is activated by both  $Ca^{2+}$  and phosphorylation reactions that triggered by protein kinase C (PKC). PKC is activated by DAG. Arachidonic acid (AA) is formed from membrane phospholipids by  $PLA_2$ . AA is a substrate of cyclooxygenase (COX) enzymes and cytochrome p450 epoxygenases to produce PG and epoxyeicosatrienoic acids (EET), respectively. PG pass across vascular smooth muscle cells and activate adenylate cyclase (AC) that catalyses the production of cyclic adenosine monophosphate (cAMP) from adenosine triphosphate (ATP). cGMP and cAMP mediate vascular smooth muscle relaxation. Actions of EET on large-conductance calcium sensitive potassium channels ( $BK_{Ca}$ ) and of  $Ca^{2+}$  on small and intermediate-conductance calcium sensitive potassium channels ( $SK_{Ca}$  and  $IK_{Ca}$  respectively) lead to increase in the potassium levels ( $K^+$ ) in the myo-endothelial space. The increase of  $K^+$  causes hyperpolarization and consequently smooth muscle relaxation occurs.

### 1.2.3. Bradykinin functions

Bradykinin exerts several beneficial actions via B<sub>2</sub>R on blood vessels, kidney, and heart (Figure 3); targeting this pathway can hold promises in treatment of hypertension, coronary artery disease and peripheral arterial disease.

#### 1.2.3.1 Blood pressure lowering effect of bradykinin

Bradykinin showed blood pressure lowering effect since it was first discovered (11). It is regarded as endothelial autacoid that provokes protective effects on endothelium through vasodilatory effect on vessels (46, 47). Notably, bradykinin acts in autocrine and paracrine mechanisms rather than an endocrine way (48). Both intravenous and intra-arterial bradykinin administration resulted in a decrease in blood pressure in anaesthetized mice, rats and rabbits. The decrease in blood pressure was more prominent after intra-arterial administration (49). Inhibition of endogenous bradykinin degradation led to decrease in blood pressure in spontaneously hypertensive rats and not in rats with normal blood pressure, suggesting that endogenous bradykinin affects blood pressure only in hypertension (50). Importantly the rats in this study underwent binephrectomy to eliminate the effect of renin-angiotensin system (RAS). Moreover, concurrent blocking of B<sub>1</sub>R and B<sub>2</sub>R caused a profound decrease in blood pressure in rats, whereas blocking of either B<sub>2</sub>R or B<sub>1</sub>R alone did not significantly decreased blood pressure (51). It is well-recognized that the vasodepressor effects of KKS counterbalance the well-described vasopressor effects of RAS (47). However, it is thought that the KKS becomes activated and starts to buffer the deleterious effects of RAS only in pathological conditions but under normal conditions KKS does not contribute substantially in blood pressure regulation (52).

Another known effect of bradykinin is its ability to cause diuresis and natriuresis, which may also contribute to its blood pressure-lowering ability (15). Chronic overexpression of bradykinin in rat's kidney led to increase in urine and sodium excretion (53). Administration of B<sub>2</sub>R antagonist decreased urinary volume and secretion of both sodium and potassium (54). Mamenko et al. reviewed the detailed mechanisms by which bradykinin induces natriuresis and showed that bradykinin inhibits the renal epithelial sodium channels through the released mediators (NO, EET and PIP<sub>2</sub>) (55). Zhang et al. demonstrated that bradykinin increases both sodium and potassium secretion by inhibiting inwardly rectifying potassium channel and sodium-chloride cotransporter in the distal convoluted tubule. They also showed an increase in urine volume in mice after 60 minutes of bradykinin infusion (56).

Despite the proof of presence of local KKS in kidney (57), the effect of bradykinin on renal blood flow and its implications on blood pressure are questionable. Local infusion of bradykinin in kidney medulla improves renal medullary blood flow but has no effect on arterial blood pressure (58). It has been shown that the effect of bradykinin is differential across different zones of the kidney. Infusion of bradykinin into the renal artery or directly into the renal cortex or medulla resulted in a sustained increase only in medullary perfusion, without affecting renal blood flow or cortical perfusion (59). Besides, it was shown that the bradykinin-induced increase in medulla perfusion is dependent on NO and Ca<sup>2+</sup> sensitive K<sup>+</sup> channels (59). In angiotensin II infused rats, bradykinin abolished the renal vasoconstrictor effect of angiotensin II but couldn't abolish angiotensin II hypertension (60). There is a consensus that bradykinin plays a minor role in renal blood flow regulation under

physiological conditions. However, when bradykinin degradation is inhibited or when the kidney is challenged by changes in volume or different salt diets, the role of bradykinin becomes prominent (52, 61).

### 1.2.3.2 Bradykinin effects on coronary arteries, heart and hindlimb ischemia

**Coronary arteries** The identification of local KKS in heart (57) and the well-described vasodilator effect of bradykinin inspired the study of bradykinin effects on heart and myocardial ischemia. Administration of B<sub>2</sub>R antagonist in left main coronary artery of patients pointed out a role of endogenous B<sub>2</sub>R in improving coronary blood flow (62). Interestingly, the bradykinin induced-coronary vasodilation was not deteriorated by twelve weeks streptozotocin-induced diabetes in rats (63). It has been shown that the bradykinin-induced vasodilation in coronary arteries as an example of resistance arteries is dependent on cytochrome P450 products and calcium sensitive potassium channels (63). A recent study demonstrated porcine and human intramyocardial coronary arteries in three-dimensional imaging to investigate the underlying signalling of bradykinin-induced vasodilation. This study showed that bradykinin induced vasodilation via calcium release with subsequent stimulation of calcium sensitive potassium channels (64). Besides, it was demonstrated that the communication between endothelial cells and smooth muscle cells cause the propagation of vasodilation along the vessel length (64).

**Myocardial ischemia and heart failure** Expression of B<sub>2</sub>R and B<sub>1</sub>R increased after induction of myocardial infarction in rats (65). Possible benefits of bradykinin after myocardial ischemia could be improving coronary blood flow, reducing infarct size, minimizing the decrease of cardiac contractility and lessening left ventricular (LV) remodelling (66). Continuous subcutaneous administration of bradykinin in myocardial infarction model in rats attenuated LV dysfunction, fibrosis, and autophagy. PI3K/Akt was shown to be the underlying pathway of bradykinin protective effect against cardiomyocyte autophagy (67). *In vitro*, bradykinin demonstrated an antiapoptotic effect via enhancing Bcl-2 expression and reducing cleaved caspase 3 and Bax expression (68). B<sub>2</sub>R expression increased in compensated LV hypertrophy and are thought to elicit cardioprotective effects. However, in heart failure the expression decreased which might indicate loss of the protective effect of bradykinin on the heart (69). Heart tissues from heart failure patients showed lower B<sub>2</sub>R expression than healthy hearts (70). Bradykinin infusion preserved vascular endothelial function, cardiac systolic and diastolic function in heart failure model in dogs (71).

**Angiogenesis and hindlimb ischemia** Another reported effect of bradykinin is the ability to promote angiogenesis, this effect was thoroughly studied in hindlimb ischemia rather than myocardial ischemia. In hindlimb ischemia rat model, administration of kinin and kallikrein increased blood perfusion and capillaries and arterioles density in ischemic limb (72). While diabetes impairs the post-ischemic neovascularization, B<sub>2</sub>R stimulation restored neovascularization in hindlimb ischemia diabetic mice model. VEGF levels and CD34<sup>+</sup>/VEGFR2<sup>+</sup> progenitor cells were increased and mediate the neovascularization induced by B<sub>2</sub>R stimulation (73). It has been shown that B<sub>2</sub>R are expressed on circulating progenitor cells CD34<sup>+</sup>. The progenitor cells play a role in vascular repair after myocardial infarction, and it is thought that B<sub>2</sub>R signalling contributes to this protective role which includes cell proliferation and angiogenesis (74). In another study, expression of B<sub>2</sub>R was

demonstrated on CD34<sup>+</sup> and CD133<sup>+</sup>; bradykinin increased the recruitment of these progenitor cells, which play a role in neovascularization following ischemia (75).

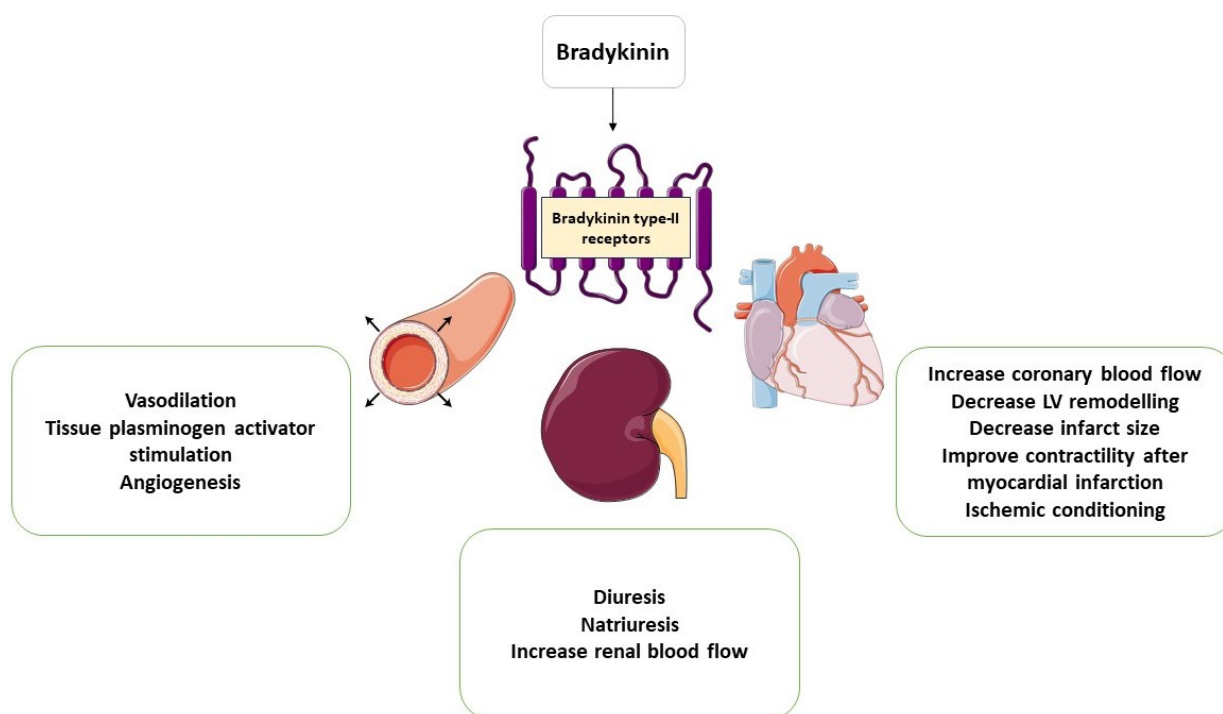


**Figure 3:** Summary of bradykinin benefits on blood vessels, kidney, and heart. LV: left ventricle.

#### 1.2.4. Regulation of bradykinin type-II receptors expression

Previous finding from our working group showed that B<sub>2</sub>R expression is not affected by NO, bradykinin or B<sub>2</sub>R antagonist icatibant (76). However, B<sub>2</sub>R expression could be affected by some drugs or changed in some conditions or diseases. An early study in hypertensive rats, administration of 1% potassium chloride in drinking water resulted in an increase in renal B<sub>2</sub>R expression after 6 weeks, suggesting that KKS may contribute to the blood pressure lowering effect of potassium supplements (77). In human coronary artery endothelial cells, a cholesterol lowering drug lovastatin increased the B<sub>2</sub>R expression (78). In rats with endothelium-specific B<sub>1</sub>R overexpression, B<sub>2</sub>R expression was increased suggesting that B<sub>1</sub>R may induce B<sub>2</sub>R upregulation (79).

B<sub>2</sub>R expression is upregulated in some diseases or pathological conditions. Hypoxia (5% oxygen) induced B<sub>2</sub>R upregulation, this upregulation may be responsible for proper cell migration and angiogenesis in LV remodelling after myocardial infarction (80). Angiotensin II and inflammatory mediators such as tumour necrosis factor alpha (TNF- $\alpha$ ) and interleukin-1 (IL-1) enhanced B<sub>2</sub>R expression (42, 81). B<sub>2</sub>R is implicated in diabetic retinopathy by increasing retinal vascular permeability via vascular endothelial cadherin phosphorylation, and an increase of B<sub>2</sub>R expression was demonstrated in the retina of diabetic rats (82). Moreover, B<sub>2</sub>R was found to be highly expressed in several types of cancers such as cervical cancer, hepatocellular carcinoma, and head and neck squamous cell carcinoma. In these studies, it was proposed that B<sub>2</sub>R is responsible for tumour cells migration, invasion, proliferation and angiogenesis; in addition, EGF-R,

COX-2, VEGF, and matrix metalloproteinases were found to mediate these actions via B<sub>2</sub>R (83-88). N-myc (and STAT) interactor, a protein that play a role of tumour growth in hepatocellular carcinoma was shown to be an upstream target of B<sub>2</sub>R expression (89).

### 1.3. Drugs that interfere with bradykinin signalling

#### 1.3.1. Drugs increasing bradykinin effects

Drugs that increase bradykinin levels due to decrease of bradykinin metabolism were investigated for possible beneficial effects of bradykinin via B<sub>2</sub>R. Although most therapeutic agents which decrease catabolism of bradykinin showed angioedema as a side effect (90, 91), the beneficial actions of bradykinin reported over years may open the door for designing new candidate entities to act as B<sub>2</sub>R agonists.

**Angiotensin-Converting Enzyme Inhibitors (ACEI)** ACEI (drug class ending with -pril such as captopril, ramipril, enalapril, perindopril) are well-known therapeutic agents in treatment of hypertension, heart failure, chronic kidney diseases, and in secondary prevention of stroke in patients who experienced previous stroke of transient ischemic attack (2, 92-94). The main mechanism of actions of ACEI is the inhibition of production of angiotensin II via inhibition of ACE which is responsible for conversion of angiotensin I to angiotensin II (95). Another mechanism of action of ACEI is the increased bradykinin levels, as a consequence of inhibition of their degradation enzymes ACE (96). *In vitro* incubation of healthy volunteers' plasma with 100 nM bradykinin and ACEI increased half-life of bradykinin from 34 seconds into 7.1 minutes (97). The increased bradykinin levels is thought to elicit beneficial functions in endothelium through increasing NO, prostacyclin, EDHF and t-PA (98).

Experimental evidence pointed out that bradykinin activity through B<sub>2</sub>R plays a role in therapeutic actions of ACEI on blood pressure, heart, and kidney. An early study on acute administration of captopril and B<sub>2</sub>R antagonist partially abolished the decrease of mean arterial pressure (MAP) caused by administration of captopril (99). A gene polymorphism association study in 106 hypertensive patients received enalapril for 60 days showed an association between BDKRB2 gene polymorphism and MAP response to enalapril suggesting a role of B<sub>2</sub>R in the antihypertensive effect of enalapril (100). PERTINENT, a sub-study of the EUROPA study, provided evidence about beneficial actions of perindopril on endothelial function through increasing bradykinin and eNOS protein levels (101).

Studies of the ACEI-induced neovascularisation revealed that B<sub>2</sub>R signalling partially underlying this effect in models of hindlimb ischemia with or without diabetes. Administration of perindopril led to an improvement in post ischemic neovascularization only in wild-type (WT) or diabetic mice and not in bradykinin type-II receptor knockout (B<sub>2</sub>R-KO) mice (102, 103). The ACEI induced neovascularisation in hindlimb ischemia was proven even in angiotensin II type-1 receptors (AT<sub>1</sub>R) knockout mice and this effect was moderately attenuated by B<sub>2</sub>R antagonist (104). Collectively, these results suggested that B<sub>2</sub>R partially contributes to the ACEI-induced benefits in neovascularisation.

Improvement of cardiac functions and LV remodelling after myocardial infarction induced by ACEI was partially attenuated in B<sub>2</sub>R-KO mice (105, 106). The attribution of bradykinin for beneficial effects on heart was further investigated in heart failure model in dogs and in isolated hearts from rats after induction of ischemia followed by reperfusion (107, 108). Not only the role of bradykinin signalling, as a part of mechanisms of action of ACEI, on blood vessels and heart were studied but also on kidney. In diabetic obese mice, oral administration of ramipril for 20 weeks protected against diabetic nephropathy, this effect was abolished by administration of B<sub>2</sub>R antagonist (109).

**Angiotensin Receptor Blockers (ARBs)** ARBs (sartans) are alternative therapeutic agents with similar indications to ACEI. They act by blocking of deleterious effects of angiotensin II on AT<sub>1</sub>R (110). In contrast to ACEI, these agents are not acting directly on ACE, therefore, few beneficial actions via B<sub>2</sub>R were reported (111, 112). Some assumptions have been raised regarding indirect mechanism of action of ARB on bradykinin, where ARBs displace the binding of angiotensin II on AT<sub>1</sub>R, angiotensin II levels increase which in turn stimulate angiotensin II type-2 receptors (AT<sub>2</sub>R). Stimulation of AT<sub>2</sub>R, may reduce ACE activity and consequently increases bradykinin levels (91). Particularly, losartan may act as a partial agonist of B<sub>2</sub>R (113) and was shown to increase bradykinin levels in a small clinical study (114).

**Angiotensin receptor-neprilysin inhibitor (ARNi)** ARNi is a complex of a neprilysin inhibitor and ARB. Neprilysin is a neutral endopeptidase that cleaves natriuretic peptides, bradykinin, adrenomedullin, so inhibition of neprilysin increase bradykinin levels (115). In endothelial cells, neprilysin inhibitor promoted proliferation that contributes to collateral formation via B<sub>2</sub>R pathway (116).

**Statins** Although not extensively studied for their effect on bradykinin, few studies showed that statins increased NO production at least partially via B<sub>2</sub>R (117, 118).

**B<sub>2</sub>R agonists** The concept of developing B<sub>2</sub>R agonists is under study. Increasing the knowledge about B<sub>2</sub>R signalling can help to optimize the structure requirements for effective B<sub>2</sub>R agonists. Labradimil is a synthesized B<sub>2</sub>R agonist with longer half-life than bradykinin. Labradimil developed to increase the blood brain permeability of chemotherapeutic agents to treat brain tumours (119). In rats, labradimil administration showed decrease in mean arterial pressure (120, 121). In preclinical study in mice, a synthesized B<sub>2</sub>R agonist showed more potent hypotensive and profibrinolytic effects than bradykinin (122).

### 1.3.2. Drugs decreasing bradykinin effects

C1 esterase Inhibitor (C1-INH), B<sub>2</sub>R antagonist, and kallikrein inhibitor are three therapeutic options used for decreasing bradykinin effects. These drugs are approved for treatment of hereditary angioedema, a condition characterized by oedema that is caused by increase production of bradykinin (123). C1-INH is a serine protease inhibitor that inactivates factor XIIa and inhibits kallikrein thus decrease production of bradykinin (13). Icatibant is a specific competitive B<sub>2</sub>R antagonist that has a short half-life (1.5-2 hours) and the maximum plasma concentration for 30 mg or 90 mg doses was achieved in less than 1 hour (124). Some clinical trials were conducted to discover other indications for icatibant, for instance, icatibant prevented intradialytic hypotension in a small randomized clinical trial in patients receiving haemodialysis (125). Recently, few small

studies were conducted in covid-19 patients to evaluate the efficacy of icatibant on improving patients' symptoms and oxygen requirements, however, the results were inconsistent (126).

#### **1.4. Interaction of bradykinin pathway and renin-angiotensin system**

RAS is the major interacting system with bradykinin pathway and the interaction between the two systems can occur on several levels (47). Bradykinin counteracts the deleterious effects of hyperactive RAS in CVDs and loss of B<sub>2</sub>R functions resulted in a counter activation of Angiotensin-(1-7)/Mas and AT<sub>2</sub>R to maintain homeostasis (127). B<sub>2</sub>R activation increased renin gene expression in mouse kidney cortical collecting duct cell line via PKC and NO release (128). Moreover, in B<sub>2</sub>R-KO mice renin gene expression was decreased but ACE, AT<sub>1</sub>R and angiotensinogen expression were not changed suggesting a role of B<sub>2</sub>R on renin secretion (129). ACE is regarded as a connection point between RAS and KKS through production of angiotensin II and inactivation of bradykinin (47).

B<sub>2</sub>R can form functional heterodimers with receptors of RAS (AT<sub>1</sub>R, AT<sub>2</sub>R and Mas receptors) with a consequent change in the net signalling. For instance, in studies on preeclampsia, B<sub>2</sub>R-AT<sub>1</sub>R heterodimer leads to enhanced G-protein coupling and activation of the AT<sub>1</sub>R that was manifested as an increase in blood pressure and oxidative stress (130, 131). AT<sub>2</sub>R and Mas receptor are the receptors in RAS which are responsible for beneficial effects on blood vessels like vasodilation and decreasing thrombosis (127). Some studies showed that AT<sub>2</sub>R can stimulate the release of bradykinin and some of the beneficial functions of AT<sub>2</sub>R are mediated via B<sub>2</sub>R (132, 133). In addition, B<sub>2</sub>R forms heterodimers with AT<sub>2</sub>R and with Mas receptor, this heterodimerization enhances the beneficial effects from each receptor separately (134, 135).

#### **1.5. Polymorphism studies of bradykinin type-II receptor gene**

Clinical studies on polymorphisms of the human BDKRB2 gene and their associations with blood pressure strengthen the evidence about human B<sub>2</sub>R gene for being a candidate gene in blood pressure regulation. One commonly studied gene polymorphism is the BDKRB2-58T/C gene polymorphism in the promoter region of BDKRB2 gene, where a cytosine (C) to thymidine (T) transition occurs 58 bp upstream of the putative transcription start site (136). The different alleles (T or C) at this site can lead to difference in the B<sub>2</sub>R transcription rate and hence affect the number of B<sub>2</sub>R. Three metanalysis addressed the association of different alleles of this polymorph with blood pressure and reported an association between BDKRB2-58T/C gene polymorphism and the risk of hypertension. -58T allele carriers showed a protective effect on hypertension, whereas -58C allele carriers are susceptible to hypertension (Table 1).

Another common polymorphism in human BDKRB2 gene is the presence (+9) or absence (-9) of nine bp repeat in exon 1 (BE1), +9 allele has been associated with decreased B<sub>2</sub>R gene transcription and messenger ribonucleic acid (mRNA) expression in comparison to the -9 allele (136, 137). Pretorius et al. showed an association between BE1 +9/+9 genotype and increased systolic blood pressure (sBP) and pulse pressure in white Americans and increased flow vascular resistance in black Americans (138). Later on, this association was demonstrated in children as well (139), and in this study BE1 +9/+9 genotype was associated with microvascular dysfunction. In normotensive healthy males, BE1 +9/+9 genotype was associated with higher LV

growth response after 10-week physical training program (140). Similar findings was shown in hypertensive patients, where BE1 +9/+9 genotype carrier showed lower improvement in response to antihypertensive medications in comparison to BE1 -9/-9 genotype carrier (141). BE1 +9/-9 and BE1-9/-9 carriers who received ACEI showed higher forearm blood flow and lower forearm vascular resistance in response to bradykinin in comparison to BE1 +9/+9 carriers (142).

**Table 1:** Meta-analysis of BDKRB2 gene polymorphism studies, number of studies included in each meta-analysis and publication year.

Site of polymorphism	Number of studies in meta-analysis	Publication year, references
Promoter region, -58 T/C polymorphism	4 studies	2010, (143)
	11 studies	2012, (144)
	13 studies	2016, (145)

C: cytosine, T: thymidine

## 1.6. Genetically modified models of kallikrein-kinin system

An essential approach to explore the physiological functions of KKS is the generation of genetically modified animal models in which specific gene is disrupted or inserted. B<sub>2</sub>R-KO mice models were generated on 129Sv/J genetic background (81, 105, 146-152) or C57BL/6 genetic background (153-157). However, the obtained results from the B<sub>2</sub>R-KO models regarding the blood pressure outcome of those mice were inconsistent (Appendix 1). The discrepancy of the obtained results from B<sub>2</sub>R-KO models can be largely attributed to several variations such as using mice with different genetic background, age, or gender. Besides, the reported heterogeneity in methodological approaches among different studies. An additional crucial aspect to be considered is the compensation from the other types of receptors such as the increase of B<sub>1</sub>R, Mas receptor and AT<sub>2</sub>R expression when BDKRB2 gene were knocked out (106, 158).

Studies on mice with double knockout of B<sub>1</sub>R and B<sub>2</sub>R mice were conducted (159-161) and these mice exhibited normal blood pressure. Likewise, tissue kallikrein-deficient mice did not show change in blood pressure (162, 163). In contrast, mice with conditional B<sub>2</sub>R-KO of collecting duct and mice with deletion of kininogen1 and kininogen2 genes (in which LMWK was decreased) showed elevated blood pressure (164, 165).

The other strategy in the genetically modified animal models is the insertion of target gene in which overexpression of a protein or a receptor occurs. Insertion of human tissue kallikrein in rats led to a decrease in blood pressure (166). Likewise, insertion of human B<sub>2</sub>R in mice resulted in the same effect (167). The studies on B<sub>2</sub>R overexpression models are scarce and the cardiovascular outcomes are not fully studied in these models.

The model description, main findings, and publication year of the genetically modified models that are described in this section are summarized in appendix 1.

## 1.7. Aim of the work

The B<sub>2</sub>R pathway, discovered several years ago, has been associated with numerous beneficial effects. These effects observed either through direct administration of bradykinin or indirectly via studies on ACEI. Despite these findings, there remains a gap in our understanding of the vascular and cardiac effects of the B<sub>2</sub>R pathway under basal conditions. To address this knowledge gap, a mouse model with endothelium-specific overexpression of human B<sub>2</sub>R was utilized to investigate the following research questions:

- Does B<sub>2</sub>R play a role in the regulation of blood pressure?
- What are the mediators responsible for the vasodilatory effects of bradykinin on B<sub>2</sub>R?
- Does B<sub>2</sub>R influence cardiac function?
- Does B<sub>2</sub>R affect flow-mediated dilation?
- What candidate proteins mediate the effects of B<sub>2</sub>R signalling on endothelial function?

## 2. Materials and Methods

### 2.1. Buffers and reagents

Ultrapure grade chemicals and reagents were purchased mainly from Merck (Darmstadt, Germany), Roth (Karlsruhe, Germany), VWR (Darmstadt, Germany) and Sigma-Aldrich (Munich, Germany), otherwise, the company will be mentioned in the specified section. Buffers were prepared using fresh ultra-pure water produced by Milli-Q® EQ 7000 water purification system (Merck, Darmstadt, Germany). The pH of buffers was measured by pH-Meter (HI 2210 pH Meter, Hanna Instruments, Vöhringen, Germany). Required pH was achieved by gradually adding 1M hydrochloride (HCl) or 1M sodium hydroxide (NaOH) aqueous solutions.

#### Lysis buffer for ear biopsies for genotyping (pH 8.0)

Tris-HCl	40 mM
EDTA	100 mM
NaCl	100 mM
SDS	0.1%

#### 50x TAE buffer for agarose gel preparation (pH 8.3)

Tris	2 M
EDTA	50 mM
Acetic acid	20 mM

#### Sample loading buffer for genotyping

Glycerol	30%
Bromophenol blue	q.s.

#### Krebs-HEPES buffer (pH 7.4)

NaCl	99 mM
KCl	4.7 mM
CaCl <sub>2</sub> · 2 H <sub>2</sub> O	1.9 mM
MgSO <sub>4</sub> · 7 H <sub>2</sub> O	1.2 mM
NaHCO <sub>3</sub>	25 mM
KH <sub>2</sub> PO <sub>4</sub>	1.0 mM
Na-HEPES	20 mM
D-Glucose · H <sub>2</sub> O	11.1 mM

**Modified Krebs- Henseleit buffer (pH 7.4, achieved by carbogen bubbling)**

NaCl	118.07 mM
KCl	4.70 mM
CaCl <sub>2</sub>	1.60 mM
MgSO <sub>4</sub>	1.18 mM
NaHCO <sub>3</sub>	25.0 mM
K <sub>2</sub> HPO <sub>4</sub>	1.18 mM
D-glucose	5.55 mM

**Radioimmunoprecipitation assay buffer (RIPA) buffer for protein lysate preparation**

Triton X	1%
SDS	0.1%
Sodium deoxycholate	0.1%
EDTA	1 mM
PBS	25 ml

**2x Lammeli buffer protein preparation (pH 6.8)**

Tris	125 mM
SDS	4%
Glycerol	20%
2-Mercaptoethanol	10%
Bromophenol blue	q.s.

**4x separating gel buffer (pH 8.8)**

Tris	1.5 M
SDS	0.4%

**4x stacking gel buffer (pH 6.8)**

Tris	0.5 M
SDS	0.4%

**10x tank buffer for sodium dodecyl sulfate Polyacrylamide Gel Electrophoresis (SDS-PAGE)**

Tris	0.25 M
Glycine	1.9 M

SDS 1%

**10x transfer buffer for SDS-PAGE**

Tris 0.25 M

Glycine 1.9 M

Methanol 20%

**Tris-Buffered Saline (TBS, pH 7.6)**

Tris 200 mM

NaCl 1500 mM

**TBST**

Tween® 20 0,1%

TBS as solvent

**Phosphate-buffered saline with tween (PBST)**

Tween® 20 0,1%

PBS as solvent

**Casein blocking buffer**

Casein 1%

PBS as solvent

**Bovine serum albumin (BSA) blocking buffer**

Bovine serum albumin 5%

TBS as solvent

## 2.2. Laboratory mice

### 2.2.1. Description of mice

All conducted animal experiments were approved by State Office for Nature, Environment and Consumer Protection (Landesamt für Natur, Umwelt und Verbraucherschutz Nordrhein-Westfalen, LANUV), approval ID: 81-02.04.2018.A354. Experiments were conducted according to article 8 of the German Animal Welfare Act (“Tierschutzgesetz”) and ARRIVE guidelines for the use of experimental animals (168).

In this study a transgenic mouse line with endothelium-specific overexpression of human B<sub>2</sub>R was used (B<sub>2</sub><sup>tg</sup>) (Figure 4). The generation of this mouse line is fully described in the PhD thesis of Dr. rer. nat. Vu Thao-Vi Dao (Dao, 2011) and was designed in cooperation with Oliver Lieven and Ulrich Rüther (Institute for Animal Developmental and Molecular Biology, Heinrich-Heine-University). The deoxyribonucleic acid (DNA) construct that was inserted in this line consists of human B<sub>2</sub>R cDNA (1.3 Kb), murine Tie-2 promoter (2.1 Kb), and Tie-2 enhancer which is a fragment of Tie-2 intron (10 Kb). Tie-2 promoter is important for endothelial-specific gene expression. The B<sub>2</sub><sup>tg</sup> mouse line was established and backcrossed with C57BL/6J more than 20 times.

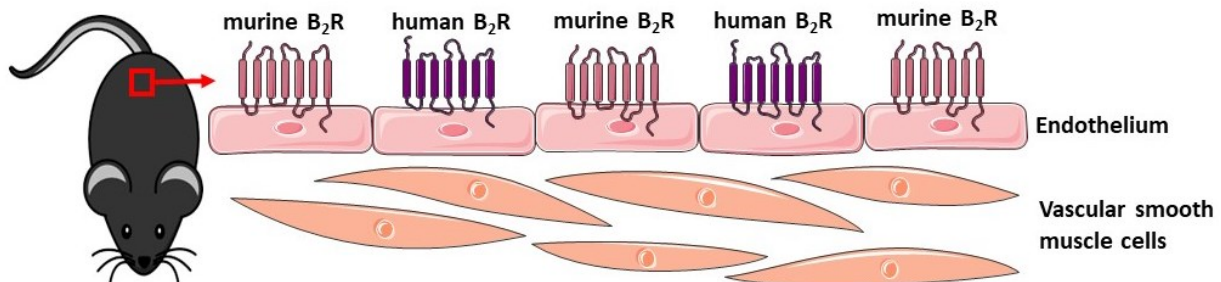


**Figure 4:** Schematic diagram describing transgenic mouse line with endothelium-specific overexpression of human B<sub>2</sub>R (B<sub>2</sub><sup>tg</sup>), where human B<sub>2</sub>R are introduced and expressed on endothelium together with murine B<sub>2</sub>R that are naturally expressed. B<sub>2</sub>R: bradykinin type-II receptors.

Mice were housed and bred in the local animal facility (Zentrale Einrichtung für Tierforschung und wissenschaftliche Tierschutzaufgaben (ZETT), Universitätsklinikum Düsseldorf, Düsseldorf, Germany), where they were under veterinary control and were tested for any possible infections and other diseases at regular intervals. Mice were housed in groups (3-6 mice per cage) and kept in specific pathogen free environment with 12-hour light/dark cycle. They had free access to food (10 mm, ssniff Spezialdiäten GmbH, Soest, Germany) and acidified water (pH=3), and bedding (straw) was changed 1-2x weekly. Room temperature and relative humidity were kept at 24-26 °C and 55±5% respectively.

Mice of age 12-16 weeks and body weight 24-32 g were used in experiments. Male mice only were used unless mentioned that female mice were used for sake of study of sex-specific effects. In some experiments C57BL/6J mice were used which were purchased from Janvier Labs (Le Genest-Saint-Isle, France) and an adaptation

phase of at least 1 week was allowed for mice to acclimatize to the new environment before they were used in experiments.

### **2.2.2. Organ harvesting**

Mice were euthanized by carbon dioxide inhalation using GasDocUnit<sup>®</sup> (Medres, Cologne, Germany) and fixed on a Styrofoam plate using needles. The fur was sanitized with 70% ethanol or isopropanol and the chest cavity was dissected to expose the internal organs. Lungs, oesophagus and inferior vena cava were removed, a 24 G butterfly needle was inserted into LV to perfuse organs with cooled Krebs-Hepes buffer to clear blood from circulation. The heart was dissected, and LV tissues were cut. The aorta was dissected and cleaned from surrounding fibrous tissues. Skeletal muscles (gastrocnemius muscle) were dissected from posterior side of legs. Dissected tissues were quickly washed in cold Krebs-Hepes buffer and flash frozen in liquid nitrogen. Tissues were stored in -80 °C until further analysis (real-time quantitative polymerase chain reaction or western blot).

## **2.3. Genotyping**

### **2.3.1. DNA isolation and purification**

DNA was isolated from ear tissues that were punched out from ears of mice at 3 weeks of age, mice were identified according to the position and number of ear pierces. DNA was first extracted from tissues by incubation in 1.5 ml Eppendorf tubes (Eppendorf, Hamburg, Germany) with 750 µl lysis buffer and 17.5 µl proteinase K (Qiagen, Hilden, Germany) at 56 °C and 600 rpm overnight in Thermocycler (Eppendorf, Hamburg, Germany). 250 µl saturated sodium chloride solution was added and incubated at the same conditions for 5 minutes. Samples were then centrifuged at 4 °C and 10,000 x g for 15 minutes and 700 µl of supernatants containing DNA were transferred into new 1.5 ml Eppendorf tubes. DNA was then purified by adding 500 µl precooled absolute ethanol, Eppendorf tubes were gently inverted up and down twice. Samples were stored at -20 °C for at least 30 minutes to allow precipitation of DNA, then centrifuged at 4 °C and 10,000 x g for at least 30 minutes. Supernatants were discarded and pellets were washed with precooled 70% (v/v) ethanol and centrifuged again at 4 °C and 10,000 x g for 10 minutes. Supernatants were discarded and Eppendorf tubes were left to dry completely from ethanol for at least 2 hours. Pellets were then dissolved in 80 µl ultra-pure water and stored overnight at room temperature. Polymerase Chain Reaction (PCR) was done on the following day or samples were stored at 4 °C until analysis. The quantity and purity of DNA were checked using NanoDrop one Microvolume UV-Vis Spectrophotometer (Thermo Fisher Scientific, Meerbusch, Germany) using 1 µl of sample. Purity of DNA were accepted if the ratio of absorbance at 260 nm and 280 nm is around 1.8.

### **2.3.2. Polymerase Chain Reaction**

Routine genotyping was done for every mouse to distinguish between transgenic mice ( $B_2^{tg}$ ) and negative littermates ( $B_2^n$ ) by using the PCR technique followed by separation of PCR products by agarose gel electrophoresis. For identification of  $B_2^{tg}$  two primer pairs (P1+P2 and R+S) were used as shown in Table 2. Reaction mixture (25 µl) was prepared for each primer pair separately from Master Mix (Taq DNA-Polymerase

2x Master Mix, VWR, Darmstadt, Germany), Q-solution (Qiagen, Hilden, Germany), primers (Thermo Fisher Scientific, Meerbusch, Germany), ultra-pure water and DNA (200-400 ng). PCR was done on the prepared reaction mixtures using Mastercycler pro S vapo.protect (Eppendorf, Hamburg, Germany) according to a specified temperature and time profile as follows:

**Step 1:** initial denaturation at 95 °C for 5 minutes

**Step 2:** amplification (35X)

Denaturation at 95 °C for 30 seconds

Annealing at 60 °C for 30 seconds

Elongation at 72 °C for 30 seconds

**Step 3:** final extension at 72 °C for 5 minutes

**Step 4:** stop at 4 °C

The amplified DNA were then mixed with 6 µl loading buffer and separated on 2% agarose gel containing 0.004 µL/ml GelRed Nucleic Acid Stain® (Biotium, Hayward, USA) at 90 volts for 45 minutes. 100 bp DNA ladder (Invitrogen, Karlsruhe, Germany) was used to identify the size of the detected bands. Finally, bands were displayed under ultraviolet (UV) light using UVP ChemStudio (Analytik Jena, Jena, Germany) and image acquisition was optimized using VisionWorks® Software. The PCR was designed to give two bands in B<sub>2</sub><sup>tg</sup> and no bands in B<sub>2</sub><sup>n</sup>. A sense primer binds to Tie-2 promoter and the antisense primer binds to coding sequence of human B<sub>2</sub>R giving a PCR product of size 497 bp which indicated the presence of Tie2 promoter and human B<sub>2</sub>R. Another sense primer binds to another region inside the coding sequence of human B<sub>2</sub>R and the antisense binds to non-coding sequence of human B<sub>2</sub>R giving a PCR product of size 855 bp. Since there are neither Tie-2 promoter nor human B<sub>2</sub>R in B<sub>2</sub><sup>n</sup>, then no bands will be detected in B<sub>2</sub><sup>n</sup> (Figure 5).

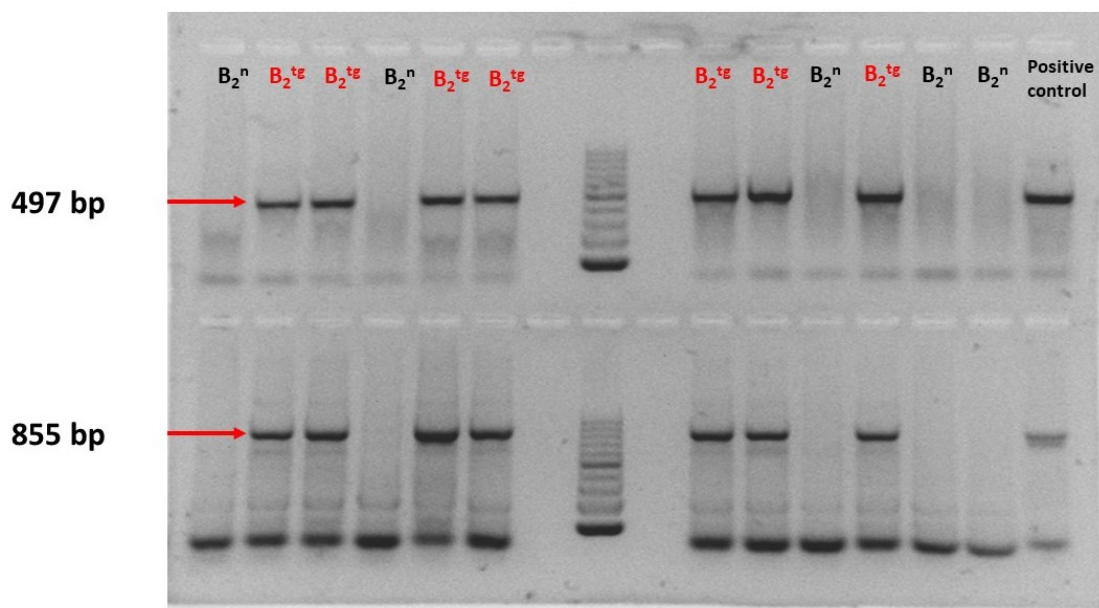


**Figure 5:** Example of agarose gel visualized under ultraviolet (UV) light showing two bands at 497 bp (indicating the presence of Tie-2 promoter and human B<sub>2</sub>R) and 855 bp (indicating the presence of human B<sub>2</sub>R) in B<sub>2</sub><sup>tg</sup>. No bands were detected in B<sub>2</sub><sup>n</sup>. 100 bp DNA ladder is shown in the middle.

**Table 2:** Primers and reaction mixture components used for genotyping of B<sub>2</sub><sup>tg</sup> mice.

Primers	Sense (P2): 5`-CCAAAGAGCCAGTCGAAGTT-3`	Inside coding sequence (CDS) of human B <sub>2</sub> R
	Antisense (P1): 5`-AACCAAGAGCGAGTGGACCAT-3`	Inside Tie-2 promoter
	Sense (R): 5`-CAGCACAACCAGGACTAGCA-3`	Inside CDS of human B <sub>2</sub> R
	Antisense (S): 5`-CACATCCCCTCTGAGTCCA-3`	outside CDS of human B <sub>2</sub> R
Reaction mixture for PCR	Master Mix	12,5 µL
	Q-solution	6,3 µL
	Primer sense (50 µM)	0,1 µL
	Primer antisense (50 µM)	0,1 µL
	Ultrapure water	4 µl
	DNA (100-200 ng/µL)	2,0 µL

## 2.4. Preparation and analysis of RNA

### 2.4.1. RNA isolation and purification

RNA was isolated from different tissues and organs using RNeasy Protect Mini Kit (Qiagen, Hilden, Germany). This kit is based on spin column technology and reagents optimized for RNA isolation via centrifugation. Briefly following the kit protocol, skeletal muscles (gastrocnemius muscle) and aortae were lysed in 700 µl and 300 µl RLT lysis buffer respectively where β-mercaptoethanol (1:100) was added. Samples were homogenized by TissueRuptor II (Qiagen, Hilden, Germany) which was washed by 0.1% NaOH followed by nuclease-free water between samples. 590 µl RNase free water and 10 µl Proteinase K (Qiagen, Hilden, Germany) were then added and incubated at 55°C for 10 minutes. After centrifugation at 10000 x g for 3 minutes, the supernatant was added to 0.5 volume of absolute ethanol and then transferred to mini spin column and centrifuged at 10000 x g for 30 seconds. The spin columns were then washed with 350 µl RW buffer and centrifuged at 10000 x g for 30 seconds. A mixture of 10 µl DNase I stock solution and 70 µl buffer RDD (RNase-free DNase set, Qiagen, Hilden, Germany) was added directly on spin column membrane and incubated at room temperature for 15 minutes and then washed again with 350 µl RW buffer and centrifuged at 10000 x g for 30 seconds. Afterwards the spin columns were washed twice with 500 µl RPE buffer and centrifuged at 10000 x g for 30 seconds and 2 minutes and then the spin columns were placed in to new 2 ml Eppendorf tubes and centrifuged at full speed to

eliminate any buffer residuals. Finally, RNA was eluted by adding 50  $\mu$ l RNase-free water over the spin column in 1.5 ml Eppendorf tubes and centrifuged at 10000 x g for 1 minute.

### 2.4.2. RNA Quantification

The quantity and purity of RNA samples were checked using NanoDrop one Microvolume UV-Vis Spectrophotometer (Thermo Fisher Scientific, Meerbusch, Germany) using 1  $\mu$ l of sample. Purity of RNA samples are accepted if the ratio of absorbance at 260 nm and 280 nm is between 1.8-2.

### 2.4.3. Complementary DNA (cDNA) synthesis

cDNA was reversely transcribed from RNA by using QuantiTect<sup>®</sup> Reverse Transcription kit (Qiagen, Hilden, Germany) following the kit protocol as follows: 2  $\mu$ l genomic DNA (gDNA) wipeout buffer was added to 500-1000 ng template RNA and incubated at 42°C for 2 minutes to remove gDNA. Afterwards samples were put immediately on ice and 6  $\mu$ l Master Mix (composed of 1  $\mu$ l Quantiscript reverse transcriptase, 4  $\mu$ l Quantiscript reverse transcriptase buffer and 1  $\mu$ l reverse transcriptase primer mix) was added and incubated for 30 minutes at 42 °C. To inactivate the reverse transcriptase, samples are then incubated for 3 minutes at 95 °C. cDNA samples are then stored in -20°C until Real-time quantitative polymerase chain reaction measurements.

### 2.4.4. Real-time quantitative polymerase chain reaction

**Theory** Real-time quantitative polymerase chain reaction (RT-qPCR) is a sensitive method for gene expression quantification through which increase or decrease in particular gene expression could be investigated. Quantification was done by measuring intensity of fluorescence emitted from fluorescent reporter molecule. RT-qPCR based on TaqMan<sup>™</sup> chemistry was used in this work. TaqMan probes contain reporter dye (such as FAM<sup>™</sup>, VIC<sup>®</sup>) that is linked to the 5' end of the probe, nonfluorescent quencher (NFQ) at the 3' end and minor groove binder (MGB) moiety attached to the NFQ. MGBs increase the melting temperature without need for increasing probe length, thus allows the design of shorter probes. The idea beyond TaqMan chemistry, as shown in Figure 6, is that the oligonucleotide probe remains intact due to the proximity of the quencher which reduces the fluorescence emitted by the reporter dye by fluorescence resonance energy transfer through space. If the target sequence is present, the probe anneals between primer sites and is cleaved by the 5' nuclease activity of the taq DNA polymerase during extension. As a result of separation of the reporter dye from the quencher, the reporter dye fluorescence signal increases. With each cycle, additional reporter dye molecules are cleaved from their respective probes, hence, increasing fluorescence intensity that is proportional to the amount of produced amplicon. The higher the starting copy number of the nucleic acid target, the sooner a significant increase in fluorescence is observed.

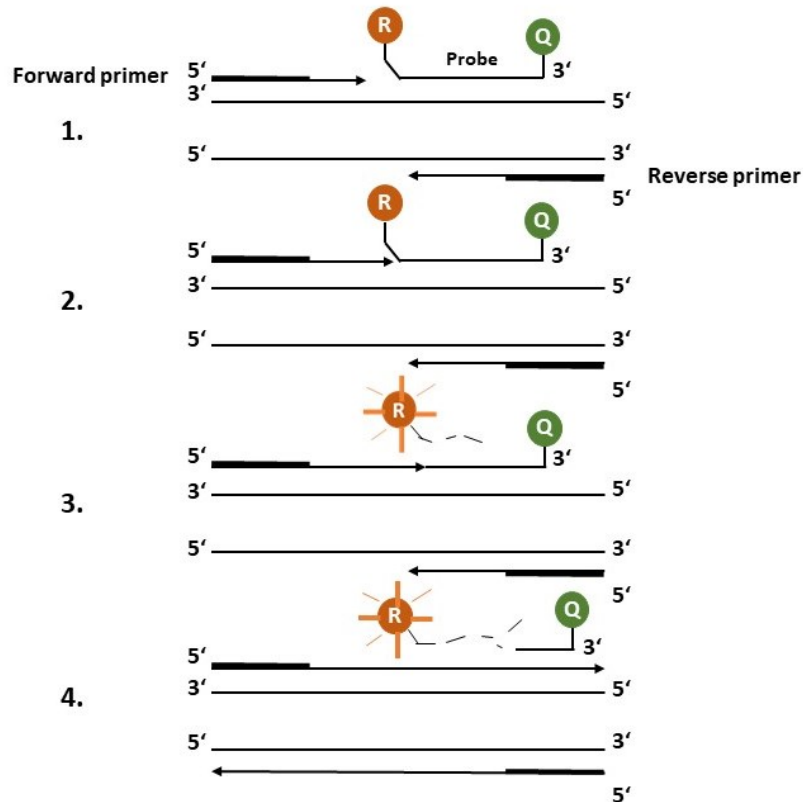


**Figure 6:** Diagram explaining the concept of TaqMan chemistry. 1. Polymerization: A fluorescent reporter dye (R) and a quencher (Q) are attached to the TaqMan probe at 5' and 3' respectively. 2. Strand displacement: when the probe is intact, the reporter dye emission is intact because of the proximity to quencher and the action of Fluorescence Resonance Energy Transfer. 3. Cleavage: During each extension cycle, the DNA polymerase cleaves the reporter dye from the probe, as the proximity between the reporter dye and the quencher is not found, the dye starts to emit its fluorescence. 4. Polymerization completed: once separated from the quencher, the reporter dye emits its characteristic fluorescence which is directly proportional to the amount of DNA (169).

**RT-qPCR experiments** Reaction mixtures of 20x TaqMan gene expression assay (applied biosystems/life technologies, Weiterstadt, Germany) and 2x TaqMan Fast Advanced Master Mix (applied biosystems/life technologies, Weiterstadt, Germany) were prepared for the specified gene of interest (Table 3). Murine Hypoxanthine Guanine Phosphoribosyltransferase (*Hprt1*) was used as housekeeping gene (endogenous control) to compensate for pipetting errors and any occasional differences of introduced cDNA. In 96-well PCR plate (applied biosystems/life technologies, Weiterstadt, Germany), 10 ng cDNA template was pipetted followed by addition of prepared reaction mixtures. Samples were pipetted in duplicates and nuclease-free water was used as non-template (negative) control. The plate was then introduced to StepOnePlus™ Real-Time PCR System (applied biosystems, Weiterstadt, Germany) with the following run:

stage 1: 95°C 20 seconds

stage 2 (40 cycles): Denature at 95°C 1 second

Anneal/extend at 60°C 20 seconds

**Table 3:** TaqMan gene expression assays and reaction mixtures components for genes measured by RT-qPCR.

Assay ID	Gene	Reference sequence	Assay design	Amplicon length
Hs00176121	Human bradykinin type-II receptor ( <i>BDKRB2</i> )	NM_000623.3	Probe spans exons 2-3	99
Mm01339907	Murine bradykinin type-II receptor ( <i>Bdkrb2</i> )	NM_009747.2	Probe spans exons 1-2	72
Mm00435217	Murine endothelial nitric oxide synthase ( <i>eNos</i> )	NM_008713.4	Probe spans exons 22-23	71
Mm01957722	Murine angiotensin II receptor, type 1a ( <i>Agtr1a</i> )	NM_177322.3	Probe spans exon 3	138
Mm03024075	Murine Hypoxanthine Phosphoribosyltransferase 1 ( <i>Hprt1</i> )	NM_013556.2	Probe spans exons 2-3	131
Reaction mixture (10 $\mu$ l)				
20x TaqMan gene expression assay			0.5 $\mu$ l	
2x TaqMan Fast Advanced Master Mix			5 $\mu$ l	
10 ng cDNA template			4.5 $\mu$ l	

cDNA: complementary DNA

**Relative gene expression analysis** Cycle threshold ( $C_t$ ) values, defined as the number of cycles required for the fluorescent signal to exceed background level, were calculated for both the gene of interest and housekeeping genes using StepOne v2.3 analysis software. Samples were measured in duplicates and then average values were calculated. Comparative  $\Delta\Delta C_t$  method was used to calculate relative gene expression according to the following equations (170):

1.  $C_t$  gene of interest -  $C_t$  internal control =  $\Delta C_t$
2.  $\Delta C_t$  transgenic mice -  $\Delta C_t$  wild-type mice =  $\Delta\Delta C_t$

Since DNA concentration doubles with each cycle, the relative gene expression was calculated as follows:

3. Relative gene expression =  $2^{-\Delta\Delta C_t}$

As human  $B_2R$  were found only in  $B_2^{tg}$  mice and not in wild-type, relative gene expression could not be calculated, and expression was calculated by:  $2^{-\Delta C_t}$

## 2.5. Preparation and analysis of proteins

### 2.5.1. Protein isolation

Proteins were prepared from flash frozen tissues or organs (aorta, LV, skeletal muscles (gastrocnemius muscle) by pulverization in a precooled metal mortar that was thoroughly washed and dried between samples. The powder was added to cold RIPA buffer (150-1000  $\mu$ l) supplemented by Protease Inhibitor Cocktail Set III (Merck, Darmstadt, Germany) and Phosphatase Inhibitor Cocktail Set V, 50x (Merck, Darmstadt, Germany). Samples were immediately homogenized by Ultra-Turrax® T8 (IKA Labortechnik, Staufen, Germany) for 30-45 seconds on ice. Samples were added in ultrasound bath for 10 minutes at 4 °C followed by centrifugation for 15 min at 4 °C, 10,000 x g or 1500 x g when cytoplasmic or membrane bound proteins were needed to be detected respectively. Supernatants were collected and proteins were further quantified.

### 2.5.2. Protein quantification

Protein concentrations were determined by Bradford Protein Assay Kit (Thermo Fisher Scientific, Meerbusch, Germany). This is a colorimetric assay based on binding coomassie Brilliant Blue G-250 dye with proteins that leads to shift in maximum absorption from 465 nm to 595 nm. A colour change from brown to blue occurs (171). Samples of unknown concentrations were diluted (1:5/1:10/1:20) and serial dilutions of standards of bovine serum albumin (125-2000  $\mu$ g/ml) were prepared freshly for each set of measurements. 5  $\mu$ L of each standard or unknown sample or blank was pipetted in duplicates into 96-Well microplate with flat bottom (Thermo Scientific™ Pierce™, Thermo Fisher Scientific, Meerbusch, Germany). 250  $\mu$ L of the Reagent was added to each well and the plate was wrapped in aluminium foil and incubated for 10 minutes at room temperature. The absorbance was measured at 595 nm with Synergy Mx microplate reader (Biotek, Vermont, USA). The average measurement for two Blank replicates was subtracted from the average measurements of standards or unknown sample replicates. A standard curve was obtained by plotting the known concentrations of prepared standards versus the corresponding absorbance and equation is generated by linear regression fit to calculate the unknown samples' protein concentrations (Figure 7).

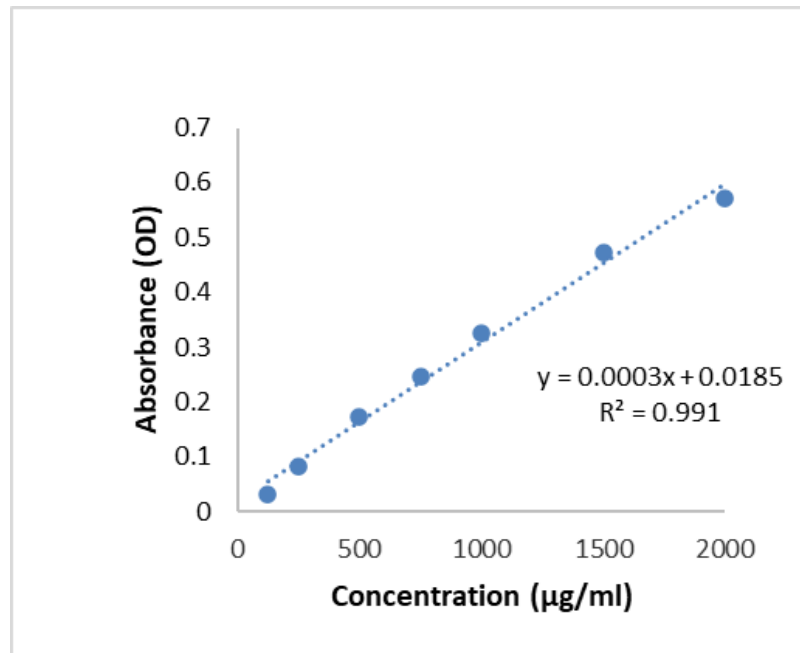


**Figure 7:** Example of standard curve obtained by Bradford method. Known concentrations of serial dilution of standards are plotted on x-axis versus the obtained absorbance measured at wavelength=595 nm on y-axis. An equation was generated by linear regression fit, from which unknown concentrations of samples were calculated by substitution of obtained absorbance. Y-axis: absorbance, X-axis: concentration,  $R^2$  is the regression coefficient, OD: optical density.

### 2.5.3. Sodium Dodecyl Sulfate Polyacrylamide Gel Electrophoresis

After protein concentration determination, lammeli buffer and 2-mercaptoethanol (reducing agent) were added to samples and heated at 95 °C for 5 minutes, so that the proteins would be in reduced and denaturated form. Then the proteins were separated based on their molecular weight with gel electrophoresis (172). For that, polyacrylamide gels were hand casted using acrylamide/bisacrylamide (37.5:1), 10 µg/ml ammonium persulfate (APS) and 1 µl/ml tetramethylethylenediamine (TEMED). 10% acrylamide/bisacrylamide separating gel solution was poured in Mini-PROTEAN Tetra Cell Casting Stand & Clamps (Bio-Rad, Feldkirchen, Germany) followed by 1 ml isopropanol. After 30 minutes, isopropanol was discarded and 4% acrylamide/bisacrylamide stacking gel solution was poured over it. Gels were stored at 4 °C until use. Electrophoresis gel chambers were filled with SDS-PAGE running buffer and gels were inserted, equal amounts of proteins (20-60 µg) were loaded into the wells. Pre-stained protein marker (PageRuler/PageRuler Plus Prestained Protein Ladder; Thermo Fisher Scientific, Meerbusch, Germany) was loaded in a separate pocket, to identify the expected molecular weight of the proteins of interest. The chamber was closed and connected, first the voltage was adjusted at 100 volts for 20 minutes until all proteins were stacked at one line and then at 150 volts for 60 minutes until the blue line reached the end of the gel. Mini-PROTEAN Tetra Cell and PowerPac HC Power Supply (Bio-Rad, Feldkirchen, Germany) were used for gel electrophoresis.

#### 2.5.4. Western Blot

**Theory** the development of western blot started in end of 1970s and beginning of 1980s (173-175). Among decades western blot became a popular technique for protein identification and quantification. This technique depends on transfer of proteins that first separated on SDS-PAGE to a membrane on which highly specific antibodies are applied to bind to specific proteins. Finally, substrate conjugated, or IR dye bound secondary antibodies are applied for visualization of target proteins bound by primary antibodies.

**Wet/tank transfer** after protein separation by SDS-PAGE, a transfer-sandwich was prepared. Nitrocellulose membrane (pore size 0.45  $\mu\text{m}$  Millipore, Schwalbach, Germany), sponges and filter papers were soaked in cold transfer buffer. In a cassette, the transfer-sandwich was arranged from downward (anode) to upward (cathode) in the following direction: sponge, 2 filter papers, gel, membrane, 2 filter papers and sponge. The cassette was inserted to into transfer-apparatus filled with cold transfer buffer and ice pack. 90 volts was applied for 90 minutes at 4  $^{\circ}\text{C}$  under slow stirring. Proteins attained negative charges from SDS should move to positively charged membrane by applying electric current. Mini Trans-Blot Electrophoretic Transfer Cell (Bio-Rad Laboratories, Feldkirchen, Germany) including all instruments needed for transfer-sandwich assembly and protein transfer from gel to membrane was used. PowerPac HC Power Supply (Bio-Rad, Feldkirchen, Germany) were used for power supply.

**Immunodetection** after successful transfer, membranes were briefly rinsed in distilled water to remove any remaining buffer and then incubated in blocking buffer (1% casein or 5% BSA) at room temperature for 1 hour on shaker (12 rpm). Membranes were then incubated with prespecified primary antibodies (Table 4) at 4  $^{\circ}\text{C}$  overnight on shaker (12 rpm), blocking buffer was used as diluent and 0.1% tween was added.  $\beta$ -ACTIN or GAPDH were used as endogenous controls, so membranes were co-incubated with primary antibodies against  $\beta$ -ACTIN or GAPDH. On the following day, membranes were washed by PBST or TBST for 5 minutes on shaker (12 rpm) 4 times. Membranes were then incubated with appropriate secondary antibodies (Table 4) at room temperature on shaker (12 rpm) for 1 hour, boxes were wrapped with aluminium foil since fluorescent antibodies were used. Membranes were then washed by PBST or TBST for 5 minutes on shaker (12 rpm) 2 times followed by washing with PBS or TBS for 5 minutes on shaker (12 rpm) 2 times. Membranes were scanned with Odyssey<sup>®</sup> Infrared Imager (LI-COR Biosciences, Nebraska, USA) and captured images were quantified by Image Studio<sup>™</sup> Lite software Ver 5.2 (LI-COR Biosciences, Nebraska, USA).

**Table 4:** List of primary and secondary antibodies with species, clones, catalogue no, dilutions and companies.

Primary antibodies				
Name	Species, clone	Catalogue no	Dilution	Company
Anti-BDKRB2	Mouse, monoclonal	MAB9434	1:500	R&D, Minneapolis, USA
Anti-BDKRB2	Rabbit, monoclonal	MA5-34627	1:1000	Invitrogen, Rockford, USA
Anti-eNOS	Mouse, monoclonal	610297	1:1000	BD Transduction Laboratories
Anti-ERK1/2	Rat, monoclonal	686902	1:1000	Biolegend, San Diego, California, USA
Phospho-p44/42 MAPK (ERK1/2) (Thr202/Tyr204) antibody	Rabbit, monoclonal	4370	1:2000	Cell Signaling Technology, Danvers, Massachusetts, USA
Anti-GAPDH	Rabbit, monoclonal	2118	1:10000	Cell Signaling Technology, Danvers, Massachusetts, USA
Anti- $\beta$ -ACTIN	Rabbit, monoclonal	A2066	1:20000	Sigma-Aldrich, Munich
Secondary antibodies				
IRDye 680LT anti-Mouse IgG	Goat, polyclonal	926-68020	1:20000	(LI-COR Biosciences, Nebraska, USA)
IRDye 800CW anti-Rabbit IgG	Goat, polyclonal	926-32211	1:15000	(LI-COR Biosciences, Nebraska, USA)
IRDye® 680RD anti-Rat IgG	Goat, polyclonal	925-68076	1:15000	(LI-COR Biosciences, Nebraska, USA)

**Abbreviations:** BDKRB2: bradykinin type-II receptor, eNOS: endothelial nitric oxide synthase, ERK1/2: Extracellular signal-regulated kinase 1/2, MAPK: Mitogen-Activated Protein Kinase, GAPDH: Glyceraldehyde 3-phosphate dehydrogenase. IR: infrared, IgG: immunoglobulin G.

## 2.6. Proteome analysis

To explore new proteins that could be related to B<sub>2</sub>R signalling, proteomic analysis was done on aortic tissues from B<sub>2</sub><sup>tg</sup> and wild-type mice. Aortic tissues were chosen for the proteomic analysis to simplify interpretation because they don't contain too many cell types like other tissues from heart or skeletal muscles.

**2.6.1. Background/theory** proteome analysis is an advanced high throughput technique to assess the proteins' fingerprint of cells/tissues/organs and hence can provide an insight about change of protein expression under specific conditions such as diseases (176). Workflow for proteomic analysis is summarized in Figure 8. Briefly, protein lysate is prepared from tissues or organs and then digested into peptides, these peptides are identified by liquid chromatography coupled with mass spectrometry (LC-MS). Generated data are inserted into specific software, where identification and quantification of proteins are obtained. Comparison of protein abundance can reflect differential increase or decrease in protein expression (177). Several databases can show relevant pathways for measured proteins and perform protein enrichment analysis.

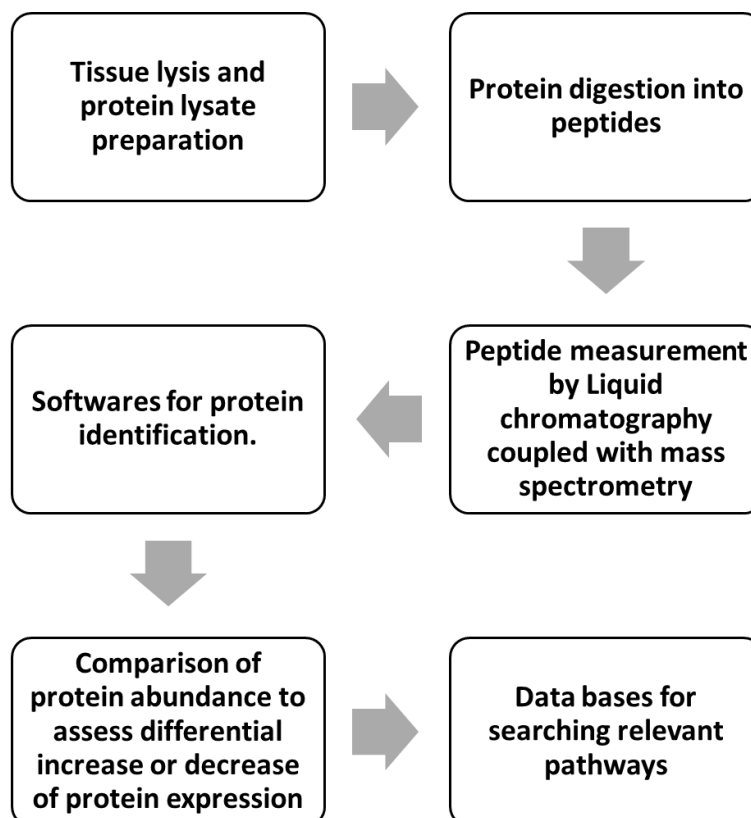


**Figure 8:** Simplified workflow of proteomic analysis.

## 2.6.2. Tissue harvesting and lysis

Aortae were harvested as previously described in section 2.2.2. and flash frozen in liquid nitrogen, transferred to local facility in Heinrich-Heine-University (Biologisch-Medizinisches Forschungszentrum, BMFZ) where

sample preparation and analysis was carried out. Frozen aortae were firstly weighed, then urea buffer (1M Tris Base, Urea 7 M, Thiourea 2M, 3-[(3-Cholamidopropyl)dimethylammonio]- 1-propanesulfonate (CHAPS) 4% (w/v), pH 8.5) was added (3 times the weight (mg) in  $\mu\text{L}$ ). Tissues were homogenized by Tissue Lyser and samples were then sonicated in ice cold ultrasonic bath 6 times for 10 seconds followed by centrifugation for 15 min at 4°C at 16,000g, supernatants were transferred to new Eppendorf tubes. Protein concentration was determined by Pierce Bicinchoninic acid (BCA) Protein Assay (Thermo Fisher Scientific, Meerbusch, Germany)

### **2.6.3. Mass spectrometry sample preparation**

1) 20  $\mu\text{g}$  protein lysate were diluted to 40  $\mu\text{L}$  with sample buffer (7.5% glycerol, 3% SDS, 37.5 mM Tris-HCl pH 7.0) to a final concentration of 0.5 $\mu\text{g}/\mu\text{L}$ .

2) Reduction/Alkylation: 10  $\mu\text{L}$  100 mM Dithiothreitol (DTT) (final 20 mM DTT) was added and incubated for 20 min, 56 °C, 1000 rpm with aluminum foil on top of the Eppendorf tubes to avoid condensation in the lids, followed by addition of 13,34  $\mu\text{L}$  300 mM IAA and incubation for 15 min at room temperature, in the dark. Finally, 10  $\mu\text{L}$  100 mM DTT was added and incubated for 15 min at room temperature.

3) Protein precipitation: 10  $\mu\text{L}$  20 mg/ml single-pot solid-phase enhanced sample preparation (SP3) bead mix was added and homogenized. An equal volume of absolute ethanol was added to achieve 50% ethanol concentration and incubated for 15 minutes at 24 °C and 1000 rpm. Beads were collected with the caproMag (a device for handling magnetic beads) and washed three times with 200  $\mu\text{L}$  80% ethanol and once with 200  $\mu\text{L}$  acetonitrile HPLC grade.

4) On-bead digestion: beads were resuspended in 20  $\mu\text{L}$  50 mM Triethylammonium bicarbonate (TEAB) in HPLC grade H<sub>2</sub>O with final 0.4  $\mu\text{g}$  trypsin/LysC (1:50  $\mu\text{g}$  Trypsin/LysC to  $\mu\text{g}$  protein) and incubated overnight at 37 °C and 1000 rpm with aluminium foil on top of the Eppendorf tubes to prevent condensation in the lids. Then samples were shortly centrifugated and 2  $\mu\text{L}$  50mM TEAB in HPLC grade H<sub>2</sub>O with final 0.4  $\mu\text{g}$  Trypsin/LysC was added and incubated for 3 hours at 37 °C and 1000 rpm with aluminium foil on top of the Eppendorf tubes. Afterwards, samples were shortly centrifugated and beads were collected with the caproMag, supernatants were transferred into new PCR tubes, and beads were discarded. Samples were dried in SpeedVac vacuum concentrators and peptides were collected in 0.1% Trifluoroacetic acid (TFA). 1 $\mu\text{g}$  peptides solubilized in 15  $\mu\text{L}$  was used for LC-MS analysis.

### **2.6.4. Liquid chromatography-mass spectrometry analysis**

For the LC-MS acquisition an Orbitrap Fusion Lumos Tribrid Mass Spectrometer coupled to an Ultimate 3000 Rapid Separation liquid chromatography system equipped with an Acclaim PepMap 100 C18 column (75  $\mu\text{m}$  inner diameter, 25 cm length, 2 mm particle size) as separation column and an Acclaim PepMap 100 C18 column (75  $\mu\text{m}$  inner diameter, 2 cm length, 2 mm particle size) as trap column were used. A LC-gradient of 180 min was applied and the mass spectrometer operated in positive mode with a scan range of 200 – 2000 m/z at a resolution of 120,000. The capillary temperature was set to 275 °C, the source voltage to 1.5 kV, the normalized AGC target was set to 62.5% and the maximum injection time was 60 ms. HCD fragmentations were carried out within a cycle time of 2 seconds.

### 2.6.5. Data analysis

Proteome Discoverer (version 2.4.1.15, Thermo Fisher Scientific) was used for data analysis. All RAW files were searched against the mouse Swissprot database (UP000000589, 55341 entries, 18.01.2022) and the Maxquant Contaminant database, using SequestHT integrated in the Label-free quantification (LFQ) Tribrid processing workflow from Thermo Fisher Scientific. The digestion enzyme was trypsin, the maximum number of missed cleavages was set to two and the peptide length was 6–144 amino acids. Precursor mass tolerance was set to 10 parts per million (PPM) and the fragment mass tolerance was 0.6 daltons (Da). As dynamic modifications: methionine oxidation, N-terminal acetylation, N-terminal methionine loss and N-terminal methionine loss combined with acetylation were used in the workflow settings. Static modification was carbamido-methylation of cysteines. Analysis was performed by **Dr. Anja Stefanski** in BMFZ, Heinrich-Heine-University, Düsseldorf, Germany.

## 2.7. Vascular reactivity studies

### 2.7.1. Preparation of aorta

Mice were euthanized by carbon dioxide inhalation using GasDocUnit® (Medres, Cologne, Germany). Mice were fixed on Styrofoam plate using needles. The fur was sanitized with 70% (v/v) ethanol or isopropanol and the chest cavity was dissected to expose the internal organs. Lungs, oesophagus, and inferior vena cava were removed. The surrounding area in chest cavity was frequently flushed with cold Krebs-Hepes buffer to rinse away the blood and make the aorta clearly visible. Using forceps to raise the heart, small and straight cuts were made to separate the aorta from the surrounding tissues till reaching the diaphragm. Special care was taken to avoid stretching aorta to keep the functionality of vessel. Heart with attached aorta were then placed in cold Krebs-Hepes buffer, heart was separated, and aorta was carefully cleaned from surrounding adipose and connective tissues. Thoracic aorta was cut into 3-4 mm rings and each ring was inserted between two metal triangles (Figure 9).

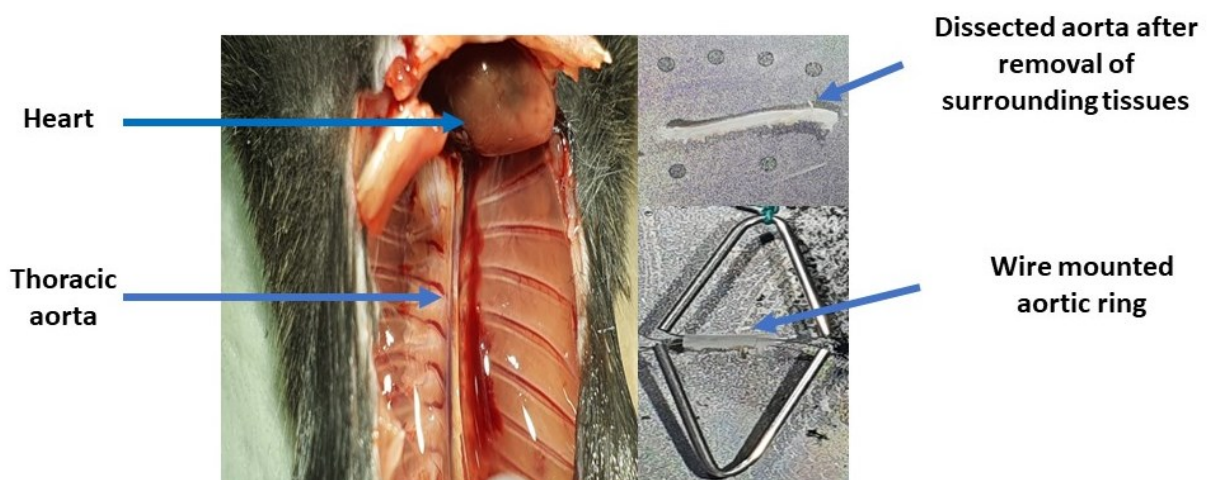


**Figure 9:** Photos showing aortic rings preparation for vascular reactivity studies.

### 2.7.2. Organ bath experiments

Wire mounted aortic rings (3-4 mm) were hanged over hooks in organ bath vessel filled with 10 ml Krebs-Henseleit buffer (PH=7.4) supplied with 95% O<sub>2</sub>/5% CO<sub>2</sub> and kept at 37 °C using water filled glass vessels (Figure 10). Tension was recorded during the whole experimental flow by force transducers which were connected to amplifiers. The recordings were measured on charts by pens connected to amplifiers. Each ring was subjected to an initial resting tension (1 g) followed by equilibration period of 60-90 minutes with washing interval every 20 minutes, all vascular rings were exposed to KCl 80 mM to check the vascular smooth muscle integrity and to use the value of maximum contraction to KCl for normalization to account for different ring lengths. Endothelium integrity was checked by calculating maximum relaxation to acetylcholine, rings with less than 80% relaxation to acetylcholine were excluded from analysis. After pre-constriction with phenylephrine (0.2 µM) and at the steady state of maximal contraction, cumulative concentration response curves were obtained for acetylcholine (1 nM – 100 µM) and bradykinin (1 nM – 10 µM). Concentration response curve of NO donor [Diethylammonium (Z)-1-(N,N-diethylamino)diazen-1-ium-1,2-diolate (DEA NONOate) 1 nM–10 µM] was obtained after pipetting increasing concentrations of phenylephrine and reaching maximum phenylephrine induced constriction. DEA NONOate is an exogenous NO donor with half-life of approximately 2 min (at 37 °C, pH 7.4) and can rapidly self-decompose when dissolved in aqueous solution releasing 2 molecules of NO (178). In some experiments different inhibitors were used as summarized in Table 5, rings were incubated with inhibitors for 20 minutes before pre-constriction with phenylephrine. All substances except DEA NONOate used were purchased from Sigma Aldrich (Munich, Germany). DEA NONOate was purchased from Enzo Life Sciences (Lörrach, Germany).

**Table 5:** Inhibitors used in vascular reactivity studies.

Substance	Function	Final concentration in organ bath
N <sup>ω</sup> -Nitro-L-arginine methyl ester hydrochloride (L-NAME) (Sigma Aldrich, Munich, Germany)	Nitric oxide synthase inhibitor	100 µM
Diclofenac sodium (Sigma Aldrich, Munich, Germany)	Cyclooxygenase inhibitor	10 µM

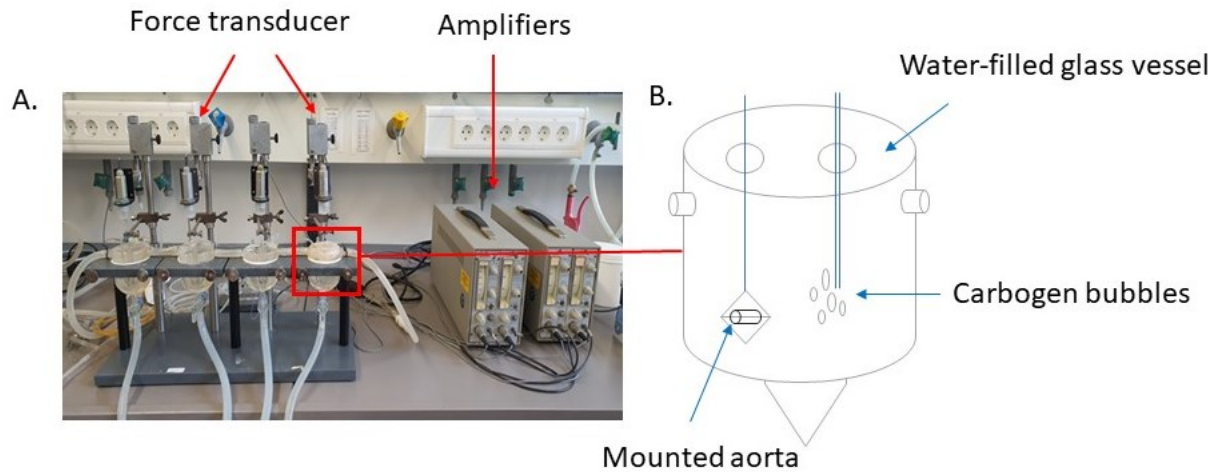


**Figure 10:** A. Organ bath setup for vascular reactivity studies. B. Schematic diagram illustrating organ bath vessel where aortic ring is incubated inside Henseleit buffer with carbogen gas. Warm water supplied from water bath run inside double wall glass vessel to keep temperature at 37 °C.

## 2.8. Aortic incubation experiments

Aortae were isolated as described in section 2.7.1. and hanged in organ bath apparatus filled with 10 ml henseleit buffer (PH=7.4) supplied with 95% O<sub>2</sub>/5% CO<sub>2</sub> and kept at 37 °C. Buffer was replaced with fresh one every 15 minutes for 1 hour. Aortae were then either stimulated with 10 μM bradykinin or PBS (vehicle) for 15 minutes and then rings were quickly collected, and flash frozen in liquid nitrogen. Samples were stored in -80 °C until downstream analysis by western blot for p-ERK1/2 at Tyr204/187 and Thr202/185 and ERK1/2.

## 2.9. Blood pressure and heart rate measurements

### 2.9.1. Theoretical background of tail-cuff method

Systolic blood pressure (sBP) and heart rate (HR) were measured in conscious mice using non-invasive tail-cuff method (179). This method measures sBP in tail of restrained conscious mice using transmission photoplethysmography. Mice were gently restrained in a tunnel which was fixed by a magnet to a plate and then the tail was inserted into a cuff and then lied into a V-groove between led light source and light sensor. Tails were taped to keep mice still during measurements. When measurements started, pulse should be first detected and then inflation of cuff started. Systolic blood pressure is calculated from the amount of light transmitted through the tail and analysed by software installed on laptop connected to the instrument. BP-2000 series II Blood Pressure Analysis System™ (Visitech Systems, Apex, USA) was used, which enabled the measurement of six mice in parallel (Figure 11). The plate where the mice sit during the measurements was heated at 35-36 °C to enhance blood flow to the tail.

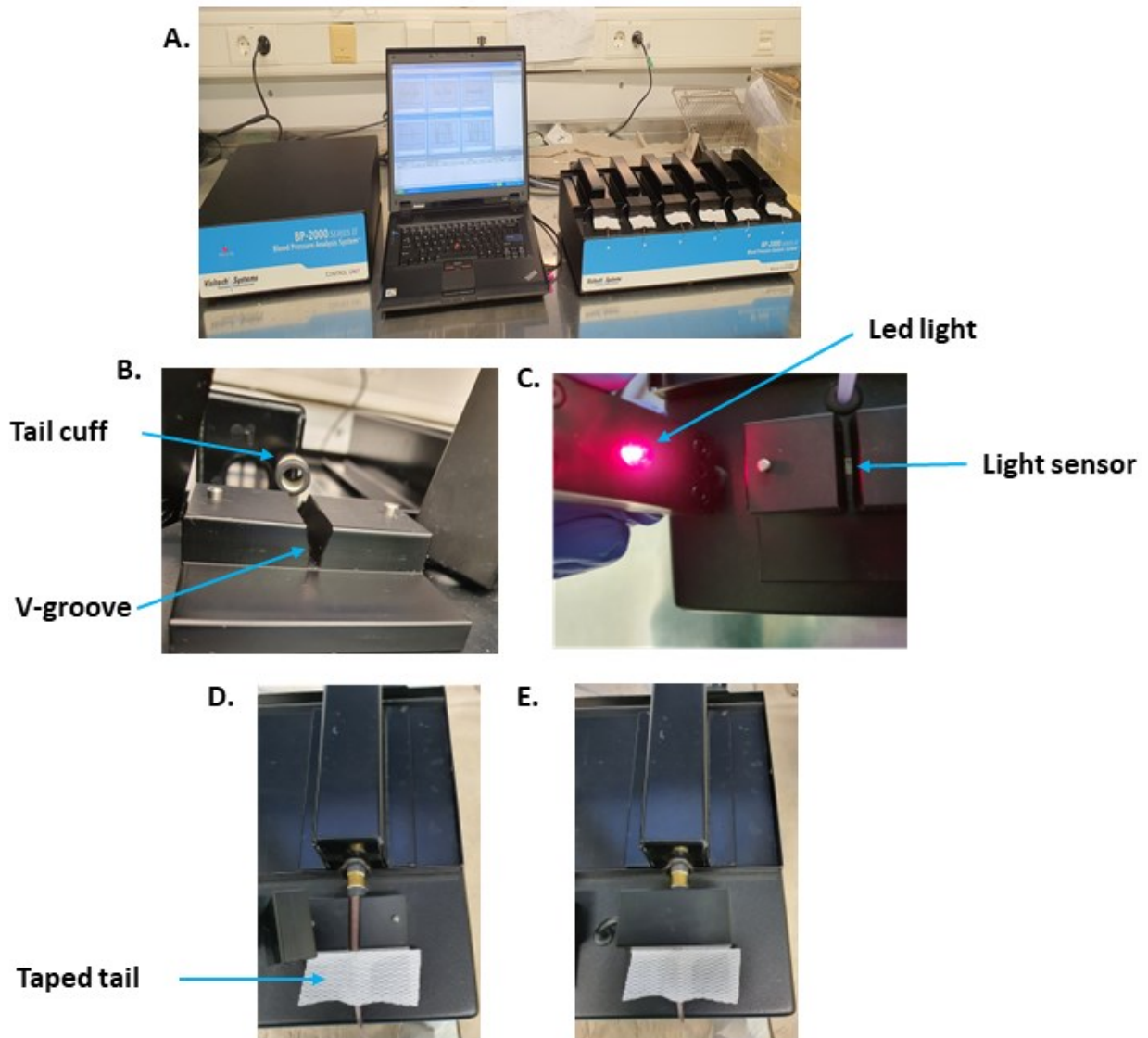


**Figure 11:** Photos of blood pressure machine. A. Mice are restrained on a warm sitting table that is connected to a machine for cuff inflation and a laptop for data acquisition. B. Tail-cuff and V-groove where mice tail lied inside. C. Position of the tail between led light and light sensor. D. Taping of tail is necessary to avoid movements. E. Led light cable is closed over mouse tail.

### 2.9.2. Protocol of measurements

Adaptation phase ranged from 7-10 days was done for all mice to get accustomed to the procedure and minimize stress during actual measurements. During this phase, mice were brought to a quiet measurement room at least 1 hour before measurements. They were placed on the heated plate 5 minutes before starting the measurements. Adaptation phase measurement sets were not used in baseline sBP calculation. Baseline values were a summary of measurements of several days to ensure reproducibility, minimize day to day variations and reflect actual blood pressure values. Measurements were done at the same time every day and for every mouse, a set of 10 consecutive measurements were done three times per day and average of these readings was calculated. To get baseline values, an average of 3-7 days of measurements was calculated for

every mouse. Depending on the objective of the experiment, different drugs were given to mice (Table 6). If the drug was given in drinking water, dose was calculated on average water intake (2 ml per day) and average mice weight (30 g). Drinking water was changed daily based on the duration of treatment. Mice underwent an adaptation phase to intraperitoneal (i.p.) injections with the vehicle in case the drug was given i.p. The percent change of sBP or HR after drug administration was calculated as follows: percent change (%) = [(sBP or HR after drug administration- sBP or HR at baseline)/ sBP or HR at baseline]\*100.

**Table 6:** Drugs used during blood pressure experiments.

Drug	Dose	Duration
Diclofenac sodium (Sigma Aldrich, Munich, Germany)	10 mg/kg, oral in drinking water.	3 days
Icatibant (Firazyr <sup>®</sup> , Shire Orphan Therapies GmbH, Berlin, Germany)	1 mg/kg, i.p.	2 days
N <sup>ω</sup> -Nitro-L-arginine methyl ester hydrochloride (L-NAME) (Sigma Aldrich, Munich, Germany)	100 mg/kg, oral in drinking water.	7 days

## 2.10. Transthoracic echocardiography

Echocardiography, a powerful tool for heart imaging in mice (180-182), was performed to assess LV function of B<sub>2</sub><sup>tg</sup> and B<sub>2</sub><sup>n</sup> mice. Transthoracic echocardiography was done under slight mask anaesthesia by an inhaled mixture of 1.5–2.0% isoflurane and 100% oxygen. Hair was gently removed from thorax by hair removal cream (Veet, Reckitt Benckiser Deutschland GmbH, Heidelberg, Germany). Aquasonic 100 gel (Parker Laboratories, Hellendoorn, The Netherlands) was applied to the thorax to optimize the visibility of the cardiac chambers. Electrocardiogram (ECG) was obtained via built-in ECG electrode contact pads. The body temperature was maintained at 36.5–37.5 °C by a heating pad and infrared lamp. Heart rate was kept in a range of 450-550 beats per minute (bpm) and respiration rate at 80-120 breaths per minute.

Cardiac imaging was performed by using a high-resolution ultrasound transducer MX400 (20-46 MHz; Vevo 3100, Visual Sonics Inc., Toronto, Canada), and the manufacturer's analysis software. Parasternal long- and short-axis views, a four-chamber view and an aortic view of ascending aorta were acquired.

LV volume during systole (volume;s) and LV volume during diastole (volume;d), stroke volume (SV), cardiac output (CO), fractional shortening (FS) and ejection fraction (EF) were calculated from B-mode images by identification of maximal and minimal cross-sectional area. LV mass, LV posterior wall thickness in systole (LVPW;s) and LV posterior wall thickness in diastole (LVPW;d) were calculated from parasternal long axis view of the heart acquired in M-mode. LV mass, LVPW;s and LVPW;d were further normalized for body weight. Diastolic function was measured by analysing the characteristic flow profile of the mitral valve Doppler, which

was visualized in apical four-chamber view. Myocardial performance index (MPI) was calculated as follows: [(isovolumetric contraction time + isovolumetric relaxation time)/aortic ejection time]. A Pulsed Wave Doppler spectrum in the ascending aorta was used to measure the velocity and gradient of aortic flow. Analysis of images was done using Vevo Lab software version 5.7.1 (Visual Sonics, Toronto, Canada). Cardiac Imaging was performed by **PD Dr. Tatsiana Suvorava**.

### 2.11. Flow-mediated dilation

Flow-mediated dilation (FMD) is a commonly used research tool for non-invasive assessment of endothelial function of conduit vessels (e.g brachial artery) in humans since it was established in 1992 (183). FMD is the dilation of blood vessel (i.e increase in diameter) that resulted from wall shear stress after ischemia (184). Diameter normally increases in non-diseased blood vessels due to increase of NO production from endothelium (185).

Mice underwent the same procedures as described in section 2.10. Imaging of the external iliac artery was performed using Vevo 3100 with a 29-71 MHz transducer MX700 (VisualSonics Inc, Toronto, Ontario, Canada). The artery was identified by its characteristic blood flow pattern using colour and pulsed wave doppler. A vascular occluder (8 mm diameter, Holly Specialty Product, California, USA) was placed around the lower limb. For measurements of FMD, first baseline B-mode images and pulse wave Doppler signal of the external iliac artery were recorded, afterwards the cuff was inflated to 200 mmHg, and pressure was kept constant for 5 min to occlude the artery. Then, the occluder was deflated to induce an increased blood flow and FMD. The images were captured every 30 seconds during artery occlusion. After cuff deflation, images were captured every 20 seconds for 2 minutes and every 30 seconds for another 3 minutes during FMD. Vessel diameter was measured for every time point using Brachial Analyzer software version 6 (Medical Imaging Applications LLC, Coralville, USA). Changes in vessel diameter were calculated as percent ratio (%) = [(diameter at each time point - diameter baseline) / diameter baseline] x 100. Mean flow velocity in the artery was calculated from average of three values at each time point using Vevo Lab software version 5.7.1 (Visual Sonics, Toronto, Canada). Acquiring of vascular images was performed by **PD Dr. Tatsiana Suvorava**.

### 2.12. Statistical analysis

Data analysis was done by GraphPad Prism software version 8.0.2 (San Diego, USA). Data were summarized as mean  $\pm$  standard error of mean (SEM), and number of biological replicates (n) that represents number of different mice. Comparison between two groups was done by unpaired t-test. D'Agostino & Pearson test, Shapiro-Wilk test or Kolmogorov-Smirnov test were used to test the normal distribution of data. Rout test was used to identify outliers. Comparison within one group after intervention or among time, was done by paired t-test. Comparison between more than two groups was done by one-way ANOVA followed by post-hoc Sidak's multiple comparisons test if P-value was significant. Two-way repeated measures ANOVA was used for comparisons between groups across different drug concentrations or time followed by post-hoc Tukey's or Dunnett's multiple comparisons test if P-value was significant. For correlation between two parameters,

Pearson correlation was used. Adjusted p-value in proteomic analysis was calculated using the Benjamini-Hochberg method. P-value < 0.05 was considered statistically significant.

### 3. Results

#### 3.1. Gene expression levels

##### 3.1.1. Gene expression levels of human and murine bradykinin type-II receptors in B<sub>2</sub><sup>tg</sup> mice

Since human *BDKRB2* gene was introduced in the B<sub>2</sub><sup>tg</sup> model, RT-qPCR was done to both confirm the expression of the inserted human gene and to evaluate whether the insertion of the human gene affect the expression of the murine *Bdkrb2* in B<sub>2</sub><sup>tg</sup> mice. Aortic tissues were used as a representation of conductive blood vessels. As expected, mRNA of human *BDKRB2* were exclusively found in B<sub>2</sub><sup>tg</sup> mice (0.53±0.11, n=6 per group, P<0.0001) and were not detected in WT mice (Figure 12). In addition, the insertion of the human *BDKRB2* gene did not affect the mRNA expression of the constitutive murine *Bdkrb2* (WT: 0.03±0.005 B<sub>2</sub><sup>tg</sup>: 0.05±0.01, n=6 per group, P=ns; Figure 12). Of note, human *BDKRB2* (0.53±0.11) mRNA expression was significantly higher than the murine *Bdkrb2* (0.05±0.01) mRNA expression in B<sub>2</sub><sup>tg</sup> mice (n=6 per group, P<0.0001; Figure 12). Collectively, these data provide evidence for both the B<sub>2</sub>R overexpression in B<sub>2</sub><sup>tg</sup> mice only and the specificity of primers for human.

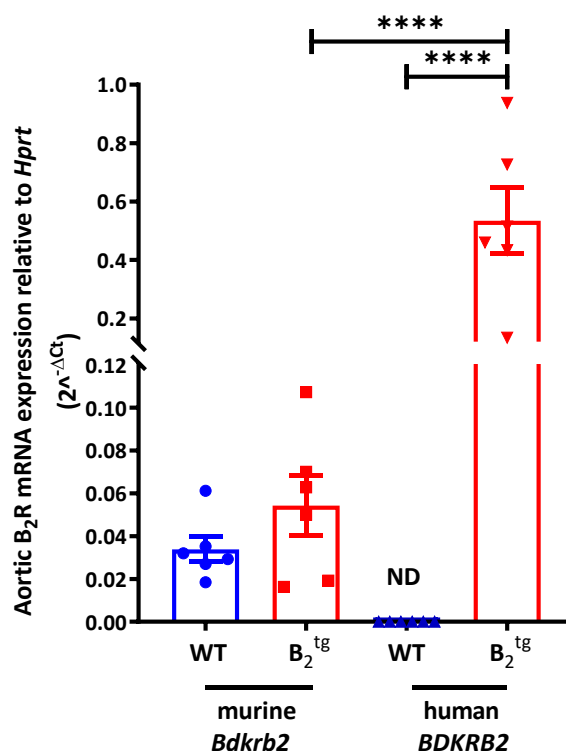


**Figure 12:** RT-qPCR data showing human *BDKRB2* and murine *Bdkrb2* mRNA expression in aorta of B<sub>2</sub><sup>tg</sup> and wild-type (WT) mice. Human *BDKRB2* mRNA were found only in B<sub>2</sub><sup>tg</sup> mice (0.53±0.11) and were not detectable in WT mice (n= 6 per group, \*\*\*\*P<0.0001). There was no significant difference in constitutive murine *Bdkrb2* mRNA expression between B<sub>2</sub><sup>tg</sup> and WT mice (WT: 0.03±0.005 B<sub>2</sub><sup>tg</sup>: 0.05±0.01, n= 6 per group, P=ns). In B<sub>2</sub><sup>tg</sup> mice, human *BDKRB2* mRNA (0.53±0.11) expression was significantly higher than the murine *Bdkrb2* mRNA (0.05±0.01) expression (n=6 per group, \*\*\*\*P<0.0001). Statistical analysis was done by Sidak's multiple comparisons test following one-way ANOVA. ND: not detected.

Skeletal muscle tissues were also analysed as a representation of resistance vessels. Similar results were shown, where human *BDKRB2* were exclusively found in  $B_2^{tg}$  mice ( $0.02 \pm 0.002$ ,  $n=6$  per group,  $P < 0.0001$ ) and the mRNA expression of the constitutive murine *Bdkrb2* was not changed in  $B_2^{tg}$  mice (WT:  $0.007 \pm 0.002$ ,  $B_2^{tg}$ :  $0.007 \pm 0.001$ ,  $n=6-7$  per group,  $P=ns$ ; Figure 13). Human *BDKRB2* mRNA expression ( $0.02 \pm 0.002$ ) was significantly higher than the murine *Bdkrb2* mRNA expression ( $0.007 \pm 0.001$ ) in  $B_2^{tg}$  mice ( $n=6-7$  per group,  $P < 0.0001$ ; Figure 13).

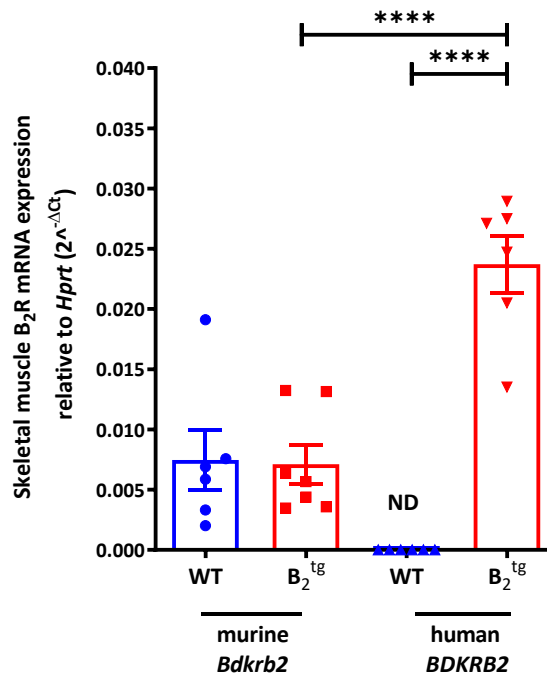


**Figure 13:** RT-qPCR data showing human *BDKRB2* and murine *Bdkrb2* mRNA expression in skeletal muscle tissues of  $B_2^{tg}$  and wild-type (WT) mice. Human *BDKRB2* mRNA were found only in  $B_2^{tg}$  mice ( $0.02 \pm 0.002$ ) and were not detectable in WT ones ( $n=6$  per group, \*\*\*\* $P < 0.0001$ ). There was no significant difference in the constitutive murine *Bdkrb2* mRNA expression between  $B_2^{tg}$  and WT mice (WT:  $0.007 \pm 0.002$ ,  $B_2^{tg}$ :  $0.007 \pm 0.001$ ,  $n=6-7$  per group,  $P=ns$ ). In  $B_2^{tg}$  mice, human *BDKRB2* mRNA expression ( $0.02 \pm 0.002$ ) was significantly higher than the murine *Bdkrb2* mRNA expression ( $0.007 \pm 0.001$ ),  $n=6-7$  per group, \*\*\*\* $P < 0.0001$ . Statistical analysis was done by Sidak's multiple comparisons test following one-way ANOVA. ND: not detected.

### 3.1.2. Gene expression levels of angiotensin II type-1 receptors in $B_2^{tg}$ mice

AT<sub>1</sub>R (*Agtr1* gene) form heterodimers with B<sub>2</sub>R (130, 186), thus investigating *Agtr1* mRNA expression was necessary. *Agtr1* plays crucial roles in blood pressure regulation as well as heart functions. There are two subtypes of *Agtr1* (*Agtr1a* and *Agtr1b*), from which *Agtr1a* is the most important (187). Measuring the protein levels of AGTR1a is challenging due to the lack of specificity of commercially available antibodies (188), therefore, the gene expression levels were measured. There was no significant change in *Agtr1a* mRNA expression neither in skeletal muscles ( $0.93 \pm 0.06$ ,  $n=6-7$  per group,  $P=ns$ ) nor in aorta ( $0.78 \pm 0.14$ ,  $n=6$  per group,  $P=ns$ ) in  $B_2^{tg}$  mice (Figure 14). These data indicate that the insertion of human *BDKRB2* gene did not influence the constitutive gene expression levels of *Agtr1a*.

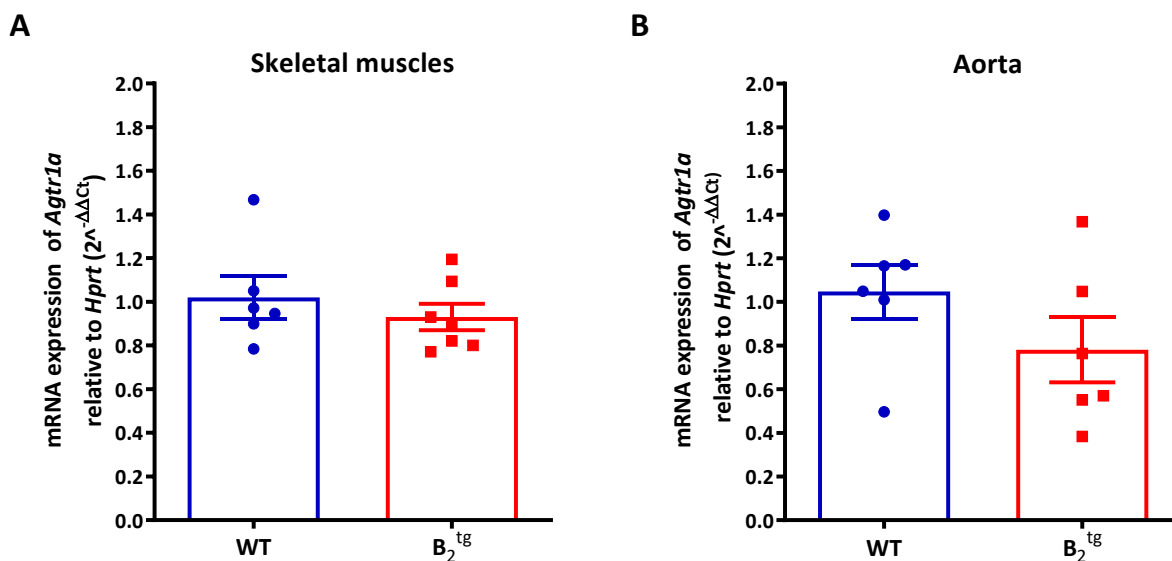


**Figure 14:** RT-qPCR data showing *Agtr1a* mRNA expression in skeletal muscle and aortic tissues of  $B_2^{tg}$  and wild-type (WT) mice. The *Agtr1a* mRNA expression was not changed in  $B_2^{tg}$  mice neither in (A) skeletal muscles ( $0.93 \pm 0.06$ ,  $n=6-7$  per group,  $P=ns$ ) nor (B) in aorta ( $0.78 \pm 0.14$ ,  $n=6$  per group,  $P=ns$ ). Statistical analysis was done by unpaired t-test.

## 3.2. Bradykinin type-II receptors protein expression

### 3.2.1. Mouse monoclonal anti-bradykinin type-II receptors antibody

BDKRB2 protein expression can be detected by western blot either in glycosylated form where the band appears around 70 kDa or in the non-glycosylated form where the band appears around 43 kDa (189). Mouse monoclonal BDKRB2 antibody showed multiple bands between 55 and 70 kDa in murine tissues from kidney, lung, and aorta (Figure 15). However, these bands were not representative of BDKRB2, as the incubation of the membranes with the secondary anti-mouse antibody alone (i.e without prior incubation with the primary antibody) showed multiple bands in the same molecular weight levels as well (Figure 15). From these findings, it was concluded that using mouse primary antibodies is not a good choice when the molecular weight of protein of interest lies between 50 and 70 kDa. Because this demands the use of anti-mouse secondary antibody which binds non-specifically to immunoglobulins in the murine tissues. Rabbit or rat primary antibodies would be rather recommended.

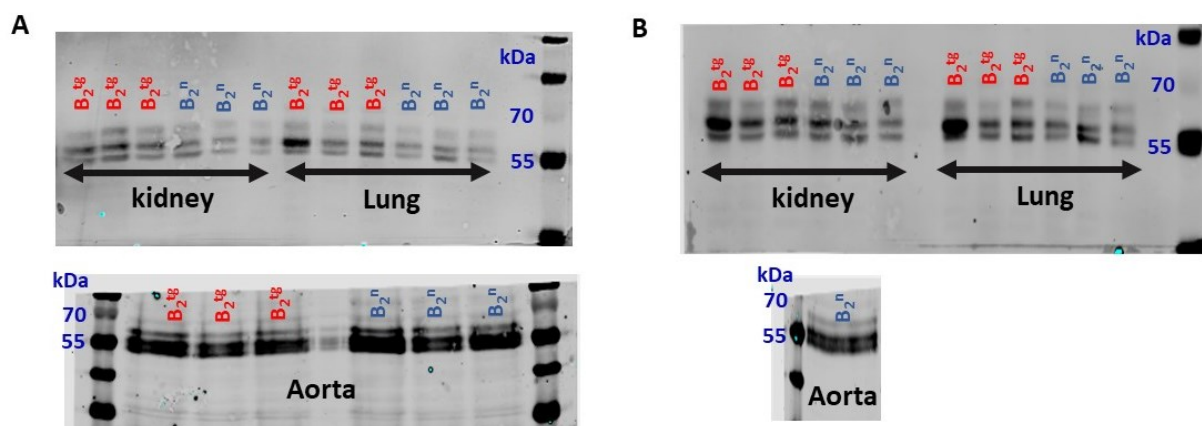


**Figure 15:** Images of membranes from western blot in different tissues (aorta, lung, and kidney) after incubation with goat anti-mouse secondary antibody with or without previous incubation of mouse monoclonal anti-BDKRB2 primary antibody. (A) Signals obtained with mouse monoclonal anti-BDKRB2 primary antibody and goat anti-mouse secondary antibody in kidney, lung (upper panel) and aortic tissues (lower panel). (B) Signals obtained with goat anti-mouse secondary antibody without incubation with primary antibody in kidney, lung (upper panel) and aortic tissues (lower panel). None of the signals appeared to be specific, visualized in red colour at 700 nm channel and depicted in black and white.

### 3.2.2. Bradykinin type-II receptors protein expression using rabbit monoclonal antibody

To avoid the nonspecific binding of the secondary anti-mouse antibody, rabbit monoclonal primary antibody was used to detect the BDKRB2 protein expression. The antibody was first tested in human and murine endothelial cells.

One band around 70 kDa was detected in the human dermal microvascular endothelial cells, while two bands were detected in the brain murine endothelial cells. Similarly, two bands were detected in aortic tissues from mice (Figure 16). The presence of two isoforms of murine B<sub>2</sub>R which consists of 392 amino acids and 366 amino acids could explain the presence of two bands in the murine samples (190). It has been shown that alternatively spliced mRNAs of B<sub>2</sub>R exist, and they may be responsible for the presence of these isoforms (191). Alternative splicing is a process in which various mRNA are produced from a single gene generating isoforms of proteins (192).

The detected bands lied between 70 and 100 kDa which suggest that this antibody detected the glycosylated BDKRB2. This antibody showed different signals between human and murine cells which might indicate the antibody's ability to differentiate between species. Nevertheless, this was not helpful in the B<sub>2</sub><sup>tg</sup> mice model as the antibody detected both human and murine B<sub>2</sub>R in the tissues from B<sub>2</sub><sup>tg</sup> mice (Figure 17). As it was not possible to quantify the human BDKRB2 protein expression separately from the murine BDKRB2, the quantification of the two bands was done to assess the total BDKRB2 protein expression. A significant increase in BDKRB2 protein expression in myocardial tissues of left ventricle ( $1.36 \pm 0.08$ ,  $n=6$  per group,  $P=0.01$ ; Figure 18A) and in aortic tissues ( $1.59 \pm 0.20$ ,  $n=6$  per group,  $P=0.03$ ; Figure 18B) of B<sub>2</sub><sup>tg</sup> mice was observed. No change was observed in skeletal muscle tissues of B<sub>2</sub><sup>tg</sup> mice ( $P=ns$ ; Figure 18C).

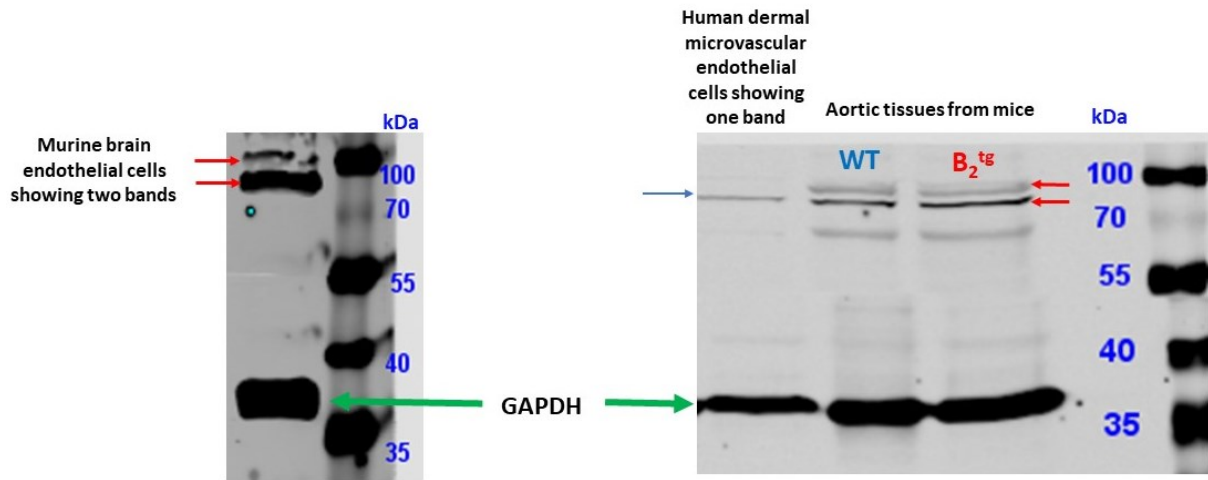


**Figure 16:** Western blot membranes showing BDKRB2 in murine brain endothelial cells and human dermal microvascular endothelial cells versus aortic tissues from mice using rabbit monoclonal anti-BDKRB2 antibody (invitrogen®). Red arrows refer to the two bands of the murine BDKRB2 detected between 70 and 100 kDa. Blue arrow refers to one band of human BDKRB2 detected around 70 kDa. Goat anti-rabbit was used as secondary antibody and GAPDH was used as endogenous control and detected at 38 kDa. Bands' signals were visualized in green colour at 800 nm channel and depicted in black and white.

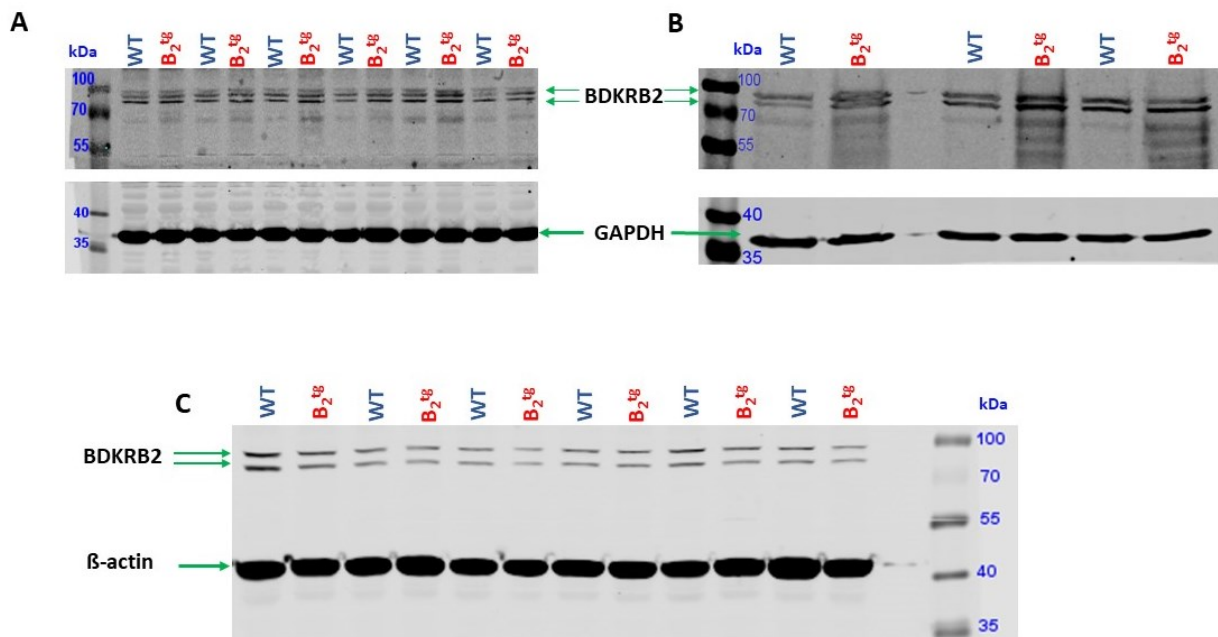


**Figure 17:** Images of membranes from western blot of BDKRB2 in  $B_2^{tg}$  and wild-type (WT) mice. (A) Myocardial tissues from left ventricle, (B) aortic tissues, and (C) skeletal muscle tissues. Two bands of the  $B_2R$  detected between 70 and 100 kDa, GAPDH was used as endogenous control and detected at 38 kDa in aortic and myocardial tissues.  $\beta$ -ACTIN was used as endogenous control and detected at 42 kDa. Bands were visualized in green colour in 800 nm channel using goat anti-rabbit secondary antibody and depicted in black and white.

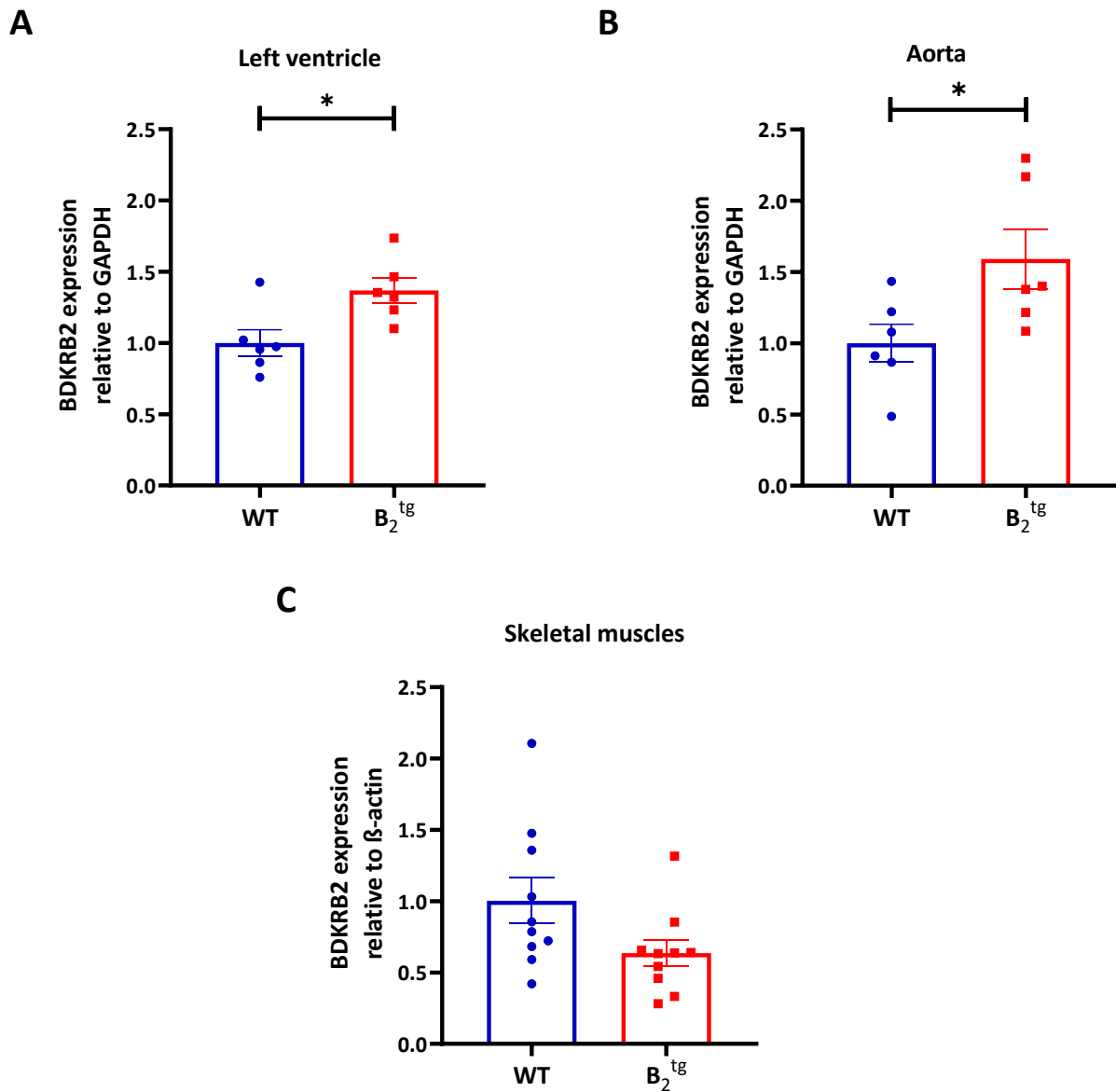


**Figure 18:** Quantification of immunodetection signals of BDKRB2 protein expression in different tissues of  $B_2^{tg}$  and wild-type (WT) mice. BDKRB2 protein expression was significantly increased in (A) left ventricle ( $1.36 \pm 0.08$ ,  $n=6$  per group,  $*P=0.01$ ) and in (B) aorta ( $1.59 \pm 0.20$ ,  $n=6$  per group,  $*P=0.03$ ) of  $B_2^{tg}$  mice. No change in BDKRB2 protein expression was detected in (C) skeletal muscles ( $0.63 \pm 0.09$ ,  $n=10$  per group,  $P=ns$ ). Statistical significance was checked by unpaired t-test.

### 3.3. Effect of endothelium-specific bradykinin type-II receptors overexpression on bradykinin signalling

#### 3.3.1. Protein expression of endothelial nitric oxide synthase in $B_2^{tg}$ mice

The enzyme eNOS is a key regulator of vasomotor tone initiating vasodilation (193).  $B_2R$  stimulation increases eNOS activity with the subsequent synthesis of the vasodilator NO (15). Therefore, it appeared to be important to determine eNOS protein expression in  $B_2^{tg}$  mice. Signal of eNOS was detected by western blot as a single band at 140 kDa and normalization was done either to GAPDH (38 kDa) for aorta and left ventricle or  $\beta$ -actin (42 kDa) for skeletal muscles (Figure 19). Protein expression of eNOS was significantly decreased in aorta of  $B_2^{tg}$  in comparison to  $B_2^n$  mice ( $0.62 \pm 0.13$ ,  $n=8$  per group,  $*P=0.04$ ), but weren't changed either in left ventricle ( $0.87 \pm 0.17$ ,  $n=5$  per group,  $P=ns$ ) or in skeletal muscles ( $0.86 \pm 0.15$ ,  $n=12$  per group,  $P=ns$ ; Figure 20). The observed decrease in eNOS protein expression in the aorta may reflect a compensatory mechanism, perhaps due to the stimulation of the increased number of  $B_2R$  in  $B_2^{tg}$ . Importantly, the 0.38-fold reduction in protein expression had no impact on eNOS-dependent vasodilation induced by acetylcholine in  $B_2^{tg}$  as shown later in section 3.5.1. Another aspect to consider is the change in eNOS protein expression was observed in aorta and not in skeletal muscles nor in left ventricle. This could be attributed to the presence of many different cell types found in tissues of skeletal muscles and left ventricle or maybe the regulatory mechanisms varying across different vascular beds that is, for example, conduit and resistance blood vessels.

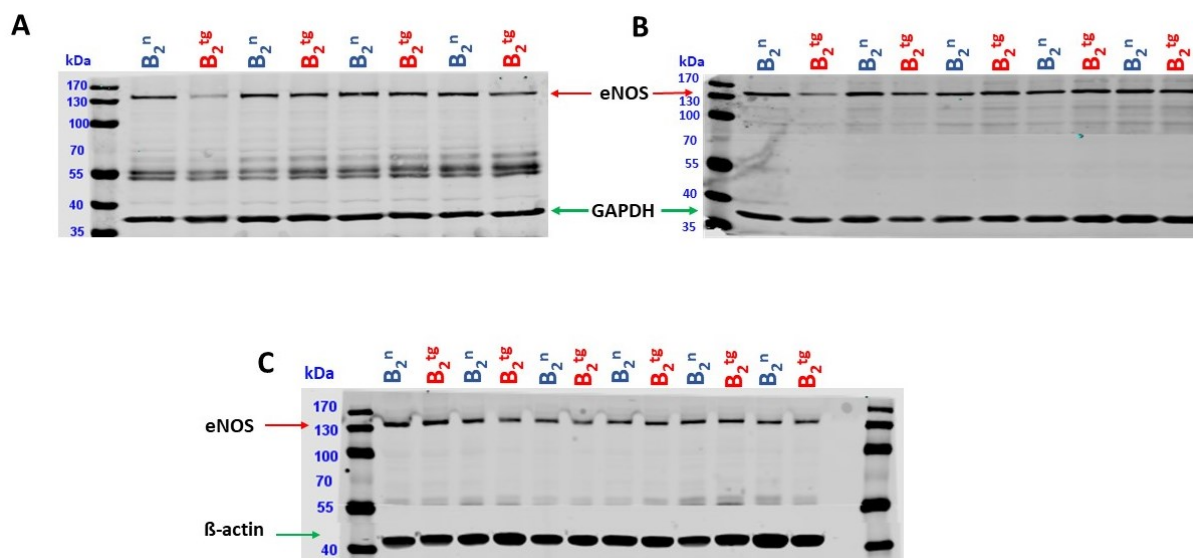


**Figure 19:** Images of membranes from western blot of eNOS protein in different tissues of  $B_2^{tg}$  and  $B_2^n$  mice. A single band of eNOS was detected at 140 kDa and visualized in red colour in 700 nm channel using goat anti-mouse secondary antibody and depicted in black and white. In (A) aorta and (B) left ventricle, GAPDH was used as endogenous control and detected at 38 kDa. GAPDH signals were visualized at 800 nm channel using goat anti-rabbit secondary antibody and depicted in black and white. In (C) Skeletal muscles,  $\beta$ -actin was used as endogenous control and detected at 42 kDa.  $\beta$ -actin signals were visualized at 800 nm channel using goat anti-rabbit secondary antibody and depicted in black and white.

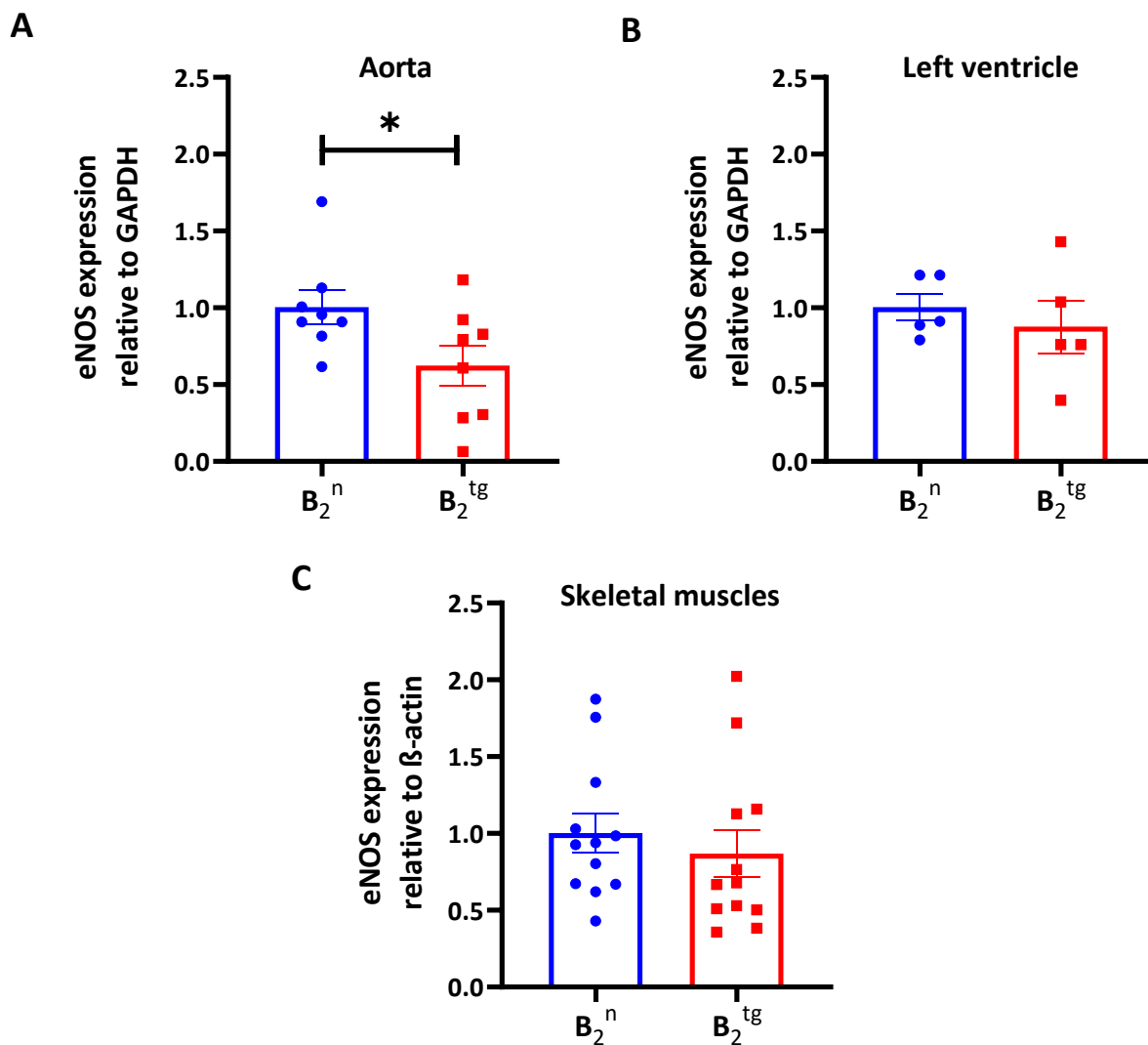


**Figure 20:** Quantification of immunodetection signals of eNOS in different tissues of  $B_2^{tg}$  and  $B_2^n$  mice. Protein expression of eNOS was significantly decreased in (A) aorta of  $B_2^{tg}$  mice ( $0.62 \pm 0.13$ ,  $n=8$  per group,  $*P=0.04$ ) and wasn't change either in (B) left ventricle ( $0.87 \pm 0.17$ ,  $n=5$  per group,  $P=ns$ ) or in (C) skeletal muscles ( $0.86 \pm 0.15$ ,  $n=12$  per group,  $P=ns$ ). Statistical significance was checked by unpaired t-test.

### 3.3.2. Protein expression of phosphorylated ERK1/2 in aorta

Extracellular signal-regulated kinase (ERK)1/2 belong to the mitogen-activated protein kinase (MAPK) signalling pathway. ERK1 (p44) and ERK2 (p42) are the dominate forms of ERK and activated via phosphorylation on both tyrosine (Tyr204/187) and threonine (Thr202/185) residues (194). Phosphorylated ERK1/2 is a part of downstream signalling in many cellular processes like proliferation, migration, and apoptosis (194).

Phosphorylation of ERK1/2 was studied in aortic tissues upon stimulation with  $10 \mu\text{M}$  bradykinin for 15 minutes as described in section 2.8. The first set of experiments was done in C57BL/6J wild-type mice to validate whether stimulation with  $10 \mu\text{M}$  bradykinin enhances phosphorylation of ERK1/2 in aortic tissues *ex vivo*. As shown in Figure 21, p-ERK1/2 was detected as two bands at 44 kDa and 42 kDa which correspond to phosphorylated ERK1 and ERK2. Total ERK1/2 was also detected simultaneously with p-ERK1/2 by multiplex

western blot and appeared as two bands at the same band sizes as p-ERK1/2. p-ERK1/2 was increased upon stimulation with bradykinin (bradykinin vs vehicle control:  $1.57 \pm 0.05$ ,  $n=2-3$  per group; Figure 21). A second set was conducted to confirm this effect in  $B_2^{tg}$  mice. As expected, a significant increase of p-ERK1/2 upon stimulation with 10  $\mu$ M bradykinin was observed in  $B_2^{tg}$  mice (bradykinin vs vehicle control:  $1.30 \pm 0.01$ ,  $n=3$  per group,  $p=0.0006$ ; Figure 22).

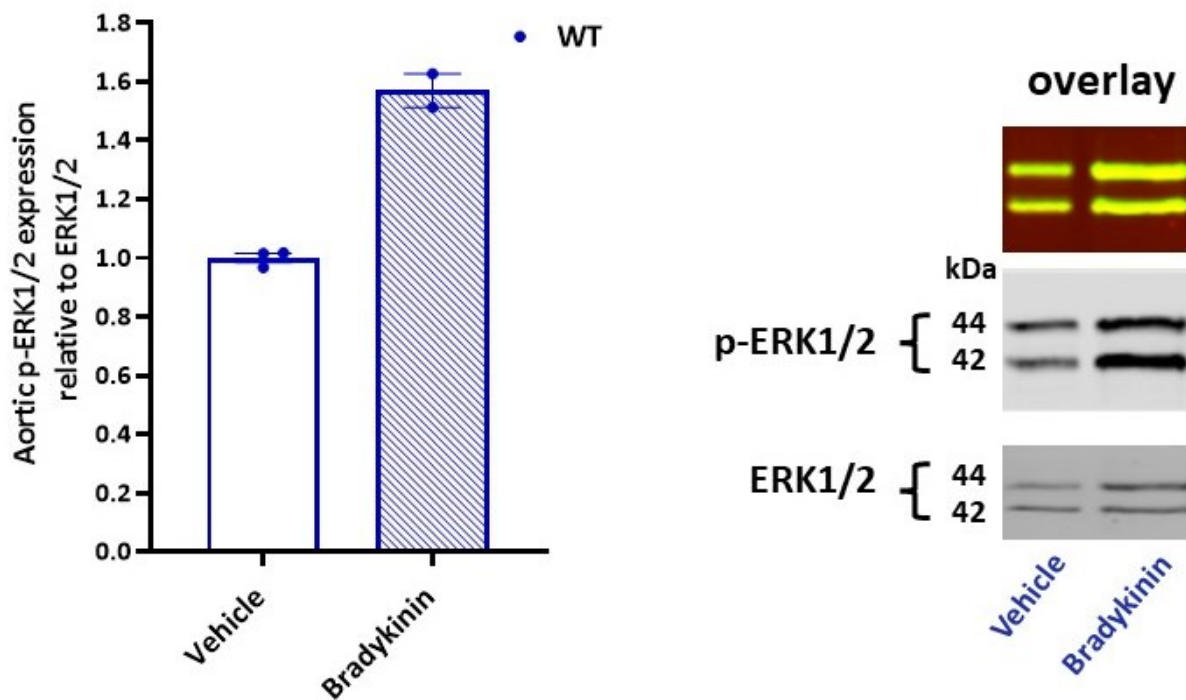


**Figure 21:** Images from western blot and quantification of immunodetection signals of p-ERK1/2 relative to total ERK1/2 in aortic tissues of C57BL/6J wild-type mice. Stimulation of aortic rings for 15 minutes with 10  $\mu$ M bradykinin increased p-ERK1/2 expression (bradykinin vs vehicle control:  $1.57 \pm 0.05$ ,  $n=2-3$  per group), statistical analysis was not conducted because of low number of samples in one group. Two bands were detected for total ERK1/2 (ERK1 at 44 kDa and ERK2 at 42 kDa) and signals were visualized in red colour at 700 nm channels using secondary goat anti-mouse antibody and depicted in black and white. Two bands were detected for p-ERK1/2 (p-ERK1 at 44 kDa and p-ERK2 at 42 kDa) and signals were visualized in green colour at 800 nm using secondary goat anti-rabbit antibody and depicted in black and white. Overlay between red and green was visualized as yellow colour.

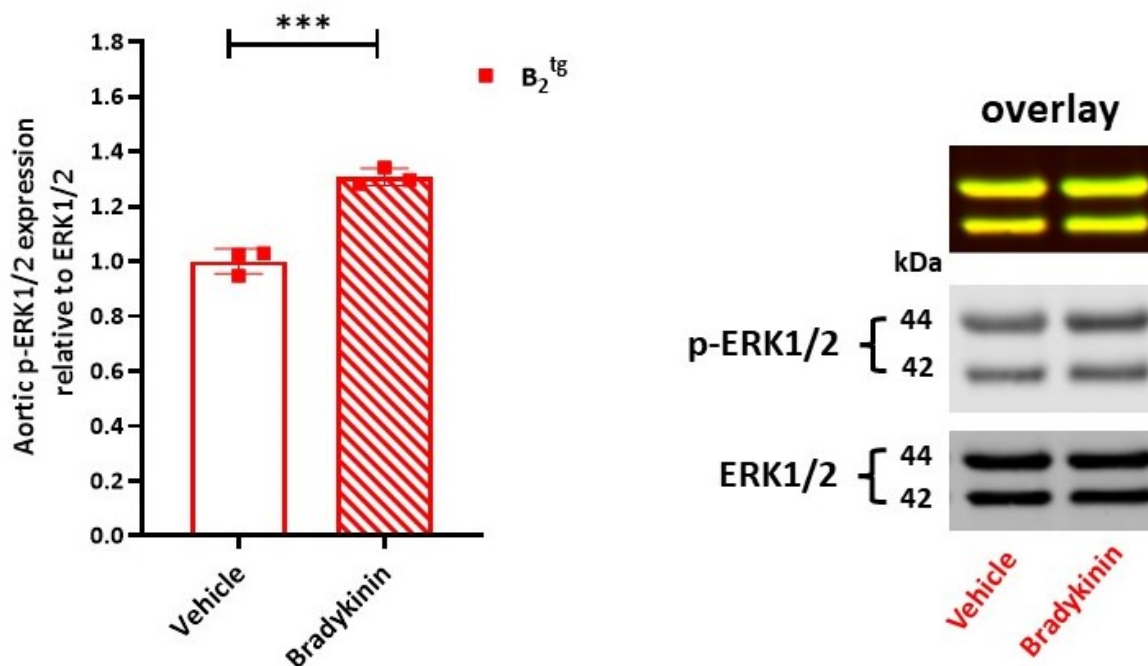


**Figure 22**:-Images from western blot and quantification of immunodetection signals of p-ERK1/2 relative to total ERK1/2 in aortic tissues of  $B_2^{tg}$  mice. Stimulation of aortic rings for 15 minutes with 10  $\mu$ M bradykinin significantly increased p-ERK1/2 expression (bradykinin vs vehicle control:  $1.30 \pm 0.01$ ,  $n=3$  per group,  $***p=0.0006$ ), unpaired t-test. Two bands were detected for total ERK1/2 (ERK1 at 44 kDa and ERK2 at 42 kDa) and signals were visualized in red colour at 700 nm channels using secondary goat anti-mouse antibody and depicted in black and white. Two bands were detected for p-ERK1/2 (p-ERK1 at 44 kDa and p-ERK2 at 42 kDa) and signals were visualized in green colour at 800 nm using secondary goat anti-rabbit antibody and depicted in black and white. Overlay between red and green was visualized as yellow colour.

### 3.4. Vascular reactivity studies

#### 3.4.1. Effect of endothelium-specific bradykinin type-II receptors overexpression on endothelium-dependent relaxation

It was important to investigate if endothelium-dependent relaxation of thoracic aortic rings was changed due to the endothelium-specific  $B_2R$  overexpression in  $B_2^{tg}$  mice. The endothelium-dependent relaxation was checked by adding cumulative concentrations of acetylcholine (final concentration in organ bath: 1 nM–100  $\mu$ M) after pre-constriction with 0.2  $\mu$ M phenylephrine. As shown in Figure 23, the maximum acetylcholine-induced relaxation was not statistically different between  $B_2^f$  ( $84.8 \pm 2.2$ ) and  $B_2^{tg}$  ( $87.1 \pm 3.0$ ),  $n=8$ ,  $P=ns$ . Likewise, negative logarithm of concentration that produce half maximal effect ( $pD_2$ ) was not different between groups ( $B_2^f$ :  $6.7 \pm 0.18$ ,  $B_2^{tg}$ :  $6.6 \pm 0.14$ ,  $P=ns$ , unpaired t-test).

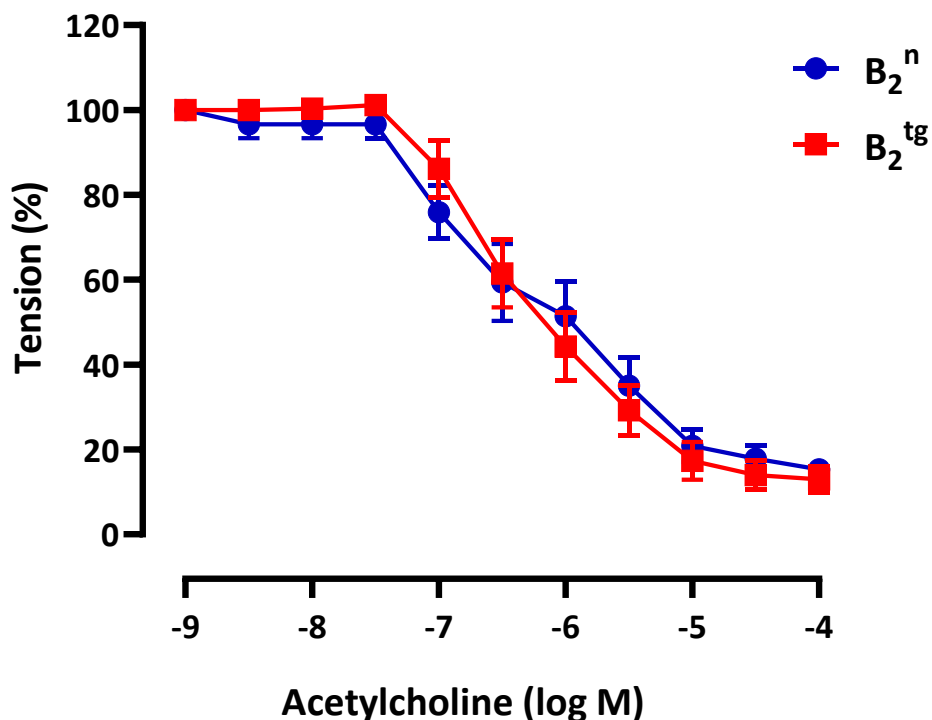


**Figure 23:** Concentration response curve of acetylcholine-induced relaxation obtained from aortic rings reactivity studies. Increasing concentrations of acetylcholine (final concentration in organ bath: 1 nM – 100  $\mu$ M) were added to aortic rings pre-constricted with 0.2  $\mu$ M phenylephrine. There was no significant difference in endothelium-dependent relaxation between  $B_2^n$  and  $B_2^{tg}$  (n=8 per group, P=ns). Statistical significance was checked by two-way repeated measures ANOVA.

### 3.4.2. Mediators of endothelium-dependent relaxation in $B_2^{tg}$ mice

It is known that the endothelium-dependent relaxation of C57BL/6 thoracic aorta is dependent on NO that is produced by eNOS enzymes. To determine whether the endothelium-dependent relaxation of  $B_2^{tg}$  mice is totally or partially dependent on NO, aortic rings were preincubated with NOS inhibitor L-NAME 100  $\mu$ M for 20 minutes. Rings were then constricted with 0.2  $\mu$ M phenylephrine and cumulative concentrations of acetylcholine (1 nM – 100  $\mu$ M) were added. As expected, L-NAME totally abolished acetylcholine induced relaxation in  $B_2^n$  (n=5 per group,  $P < 0.0001$  vs vehicle; Figure 24). Similar results were shown in  $B_2^{tg}$  (n=5 per group,  $P < 0.0001$  vs vehicle; Figure 24). In addition, there was no significant difference between  $B_2^n$  and  $B_2^{tg}$  after preincubation with L-NAME (n=5 per group, P=ns; Figure 24).

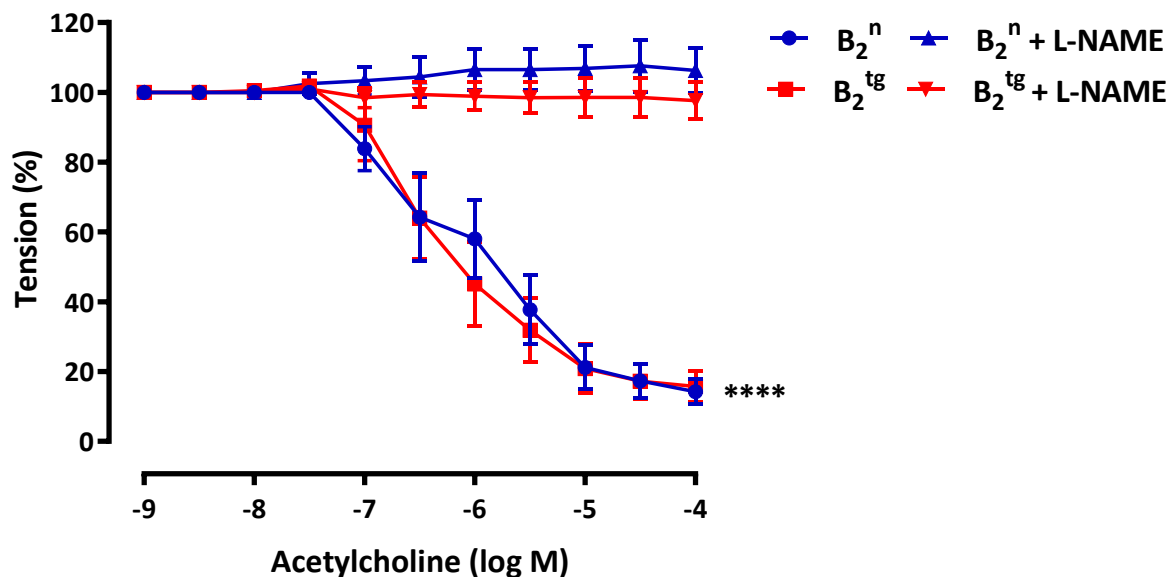


**Figure 24:** Concentration response curve of acetylcholine-induced relaxation obtained from aortic rings reactivity studies after incubation with 100  $\mu\text{M}$  L-NAME or vehicle for 20 minutes. Increasing concentrations of acetylcholine (final concentration in organ bath: 1 nM – 100  $\mu\text{M}$ ) were then added to aortic rings pre-constricted with 0.2  $\mu\text{M}$  phenylephrine. L-NAME totally abolished acetylcholine-induced relaxation in both  $B_2^n$  (n=5 per group, \*\*\*\* $P$ <0.0001 vs vehicle) and  $B_2^{tg}$  (n=5 per group, \*\*\*\* $P$ <0.0001 vs vehicle). There was no significant difference between  $B_2^n$  and  $B_2^{tg}$  after addition of L-NAME (n=5 per group,  $P$ =ns). Statistical significance was checked by Tukey's multiple comparisons test following two-way repeated measures ANOVA.

### 3.4.3. Effect of endothelium-specific bradykinin type-II receptors overexpression on phenylephrine-induced vasoconstriction

Regarding the evaluation of phenylephrine induced vasoconstriction, no significant difference was found between groups (maximum contraction  $73.49 \pm 8.22\%$  in  $B_2^n$  and  $76.38 \pm 11.21\%$  in  $B_2^{tg}$ , n=4 per group,  $P$ =ns; Figure 25). Likewise,  $pD_2$  was similar between groups ( $B_2^{tg}$ :  $6.7 \pm 0.13$ ,  $B_2^n$ :  $6.6 \pm 0.12$ ,  $P$ =ns, unpaired t-test).

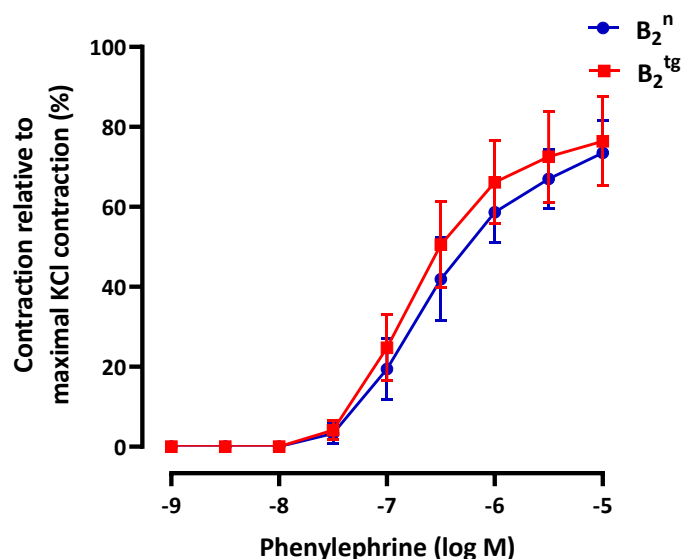


**Figure 25:** Concentration response curve of phenylephrine-induced constriction obtained from aortic rings reactivity studies. Increasing concentrations of phenylephrine (1 nM – 10  $\mu$ M) were added to aortic rings. There was no significant difference in phenylephrine-induced constriction between B<sub>2</sub><sup>n</sup> and B<sub>2</sub><sup>tg</sup> (n=4 per group, P=ns, two-way repeated measures ANOVA).

### 3.4.4. Effect of endothelium-specific bradykinin type-II receptors overexpression on endothelium-independent relaxation

After reaching maximal phenylephrine constriction, the effect of exogenous NO (i.e not dependent on NO that is produced in endothelium) on aortic relaxation was evaluated. DEA NONOate, a spontaneous NO-donor releasing NO rapidly (178), was used as a source of exogenous NO. Aortic rings from B<sub>2</sub><sup>n</sup> and B<sub>2</sub><sup>tg</sup> relaxed similarly in response to DEA NONOate (n=3 per group, P=ns, two-way repeated measures ANOVA), pD<sub>2</sub> values were 7.01 $\pm$ 0.12 in B<sub>2</sub><sup>tg</sup> and 6.88 $\pm$ 0.12 in B<sub>2</sub><sup>n</sup>, P=ns, unpaired t-test (Figure 26).

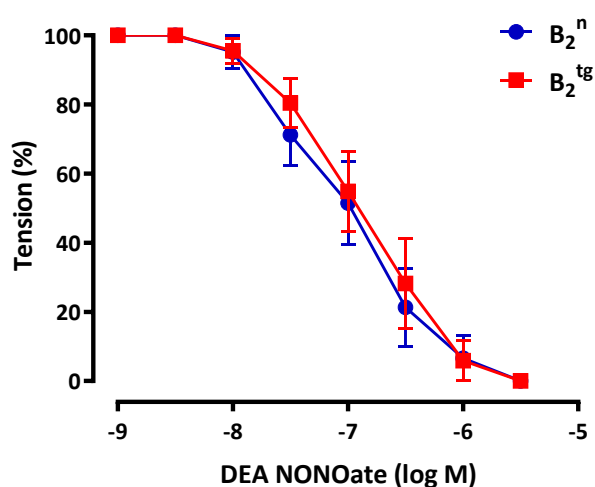


**Figure 26:** Concentration response curve of DEA NONOate-induced relaxation obtained from aortic rings reactivity studies. Increasing concentrations of DEA NONOate were added to aortic rings (final concentration in organ bath: 1 nM – 3  $\mu$ M). There was no significant difference in DEA NONOate-induced relaxation between B<sub>2</sub><sup>n</sup> and B<sub>2</sub><sup>tg</sup> (n=3 per group, P=ns, two-way repeated measures ANOVA).

### 3.4.5. Effect of endothelium-specific bradykinin type-II receptors overexpression on bradykinin mediated vasoconstriction

To prove the functional B<sub>2</sub>R overexpression, effect of bradykinin was evaluated in aortic rings of B<sub>2</sub><sup>tg</sup> mice. Previous work showed bradykinin-induced concentration-dependent vasoconstriction in aortic rings of WT mice (76, 195), which was abolished by diclofenac. Similar results were observed in this investigation as shown in Figure 27 (maximum vasoconstriction in WT: 9.6±3.0, n=4-5 per group, P=ns vs diclofenac). In contrast, bradykinin induced a concentration-dependent vasorelaxation in B<sub>2</sub><sup>tg</sup> mice confirming functional overexpression of B<sub>2</sub>R (maximum vasorelaxation: -31.23±2.48%, n=5-6 per group, P<0.0001 B<sub>2</sub><sup>tg</sup> vs WT). Moreover, this vasorelaxation wasn't affected by addition of diclofenac (n=6 per group, P=ns).

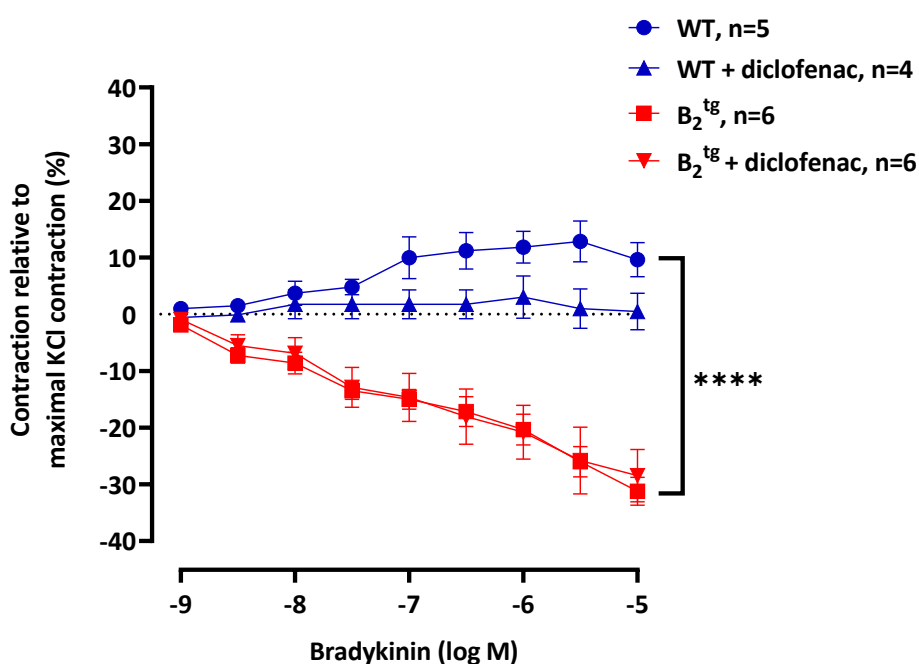


**Figure 27:** Concentration response curve of bradykinin obtained from aortic rings reactivity studies. Preincubation with 10  $\mu$ M diclofenac was done in some rings 20 minutes before pre-constriction with 0.2  $\mu$ M phenylephrine. Bradykinin induced concentration-dependent vasoconstriction in wild-type (WT) mice which is abolished by addition of diclofenac (n=4-5 per group, P=ns), while bradykinin induced concentration-dependent vasorelaxation in B<sub>2</sub><sup>tg</sup> mice (n=5-6 per group, \*\*\*\*P<0.0001 vs WT) that is not affected by diclofenac (n=6 per group, P=ns). Statistical test: Tukey's multiple comparisons test following two-way repeated measures ANOVA.

Another set of experiments was conducted in B<sub>2</sub><sup>tg</sup> mice to identify which mediators were responsible for bradykinin-induced vasorelaxation. Aortic rings were preincubated with 100  $\mu$ M L-NAME or vehicle for 20 minutes before pre-constriction with 0.2  $\mu$ M phenylephrine. L-NAME totally abolished bradykinin-induced vasorelaxation and even showed vasoconstriction (n=8, P<0.0001; Figure 28), suggesting that the bradykinin-induced vasorelaxation is eNOS-dependent. The vasoconstrictive effect seen after inhibition with L-NAME could be due to the constrictive effect of COX products, as shown to occur in WT mice (Figure 27), which was likely masked by NO-mediated vasorelaxation.

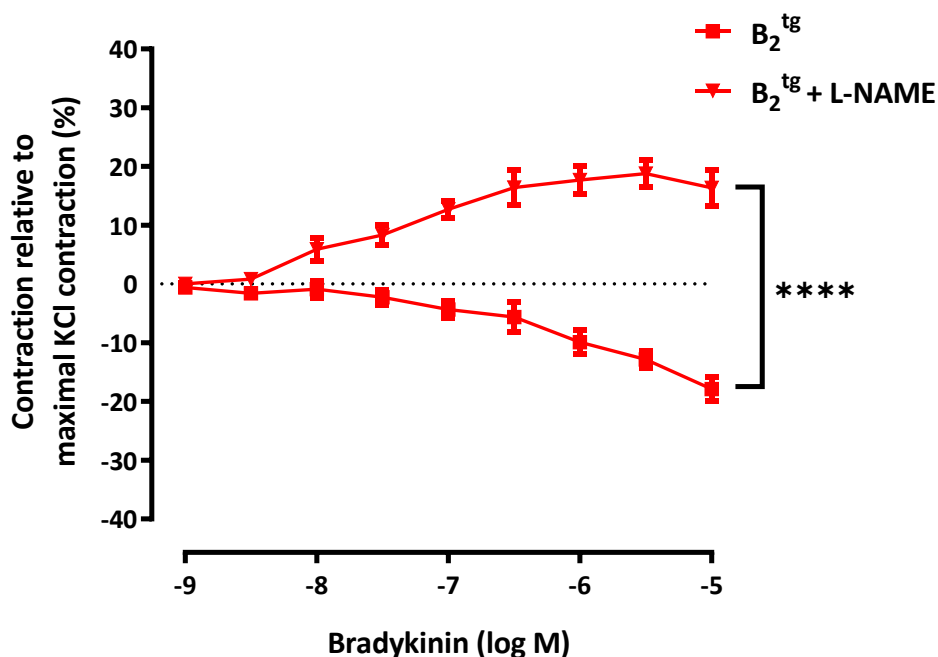


**Figure 28:** Concentration response curve of bradykinin obtained from aortic rings reactivity studies. Bradykinin-induced concentration-dependent relaxation in B<sub>2</sub><sup>tg</sup>. L-NAME abolished bradykinin-induced vasorelaxation and turned it to vasoconstriction (n=8 per group, \*\*\*\*P<0.0001, two-way repeated measures ANOVA). Preincubation with 100 μM L-NAME was done in some rings for 20 minutes before pre-constriction with 0.2 μM phenylephrine.

### 3.5. Systolic blood pressure and heart rate measurements

#### 3.5.1. Effect of endothelium-specific bradykinin type-II receptors overexpression on systolic blood pressure and heart rate

Studies of B<sub>2</sub>R signalling revealed that these receptors play a crucial role in blood pressure regulation and activation of B<sub>2</sub>R leads to vasodilation and decrease in blood pressure (section 1.2.3.1). Early generations of B<sub>2</sub><sup>tg</sup> mice showed significant reduction in systolic blood pressure as compared to B<sub>2</sub><sup>n</sup> (195). Surprisingly, in a series of sets in later generations, systolic blood pressure was not different between B<sub>2</sub><sup>n</sup> and B<sub>2</sub><sup>tg</sup> (B<sub>2</sub><sup>n</sup>: 104.5±5.4 mmHg, n=10 and B<sub>2</sub><sup>tg</sup>: 104.8±3.2 mmHg, n=10-15, P=ns; Figure 29). These measurements were done on mice from generation N=27, F=7, where 'N' refers to number of backcrossing with C57BL/6J and 'F' refers to number of siblings breeding (196). In one set of measurements, B<sub>2</sub><sup>tg</sup> was compared to WT strain and systolic blood pressure was significantly reduced in B<sub>2</sub><sup>tg</sup> (102.9±2.2 mmHg, n=6) vs WT (119.9±3.1 mmHg, n=3), P=0.003 (Figure 30). B<sub>2</sub><sup>n</sup> mice are the siblings of B<sub>2</sub><sup>tg</sup> that do not carry the genetic modification (i.e, the human B<sub>2</sub>R cDNA, the murine Tie-2 promoter, and the Tie-2 enhancer). Whereas WT mice are the standard mice that possess the naturally occurring alleles of all genes. Remarkably, the difference in systolic blood pressure was evident when B<sub>2</sub><sup>tg</sup> mice were compared to WT mice, but not when compared to B<sub>2</sub><sup>n</sup>, suggesting that genetic drift might have occurred. Therefore, a refreshment of the line with backcrossing to the parental strain C57BL/6J was initiated.

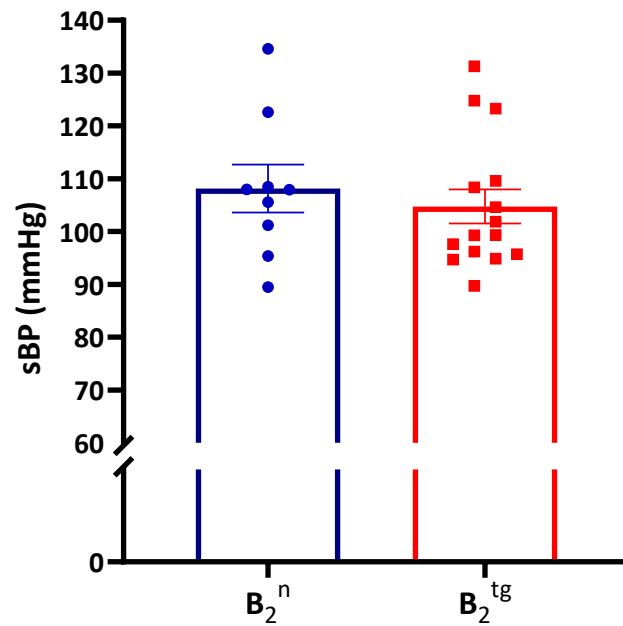


**Figure 29:** Systolic blood pressure (sBP) measurements using tail-cuff method in conscious  $B_2^{tg}$  and  $B_2^n$  mice. No significant difference was shown between  $B_2^{tg}$  and  $B_2^n$  mice ( $B_2^{tg}$ :  $104.8 \pm 3.2$ ,  $n=15$  and  $B_2^n$   $104.5 \pm 5.4$ ,  $n=10$ ,  $P=ns$ , unpaired t-test).

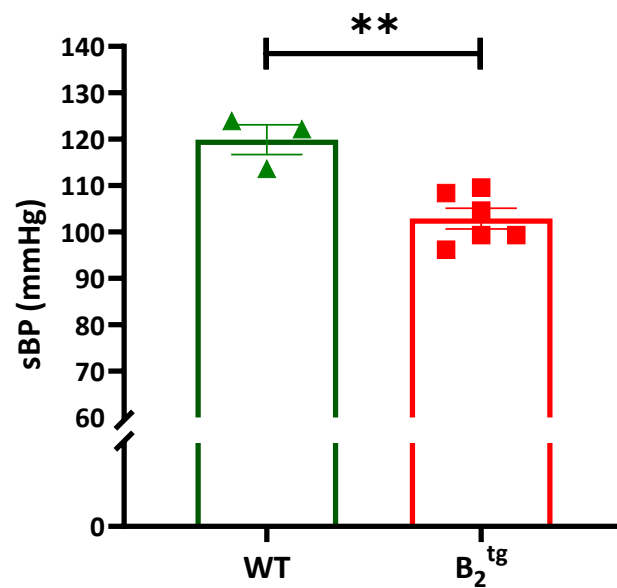


**Figure 30:** Systolic blood pressure (sBP) measurements using tail-cuff method in conscious  $B_2^{tg}$  and wild-type (WT) mice. sBP was significantly reduced in  $B_2^{tg}$  ( $102.9 \pm 2.2$  mmHg,  $n=6$ ) vs WT ( $119.9 \pm 3.1$  mmHg,  $n=3$ ),  $**P=0.003$ , unpaired t-test.

$B_2^{tg}$  mice were backcrossed with parental strain C57BL/6J two times sequentially. To verify the reduction of sBP, a new set of measurements was carried out. As expected, sBP was significantly lower in  $B_2^{tg}$  ( $120.6 \pm 2.1$  mmHg,  $n=15$ ) in comparison to  $B_2^n$  ( $126.4 \pm 1.6$  mmHg,  $n=14$ ),  $P=0.03$  (Figure 31A). Interestingly, HR was as well significantly lower in  $B_2^{tg}$  mice ( $555.3 \pm 13.5$  bpm,  $n=15$ ) than  $B_2^n$  ( $600.6 \pm 13.8$  bpm,  $n=14$ ),  $P=0.02$  (Figure 31B). Only in  $B_2^{tg}$  there was a significant strong correlation between sBP and HR ( $B_2^{tg}$ :  $r=0.73$ ,  $P=0.002$ ,  $B_2^n$ :  $r=0.13$ ,  $P=ns$ ; Figure 32).

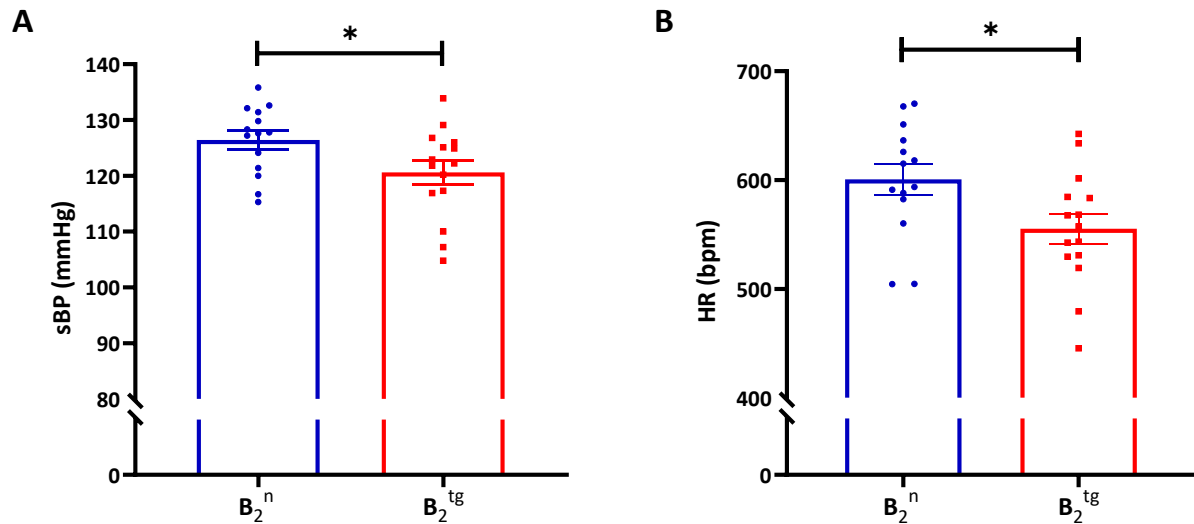


**Figure 31:** Systolic blood pressure (sBP) and heart rate (HR) data using tail-cuff method in conscious  $B_2^n$  and  $B_2^{tg}$  mice after refreshing the line by backcrossing with parental strain C57BL/6J mice. (A) sBP was significantly lower in  $B_2^{tg}$  than  $B_2^n$  ( $B_2^{tg}$ :  $120.6 \pm 2.1$  mmHg vs  $B_2^n$ :  $126.4 \pm 1.6$  mmHg,  $n=14-15$ ,  $*P=0.03$ , unpaired t-test). (B) HR was significantly lower in  $B_2^{tg}$  than  $B_2^n$  ( $B_2^{tg}$ :  $555.3 \pm 13.54$  bpm vs  $B_2^n$ :  $600.6 \pm 13.89$  bpm,  $n=14-15$ ,  $*P=0.02$ , unpaired t-test).

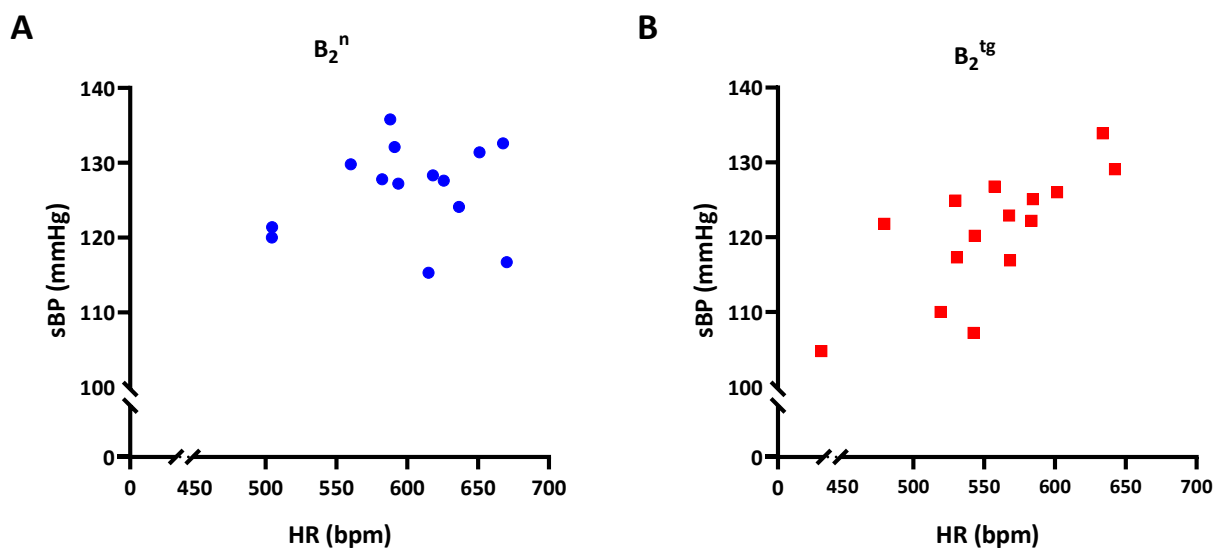


**Figure 32:** Pearson correlation between systolic blood pressure (sBP) and heart rate (HR) in  $B_2^{tg}$  and  $B_2^n$  mice. (A)  $B_2^n$  mice showed no correlation between sBP and HR ( $n=14$ ,  $r=0.13$ ,  $P=ns$ ). (B)  $B_2^{tg}$  mice showed significant strong correlation between sBP and HR ( $n=15$ ,  $r=0.73$ ,  $P=0.002$ ).

### 3.5.2. Effect of cyclooxygenase inhibitor on blood pressure and heart rate in $B_2^{tg}$ mice

One of the important mediators of bradykinin-induced vasorelaxation are the products of COX enzymes (15). Diclofenac, a non-selective inhibitor of COX enzymes, was used to assess if the decrease in blood pressure observed in  $B_2^{tg}$  is dependent on COX pathway. After baseline measurements, diclofenac (10 mg/kg/day) was added to drinking water for 3 days. As shown in Figure 33A, at baseline before diclofenac administration sBP was significantly lower in  $B_2^{tg}$  ( $125.0 \pm 1.6$  mmHg) in comparison to  $B_2^n$  ( $129.9 \pm 1.1$  mmHg),  $n=9$  per group,  $P=0.02$ . Likewise, HR was significantly lower in  $B_2^{tg}$  ( $567.0 \pm 17.7$  bpm) in comparison to  $B_2^n$  ( $614.7 \pm 11.4$  bpm),  $n=9$  per group,  $P=0.03$  (Figure 33B). Although not statistically significant, administration of diclofenac slightly reduced sBP in both  $B_2^n$  (from  $129.9 \pm 1.1$  into  $125.5 \pm 2.4$  mmHg,  $n=9$ ,  $P=0.09$ ; Figure 34A) and  $B_2^{tg}$  (from  $125.0 \pm 1.6$  into  $119.8 \pm 2.8$  mmHg,  $n=9$ ,  $P=0.12$ ; Figure 34B). Mild non-significant reduction of sBP presumed that COX signalling may be involved in blood pressure regulation in mice. Percent change of sBP in  $B_2^{tg}$  ( $-4.0 \pm 2.4\%$ ) was not significantly different from  $B_2^n$  ( $-3.3 \pm 1.7\%$ ),  $n=9$ ,  $P=ns$  (Figure 34C). These data suggest that sBP reduction in  $B_2^{tg}$  is not dependent on COX pathway. Regarding heart rate, there was no change from baseline after diclofenac administration ( $B_2^n$ : from  $617.7 \pm 11.45$  into  $598.1 \pm 13.03$  bpm,  $n=9$ ,  $P=ns$ ,  $B_2^{tg}$ : from  $567.0 \pm 17.7$  into  $553.3 \pm 16.0$  bpm,  $n=9$ ,  $P=ns$ ; Figure 35).

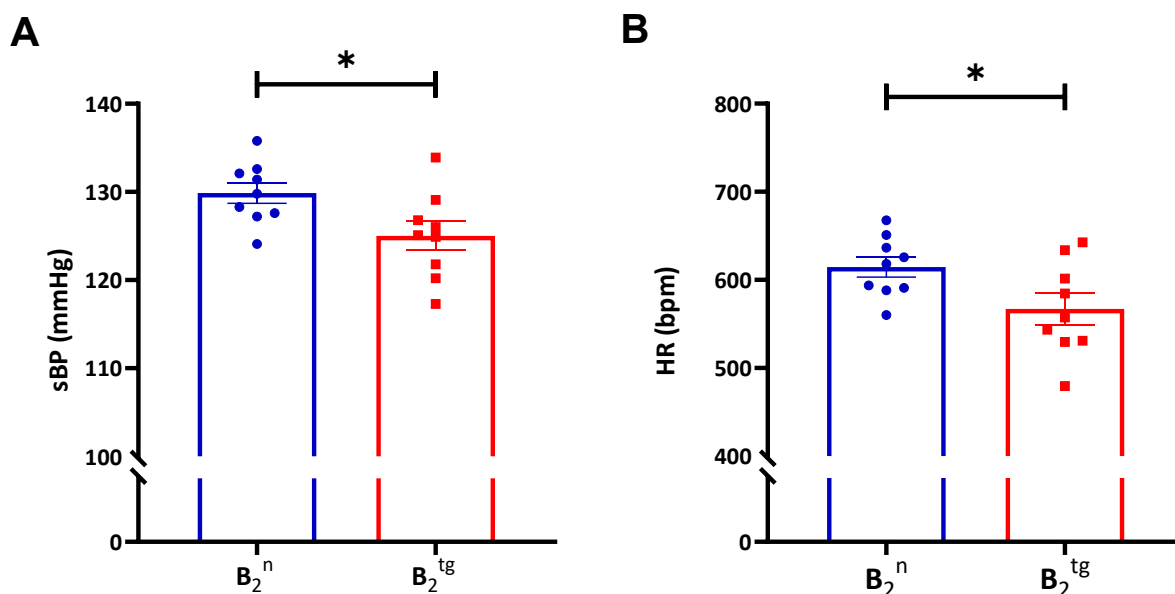


**Figure 33:** Systolic blood pressure (sBP) and heart rate (HR) data using tail-cuff method in conscious  $B_2^n$  and  $B_2^{tg}$  mice after refreshing the line by backcrossing with parental strain C57BL/6J mice. (A) sBP was significantly lower in  $B_2^{tg}$  than  $B_2^n$  ( $B_2^{tg}$ :  $125.0 \pm 1.6$  mmHg vs  $B_2^n$ :  $129.9 \pm 1.1$  mmHg,  $n=9$ ,  $*P=0.02$ , unpaired t-test). (B) HR was significantly lower in  $B_2^{tg}$  than  $B_2^n$  ( $B_2^{tg}$ :  $567.0 \pm 17.7$  bpm vs  $B_2^n$ :  $614.7 \pm 11.4$  bpm,  $n=9$ ,  $*P=0.03$ , unpaired t-test).

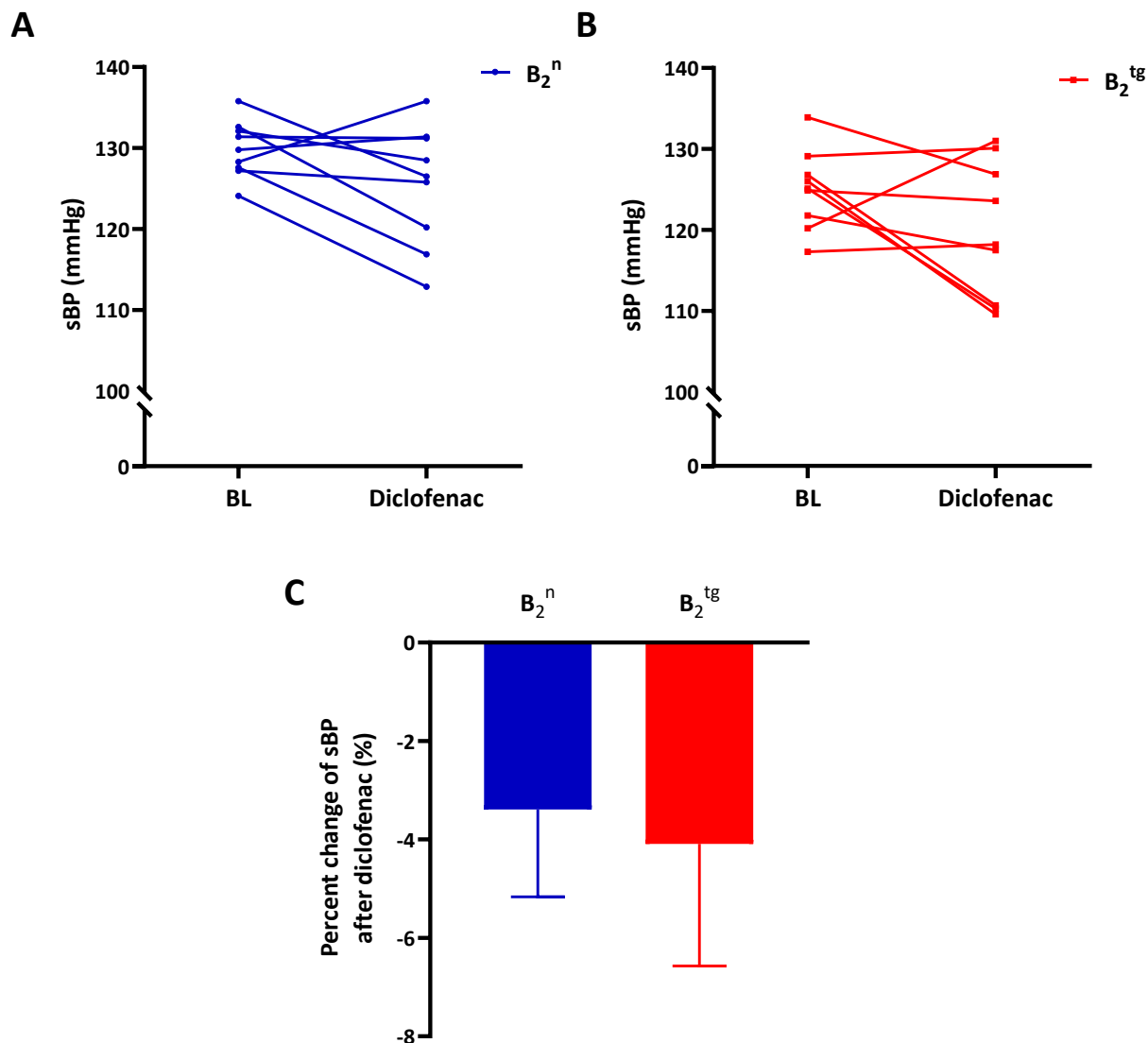


**Figure 34:** Systolic blood pressure measurements (sBP) using tail-cuff method in conscious  $B_2^{tg}$  and  $B_2^n$  mice after refreshing the line by backcrossing with parental strain C57BL/6J mice. After diclofenac administration, there was a non-significant decrease in sBP in both (A)  $B_2^n$  (from  $129.9 \pm 1.1$  into  $125.5 \pm 2.4$  mmHg,  $n=9$ ,  $P=0.09$ , paired t-test) and (B)  $B_2^{tg}$  (from  $125.0 \pm 1.6$  into  $119.8 \pm 2.8$  mmHg,  $n=9$ ,  $P=0.12$ , paired t-test). (C) The percent change of sBP in  $B_2^{tg}$  ( $-4.0 \pm 2.4\%$ ) was the same as in  $B_2^n$  ( $-3.3 \pm 1.7\%$ ),  $n=9$ ,  $P=ns$ , unpaired t-test. BL: baseline.

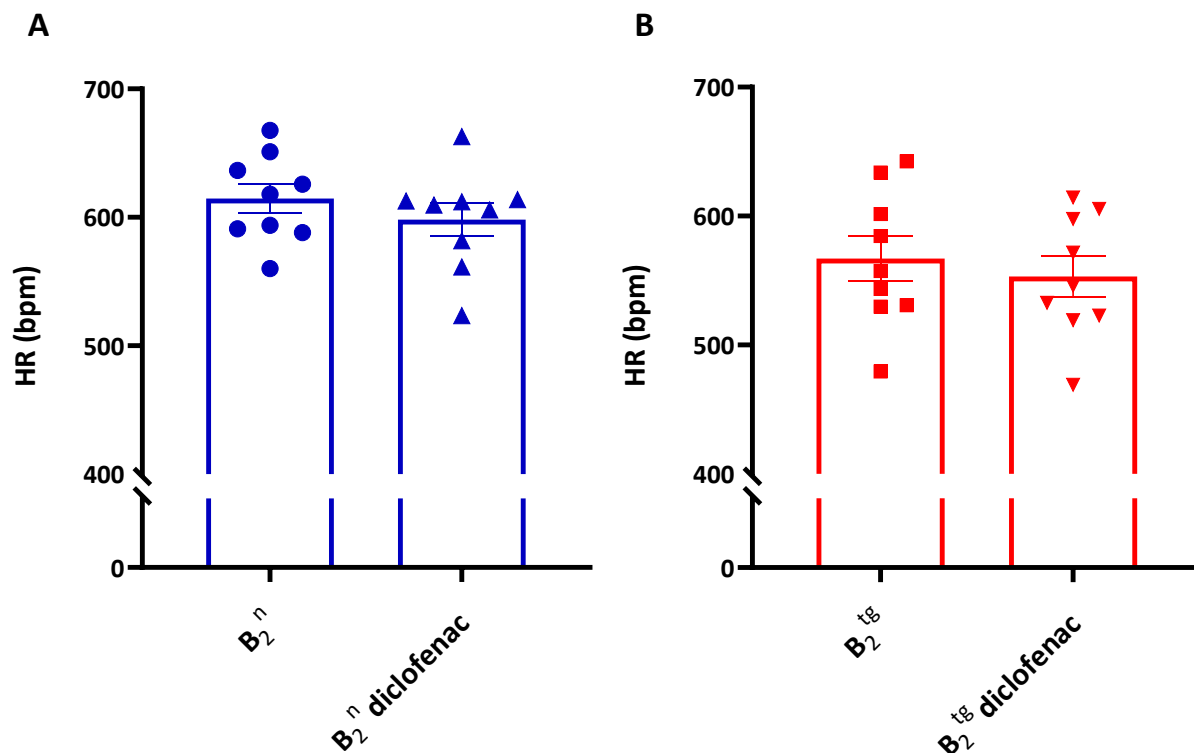


**Figure 35:** Heart rate (HR) data measured by tail-cuff method in conscious  $B_2^{tg}$  and  $B_2^n$  after refreshing the line by backcrossing with parental strain C57BL/6J mice. Diclofenac administration did not affect HR in (A)  $B_2^n$  (from  $617.7 \pm 11.45$  into  $598.1 \pm 13.03$  bpm,  $n=9$  per group,  $P=ns$ , paired t-test) and in (B)  $B_2^{tg}$  (from  $567.0 \pm 17.7$  into  $553.3 \pm 16.0$  bpm,  $n=9$ ,  $P=ns$ , paired t-test).

### 3.5.3. Effect of bradykinin type-II receptor antagonist on blood pressure and heart rate in $B_2^{tg}$ mice

To verify that the decrease in sBP was related to endothelium-specific  $B_2R$  overexpression, the same group of mice was administrated i.p. icatibant, a  $B_2R$  antagonist, on two days. A washout period of one week was implemented to ensure that the diclofenac effect completely disappeared. During the washout period, one mouse per each group died after stopping diclofenac treatment. After that, an adaptation phase of 4 days of i.p. PBS injection was carried out to rule out any effects of i.p. injection per se on sBP and HR. During adaptation phase, i.p. PBS was injected once per day and after 30 minutes of injection, sBP and HR were measured. No change in sBP was observed after the adaptation phase as compared to baseline values in  $B_2^n$  ( $127.3 \pm 2.9$  vs  $129.9 \pm 1.1$  mmHg,  $P=ns$ ), and in  $B_2^{tg}$  ( $123.4 \pm 2.5$  vs  $125 \pm 1.6$  mmHg,  $P=ns$ ) (Figure 36A,B). Likewise, no change in HR was observed in  $B_2^n$  ( $626.7 \pm 13.7$  vs  $614.7 \pm 11.4$  bpm,  $P=ns$ ), and in  $B_2^{tg}$  ( $571.4 \pm 20.8$  vs  $567.0 \pm 17.7$  bpm,  $P=ns$ ) (Figure 36C,D).

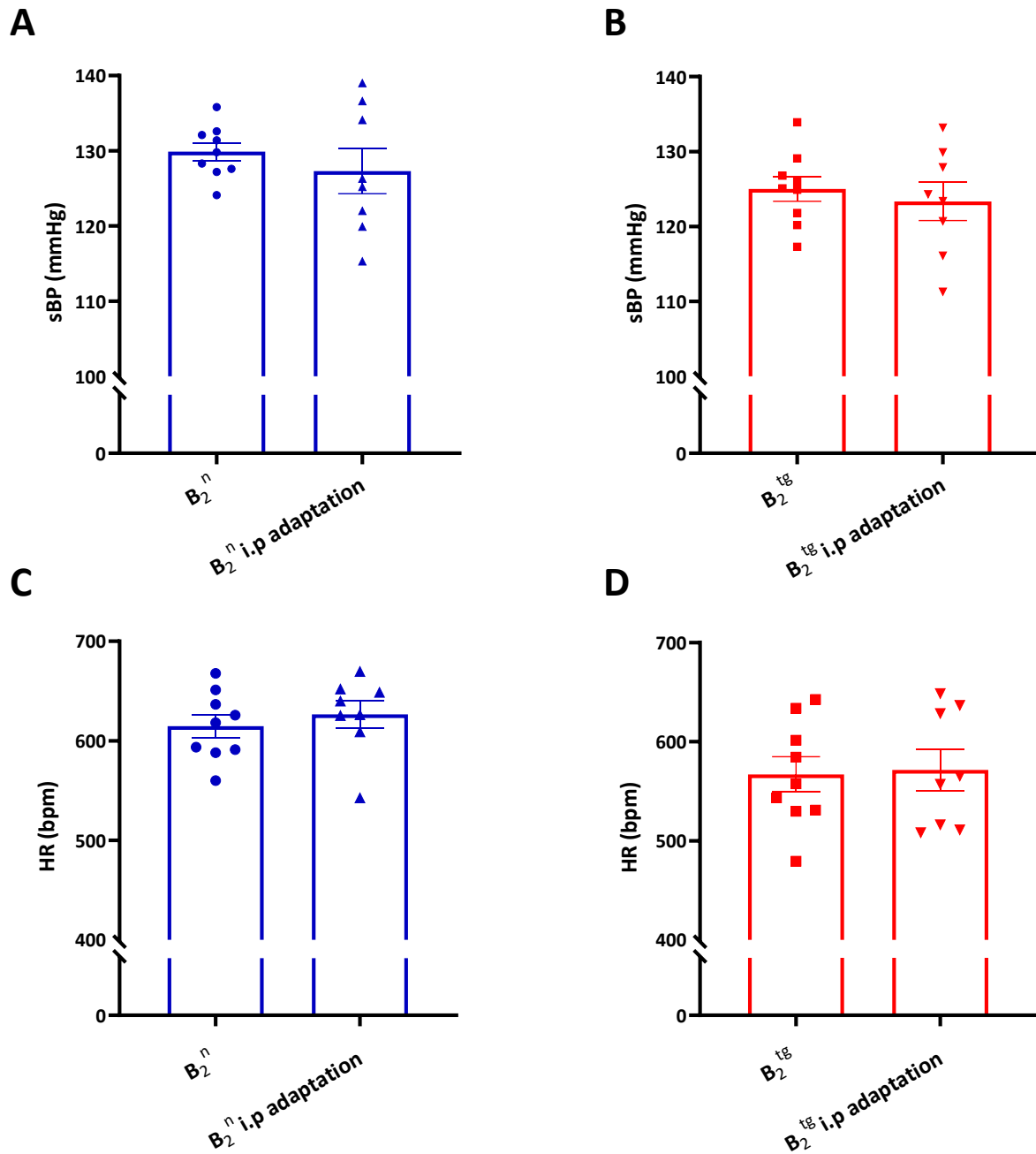


**Figure 36:** Systolic blood pressure (sBP) and heart rate (HR) data using tail-cuff method in conscious  $B_2^n$  and  $B_2^{tg}$  mice after refreshing the line by backcrossing with parental strain C57BL/6J mice. In both groups, the i.p. injections did not affect neither the (A), (B) sBP ( $B_2^n$ :  $127.3 \pm 2.9$  vs  $129.9 \pm 1.1$  mmHg,  $n=8$  per group,  $P=ns$ , paired t-test;  $B_2^{tg}$ :  $123.4 \pm 2.5$  vs  $125 \pm 1.6$  mmHg,  $n=8$  per group,  $P=ns$ , paired t-test) nor (C), (D) HR ( $B_2^n$ :  $626.7 \pm 13.7$  vs  $614.7 \pm 11.4$  bpm,  $n=8$  per group,  $P=ns$ , paired t-test;  $B_2^{tg}$ :  $571.4 \pm 20.8$  vs  $567.0 \pm 17.7$  bpm,  $n=8$  per group,  $P=ns$ , paired t-test)

Icatibant administration did not affect sBP in  $B_2^n$  (from  $127.3 \pm 2.9$  into  $128.6 \pm 4.6$  mmHg,  $P=ns$ ; Figure 37A), and slightly increased sBP in  $B_2^{tg}$  (from  $123.4 \pm 2.5$  into  $128.3 \pm 2.0$  mmHg,  $P=ns$ ; Figure 37B), and The sBP difference between groups abolished after icatibant administration ( $B_2^n$ :  $128.6 \pm 4.6$  vs  $B_2^{tg}$ :  $128.3 \pm 2.0$  mmHg,  $P=ns$ ; Figure 37C) suggesting a role of  $B_2R$  overexpression in sBP reduction. Interestingly, icatibant administration significantly increased HR in both  $B_2^n$  (from  $626.7 \pm 13.7$  into  $685.5 \pm 16.4$  bpm,  $P=0.02$ ; Figure 38A), and  $B_2^{tg}$

(from  $571.4 \pm 20.8$  into  $630.8 \pm 21.8$  bpm,  $P=0.01$ ; Figure 38B). The increase in HR after icatibant administration together with the lower HR in  $B_2^{tg}$  in comparison to  $B_2^n$  suggest a role of  $B_2R$  in HR regulation. In addition, the  $B_2R$ -induced decrease in HR might point to the underlying mechanism in sBP reduction in  $B_2^{tg}$ . The significant difference in HR between groups was abolished after administration of icatibant ( $B_2^{tg}$ :  $630.8 \pm 21.8$  bpm vs  $B_2^n$ :  $685.5 \pm 16.4$  bpm,  $P=ns$ ; Figure 38C), which indicates that  $B_2R$  overexpression is responsible for the difference in HR between groups.

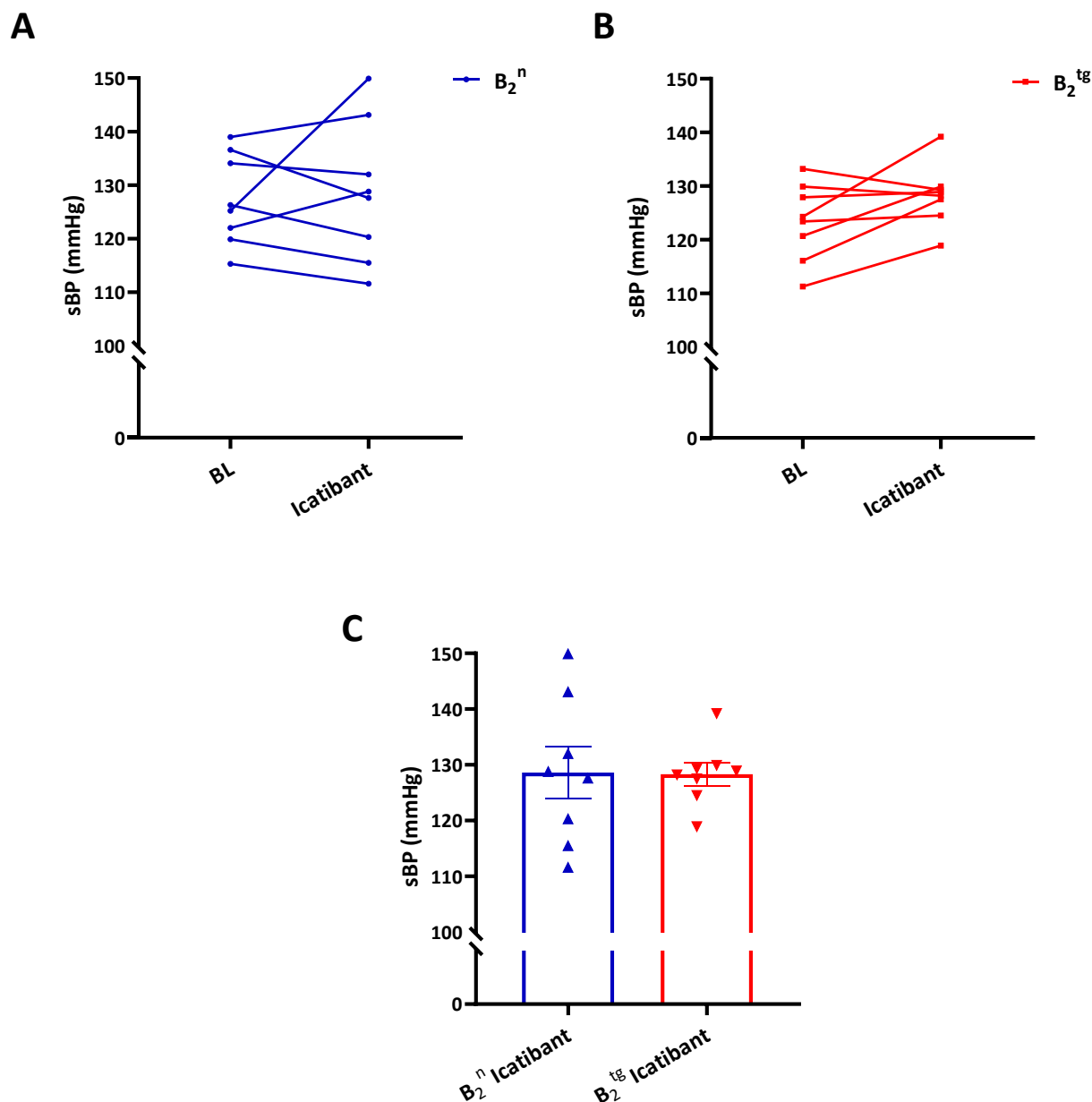


**Figure 37:** Systolic blood pressure data (sBP) using tail-cuff method in conscious  $B_2^n$  and  $B_2^{tg}$  mice after refreshing the line by backcrossing with parental strain C57BL/6J mice. Measurements were done 30 minutes after icatibant administration. (A) In  $B_2^n$ , icatibant administration did not affect sBP (from  $127.3 \pm 2.9$  into  $128.6 \pm 4.6$  mmHg,  $P=ns$ , paired t-test), and slightly increased sBP in (B)  $B_2^{tg}$  (from  $123.4 \pm 2.5$  into  $128.3 \pm 2.0$  mmHg,  $P=ns$ , paired t-test). (C) The sBP difference between groups abolished after icatibant administration ( $B_2^n$ :  $128.6 \pm 4.6$  vs  $B_2^{tg}$ :  $128.3 \pm 2.0$  mmHg,  $P=ns$ , unpaired t-test). BL: baseline.

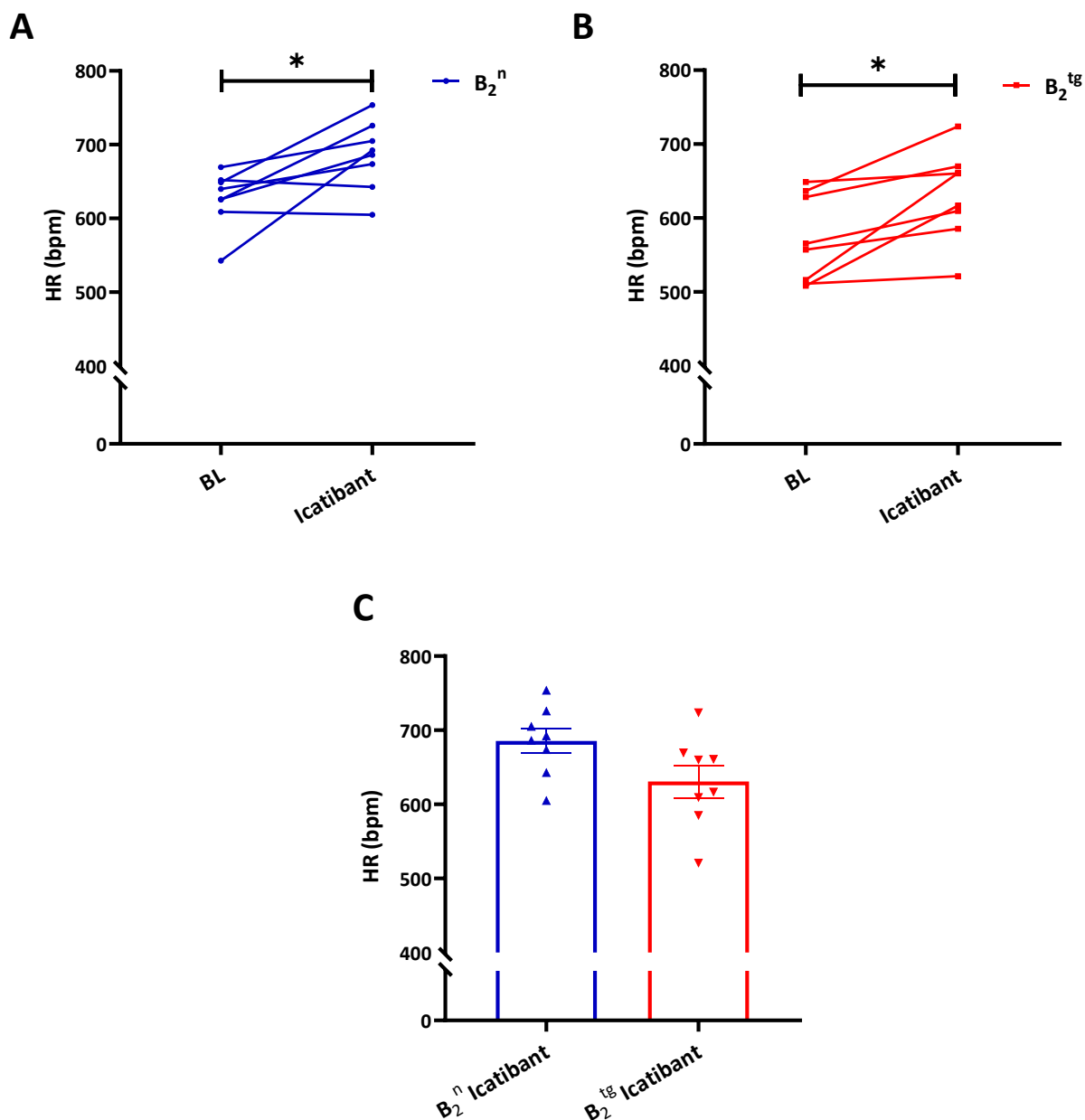


**Figure 38:** Heart rate data (HR) using tail-cuff method in conscious  $B_2^n$  and  $B_2^{tg}$  mice after refreshing the line by backcrossing with parental strain C57BL/6J mice. Measurements were done 30 minutes after icatibant administration. Icatibant administration significantly increased HR in both (A)  $B_2^n$  (from  $626.7 \pm 13.7$  into  $685.5 \pm 16.4$  bpm,  $*P=0.02$ , paired t-test), and (B)  $B_2^{tg}$  (from  $571.4 \pm 20.8$  into  $630.8 \pm 21.8$  bpm,  $*P=0.01$ ,  $n=8$  per group, paired t-test). (C) The significant difference in HR between groups was abolished after administration of icatibant ( $B_2^{tg}$ :  $630.8 \pm 21.8$  bpm vs  $B_2^n$ :  $685.5 \pm 16.4$  bpm,  $P=ns$ ,  $n=8$  per group, unpaired t-test). BL: baseline.

### 3.5.4. Effect of nitric oxide synthase inhibitor on blood pressure and heart rate in $B_2^{tg}$ mice

It is known that eNOS plays a role in blood pressure regulation and is one of the downstream signalling proteins through which bradykinin causes vasodilation (15, 193). In one set of mice, the NOS-inhibitor L-NAME was administered in drinking water for one week to investigate if eNOS is responsible for the decrease in sBP in  $B_2^{tg}$ . As expected, inhibition of eNOS resulted in significant increase in sBP in both  $B_2^n$  ( $131.4 \pm 1.6$  mmHg,  $n=6$ ,

$P=0.002$ ; Figure 39A) and  $B_2^{tg}$  ( $138.7\pm 2.9$  mmHg,  $n=6$ ,  $P=0.003$ ; Figure 39B). However, the effect of L-NAME was comparable between the two groups as the percent of increase in sBP after L-NAME administration in  $B_2^{tg}$  ( $11.3\pm 2.2\%$ ) was not statistically different from  $B_2^n$  ( $7.1\pm 1.3\%$ ),  $n=6$  per group,  $P=ns$  (Figure 39C). Therefore, it is unlikely that eNOS is responsible for the reduction of sBP observed in  $B_2^{tg}$  mice. Moreover, heart rate decreased significantly in both  $B_2^n$  ( $443.9\pm 17.6$  bpm,  $n=6$ ,  $P=0.0009$ ; Figure 39D) and  $B_2^{tg}$  ( $476.7\pm 22.9$  bpm,  $n=6$ ,  $P=0.001$ ; Figure 39E). Percent of decrease in HR after L-NAME administration in  $B_2^{tg}$  ( $-19.1\pm 3.1\%$ ) was not statistically different from  $B_2^n$  ( $-23.4\pm 2.9\%$ ),  $n=6$ ,  $P=ns$ , (Figure 39F).

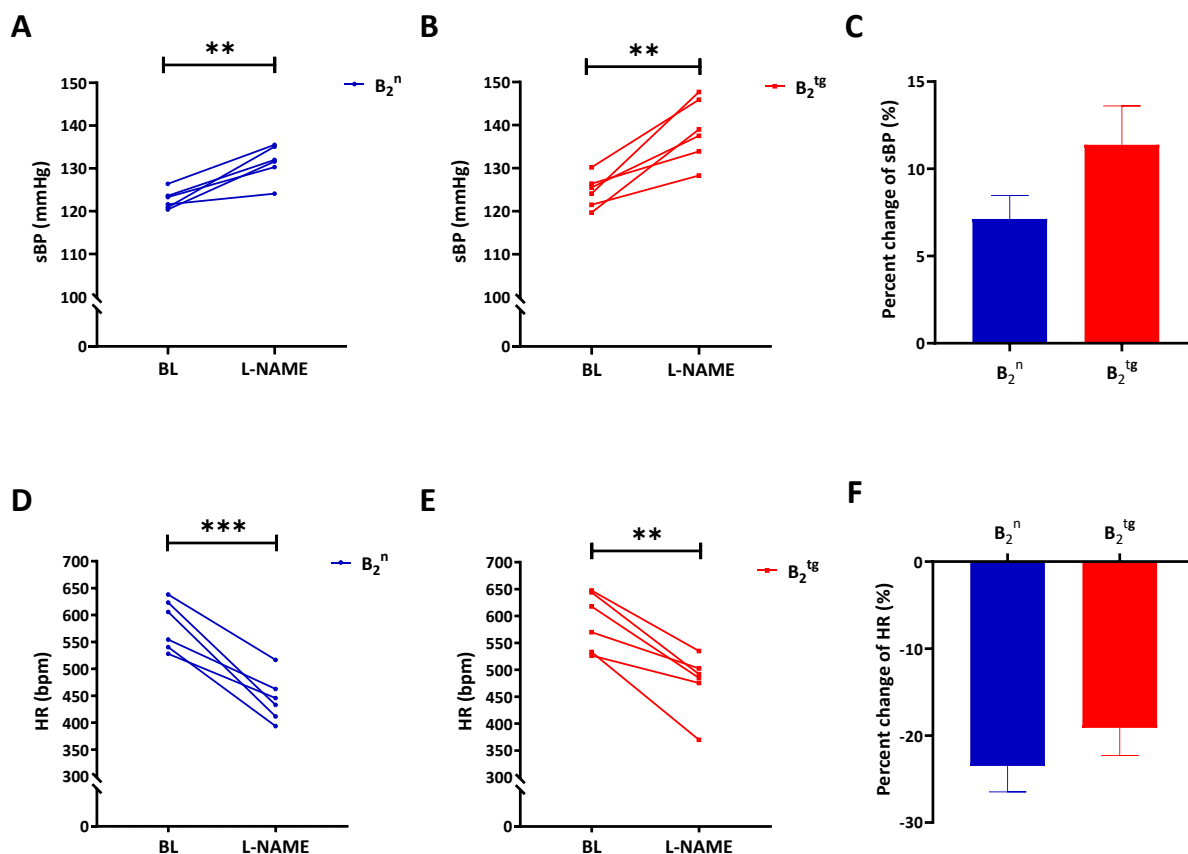


**Figure 39:** Systolic blood pressure (sBP) and heart rate (HR) data using tail-cuff method in conscious  $B_2^n$  and  $B_2^{tg}$  mice after refreshing the line by backcrossing with parental strain C57BL/6J mice.  $N^\omega$ -Nitro-L-arginine methyl ester hydrochloride (L-NAME) administration led to significant increase in sBP in (A)  $B_2^n$  ( $131.4\pm 1.6$  mmHg,  $n=6$ ,  $**P=0.002$ , paired t-test), and in (B)  $B_2^{tg}$  ( $138.7\pm 2.9$  mmHg,  $n=6$ ,  $**P=0.003$ , paired t-test). (C) The percent change of sBP in  $B_2^{tg}$  ( $11.3\pm 2.2\%$ ) was the same as in  $B_2^n$  ( $7.1\pm 1.3\%$ ),  $n=6$  per group,  $P=ns$ , unpaired t-test. Additionally, heart rate decreased significantly in both (D)  $B_2^n$  ( $443.9\pm 17.6$  bpm,  $n=6$ ,  $***P=0.0009$ , paired t-test) and in (E)  $B_2^{tg}$  ( $476.7\pm 22.9$  bpm,  $n=6$ ,  $**P=0.001$ , paired t-test). (F) The percent change of HR in  $B_2^{tg}$  ( $-19.1\pm 3.1\%$ ) was the same as in  $B_2^n$  ( $-23.4\pm 2.9\%$ ),  $n=6$  per group,  $P=ns$ , unpaired t-test. BL: baseline.

### 3.6. Assessment of flow-mediated dilation in B<sub>2</sub><sup>tg</sup> mice

*In vivo*, vascular function of B<sub>2</sub><sup>tg</sup> mice was further explored through flow-mediated dilation analysis of external iliac artery. Blood flow pattern was visualized by doppler imaging, where the diastolic component was clearly seen at baseline as shown in Figure 40A. During cuff inflation, absence of diastolic component indicates occlusion of the artery (Figure 40B). After cuff release, the diastolic component reappears indicating the reperfusion of the artery (Figure 40C).

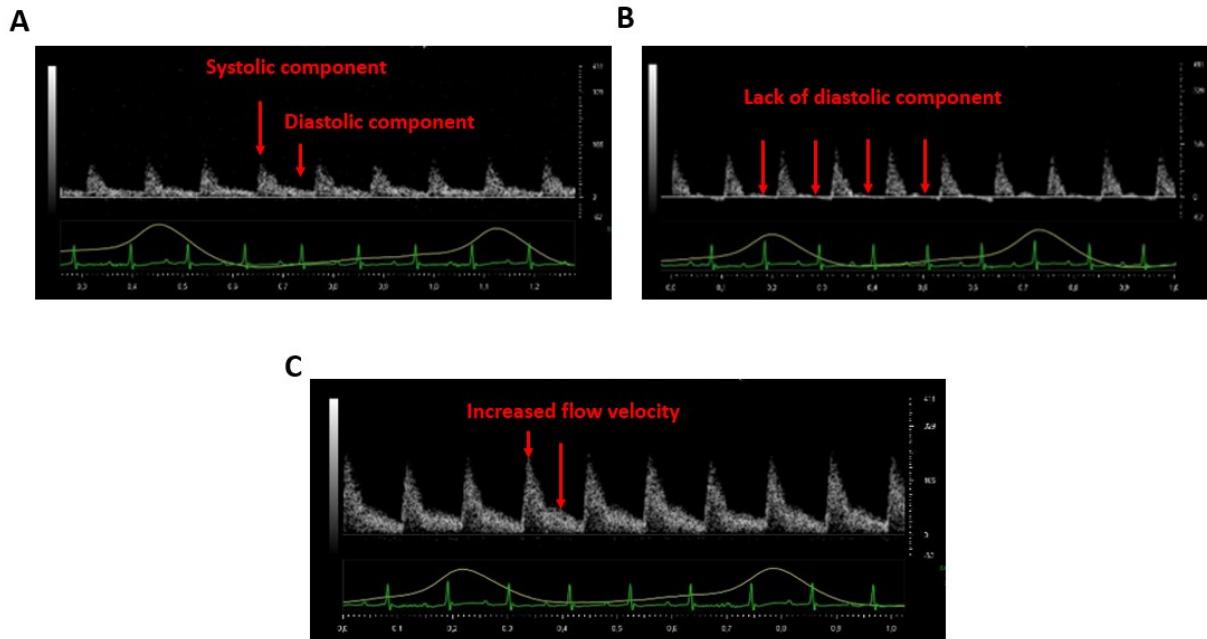


**Figure 40:** Representative photos of doppler flow of external iliac artery. Red arrows refer to systolic and diastolic components of blood flow inside the artery which is shown at baseline (A). The diastolic component disappeared during cuff inflation (B) and reappeared after deflation of cuff (C). ECG and respiratory pattern were shown below the doppler flow. Vertical line (on the right) shows velocity in mm/sec and horizontal line (at the bottom) shows time in seconds.

As expected, the mean flow velocity increased significantly after 20 seconds of cuff release in both  $B_2^n$  (from  $54.21 \pm 5.79$  into  $111.75 \pm 11.96$  mm/sec,  $n=7$ ,  $P=0.03$ ) and  $B_2^{tg}$  (from  $53.37 \pm 5.81$  into  $111.12 \pm 9.60$  mm/sec,  $n=9$ ,  $P=0.0003$ ) (Figure 41). After 5 minutes, the mean flow velocity values returned nearly to baseline values ( $B_2^n$ :  $52.51 \pm 4.62$ ,  $B_2^{tg}$ :  $51.27 \pm 3.95$  mm/sec). Importantly, there was no difference in mean flow velocity between  $B_2^n$  and  $B_2^{tg}$  at all time points,  $P=ns$  (Figure 41). Worth mentioning, the blood flow velocity returned to baseline levels by the end of five minutes. However, the increase in vessel diameter persisted even after the flow velocity returned to baseline values (Figure 42). This implies that the released mediators exert a sustained effect on vessel diameter.

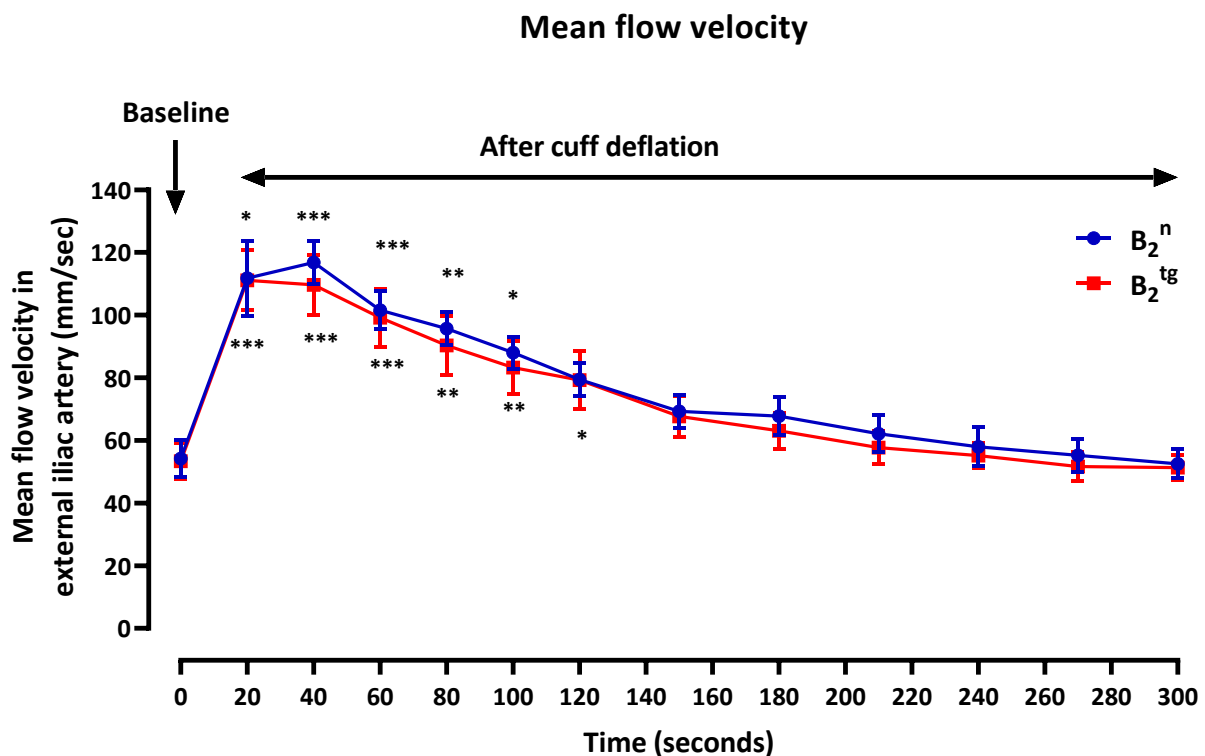


**Figure 41:** Mean flow velocity in external iliac artery in  $B_2^{tg}$  and  $B_2^n$  mice. No significant difference was shown between  $B_2^{tg}$  and  $B_2^n$  mice,  $P=ns$ , two-way repeated measures ANOVA. Mean flow velocity increased significantly after cuff release at 20, 40, 60, 80, 100, 120 in  $B_2^{tg}$  ( $n=9$ ,  $P=0.0002$ ,  $P=0.0001$ ,  $P=0.0003$ ,  $P=0.001$ ,  $P=0.006$ ,  $P=0.02$  respectively vs baseline) and in  $B_2^n$  ( $n=7$ ,  $P=0.02$ ,  $P=0.0003$ ,  $P=0.0004$ ,  $P=0.001$ ,  $P=0.01$  respectively vs baseline). Mean flow velocity returned nearly to baseline values after 5 minutes. Statistical analysis was done using Dunnett's multiple comparisons test following two-way repeated measures ANOVA.

The diameter of the artery was measured from the marked region of interest at baseline and different time points (Figure 42A). No change in FMD was observed in  $B_2^{tg}$  mice ( $n=7-9$  per group,  $P=ns$  vs  $B_2^n$ ; Figure 42B). This data indicates that the vascular  $B_2R$  overexpression per se doesn't affect the ability of conduit arteries to dilate in response to an increase in blood flow.

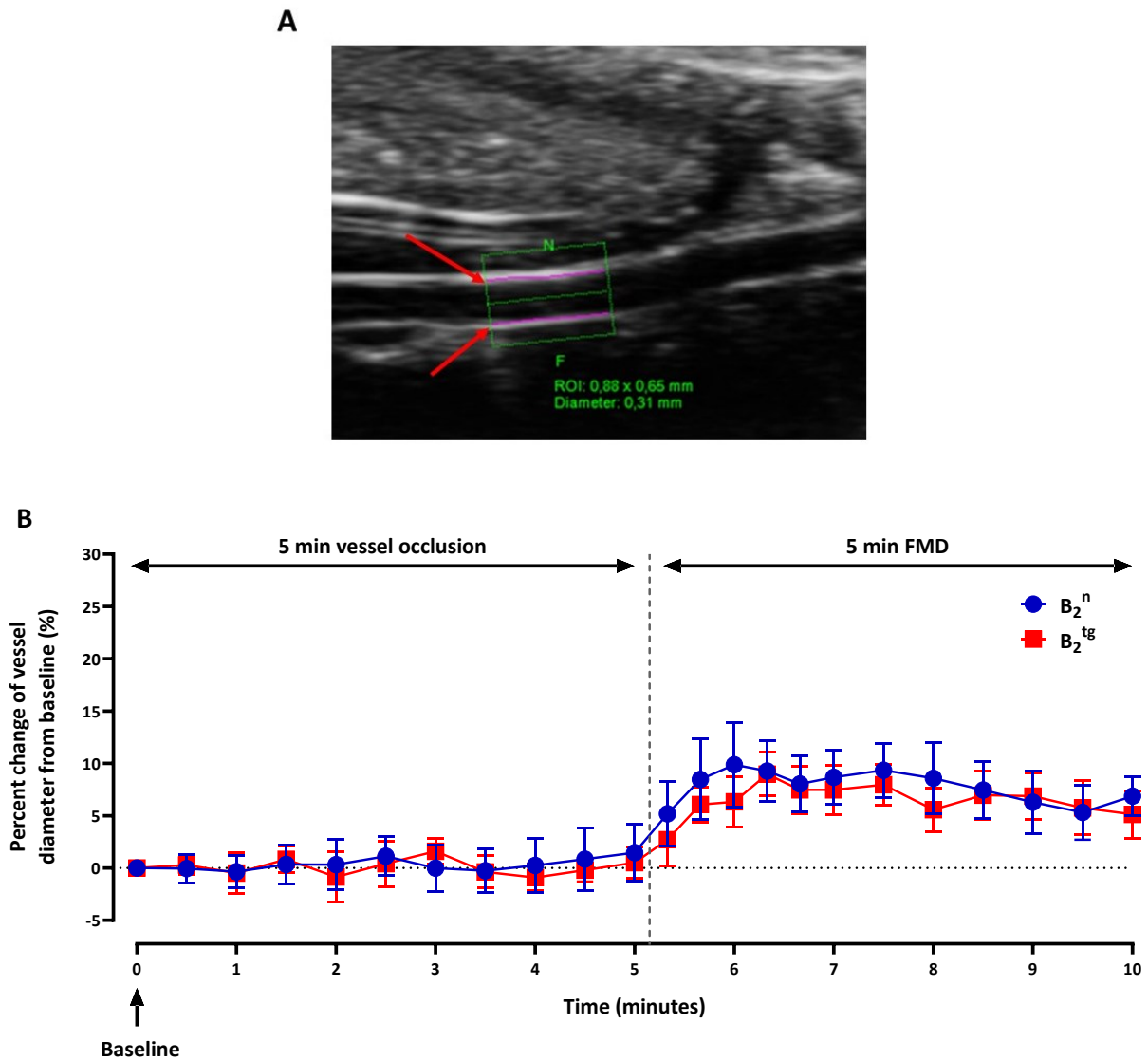


**Figure 42:** Flow-mediated dilation (FMD) data in  $B_2^{tg}$  and  $B_2^n$  mice. (A) Representative photo of analysis of diameter of external iliac artery. Pink dots marked the internal diameter of the artery as shown by red arrows and the green square represents the region of interest (ROI), where the diameter of artery is measured. (B) Baseline was recorded before cuff inflation, represented as zero time (i.e. baseline). No significant difference was shown in FMD between  $B_2^{tg}$  and  $B_2^n$  mice,  $n=7-9$  per group,  $P=ns$ , two-way repeated measures ANOVA.

### 3.7. Effect of endothelium-specific bradykinin type-II receptors overexpression on cardiac function

To explore the effect of endothelium-specific B<sub>2</sub>R overexpression on cardiac function, non-invasive transthoracic echocardiography was done in anesthetized B<sub>2</sub><sup>tg</sup> and B<sub>2</sub><sup>n</sup> mice. LV volumes during systole and diastole were calculated from B-mode of LV parasternal long axis view (Figure 43A,B). Ejection fraction, fractional shortening, stroke volume, cardiac output are calculated from LV volumes. LV diameters, LV mass and posterior wall thickness during systole and diastole were calculated from M-mode of LV parasternal long axis view (Figure 43C). Early to late diastolic transmitral flow velocity (E/A), isovolumetric contraction time (IVCT), isovolumic relaxation time (IVRT), deceleration time of the E wave (MV DT), and aortic ejection time (AET) were calculated from doppler images of mitral flow valve (Figure 44A) and aortic valve velocities were calculated from doppler aortic valve flow (Figure 45A,B).

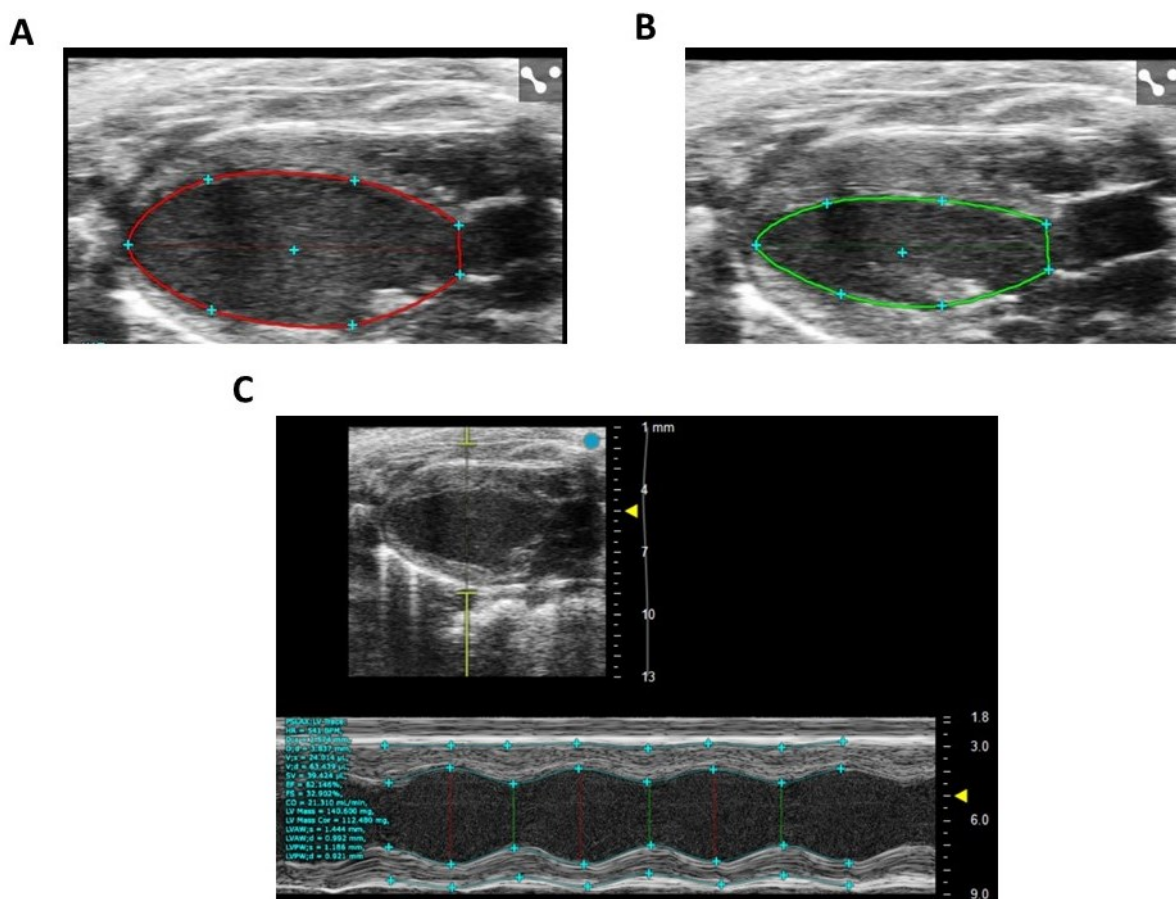


**Figure 43:** Representative photos of analysis of echocardiographic parameters related to left ventricular systolic function. (A) B-mode of parasternal longitudinal axis of heart, red colour frame represents maximum cross-sectional area during diastole. (B) B-mode of parasternal longitudinal axis of heart, green colour frame represents minimum cross-sectional area during systole. (C) Parasternal longitudinal axis view (upper panel) and M-mode tracing (lower panel) of the left ventricle. Yellow arrow indicates the focus depth of the transducer.

As shown in Table 7, parameters of LV function in  $B_2^{tg}$  were comparable to those in  $B_2^n$  as no significant differences were found in ejection fraction, fractional shortening, stroke volume and cardiac output. The LV mass was significantly larger in  $B_2^{tg}$  ( $123.1 \pm 8.9$  mm) than in  $B_2^n$  ( $99.9 \pm 5.5$  mm),  $n=10$  per group,  $P=0.04$ . Similarly, LV posterior wall thickness in systole (LVPW;s) was significantly larger in  $B_2^{tg}$  ( $0.8 \pm 0.04$  mm) than in  $B_2^n$  ( $0.7 \pm 0.03$  mm),  $n=10$  per group,  $P=0.03$ , as well as non-significant higher LV posterior wall thickness in diastole (LVPW;d) in  $B_2^{tg}$  ( $1.1 \pm 0.05$  mm) versus  $B_2^n$  ( $0.9 \pm 0.05$  mm),  $n=10$  per group,  $P=ns$ . However, after normalization to body weight, no significant differences were shown for these parameters. These observations indicate that  $B_2R$  overexpression did not affect the LV cardiac function.

Moreover, parameters of cardiac diastolic function in  $B_2^{tg}$  were comparable to those in  $B_2^n$  as no significant differences were found in passive early diastolic filling to atrial contraction ratio, deceleration time of passive early diastolic filling, and isovolumic relaxation time (Table 7). Interestingly, MPI was significantly higher in  $B_2^{tg}$  ( $0.6 \pm 0.03$ ) than in  $B_2^n$  ( $0.5 \pm 0.02$ ),  $n=9$  per group,  $P=0.017$ ; and AET was significantly lower in  $B_2^{tg}$  ( $39.2 \pm 1.8$  ms) than in  $B_2^n$  ( $45.8 \pm 1.1$  ms),  $n=9-10$  per group,  $P=0.009$  (Figure 44). Since IVCT and IVRT in  $B_2^{tg}$  were similar to  $B_2^n$ , the increase in MPI is attributed to the decrease in AET. Notably, an increase in aortic valve mean velocity was shown in  $B_2^{tg}$  ( $898.58 \pm 38.72$  mm/sec) as compared to  $B_2^n$  mice ( $779.02 \pm 41.5$  mm/sec),  $n=10$  per group,  $P=0.049$  (Figure 45C). In addition, non-significant increase in aortic valve peak velocity was found in  $B_2^{tg}$  ( $1387.09 \pm 72.43$  mm/sec) as compared to  $B_2^n$  ( $1194.99 \pm 68.37$  mm/sec),  $n=9-10$  per group,  $P=ns$  (Figure 45D). Collectively, these findings exclude any effects of  $B_2R$  overexpression on cardiac diastolic function but introduced a possible contribution of  $B_2R$  in regulation of aortic valve functions.

**Table 7:** Echocardiographic parameters values and p-values of B<sub>2</sub><sup>tg</sup> and B<sub>2</sub><sup>n</sup> mice.

Parameter	B <sub>2</sub> <sup>n</sup> , n=9-10	B <sub>2</sub> <sup>tg</sup> , n=10	P-value
Age, weeks	12-14	12-14	ns
Weight, g	28.3±0.3	29.3±0.4	ns
Heart Rate, bpm	463.8±13.1	494.6±15.8	ns
Volume;s, µL	28.8±1.3	30.4±2.0	ns
Volume;d, µL	62.2±2.1	67.1±4.6	ns
Stroke Volume, µL	33.4±1.2	36.6±2.7	ns
Ejection Fraction, %	53.8±1.2	54.51±0.8	ns
Fractional Shortening, %	10.0±0.6	9.5±1.4	ns
Cardiac Output, ml/min	15.6±0.8	17.9±1.2	ns
Diameter;s, mm	3.2±0.1	3.1±0.12	ns
Diameter;d, mm	4.3±0.07	4.3±0.1	ns
LV mass, corrected, mg	99.9±5.5	123.1±8.9	0.04
LV mass/BW, mg/g	3.5±0.1	4.1±0.2	ns
Heart weight/BW, mg/g	5.2±0.13	5.1±0.15	ns
LVPW;d, mm	0.9± 0.05	1.1±0.05	ns
LVPW;d, mm/g	0.03±1.91	0.04±1.59	ns
LVPW;s, mm	0.7±0.03	0.8±0.04	0.03
LVPW;s, mm/g	0.026±0.0	0.029±0.0	ns
Cardiac Index, ml/min/g	0.5±0.02	0.6±0.03	ns
IVCT, ms	10.7±0.4	11.5±0.4	ns
IVRT, ms	14.7±0.9	14.5±0.5	ns
E/A	1.3±0.07	1.2±0.05	ns
MV DT, ms	24.72±1.3	26.2±1.6	ns
MPI	0.5±0.02	0.6±0.03	0.017
AET, ms	45.8±1.1	39.2±1.8	0.009

LV: left ventricular, LVPW;d: left ventricular posterior wall thickness in diastole, LVPW;s: left ventricular posterior wall thickness in systole, s: systole, d: diastole, IVCT: isovolumic contraction time, interval between mitral valve closure and aortic valve opening, BW: body weight, IVRT: isovolumic relaxation time, interval between aortic valve closure and mitral valve opening, E/A: early to late diastolic transmitral flow velocity (ratio of peak velocity blood flow in passive early diastolic filling 'E wave' to peak velocity flow in late diastole caused by the atrial contraction 'A wave'), MV DT: deceleration time of the E wave, MPI: myocardial performance index, AET: aortic ejection time. ms: milliseconds. Statistical analysis was done using unpaired t-test.

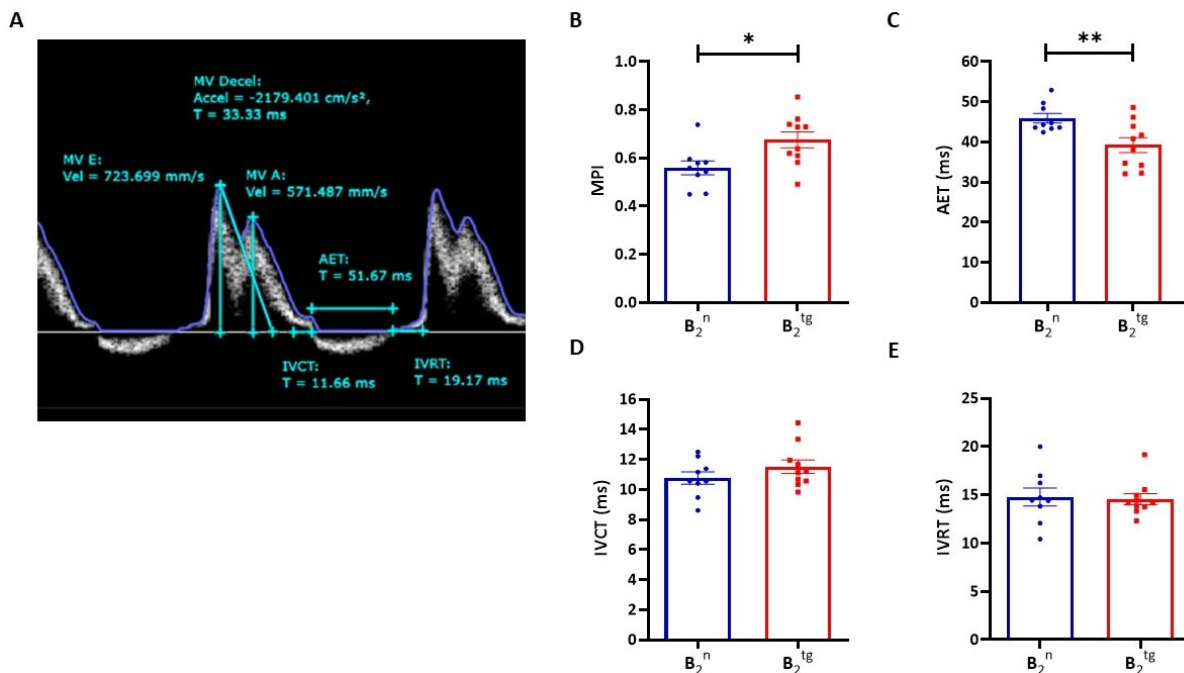


**Figure 44:** Cardiac parameters calculated from mitral flow doppler from echocardiography. (A) Representative photo of analysis of mitral valve flow parameters (E/A, MV deceleration time, IVCT, IVRT, and aortic ejection time). (B) MPI was significantly higher in B<sub>2</sub><sup>tg</sup> (0.6±0.03) than B<sub>2</sub><sup>n</sup> (0.5±0.02), \*P=0.017. (C) AET was significantly shorter in B<sub>2</sub><sup>tg</sup> (39.2±1.8 ms) than in B<sub>2</sub><sup>n</sup> (45.8±1.1 ms), \*\*P=0.009. (D) IVCT (B<sub>2</sub><sup>n</sup>: 10.7±0.4, B<sub>2</sub><sup>tg</sup>: 11.5±0.4 ms) and (E) IVRT (B<sub>2</sub><sup>n</sup>:14.7±0.9, B<sub>2</sub><sup>tg</sup>:14.5±0.5 ms) were comparable between B<sub>2</sub><sup>n</sup> and B<sub>2</sub><sup>tg</sup>, n=9-10 per group, P=ns. Statistical test: unpaired t-test. MPI: myocardial performance index, AET: aortic ejection time, IVCT: isovolumetric contraction time, IVRT: isovolumetric relaxation time, ms: millisecond.

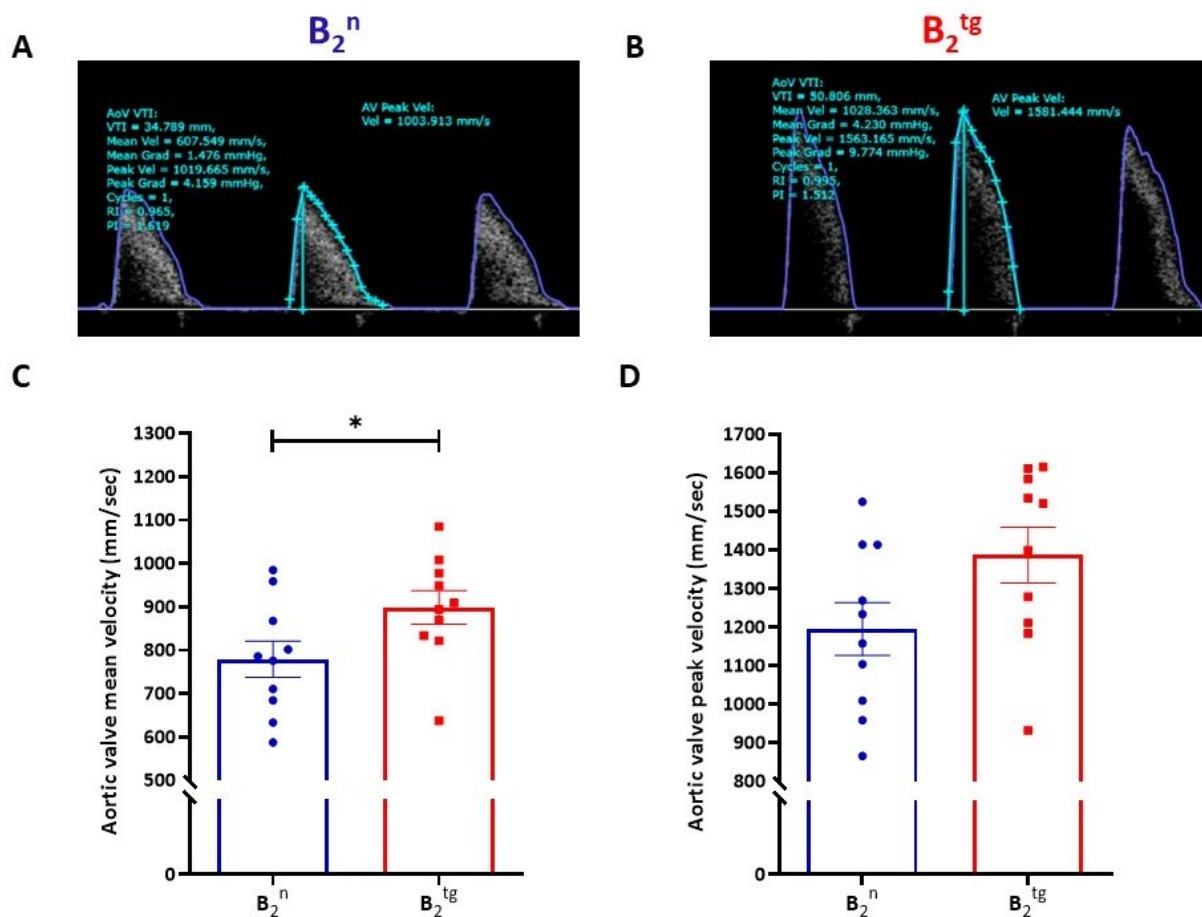


**Figure 45:** Aortic valve parameters from aortic valve flow doppler from echocardiography. (A) and (B) Representative photos of analysis of aortic valve flow in  $B_2^n$  and  $B_2^{tg}$  mice, respectively. (C) Aortic valve mean velocity was significantly higher in  $B_2^{tg}$  mice ( $898.58 \pm 38.72$  mm/sec) as compared to  $B_2^n$  mice ( $779.02 \pm 41.5$  mm/sec),  $n=10$  per group,  $*P=0.049$ . (D) Non-significant increase in aortic valve peak velocity was found in  $B_2^{tg}$  mice ( $1387.09 \pm 72.43$  mm/sec) as compared to  $B_2^n$  mice ( $1194.99 \pm 68.37$  mm/sec),  $n=10$  per group,  $P=ns$ . Statistical analysis was done using unpaired t-test.

### 3.8. Effect of endothelium-specific bradykinin type-II receptors overexpression on expression of different proteins: Proteomic analysis

The primary objective of the proteomic analysis was to investigate the alterations in the proteome profile of aortic tissue in  $B_2^{tg}$  mice compared to wild-type mice, given that overexpression of the  $B_2R$  in the endothelium was expected to influence the expression of various proteins. Specifically, the analysis aimed to identify changes in proteins associated with blood pressure regulation, to help elucidate the mediators responsible for the observed reduction in sBP in  $B_2^{tg}$  mice. Additionally, the proteomic analysis sought to provide an overview of the protein profile modifications that could explain the observed changes in aortic valve velocity and the lack of effect in the FMD study in  $B_2^{tg}$  mice. Overall, 4,240 proteins were detected in the murine aortic tissues, from which 47 proteins were identified as contaminants and therefore were excluded from analysis. For quantification, only proteins with solid values in at least five biological replicates per group were considered. In  $B_2^{tg}$  mice, there was a significant change in expression of 148 proteins (3.79%) out of 3,896

totally identified proteins in aorta. A full list of the significantly modified proteins in  $B_2^{tg}$  mice relative to WT ( $p < 0.05$ ) along with their accession numbers, protein symbols, abundance ratio,  $\log_2$  abundance ratio and P-values are summarized in appendix 2. Thirty-seven proteins (25%) were differentially upregulated, and 111 proteins (75%) were differentially downregulated (Figure 46). The hierarchical clustering of the significantly changed proteins' profiles for each replicate in  $B_2^{tg}$  and WT groups were visualized in heat map (Figure 47).

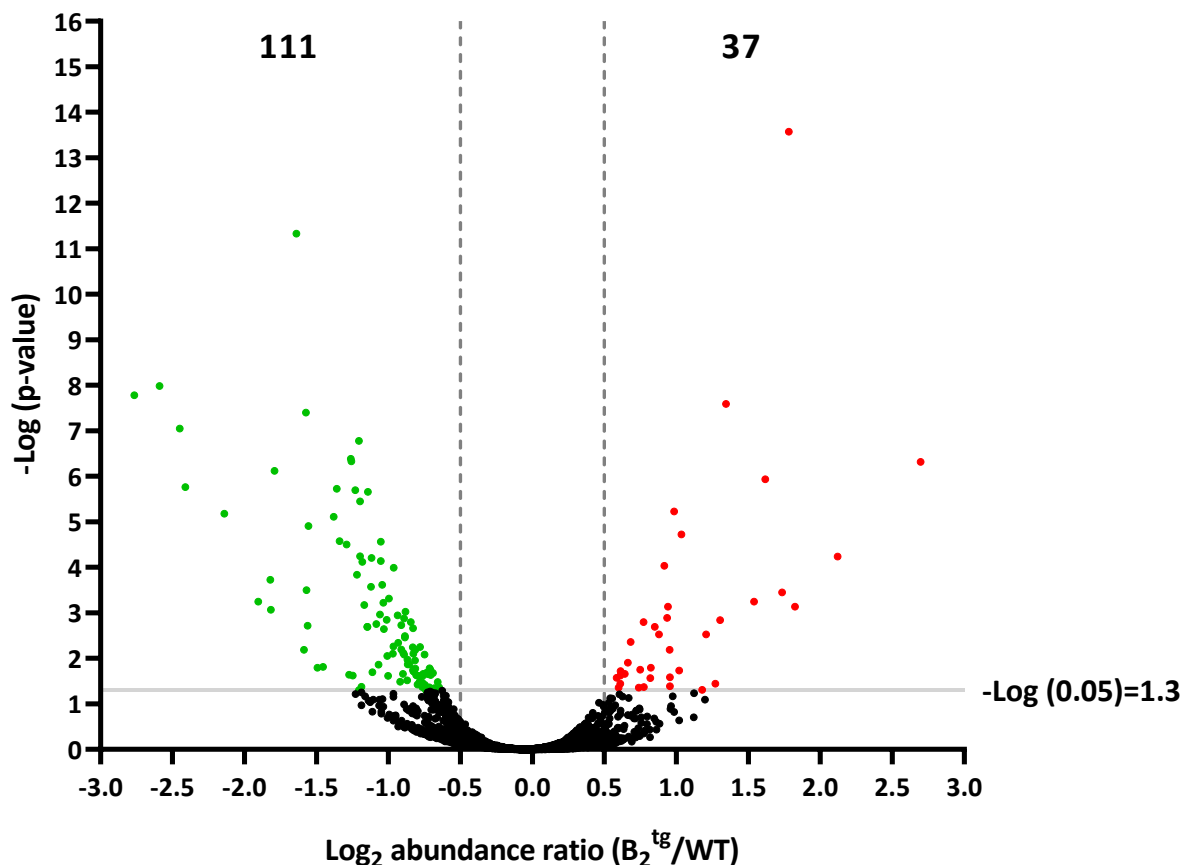


**Figure 46:** Volcano plot showing the distribution of  $-\log$  P-values vs  $\log_2$  abundance ratio of proteins obtained from proteomic analysis of aortic tissues of  $B_2^{tg}$  relative to wild-type (WT). Solid line shows the significance cutoff value which is equivalent to  $-\log(p\text{-value}=0.05) = 1.3$ . Red dots represent 37 significantly upregulated proteins ( $\log_2$  abundance ratio  $> 0.5$  and P-value  $< 0.05$ ). Green dots represent 111 significantly downregulated proteins ( $\log_2$  abundance ratio  $< -0.5$  and P-value  $< 0.05$ ). Black dots represent proteins that were not statistically significant changed (P-value  $> 0.05$ ). N=5-7 per group, statistical analysis was done by Benjamini-Hochberg method.

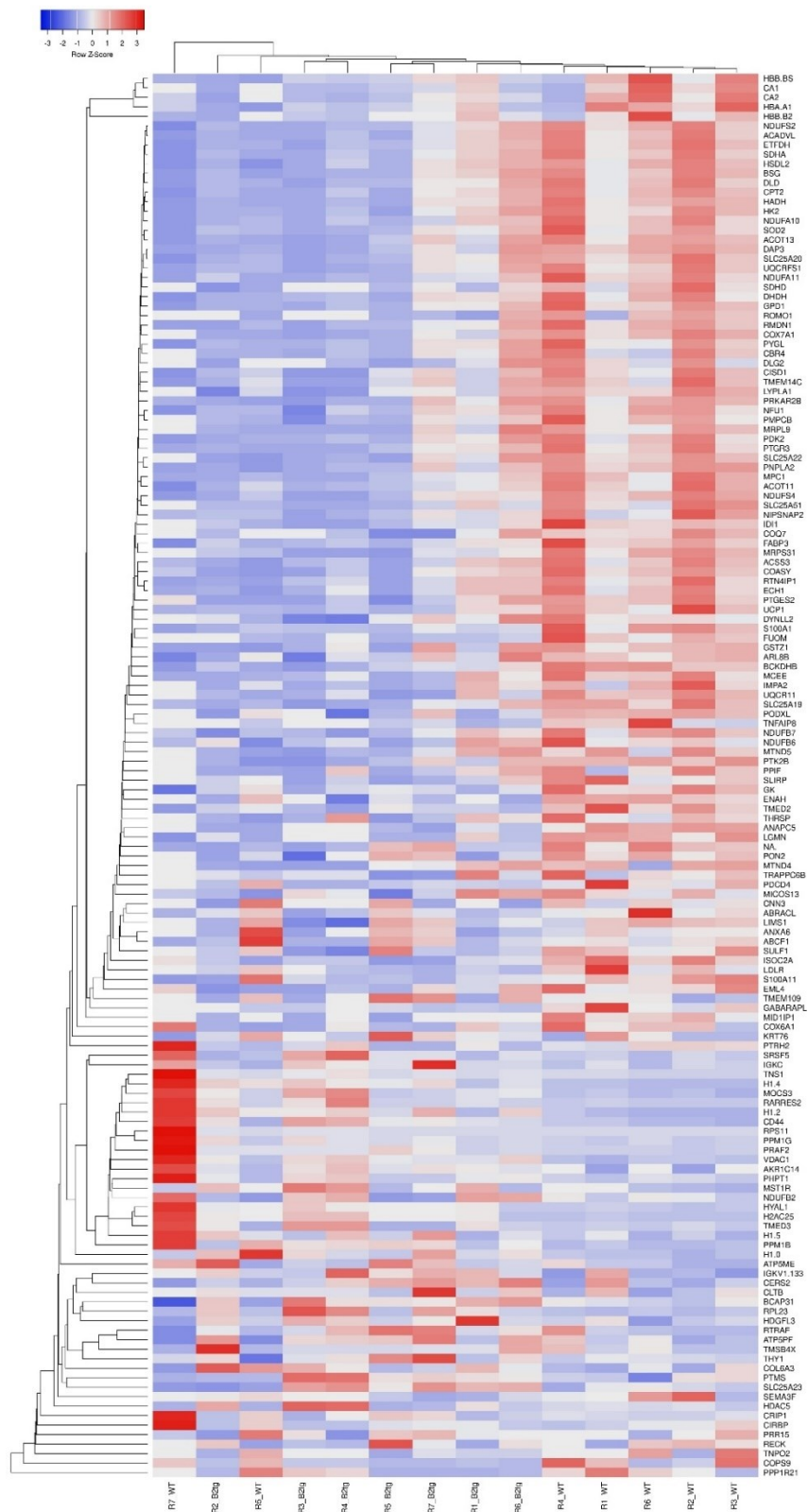


**Figure 47:** Heat map showing hierarchical expression of 148 proteins that were significantly (i.e differentially) up-/down-regulated in aortic tissues of  $B_2^{tg}$  relative to wild-type (WT). The down-regulated proteins are represented in blue, while the up-regulated proteins are represented in red. Colour intensity that represents the degree of protein expression was generated by z-score calculation. Symbols of proteins were listed on rows, and numbers of replicates per group were listed on columns. R1-R7\_  $B_2^{tg}$  and R1-R7\_WT refer to replicate numbers in  $B_2^{tg}$  and wild-type groups respectively. Horizontal dendrogram shows clustering of the proteins and vertical dendrogram shows clustering of the samples with each other.

Endothelial cell markers such as. platelet endothelial cell adhesion molecule and von Willebrand factor (197) were identified in all samples. As shown in Table 8, the expression of both proteins was comparable between groups (P=ns) confirming the presence of a comparable number of endothelial cells between groups.

**Table 8:** Protein expression of endothelial cells markers obtained from proteomic analysis of aortic tissues of B<sub>2</sub><sup>tg</sup> mice relative to wild-type mice.

Protein	Symbol	Abundance Ratio: B <sub>2</sub> <sup>tg</sup> /wild-type	B <sub>2</sub> <sup>tg</sup> group	Wild-type group	P-value
Platelet endothelial cell adhesion molecule	PECAM1	0.82	n=7	n=7	ns
von Willebrand factor	VWF	0.92	n=7	n=7	ns

Statistical analysis was done by Benjamini-Hochberg method.

Proteins related to bradykinin production, such as kininogen 1 and plasma kallikrein, were identified in the aortic tissues. Kininogen 1 is responsible for the production of high molecular weight kininogen, the precursor of bradykinin (198). Plasma kallikrein is involved in the production of bradykinin from high molecular weight kininogen (14). Additionally, some enzymes involved in bradykinin breakdown, such as: angiotensin-converting enzyme, carboxypeptidase N subunit 2, and prolyl endopeptidase, were identified (breakdown of bradykinin is described in section 1.2.1.). The presence of proteins involved in bradykinin production and metabolism confirms the presence of a local KKS in the aorta. As shown in Table 9, there were no significant changes in these proteins (P=ns), indicating that the production and metabolism of bradykinin were unlikely to be influenced by B<sub>2</sub>R overexpression.

**Table 9:** Expression of proteins relevant to bradykinin production or metabolism obtained from proteomic analysis of aortic tissues of B<sub>2</sub><sup>tg</sup> mice relative to wild-type mice.

Protein	Symbol	Abundance Ratio: B <sub>2</sub> <sup>tg</sup> /wild-type	B <sub>2</sub> <sup>tg</sup> group	Wild-type group	P-value
Kininogen-1	KNG1	0.93	n=7	n=7	ns
Plasma kallikrein	KLKB1	0.61	n=4	n=7	ns
Angiotensin-converting enzyme	ACE	0.92	n=7	n=7	ns
Carboxypeptidase N subunit 2	CPN2	0.78	n=6	n=6	ns
Prolyl endopeptidase	PREP	0.87	n=7	n=7	ns

Statistical analysis was done by Benjamini-Hochberg method

The data were screened for the mediators, enzymes, and receptors involved in B<sub>2</sub>R signalling, as described in detail in section 1.2.2. None of these proteins were changed in B<sub>2</sub><sup>tg</sup> mice (P=ns; Table 10).

**Table 10:** Protein expression of mediators involved in bradykinin signalling via bradykinin type-II receptors obtained from proteomic analysis of aortic tissues of B<sub>2</sub><sup>tg</sup> mice relative to wild-type mice.

Protein	Symbol	Abundance Ratio: B <sub>2</sub> <sup>tg</sup> /wild-type	B <sub>2</sub> <sup>tg</sup> group	Wild-type group	P-value
Adenylate cyclase type 5	ADCY5	1.12	n=7	n=7	ns
Adenylate cyclase type 7	ADCY7	0.82	n=6	n=6	ns
Adenylate cyclase type 9	ADCY9	1.06	n=6	n=6	ns
Beta-arrestin-1	ARRB1	1.11	n=7	n=7	ns
Calmodulin-2	CALM2	0.99	n=7	n=7	ns
Calcium/calmodulin-dependent protein kinase	CAMK2D	1.10	n=7	n=7	ns
Cytosolic phospholipase A2	PLA2G4A	0.84	n=7	n=7	ns
Guanylate cyclase soluble subunit beta-1	GUCY1B1	0.81	n=7	n=7	ns
Guanylate cyclase soluble subunit alpha-1	GUCY1A1	1.01	n=7	n=7	ns
Inositol 1,4,5-trisphosphate receptor type 1	ITPR1	1.01	n=7	n=7	ns
Prostaglandin G/H synthase 1	PTGS1	0.94	n=7	n=6	ns
Protein kinase C delta	PRKCA	1.18	n=7	n=7	ns

Statistical analysis was done by Benjamini-Hochberg method.

Regarding the proteins that might be related to blood pressure regulation, a significant reduction in carbonic anhydrase 1 (abundance ratio=0.41, P=4.65E-07) and carbonic anhydrase 2 (abundance ratio=0.48, P=0.00024) was found in B<sub>2</sub><sup>tg</sup> mice (Table 11). Accumulating evidence demonstrated that carbonic anhydrase enzymes are present in vascular cells and their inhibitors enhance blood flow to many organs through a vasodilatory effect (199). The observed reduction in carbonic anhydrase enzymes might be a contributor to the reduction in systolic blood pressure seen in B<sub>2</sub><sup>tg</sup> mice.

**Table 11:** Expression of proteins that may be related to blood pressure regulation obtained from proteomic analysis of aortic tissues of B<sub>2</sub><sup>tg</sup> mice relative to wild-type mice.

Protein	Symbol	Abundance Ratio: B <sub>2</sub> <sup>tg</sup> /wild-type	B <sub>2</sub> <sup>tg</sup> group	Wild-type group	P-value
Carbonic anhydrase 1	CA1	0.41	n=7	n=5	4.65E-07
Carbonic anhydrase 2	CA2	0.48	n=7	n=6	0.00024

Statistical analysis was done by Benjamini-Hochberg method

The Database for Annotation, Visualization and Integrated Discovery (DAVID) was used for gene ontology (GO) annotation of the proteins for biological processes (200, 201). This database provides functional annotation to facilitate the biological interpretation of large lists of proteins by showing enriched proteins in the dataset and their most relevant GO terms. GO annotation could be done for biological processes, molecular functions, and cellular components. According to the required depth of GO, levels from 1 to 5 can be chosen. Due to our interest in biological processes, GO was done only for biological processes with level 3. Functional GO annotation showed significant enrichment (i.e. specifically associated) of proteins related to 77 biological processes in B<sub>2</sub><sup>tg</sup> mice (Table 12). Notably, some of these biological processes are related to endothelial functions such as electron transport chain, cellular lipid metabolic process, reactive oxygen species (ROS) metabolic process, cell migration, and angiogenesis (8, 202). This suggests that B<sub>2</sub>R can influence endothelial functions through these processes

The significantly changed proteins associated with electron transport chain were generally downregulated in B<sub>2</sub><sup>tg</sup> mice (Figure 48). These proteins include NADH-ubiquinone oxidoreductase chain 4, succinate dehydrogenase [ubiquinone] cytochrome b small subunit, cytochrome c oxidase subunit 6A1, and cytochrome b-c1 complex subunit 10, which are related to complex I, complex II; complex III, and complex IV, respectively. These complexes comprise the electron transport chain (203). As shown in Figure 49, most of the significantly changed proteins that are associated with lipid metabolic process were down regulated in B<sub>2</sub><sup>tg</sup> mice. This includes proteins involved in fatty acid oxidation, a secondary source of energy fuel in endothelial cells, such as carnitine O-palmitoyltransferase 2 and very long-chain specific acyl-CoA dehydrogenase (204), which were significantly down regulated. Out of the proteins enriched in the ROS metabolic process, superoxide dismutase [Mn] (SOD2) and mitochondrial brown fat uncoupling protein 1 (UCP1) were significantly downregulated in B<sub>2</sub><sup>tg</sup>

mice (Figure 50). SOD2 is a mitochondrial antioxidant enzyme (205), and UCP1 is a marker of thermogenesis (206). A common protein enriched in both cell migration and angiogenesis, hyaluronidase 1, was significantly upregulated in B<sub>2</sub><sup>tg</sup> mice (Figure 51, Figure 52). Hyaluronidase 1 is a hyaluronan processing enzyme (207). Interestingly, the hyaluronan receptor CD44 (208) was also significantly upregulated in B<sub>2</sub><sup>tg</sup> mice and enriched in cell migration (Figure 51).

The proteomic data introduced several proteins that might be newly connected to B<sub>2</sub>R signalling in the endothelium. Further investigations into each biological process and the associated proteins should be conducted to explore novel mechanisms for B<sub>2</sub>R signalling.

**Table 12:** Functional GO annotation of significantly changed proteins from the proteomic analysis using the Database for Annotation, Visualization and Integrated Discovery. For each GO term, the number of enriched proteins, and P-value are stated.

GO term based on biological process	Number of proteins	P-value
Electron transport chain	19	2.4E-20
Generation of precursor metabolites and energy	29	1.1E-19
Small molecule metabolic process	54	9.1E-18
Oxidation-reduction process	28	6.3E-17
Energy derivation by oxidation of organic compounds	23	6.8E-17
Organophosphate metabolic process	35	1.3E-13
Organonitrogen compound metabolic process	50	2.3E-12
Nucleobase-containing small molecule metabolic process	26	6.4E-12
Carbohydrate derivative metabolic process	32	8.5E-11
Single-organism biosynthetic process	35	2.9E-10
Sulfur compound metabolic process	16	3.8E-8
Phosphorus metabolic process	50	1.2E-7
Organic acid metabolic process	26	1.9E-7
Cofactor metabolic process	16	3.8E-7
Cellular lipid metabolic process	25	5.5E-7
Lipid metabolic process	29	1.3E-6
Reactive oxygen species metabolic process	12	3.8E-6

Cellular oxidant detoxification	5	1.4E-5
Single-organism catabolic process	21	1.4E-5
Single-organism cellular localization	22	2.7E-5
Single-organism transport	43	3.1E-5
Transport	57	4.6E-5
Response to oxidative stress	13	7.1E-5
Response to cold	5	7.7E-5
Thioester metabolic process	6	8.6E-5
Cellular ketone metabolic process	9	1.3E-4
Age-dependent general metabolic decline	2	1.5E-4
Cellular catabolic process	30	3.9E-4
Cellular component disassembly	10	7.3E-4
Response to antibiotic	4	8.1E-4
Intracellular transport	25	9.9E-4
Macromolecular complex subunit organization	27	1.2E-3
Establishment of localization in cell	30	1.3E-3
Organelle organization	47	1.4E-3
Response to toxic substance	6	1.9E-3
Tricarboxylic acid cycle	3	2.0E-3
Organic substance biosynthetic process	63	2.3E-3
Positive regulation of cell motility	12	2.3E-3
Organic substance catabolic process	27	2.9E-3
Positive regulation of cellular component movement	12	3.0E-3
Positive regulation of locomotion	12	3.0E-3
Protein complex biogenesis	18	3.8E-3
Cellular modified amino acid metabolic process	6	3.8E-3
Response to inorganic substance	12	4.5E-3
Cellular biosynthetic process	61	4.9E-3

Single-organism carbohydrate metabolic process	10	5.1E-3
Maintenance of location	8	5.3E-3
Regulation of cell motility	16	5.4E-3
Maintenance of protein location	4	5.7E-3
Response to oxygen-containing compound	26	6.0E-3
Response to organonitrogen compound	16	6.4E-3
Carbohydrate metabolic process	11	7.7E-3
Cellular carbohydrate metabolic process	7	9.0E-3
Regulation of locomotion	16	9.7E-3
Regulation of cellular component movement	16	1.1E-2
Response to ischemia	3	1.2E-2
Cell motility	22	1.3E-2
Maintenance of location in cell	4	1.4E-2
Response to temperature stimulus	5	1.6E-2
Response to oxygen levels	8	1.6E-2
Cellular component assembly	33	1.7E-2
Regulation of sequestering of calcium ion	4	1.9E-2
Cellular nitrogen compound metabolic process	63	1.9E-2
Cell migration	19	1.9E-2
Positive regulation of lipid metabolic process	5	1.9E-2
Positive regulation of vasculature development	5	2.2E-2
Response to nitrogen compound	16	2.4E-2
Angiogenesis	9	2.5E-2
Regulation of localization	32	2.6E-2
Blood vessel morphogenesis	10	2.8E-2
Blood vessel development	11	3.0E-2
Organic cyclic compound metabolic process	58	3.1E-2
Cellular aromatic compound metabolic process	56	3.2E-2

Cellular response to stress	23	3.9E-2
Movement of cell or subcellular component	24	4.0E-2
Homeostatic process	23	4.1E-2
Negative regulation of developmental process	15	4.3E-2

Fisher exact test was used to check the significance that the differentially expressed proteins are specifically associated (enriched) to the GO terms.

### Electron transport chain

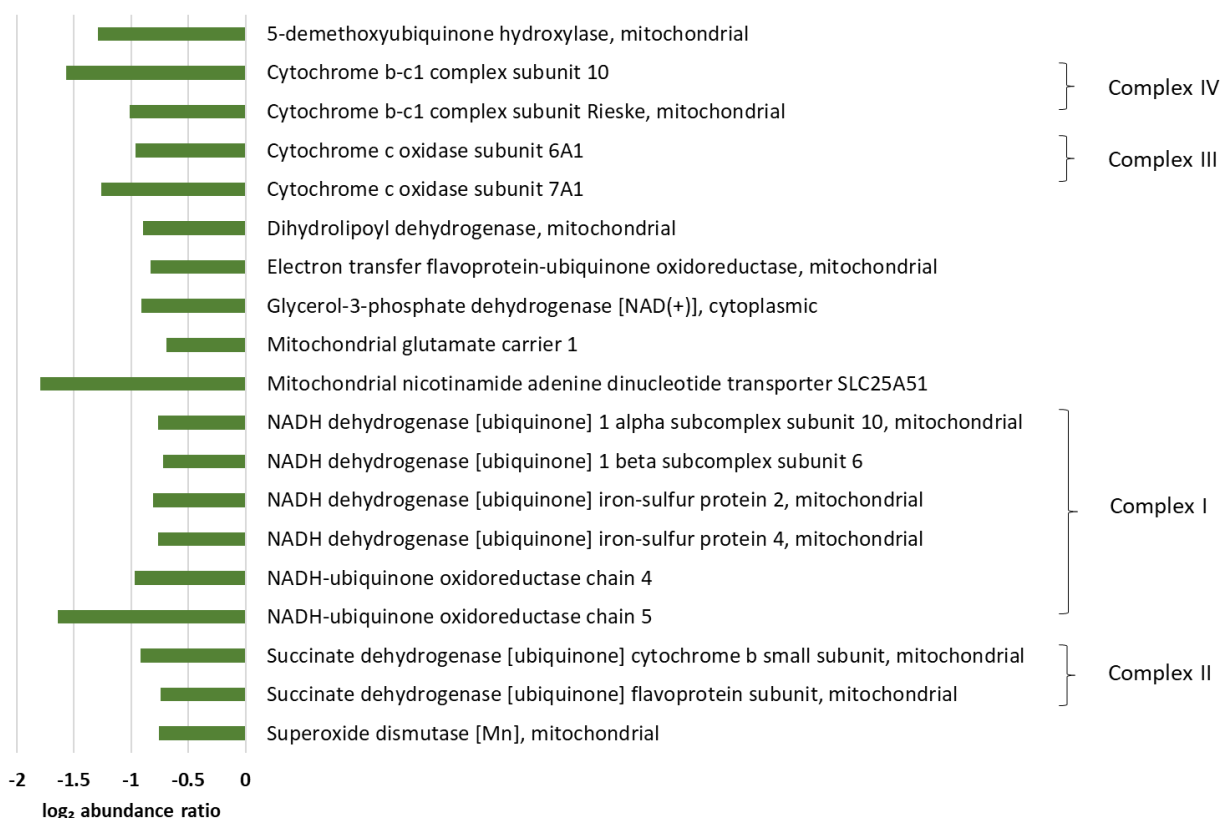


**Figure 48:** Log<sub>2</sub> abundance ratio of proteins enriched to electron transport chain. Red bars indicate upregulation and green bars indicate downregulation.

### Cellular lipid metabolic process

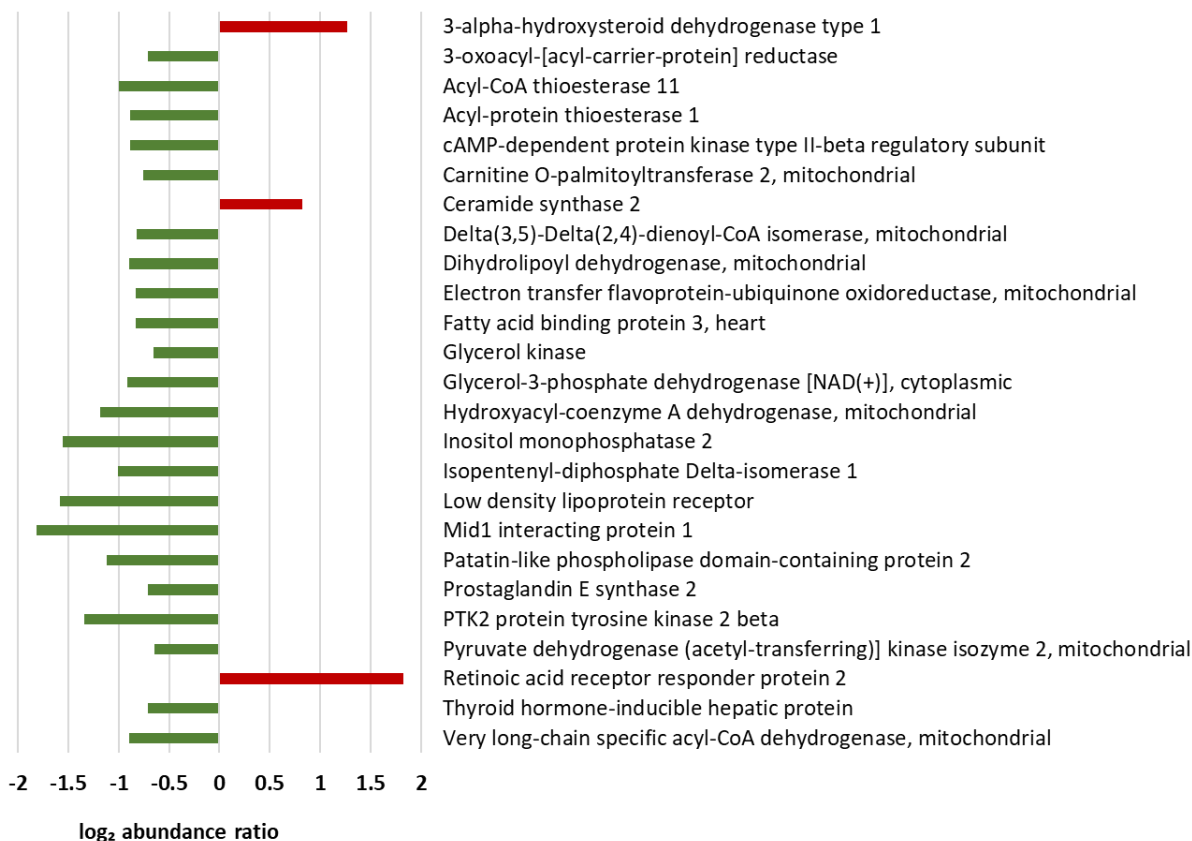


**Figure 49:** Log<sub>2</sub> abundance ratio of proteins enriched to cellular lipid metabolic process. Red bars indicate upregulation and green bars indicate downregulation.

### Reactive oxygen species metabolic process

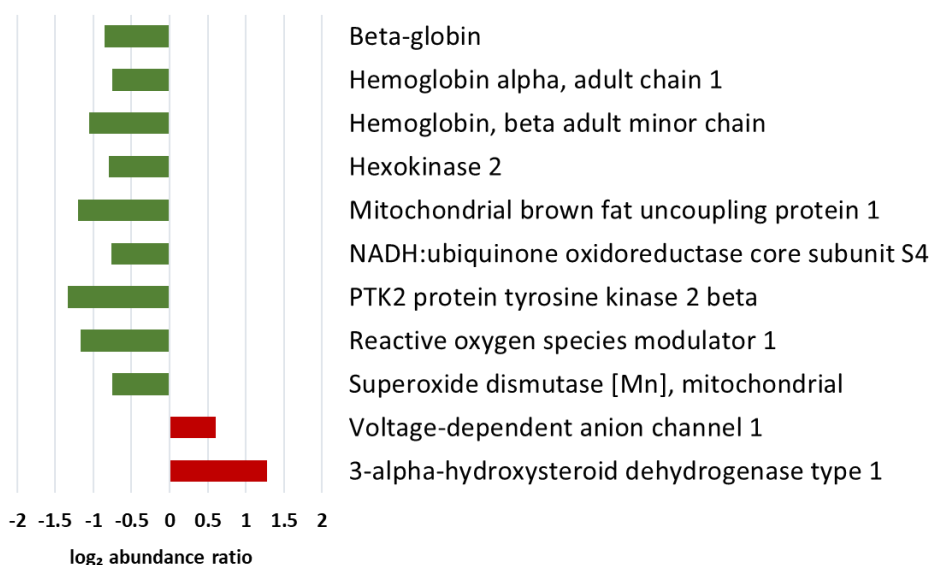


**Figure 50:** Log<sub>2</sub> abundance ratio of proteins enriched to reactive oxygen species metabolic process. Red bars indicate upregulation and green bars indicate downregulation.

### Cell migration

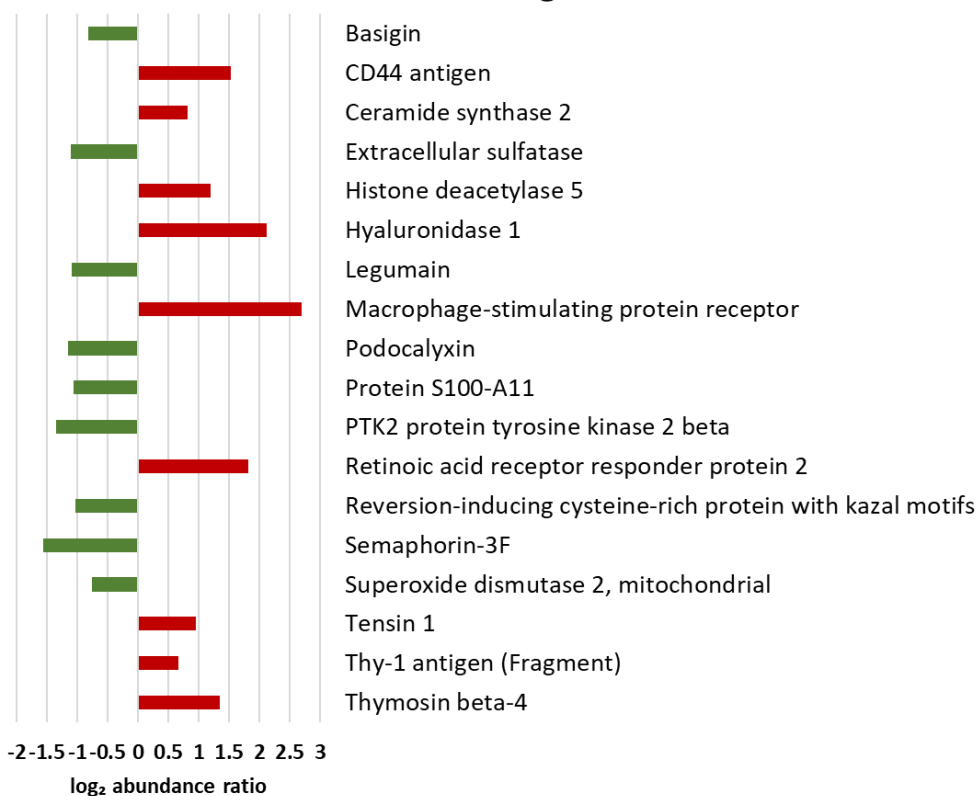


**Figure 51:** Log<sub>2</sub> abundance ratio of proteins enriched to cell migration. Red bars indicate upregulation and green bars indicate downregulation.

### Angiogenesis

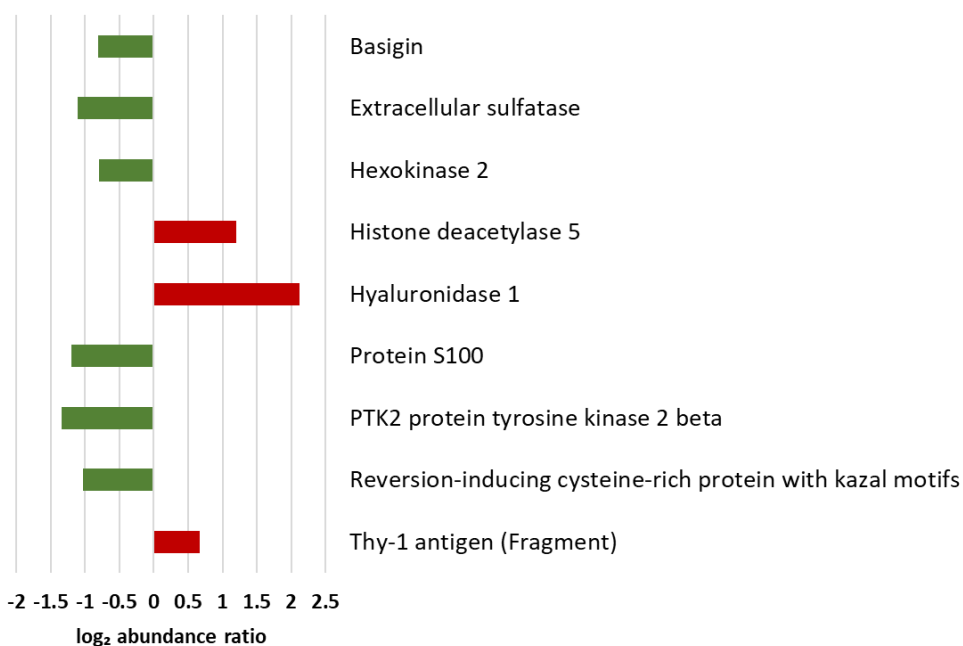


**Figure 52:** Log<sub>2</sub> abundance ratio of proteins enriched to angiogenesis. Red bars indicate upregulation and green bars indicate downregulation.

### 3.9. Sex-specific effects of bradykinin signalling

#### 3.9.1. Vascular reactivity studies

In order to explore the sex-specific effects of vascular bradykinin signalling, aortic rings from male and female mice were stimulated with increasing concentration of bradykinin using organ bath apparatus as explained in section 2.7.2. A set of experiments was conducted in  $B_2^{\text{fl}}$ , where aortic rings from female mice showed non-significant lower concentration-dependent constriction than those of male mice in response to bradykinin,  $P=\text{ns}$  (Figure 53).

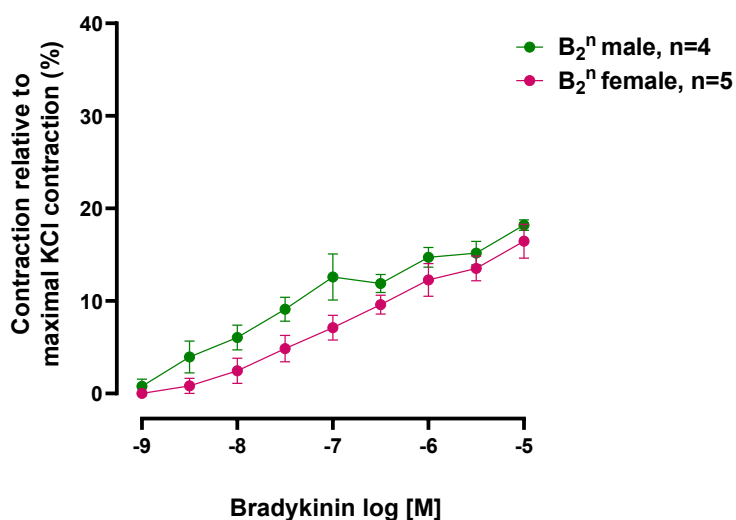


**Figure 53:** Concentration response curve of bradykinin obtained from aortic rings reactivity studies in male and female  $B_2^{\text{fl}}$ . Aortic rings from female  $B_2^{\text{fl}}$  showed slight lower concentration-dependent contraction than those from male mice,  $P=\text{ns}$ , two-way repeated measures ANOVA.

Another set of experiments was then conducted in  $B_2^{\text{tg}}$ , where aortic rings from female mice showed a higher concentration-dependent relaxation than those of male mice in response to bradykinin,  $P=0.013$  (Figure 54). L-NAME abolished the relaxation and even turned it to constriction in both female ( $P=0.002$ ) and male mice ( $P=0.003$ ) (Figure 54), indicating that the bradykinin-induced concentration-dependent relaxation in both aortic rings of female and male mice is fully dependent on NOS enzymes.

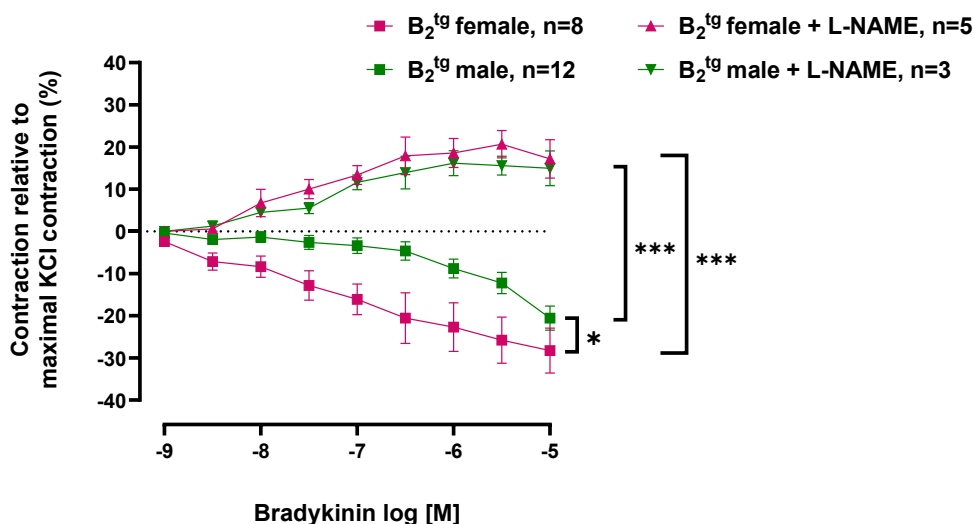


**Figure 54:** Concentration response curve of bradykinin obtained from aortic rings reactivity studies in male and female  $B_2^{tg}$  mice. Aortic rings from female  $B_2^{tg}$  showed more concentration-dependent relaxation than those from male mice,  $*P=0.013$ , two-way repeated measures ANOVA. Preincubation with  $100 \mu\text{M}$  L-NAME was done in some rings for 20 minutes before pre-constriction with  $0.2 \mu\text{M}$  phenylephrine. L-NAME abolished bradykinin-induced vasorelaxation and turned to vasoconstriction in male ( $***P=0.003$ ) and female ( $***P=0.002$ )  $B_2^{tg}$  mice, two-way repeated measures ANOVA.

### 3.9.2. Bradykinin type-II receptors and endothelial nitric oxide synthase gene expression levels in aorta of $B_2^{tg}$ mice

Based on the differential response to bradykinin between male and female  $B_2^{tg}$  mice which was abolished by L-NAME, gene expression levels of human *BDKRB2*, murine *Bdkrb2* and *eNos* was measured in aortic tissues of male and female  $B_2^{tg}$  mice. No significant difference was observed in human *BDKRB2* (male:  $1.0 \pm 0.17$ , female:  $0.6 \pm 0.19$ ,  $n=5-6$  per group,  $P=ns$ ; Figure 55A) and murine *Bdkrb2* (male:  $1.2 \pm 0.35$ , female:  $0.6 \pm 0.09$ ,  $n=5-6$  per group,  $P=ns$ ; Figure 55B) mRNA expression between male and female. These data may suggest that the differential response in vascular reactivity in response to bradykinin is related to a difference in bradykinin downstream signalling per se rather than number of receptors.

Vascular reactivity studies showed that the bradykinin-induced concentration-dependent relaxation in both aortic rings of female and male  $B_2^{tg}$  mice is mediated by NOS enzymes (section 3.9.1.). No difference was observed in *eNos* mRNA expression between male and female  $B_2^{tg}$  mice (male:  $1.0 \pm 0.12$ , female:  $1.0 \pm 0.12$ ,  $n=5-6$  per group,  $P=ns$ ; Figure 55C). Although *eNos* expression did not change at the transcriptional level, changes might still occur at the translational and post-translational levels. Further studies are needed to investigate the sex-specific differences in *eNos* expression across various levels.

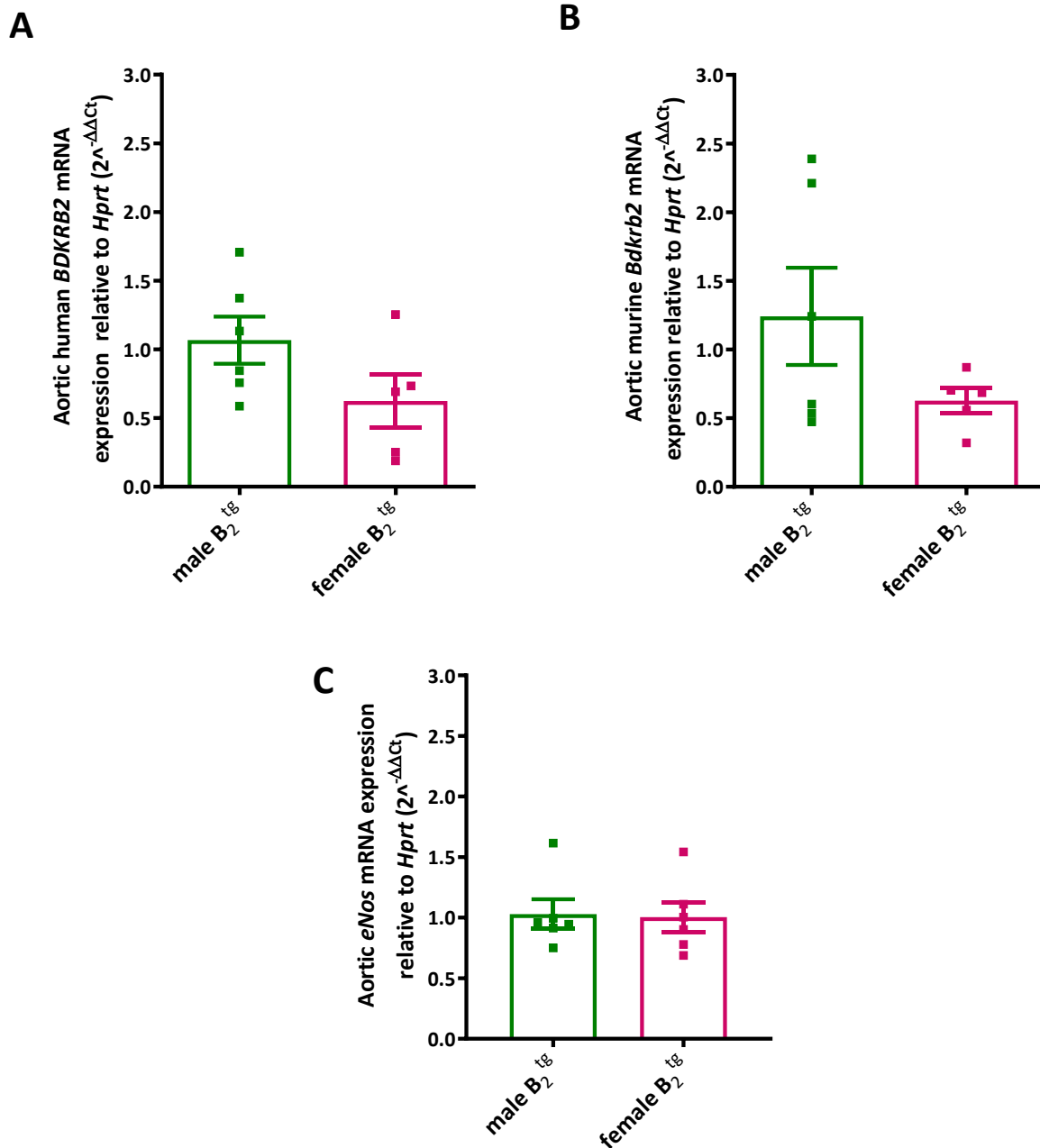


**Figure 55:** RT-qPCR data in aortic tissues of male and female  $B_2^{tg}$  mice. (A) mRNA expression of human *BDKRB2* was not statistically different between male and female mice (male:  $1.0 \pm 0.17$ , female:  $0.6 \pm 0.19$ ,  $n=5-6$  per group,  $P=ns$ ). (B) mRNA expression of murine *Bdkrb2* was not statistically different between male and female mice (male:  $1.2 \pm 0.35$ , female:  $0.6 \pm 0.09$ ,  $n=5-6$  per group,  $P=ns$ ). (C) mRNA expression of *eNos* was not statistically different between male and female mice (male:  $1.0 \pm 0.12$ , female:  $1.0 \pm 0.12$ ,  $n=5-6$  per group,  $P=ns$ ). Statistical analysis was done by unpaired t-test.

## 4. Discussion

Experimental evidence, clinical studies and evidence from ACE inhibitors' activity on bradykinin metabolism have demonstrated beneficial effects of bradykinin signalling via B<sub>2</sub>R. However not all the effects of bradykinin are fully understood, and many underlying mechanisms remain to be elucidated. Thus, the aim of this work is to gain new insights and have a better understanding of the bradykinin actions via B<sub>2</sub>R and the underlying mediators. To accomplish this, cardiac and vascular characterization of endothelium-specific B<sub>2</sub>R overexpression mice model was performed. The vascular characterization of B<sub>2</sub><sup>tg</sup> mice was done at different levels ranging from conductive arteries to resistance arteries. Aorta and external iliac arteries which represent conductive arteries were evaluated by vascular reactivity studies and FMD, respectively. Since total peripheral resistance is one of the determinants of blood pressure regulation, sBP measurements were done to investigate changes in resistance arteries which control the total peripheral resistance (3, 7). The role of endothelial B<sub>2</sub>R in cardiac functions under basal conditions was assessed by echocardiography and by changes in heart rate. On the molecular level, proteomic analysis and western blot were used. In this work, evidence of B<sub>2</sub>R overexpression was shown by RT-qPCR and western blot data. Functional B<sub>2</sub>R overexpression was proven by aortic reactivity studies with bradykinin stimulation.

The main results of this work strongly suggest that endothelial B<sub>2</sub>R play a role in regulating sBP and HR. The observed reduction in sBP does not appear to be dependent on COX and NOS pathways. In contrast, NOS-dependent vasodilation induced by bradykinin could be demonstrated *ex vivo* in aortic rings, while *in vivo* endothelial B<sub>2</sub>R overexpression itself didn't change FMD of external iliac artery. Likewise, endothelial B<sub>2</sub>R didn't affect systolic and diastolic cardiac functions but increased aortic flow velocity under basal conditions. Increased B<sub>2</sub>R expression led to a decrease in eNOS protein expression in conductance arteries but not in resistance arteries. Investigation of differential protein expression in aortic tissues revealed proteins that were not yet known to be associated with B<sub>2</sub>R signalling, namely CD44, HYAL 1 and UCP-1.

### 4.1. Quantification of bradykinin type-II receptors

B<sub>2</sub>R overexpression was quantified on both translational level using western blot and transcriptional level using RT-qPCR. The RT-qPCR data confirmed the presence of human B<sub>2</sub>R exclusively in B<sub>2</sub><sup>tg</sup> mice among various tissues, including aorta and skeletal muscles. Moreover, it was demonstrated that the constitutive murine B<sub>2</sub>R levels in B<sub>2</sub><sup>tg</sup> mice remained unaffected by the insertion of human BDKRB2 gene, thus verifying the overexpression of B<sub>2</sub>R. The later finding is in contrast to transgenic mice with endothelium-specific eNOS overexpression, where the introduction of bovine eNOS decreased the murine eNOS expression (209). The RT-qPCR primers targeting B<sub>2</sub>R are species-specific, enabling differentiation between human and murine B<sub>2</sub>R. In contrast, commercially available antibodies used for western blot to detect B<sub>2</sub>R proteins are not species-specific.

The detection of B<sub>2</sub>R by western blot represents a scientific dilemma for several reasons. First, studies on some commercially available antibodies for GPCRs (such as angiotensin II type-1 receptors, angiotensin II type-2 receptors, histamine H<sub>4</sub>-receptor, and cannabinoid CB<sub>2</sub> receptor) have demonstrated a lack of antibody

specificity (188, 210-212). Second, finding a species-specific antibody capable of distinguishing between human and murine B<sub>2</sub>R is highly challenging due to the nearly 80% homology (calculated using NCBI Blast alignment tool) between murine and human B<sub>2</sub>R (uniprot accession IDs: P32299, P30411). Third, there is inconsistency in the reported number of bands detected for B<sub>2</sub>R via western blot, with some studies reporting a single band and others reporting multiple bands (78, 213-216).

To overcome the challenges mentioned above, two monoclonal B<sub>2</sub>R antibodies (one from mouse and one from rabbit) were analysed. Polyclonal antibodies were generally avoided to minimize nonspecific binding. These antibodies were tested on different cells and mouse tissues. The mouse monoclonal antibody was excluded because anti-mouse secondary antibody bound to proteins in murine tissues and resulted in multiple bands suggesting non-specific binding. Therefore, the rabbit monoclonal antibody was selected for further validation. In human dermal microvascular endothelial cells, a single band was detected, while in murine brain endothelial cells and various tissues from mice, two bands were observed. These observations suggest that the rabbit monoclonal antibody may be species-specific. Of note, both murine and human B<sub>2</sub>R are present in B<sub>2</sub><sup>tg</sup> mice, thus the two bands of murine B<sub>2</sub>R most probably overshadow the single band corresponding to human B<sub>2</sub>R. This could explain the difficulty of differentiation between human and murine B<sub>2</sub>R via western blot in B<sub>2</sub><sup>tg</sup> mice.

## **4.2. Vascular effects of endothelium-specific bradykinin type-II receptors overexpression**

### **4.2.1. Aortic reactivity studies in B<sub>2</sub><sup>tg</sup> mice**

Although B<sub>2</sub>R-KO mice showed impaired aortic relaxation in response to acetylcholine (217), no additional beneficial effect on endothelial function could be demonstrated in B<sub>2</sub><sup>tg</sup> mice as the concentration-dependent vasorelaxation in response to acetylcholine was similar in B<sub>2</sub><sup>tg</sup> and B<sub>2</sub><sup>n</sup> mice. Given that NO mediates acetylcholine-induced endothelium-dependent relaxation in murine aorta (218), it was important to explore whether the endothelium-dependent relaxation in response to acetylcholine is eNOS-dependent or the overexpression of B<sub>2</sub>R alters the signalling pathway in endothelium. Inhibition of NOS by L-NAME abolished the acetylcholine-induced concentration-dependent relaxation in B<sub>2</sub><sup>tg</sup> mice, confirming that endothelium-dependent relaxation in aorta is eNOS dependent.

In early generations of B<sub>2</sub><sup>tg</sup>, bradykinin-induced concentration-dependent vasoconstriction was lower in B<sub>2</sub><sup>tg</sup> than B<sub>2</sub><sup>n</sup> (195). However, in this work where later B<sub>2</sub><sup>tg</sup> generations were investigated, the effect was shifted to a marked vasorelaxation. A plausible explanation for this observation is the elevation in human B<sub>2</sub>R expression over generations which might shift the signalling toward vasorelaxation. This finding validates the vasodilatory effect of bradykinin *ex vivo* and confirms the functional human B<sub>2</sub>R overexpression in aortic vessels of B<sub>2</sub><sup>tg</sup>.

Bradykinin exerted different vascular reactivity effects across different species in *ex vivo* studies. In agreement to the finding from B<sub>2</sub><sup>tg</sup> model with human B<sub>2</sub>R overexpression, rats with B<sub>2</sub>R overexpression showed concentration-dependent relaxation to bradykinin stimulation (219). Moreover, bradykinin-induced vasodilation was shown in rabbit aortic rings and in human and porcine coronary arteries (220-222). While in this work and in previous publications, it was shown that bradykinin elicited concentration-dependent

vasoconstriction in wild-type mice (76, 195), no response in aorta of rats was demonstrated (223). The response to bradykinin-induced vasoreactivity is not only variable across species, but also across vascular beds. In mesenteric arteries of mice, bradykinin elicited vasorelaxant effect (224), whereas in thoracic and abdominal segments of aorta bradykinin elicited vasoconstrictive effect (76, 225, 226). Furthermore, no effect was detected in murine coronary arteries in response to bradykinin (227). In the same manner, bradykinin-induced concentration-dependent vasodilation was shown in mesenteric arteries from rats, while in thoracic aorta from rats no response to bradykinin was noted (223). In porcine coronary arteries and in sheep pulmonary arteries, bradykinin-induced concentration-dependent vasodilation was reported (228-230). Stimulation of porcine aortic endothelial cells with bradykinin induced NO release confirming that endothelium-dependent vasorelaxation by bradykinin is mediated via NO (231). Age also plays a role in vasoreactivity to bradykinin as shown in human and rat mesenteric arteries (223, 232). This may be attributed to a decrease in B<sub>2</sub>R expression with age as shown in a study by Nurmi et al. (233), where it was demonstrated that the senescence process of endothelial cells is associated with downregulation of B<sub>2</sub>R expression. In addition, a decrease in B<sub>2</sub>R expression in myocardial tissues was shown in C57BL/6J mice at 12 and 18 months of age (234), and in rats at 24 months of age (235).

The bradykinin-induced vasorelaxation in B<sub>2</sub><sup>tg</sup> mice is dependent on eNOS because the NOS inhibitor L-NAME abolished vasodilation and even vasoconstriction was shown. This observed vasoconstriction after L-NAME pointing out that bradykinin-induced vasoconstriction can occur via other mediators (such as COX products) in murine aorta (76). To this point, bradykinin appears to exert both vasoconstriction and vasorelaxation and the net observed effect will be attributed to the dominating mediator. In B<sub>2</sub><sup>tg</sup> mice, NO is the dominating mediator and therefore aortic vasorelaxation was observed. Conversely, when NOS signalling pathway is blocked with L-NAME, only then the contractile mediators become dominant exerting vasoconstriction. In line with this finding, bradykinin-induced relaxation was abolished in isolated human mesenteric microvessels pretreated with L-NAME. Additionally, a contractile response, that was reduced by nonspecific inhibition of COX, was observed (232).

#### **4.2.2. Systolic blood pressure measurements**

Studies in rodents and humans, in which bradykinin injections reduced blood pressure, pointed out the blood pressure lowering effect of bradykinin (49, 236). To elucidate this effect and to study the molecular mechanisms in detail, B<sub>2</sub>R-KO and overexpression models were developed. However, the obtained results from these models were contradictory (summarized in section 1.6, Appendix 1.). In this work, sBP of endothelium-specific human B<sub>2</sub>R overexpression mice was evaluated to study the effect of B<sub>2</sub>R specifically overexpressed in endothelial cells on sBP. In the early generations of this mice model, sBP was studied using tail-cuff method by Bisha et al., and there was a profound decrease in sBP in B<sub>2</sub><sup>tg</sup> which was not dependent on eNOS enzymes (195). Whereas in later generations when this work begins, this phenotype was not shown which raised the possibility of presence of genetic drift in the model. Genetic drift refers to the constant tendency of genes to evolve even in the absence of selective forces, this drift is powered by spontaneous neutral mutations that may disappear or become fixed in a population at random (237). This phenomenon was demonstrated in some

models, for instance, loss of previously observed phenotype in a knockout mice model due to spontaneous genetic variations was reported by Ji et al. (238). Compensatory mechanisms were reported in some transgenic mice models, for example, transgenic mice of B<sub>2</sub>R overexpression mice showed compensatory increase of angiotensinogen but no changes in ACE and renin levels (239). In transgenic mice overexpressing endothelin-1, an increase of NO occurred which counteracted the contractile effect of elevated endothelin-1 levels (240). These mice showed comparable sBP to wild-type mice and showed higher sBP only when backcrossed with eNOS knockout mice (241). In this study that was conducted in 2007, the endothelin-1 overexpression/eNOS knockout mice showed higher sBP than eNOS knockout mice, but this effect disappeared with time as reported in another study by the same group in 2015 (242). Adaptive mechanisms in eNOS knockout mice were also reported (243).

To resolve the genetic drift phenomenon, the B<sub>2</sub><sup>tg</sup> mice were backcrossed to the parental strain (C57BL/6J) for two consecutive generations (196, 244). Successfully, the phenotype of decrease in sBP reappeared after that backcross procedure. Worth to mention that the sBP of B<sub>2</sub><sup>n</sup> is about 10 mmHg above the average physiological values (i.e 120 mmHg) which is likely attributed to the variability related to the tail-cuff method (245, 246). To minimize this variability, measurements were done over many days in both groups simultaneously to improve the accuracy of measurements.

The reduction in sBP observed in B<sub>2</sub><sup>tg</sup> mice is around 5-7 mmHg, which is similar to the decrease in sBP following intravenous administration of 1 nmol/kg bradykinin, but less than the decrease seen after intra-arterial administration of the same dose (49). Importantly, our B<sub>2</sub><sup>tg</sup> model differs from studies examining the pharmacological effects of bradykinin, as in our model, only the number of B<sub>2</sub>R was increased without elevating endogenous bradykinin levels.

Icatibant administration normalizes the sBP difference between groups, confirming that the decrease in sBP in B<sub>2</sub><sup>tg</sup> mice is related to B<sub>2</sub>R overexpression. Similar finding was reported in the transgenic mice model established by Wang et al (167). It was shown that icatibant does not influence blood pressure in rats and mice (51, 247). However, icatibant could block the blood pressure lowering effect of bradykinin (109, 248). The i.p. dose of 1 mg/kg of icatibant had been previously administered in mice, demonstrating safety (249).

Mice were administered the non-selective COX inhibitor diclofenac for three days to study the underlying mechanisms of sBP reduction in B<sub>2</sub><sup>tg</sup> mice. Surprisingly, diclofenac administration showed a non-significant decrease of sBP in both B<sub>2</sub><sup>tg</sup> and B<sub>2</sub><sup>n</sup>. Due to the mild sBP decrease after diclofenac administration and the similar percent change of sBP decrease from baseline in both B<sub>2</sub><sup>tg</sup> and B<sub>2</sub><sup>n</sup> mice, it is unlikely that COX-enzymes products play a role in B<sub>2</sub>R mediated decrease of sBP in mice. Results of COX-1 gene deficient mice models regarding effect on BP were heterogeneous. Scotland et al. showed no difference in sBP between male COX-1 gene deficient and wild-type mice (250), while Athirakul et al. reported a trend of lower sBP in COX-1 gene deficient than wild-type mice (251) and Kawada et al. reported high MAP in COX-1 gene deficient during sleep time (252). Considering the other COX isoform, a mice model with reduced COX-2 expression did not show any changes in blood pressure (253). In general, complete disruption of the COX-2 gene led to renal abnormalities and reduced mice viability (254-256). Yang et al. developed three COX-2 gene deficient mice models with

different genetic background strains (129/Sv, C57BL/6, and Balb/C). Elevated sBP was observed in 129/Sv COX-2 gene deficient male mice, but no change in sBP was demonstrated in C57BL/6 COX-2 gene deficient and Balb/C COX-2 gene deficient mice (257).

In our work, inhibition of COX enzymes using diclofenac showed a mild non-significant decrease of blood pressure in mice. A plausible rationale for this observation might be the inhibited generation of vasoconstrictor prostanoids which could play a role in maintaining normal blood pressure in mice. This is in line with the previous finding of our working group that diclofenac inhibited bradykinin-induced vasoconstriction in aorta which suggested that COX enzymes mediated murine aortic constriction (76). Further support for this idea is a study of endothelial-specific COX-1 knockout mice where the authors observed that COX-1 driven products can drive vasoconstriction *in vitro* (258). These observations are different from what is known about human physiology since evidence from clinical trials stated that diclofenac administration causes an increase in sBP (around 5-10 mmHg) especially in hypertensive patients or elderly (259-261).

The contribution of eNOS pathway to sBP decrease in  $B_2^{tg}$  was studied by giving NOS inhibitor L-NAME in drinking water for seven days. As anticipated, the administration of L-NAME led to elevated sBP in both  $B_2^n$  and  $B_2^{tg}$  mice. These findings are consistent with hypertensive outcomes observed in studies involving eNOS knockout mice (262) and L-NAME administration studies (263, 264). Moreover, this observation aligns with results from eNOS overexpression mice models, where transgenic mice exhibited a decrease in blood pressure (209, 265). However, inhibition of endogenous NO synthesis induced a comparable percentage increase of sBP in  $B_2^{tg}$  and  $B_2^n$  suggesting that the decrease in sBP in  $B_2^{tg}$  mice is likely not mediated by the increase of NOS activity. The decrease in HR after L-NAME administration was expected as shown in a previous study by Kojda et al. (266) and is likely attributed to the effect of NO on the sinoatrial node (267).

Bradykinin did not decrease the MAP in male eNOS/COX-1 double KO mice (250) which suggests that the bradykinin-induced decrease in blood pressure might be dependent on these two pathways. However, the results from sBP measurements of  $B_2^{tg}$  mice in our work and from previous work (195) did not support this finding.

The findings obtained from the  $B_2^{tg}$  mice pointed out that the underlying mediators vary depending on bradykinin-elicited effect. For example, in the present work, we demonstrated that bradykinin-induced aortic relaxation in  $B_2^{tg}$  mice is NOS-dependent, unlike bradykinin-induced angioedema (268). Despite the  $B_2$ R mediated sBP decrease in  $B_2^{tg}$  mice was not dependent on COX-derived products, it was proven that COX-derived products play an important role in bradykinin-induced angioedema (269). Furthermore, the bradykinin-induced contraction in murine aorta is dependent on COX-derived products as demonstrated by Khorsavani et al. (76). Among these COX-derived products, thromboxane  $A_2$ , prostaglandin  $H_2$ , prostaglandin  $F_2\alpha$ , and prostaglandin  $E_2$  were identified as endothelium-derived contractile factors (270). These findings suggest that the effects of bradykinin on resistance vessels and conduit vessels are regulated in distinct manners.

In the proteomic analysis of aortic tissues, a significant downregulation of carbonic anhydrase enzymes was observed in  $B_2^{tg}$  mice. Given that inhibiting carbonic anhydrase lowers blood pressure and exhibits vasodilatory properties through the activation of vascular calcium-activated potassium channels, as demonstrated in studies

on the carbonic anhydrase inhibitor acetazolamide (271-273). Therefore, the downregulation of carbonic anhydrase enzymes could contribute to the decrease in sBP in  $B_2^{\text{tg}}$  mice. Furthermore, this finding suggests a possible link between  $B_2$ R signalling and carbonic anhydrase enzymes, which warrants further investigation.

Generally, blood pressure in mice can be measured either by tail-cuff system, fluid-filled catheter system, Millar catheter or telemetry (274). In this work, sBP was measured by the tail-cuff photoplethysmography method which offers several advantages (245). Firstly, it enables non-invasive recording of sBP, ensuring the safety of mice as it eliminates the risks associated with surgical procedures, thereby minimizing the mortality rate. Secondly, it allows for the continuous monitoring of the response to drugs over extended periods. Thirdly, measurements are conducted in conscious mice, mitigating any potential influence of anaesthesia on hemodynamics, and ensuring more accurate physiological representation. It is reported that anaesthetics caused reduction in heart rate, blood pressure and cardiac index (275). However, the tail-cuff method measures peripheral and not central arterial pressure in conductance arteries as measured by other methods. Another aspect is that the blood pressure recordings are done in restrained mice which may add some stress on mice during measurements. Therefore, at least 5 adaptation days were included before the actual sBP measurements were recorded (245, 274). Radiotelemetry is considered the gold standard of blood pressure measurements because it gives a continuous blood pressure measurement over the 24 hours and can be used to monitor blood pressure for many days. On the other hand, the need of surgical procedures to implement the transmitters is associated with a documented failure rate which, together with the high costs, represent limitation for this method. Additionally, the mice need to be housed individually in special housing conditions which are not provided in every animal facility (246).

#### **4.2.3. Flow-mediated dilation**

Brachial FMD is considered a valuable non-invasive tool for evaluating arterial endothelial function in diseases and the response to drugs in clinical trials (184). Likewise, FMD is measured in the femoral artery to assess endothelial function in transgenic mice models (276). The idea of FMD measurements is based on assessing the ability of the vascular endothelium to elicit an increase in vessel diameter after a period of ischemia induced by cuff occlusion of conduit arteries namely brachial or femoral arteries. The vasodilation that occurs after cuff release is caused by the increase of blood flow velocity and the subsequent increase of shear stress (185, 277). The main mediator for FMD in brachial and femoral arteries is NO which is generated by flow-dependent activation of eNOS (278, 279). Some studies reported that EDHF may play a role in FMD, but COX-mediated products are presumably not involved (280-282).

Shear stress has been reported to activate mechanosensors on endothelial cells promoting FMD and GPCRs are proposed endothelial mechanosensors (283). Interestingly, shear stress can stimulate GPCRs independently of ligand binding (284, 285).  $B_2$ Rs in endothelial cells were identified as mechanosensitive GPCRs, where stimulation of  $B_2$ Rs by fluid shear stress led to conformational changes in the receptors (285). Bradykinin exerts protective effects on endothelial function endogenously via NO and prostacyclins (46, 286). In healthy volunteers, infusion of bradykinin in the radial artery preserved endothelial function against ischemia-reperfusion injury, which was induced by occluding the brachial artery with a pressure tourniquet for 20

minutes followed by its release. The endothelial function was assessed by FMD, and the observed protective effect of bradykinin was attributed to its ability to inhibit vasospasm and thrombus formation (287). Intracoronary administration of bradykinin increased both epicardial coronary diameter and coronary blood flow. Interestingly, these effects on coronary blood flow were positively correlated to brachial FMD which was measured in the same patients with suspected coronary artery disease (288, 289). These data highlighted that brachial FMD can be viewed as a surrogate parameter for the bradykinin-induced vasomotor response on coronary endothelial function. In addition to the beneficial effects of bradykinin on endothelial function in ischemia-reperfusion and coronary blood flow, bradykinin can promote angiogenesis in hindlimb ischemia as shown in a number of studies (72, 73, 290, 291).

In this study, FMD values were comparable between  $B_2^{tg}$  and  $B_2^n$ . The maximum increase in FMD was found at 80 seconds after cuff deflation, coinciding with the reported peak of NO, which occurs approximately 45–90 seconds after cuff deflation (292). Based on the knowledge that bradykinin can cause arterial dilation via  $G\alpha_q$  signalling (19), as well as the identification of  $B_2R$  as flow mechanosensors (285), it was expected that FMD would be enhanced in the  $B_2^{tg}$  mice model. However, no improvement of FMD was observed in this mice model, thus the role of  $B_2R$  as mechanosensors is most likely refuted. Several reasons might be suitable to explain this rather unexpected finding. For example, compensatory mechanisms might have happened over time, leading to a change in endothelial mechanosensors and consequently altering the net effect of FMD. Proteomic data showed an increase in expression of CD44 antigen which plays a role in FMD (293) and a decrease in expression of SOD2 which might have affected vasodilatory effect of  $B_2R$  (detailed explanation in section 4.4.1). Additionally, it is possible that heterodimers of different receptors might have been formed, thereby modifying the vascular reactivity to mechanical stimulation (131). It is important to note that the reported beneficial effects of bradykinin were demonstrated after pharmacological administration of bradykinin. In contrast, this study focused on the effect of endothelium-specific  $B_2R$  overexpression, which unlikely increases endogenous bradykinin levels.

### **4.3. Cardiac effects of endothelium-specific bradykinin type-II receptors overexpression**

#### **4.3.1. Heart rate**

A significant decrease of HR in  $B_2^{tg}$  mice was observed using the tail-cuff method. In addition, administration of the  $B_2R$  antagonist icatibant resulted in an increase in HR in both  $B_2^{tg}$  and  $B_2^n$ , indicating a potential influence of  $B_2R$  activity on HR. Furthermore, icatibant abolished the HR difference between  $B_2^{tg}$  and  $B_2^n$ . Taken together, these findings imply a role of  $B_2R$  in HR regulation. The effect of bradykinin on HR via  $B_2R$  is an area of study over years because from its name, bradykinin should elicit bradycardia, as shown after intracarotid injection of bradykinin in dogs (294), and direct injection in lung parenchyma in rabbits (295). Moreover, there was a tendency toward bradycardia after intravenous injection in cats (296). Notably, bradykinin has been identified as a mediator of ischemic preconditioning, contributing to a reduction in the number of ventricular premature beats, and the incidence of ventricular tachycardia and ventricular fibrillation during myocardial ischemia (297). Furthermore, some studies utilizing  $B_2R$ -KO models showed an increase in HR in those mice (151, 154), and the

B<sub>2</sub>R disruption was responsible for an alteration of the autonomic control of HR (298). These findings strengthen the evidence of the role of B<sub>2</sub>R in HR regulation. Turning to evidence from clinical studies, a series of a few patients with hereditary angioedema were described by vagal hyperactivity during the prodromal phase of an acute attack. Since bradykinin is the known main mediator of the hereditary angioedema, the authors justified this increased vagal modulation directed to the sinus node as a possible reflection of the localized bradykinin-mediated vasodilation (299). Nevertheless, some studies in B<sub>2</sub>R-KO mice did not show an effect of B<sub>2</sub>R signalling on HR. For example, in one study lower HR was reported in B<sub>2</sub>R-KO mice (163) and in other study no change in HR was demonstrated in B<sub>2</sub>R-KO mice (152).

Some studies were conducted to explore the possible mechanisms underlying bradykinin-mediated decrease in HR, which could be mediated by cardiac vagal tone modulation. The first findings were reported from studies on isolated hearts from rabbits showing that the negative chronotropic action of bradykinin was mediated by intrinsic cardiac cholinergic neurons (300). Later on, it was found that stimulation of B<sub>2</sub>R in the nucleus ambiguus, which include preganglionic parasympathetic neurons innervating postganglionic parasympathetic neurons in the heart, elicited bradycardia in rabbits (301). In another study in dogs, a negative chronotropic effect of bradykinin related to a direct effect on the sinus node was reported. Of note, the animals were vagotomised and pretreated with a beta blocker to exclude any baroreceptors mediated effects (302). The results of these studies are in line with our finding that endothelial overexpression of B<sub>2</sub>R directly affect the HR and manifested as bradycardia in B<sub>2</sub><sup>tg</sup>.

Although in some studies icatibant did not affect HR (248, 303), in our study icatibant increased HR in mice regardless the B<sub>2</sub>R overexpression. In agreement with this, intravenous icatibant administration in conscious rats and intra-arterial icatibant administration in conscious spontaneously hypertensive rats led to an increase in HR (304, 305). In humans, intravenous icatibant infusion for 6 hours enhanced the increase in HR that was already observed after 1 month administration of AT<sub>1</sub>R antagonist valsartan (306). The discrepancy on the effect of icatibant on HR may be related to differences in routes of administration, doses, use of anaesthesia, and studied species. Therefore, the role of B<sub>2</sub>R in HR regulation should not be rejected.

Noteworthy, the decrease in HR in B<sub>2</sub><sup>tg</sup> mice was not evident in echocardiographic measurements. An explanation for this discrepancy is the HR lowering effect of isoflurane used for anaesthesia (275, 307) which most likely influenced the HR results. It is recommended during the echocardiographic measurements in mice that the heart rate should be kept over 450 bpm to avoid cardio-depression effect of anaesthesia (181). It would have been appropriate to confirm these results with telemetry in conscious mice, however several aspects such as the costs, the necessity for special technical skills and the invasive nature of device implantation precluded the use of telemetry in this work (246).

#### **4.3.2. Echocardiography**

Data regarding the cardiac effects of B<sub>2</sub>R specifically expressed in endothelium is scarce. The use of the B<sub>2</sub><sup>tg</sup> model enabled us to study the impact of endothelium-specific B<sub>2</sub>R on both systolic and diastolic function, as well as aortic valve flow parameters, using non-invasive echocardiography in anesthetized mice. Under basal conditions, no changes were observed in systolic and diastolic functions of 3-4 months old B<sub>2</sub><sup>tg</sup> mice. These

findings are in line with results from B<sub>2</sub>R-KO models in which normal systolic and diastolic functions was demonstrated after disruption of BDKRB2 gene (105, 157, 163). However, this evidence does not rule out the potential benefits of B<sub>2</sub>R pathway on heart functions. It could be that possible protective effects of B<sub>2</sub>R will manifest only in advanced age as seen in 6, 12 and 18 months old B<sub>2</sub>R-KO, which exhibited impairment in cardiac structure and functions (151, 234). Additionally, induction of myocardial ischemia may accelerate the demonstration of the cardioprotective role of B<sub>2</sub>R as shown in the experimental models of myocardial infarction (308-310). In these studies, myocardial ischemia was induced by ligation of left anterior descending coronary artery followed by reperfusion and B<sub>2</sub>R signalling showed protective effects such as reduction of infarct size, decrease in apoptosis of cardiomyocytes and minimizing the impairment in LV systolic function. Moreover, part of the cardioprotective effects of ACEI in heart failure and after myocardial infarction have been attributed to bradykinin via B<sub>2</sub>R because of the decrease in bradykinin breakdown (107, 311, 312). Taken together, the evidence from models of myocardial infarction and studies on ACEI suggests a beneficial impact of B<sub>2</sub>R pathway in pathological conditions. However, in the basal state, the B<sub>2</sub>R overexpression per se didn't show additional benefits on the heart functions in the B<sub>2</sub><sup>tg</sup> model.

Surprisingly, a lower aortic ejection time and a higher aortic valve mean flow velocity were observed in B<sub>2</sub><sup>tg</sup> mice in comparison to B<sub>2</sub><sup>n</sup>. The decrease in aortic ejection time was reflected as an increase in myocardial performance index. Myocardial performance index, the overall cardiac performance index, usually increases when there are changes in LV contractility and/or relaxation, as indicated by an increase in isovolumic contraction time and isovolumic relaxation time respectively (313, 314). The aortic ejection time, also known as LV ejection time, is the time interval from aortic valve opening to aortic valve closure, during which LV ejects blood into aorta (315). Given that all parameters of systolic and diastolic functions are within the normal range, the rise in myocardial performance index is most likely attributable to the decrease in aortic ejection time. Generally, potential causes of decrease in aortic ejection time are an acute decrease in preload, an increase in afterload or an impaired systolic function as in heart failure with reduced ejection fraction (315). It is highly probable that the decrease in aortic ejection time is associated with the increase in aortic flow velocity. Two possible explanations can account for the observed rise in aortic flow velocity. First one is that the endothelium-specific B<sub>2</sub>R overexpression led to structural changes in the aortic valve, that subsequently affected the aortic ejection time and the blood flow velocity through the valve. Another less likely explanation is that the overexpression of B<sub>2</sub>R directly impacts blood flow velocity without affecting the valve's structure.

Valvular cusps are enveloped by an endothelial layer composed of valvular endothelial cells. The calcification of valves occurs due to dysfunction of this layer, resulting in endothelial to mesenchymal transition (EndMT) of valvular endothelial cells to myofibroblastic cells and endothelial-derived valvular interstitial cells (316). The response of the endothelial layer in aortic valves to bradykinin stimulation has been demonstrated in human and porcine valve allografts (317, 318), where prostacyclin levels increased with bradykinin stimulation. An increase in angiotensin-converting enzyme expression (319), and in neutral endopeptidase activity (320) which are responsible for bradykinin breakdown, were reported in studies investigating pathophysiologic mechanisms of aortic valve calcification. Furthermore, an increase in B<sub>2</sub>R expression was shown in aortic valves obtained from patients with aortic valve stenosis during valvular replacement therapy (320). Interestingly, in the same

study, stimulation of isolated myofibroblasts with bradykinin led to a decrease in the expression of collagen I and III, suggesting an antifibrotic effect of bradykinin.

An important aspect to mention is that the observed increase in mean aortic blood flow velocity falls within the physiological range that is totally distant from the values reported in pathological aortic stenosis models (2000-4000 mm/sec) (321-323). These findings only pointed out a potential role of endothelial B<sub>2</sub>R in regulation of aortic valve functions, and therefore, it could be a target in calcific aortic valve disease, as reviewed by Peltonen et al. (324). To further investigate the role of B<sub>2</sub>R in aortic valve functions, it would be beneficial to apply the aortic stenosis model using B<sub>2</sub><sup>tg</sup> mice. Additionally, the age of the mice should be taken into consideration, as more prominent effects may be manifested in advanced age (18 months old) (325) which match the elderly population in which aortic valve diseases are most commonly occurring (326).

#### **4.4. Expression of proteins relevant to bradykinin type-II receptors signalling**

##### **4.4.1. Proteomics data**

Proteomic analysis conducted on aortic tissues from B<sub>2</sub><sup>tg</sup> mice did not introduce additional knowledge about changes in proteins related to blood pressure regulation. However, it revealed changes in several proteins associated with various endothelial functions such as angiogenesis, cell migration, cellular lipid metabolic process, reactive oxygen species metabolic process and electron transport chain (Figure 56). These findings could be directly associated to endothelial B<sub>2</sub>R signalling because of endothelium-specific B<sub>2</sub>R overexpression in B<sub>2</sub><sup>tg</sup> mice.

Kininogenin 1 and plasma kallikrein, proteins involved in bradykinin production, were not significantly changed in B<sub>2</sub><sup>tg</sup> mice. This finding did not denote unchanged bradykinin levels in B<sub>2</sub><sup>tg</sup> mice but might indicate that the production of bradykinin was unlikely to be influenced by B<sub>2</sub>R overexpression.

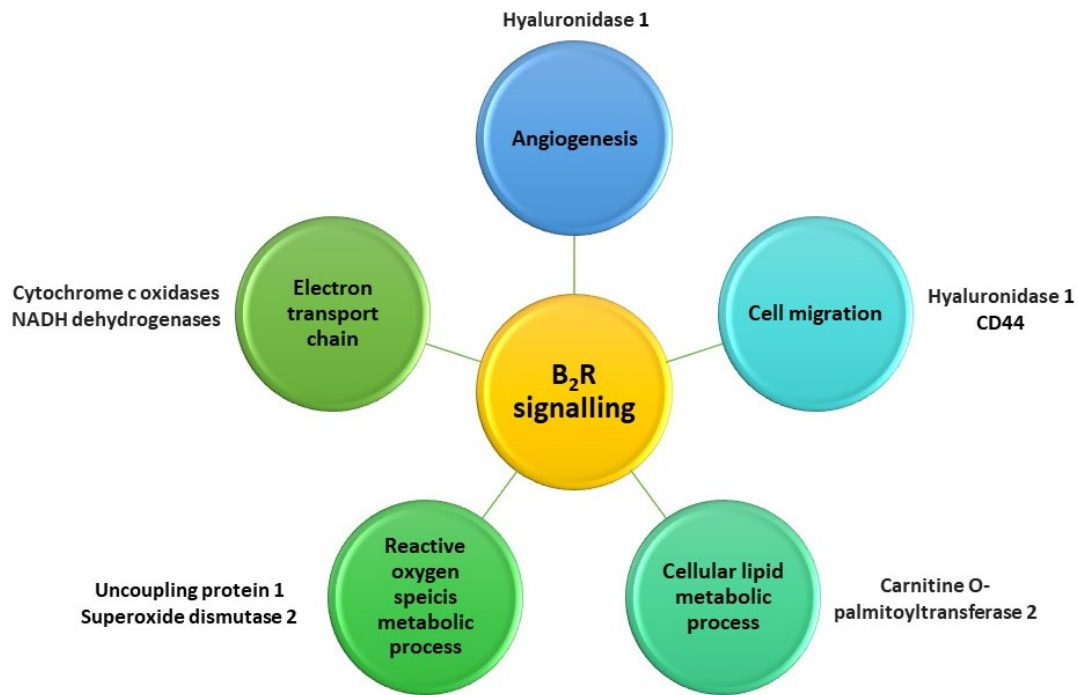


**Figure 56:** Diagram summarizing potential relation between bradykinin type-II receptors ( $B_2R$ ) signalling and biological processes (and exemplary proteins) related to endothelial functions based on proteomic data analysis.

### Angiogenesis and cell migration

Angiogenesis and cell migration are closely related processes that often occur simultaneously in the context of endothelial function and cardiovascular disease. Endothelial cells undergo migration and proliferation, which are fundamental processes for the formation of new blood vessels (327). Bradykinin has been shown to promote angiogenesis via VEGF in tumours such as prostate and cervical cancer (87, 88, 328). Furthermore, bradykinin is known to promote cell migration (83, 329, 330), although its precise role in regulating endothelial functions is not fully understood.

Proteomic data revealed changes in proteins that could be associated with  $B_2R$  mediated angiogenesis and cell migration, one of these proposed proteins is a hyaluronan processing enzyme, HYAL1. Increased expression of HYAL1 has been shown to promote angiogenesis in tumours by providing hyaluronan oligomers (207, 331). Another promising protein which was significantly upregulated in  $B_2^{tg}$  mice is CD44, a receptor for several extracellular matrix components, including hyaluronan. CD44 mediates various effects in both physiological and pathological conditions. CD44 plays a role in angiogenesis, cell migration and heart repairing mechanisms after myocardial infarction (208, 332, 333). While CD44 has been implicated in the development of atherosclerosis (208), a recent study reported that hyaluronan/CD44 interaction contributes to collateral artery formation after hindlimb ischemia (293). Therefore, the observed change in CD44 levels in  $B_2^{tg}$  mice would be better interpreted within the context of specific pathological conditions.

### Cellular lipid and reactive oxygen species metabolic processes

Proteomic data showed enrichment of proteins associated with reactive oxygen species and cellular lipid metabolic processes in  $B_2^{tg}$ . Alteration of these processes can improve endothelial function or lead to endothelial dysfunction (8). Therefore, these findings argue for the association of  $B_2R$  signalling and modulation of endothelial function.

The association between bradykinin and lipid metabolism has not received much attention, except for few studies like that conducted by Mount et al. that suggested that bradykinin may have an impact on endothelial lipid metabolism, opening a new pathway for  $B_2R$  on endothelial cell function (334). Carnitine O-palmitoyltransferase 2 (CPT2), an enzyme that plays a role in fatty acid oxidation, was differentially downregulated in  $B_2^{tg}$  mice. Fatty acid oxidation is a secondary source of energy fuel in endothelial cells and it was demonstrated that fatty acid oxidation is an important process maintaining endothelial cell functions and can affect the endothelial to mesenchymal transition and heart valves thickening (335). The differential downregulation of CPT2 may indicate an initial deleterious structural change in the aortic valve. This could justify the observed increase in aortic valve mean velocity. However, further investigations are required to confirm these findings.

The observed changes in expression of several proteins related to ROS metabolic process in  $B_2^{tg}$  mice is not unexpected as the effect of bradykinin on ROS was previously investigated in many studies. Overall, the effect of bradykinin on ROS regulation appears to be contradictory in different types of cells. In rat aortic smooth muscle cells, an increase in oxidative stress proteins was demonstrated after stimulation with bradykinin (336). In contrast, upregulation of ROS scavenging enzymes (SOD) and downregulation of ROS generation enzymes (NADPH oxidases) were observed after stimulation of rat cardiomyocytes with bradykinin (337). Moreover, increased oxidative stress was shown in the hearts of 18 months old and 2-3 months old  $B_2R$ -KO mice, suggesting a role of  $B_2R$  against ROS (234, 338). In our work, a differential downregulation in SOD2 was found in  $B_2^{tg}$  mice. This finding is in line with the increase in ROS production in Apo-E KO/  $B_2R$  overexpression mice (339). The finding from the ApoE-KO/  $B_2R$  overexpression mice may indicate that the role of  $B_2R$  on ROS modulation is disease-dependent. This is due to the overexpression of  $B_2R$  in the ApoE-KO model, which serves as a model of atherosclerosis, resulted in an increase of the ROS production rather than a decrease.

A plausible explanation behind the decrease in SOD2 protein expression in  $B_2^{tg}$  mice could be an increase in heterodimerization of  $B_2R$  with  $AT_1R$  which might enhance  $AT_1R$  signalling and consequently resulted in a decrease in SOD2. This heterodimerization might be triggered by the increased of number of  $B_2R$  in  $B_2^{tg}$  mice. It is known that heterodimers of  $B_2R$  and  $AT_1R$  sensitize and enhance the  $AT_1R$  signalling, and the dimer formation between these receptors was evident in pre-eclampsia and upon stimulation with endotoxin (131, 186, 340, 341). Importantly, the decrease in SOD2 protein expression might partially explain the unexpected absence of improvement in FMD in  $B_2^{tg}$  mice, as it has been shown that inhibition of SOD impairs bradykinin-induced relaxation (342).

Another associated protein with ROS metabolic process that was significantly downregulated in  $B_2^{tg}$  mice is UCP1. UCP1 is highly expressed in mitochondria of brown adipocytes and mediates heat production (206).

A recent study found that bradykinin induces brown adipose tissue thermogenesis via B<sub>2</sub>R and increases UCP1 expression in adipose tissue (249).

The observed decrease in protein expression of SOD2 and UCP1 in B<sub>2</sub><sup>tg</sup> mice might indicate a potentially adverse impact on endothelial function rather than a beneficial one. It's crucial to interpret these findings cautiously, considering that this effect resulted from increase of B<sub>2</sub>R activity in B<sub>2</sub><sup>tg</sup> rather than a direct pharmacological effect of bradykinin. Nevertheless, these results contribute to our understanding of the putative role of B<sub>2</sub>R signalling in modulating oxidative stress.

#### **Electron transport chain**

Mitochondrial respiratory chain complex comprised of NADH dehydrogenase (complex I), succinate dehydrogenase (complex II), cytochrome c reductase (complex III), cytochrome c oxidase (complex IV), and ATP synthase (complex V) (203). Through this chain a series of electron transfer reactions occur to generate ATP via oxidative phosphorylation and ROS as a byproduct (343). Decrease in oxidative phosphorylation and mitochondrial dysfunction is linked to atherosclerosis and cardiac hypertrophy (344, 345). Surprisingly, proteomic data showed a decrease in proteins related to electron transport chain in B<sub>2</sub><sup>tg</sup> which might be a sign of mitochondrial dysfunction. It has been shown that bradykinin induces an increase of calcium concentration in mitochondria of bovine endothelial cells (346) and the elevation of intramitochondrial calcium concentration with depletion of cellular ATP was further increased by bradykinin and led to loss of mitochondrial membrane potential (347). In addition, bradykinin modulates mitochondrial permeability transition pore opening (348). Deletion of BDKRB2 gene led to an increase in mitochondrial oxidative phosphorylation genes in skeletal muscles (349) and promoted age-induced mitochondria structural changes and dysfunction in cardiomyocytes (234). It is worth mentioning that changes in proteins relevant to the electron transport chain may have prevented the beneficial effects of B<sub>2</sub>R in the heart from being demonstrated. However, this did not result in any deleterious effects as the systolic and diastolic functions were preserved in B<sub>2</sub><sup>tg</sup> and were comparable to those of the negative littermates. Moreover, these findings are related to changes of proteins in the aorta and not reflecting protein changes in heart.

In general, proteomic data is exploratory rather than conclusive. It sheds light on new proteins that might be related to B<sub>2</sub>R signalling pathway and the associated biological processes which are known to be regulated by B<sub>2</sub>R. Moreover, proteomic analysis was done in aortic tissues under basal conditions and without bradykinin stimulation. It is worthwhile to evaluate each pathway separately with its relevant proteins in B<sub>2</sub><sup>tg</sup> model under pathological conditions to get deeper insight into the benefits of B<sub>2</sub>R and, consequently, the modulation of B<sub>2</sub>R activity as a therapeutic target.

#### **4.4.2. Protein expression of endothelial nitric oxide synthase**

Despite the established role of bradykinin in inducing an increase in eNOS activity (42, 350), the detailed regulation of B<sub>2</sub>R on eNOS protein expression is still under study. On molecular basis, bradykinin increases eNOS activity via increase intracellular calcium in endothelial cells by activation of calcium/calmodulin-dependent kinase II, increase calcium/calmodulin association, increase in Ser1177 phosphorylation and Thr497 dephosphorylation of eNOS (351-353). In line with this, stimulation of B<sub>2</sub>R using bradykinin or Maximakinin

(a potent B<sub>2</sub>R agonist), increased phosphorylation of eNOS at Ser1179 (bovine sequence) and Ser1177 respectively via activation of PI<sub>3</sub>K/AKT (354, 355). Furthermore, in an *in vitro* vascular cell co-culture model (combined human coronary artery endothelial cells, vascular smooth muscle cells, and myoendothelial junctions), stimulation of endothelial cells with 10 μM bradykinin increased phosphorylation at ser1177 position of eNOS found on apical side of endothelial cells. However, no effect was observed on eNOS found on basal side of endothelial cells which is related to myoendothelial junctions (356).

Increase in forearm blood flow in response to bradykinin infusion in humans is partially mediated by NOS (357, 358). NO mediates several bradykinin-induced effects such as protection of the arterial endothelial function in ischemic/reperfusion injury, recruitment of progenitor cells in angiogenesis, and stimulation of cell uptake of glucose (75, 287, 359). Not all the bradykinin-provoked vascular effects are mediated via NO, some studies showed that bradykinin-induced angioedema is not mediated by eNOS (76, 268). An *ex vivo* study showed that bradykinin-induced relaxation of efferent arterioles from rabbit kidneys is not NO mediated (360). Moreover, when NOS and COX enzymes were inhibited in porcine coronary artery segments, bradykinin relaxation was mediated by EDHF (361). In our work, it has been shown that bradykinin induced aortic relaxation via eNOS enzymes, whereas the decrease in sBP observed in B<sub>2</sub><sup>tg</sup> mice was not eNOS dependent.

A significant reduction of eNOS protein expression in aortic tissues of B<sub>2</sub><sup>tg</sup> mice was detected, while the eNOS protein expression was not changed in either myocardial or skeletal muscle tissues of B<sub>2</sub><sup>tg</sup> mice. Difference in findings among various tissues can be attributed to the difference of eNOS expression in different vascular beds (362). The decrease of eNOS protein expression in aortic tissues of B<sub>2</sub><sup>tg</sup> mice may represent a compensatory physiological response triggered by stimulation of overexpressed B<sub>2</sub>R. In line with this finding, Vaziri et al. showed that sustained activation of human coronary endothelial cells with bradykinin for 24 hours resulted in decrease of eNOS expression (363). In addition, aortic nitrate levels were lower in ApoE-KO/B<sub>2</sub>R overexpression mice in comparison to ApoE-KO mice suggesting that B<sub>2</sub>R overexpression has an impact on nitric oxide bioavailability (339).

Although the 0.38-fold reduction of eNOS protein expression in the aorta of B<sub>2</sub><sup>tg</sup> mice was statistically significant, its impact on functional outcomes are likely limited, as numerous post-translational modifications of eNOS exist and can either enhance or diminish the enzyme activity (193). The preserved function of aortic endothelium was confirmed by acetylcholine-induced concentration-dependent relaxation in aortic reactivity studies (section 3.4.1.). Similar findings were reported recently in arginase-1 deficient mice, where the downregulation of aortic eNOS protein expression did not affect the endothelial function (364). Furthermore, in a transgenic mice model expressing eNOS only in the vascular endothelium (eNOS-Tg/KO), that was generated by endothelial-specific targeting of bovine eNOS in eNOS-deficient mice, a reduction in aortic eNOS expression did not reduce the endothelium-dependent relaxation in aortic rings (365).

#### **4.4.3. Protein expression of p-ERK1/2/ERK1/2**

Bradykinin induced an increase in the phosphorylation of ERK1/2 in aortic tissues of both wild-type and B<sub>2</sub><sup>tg</sup> mice. This finding aligns with previous cell culture studies, which suggested that phosphorylation of ERK1/2 plays a role in various bradykinin effects, including migration, inflammation, permeability, proliferation,

angiogenesis, and vasodilation (45, 291, 354, 366, 367). Most studies investigating the p-ERK1/2 pathway have focused on one specific cell type such as endothelial cells and smooth muscle cells (366, 368, 369). In contrast, in our study stimulation with bradykinin was done *ex vivo* on aortic tissues encompassing both endothelial cells and smooth muscle cells (370). This argues for the presence of this downstream pathway in aortic tissues that represent different types of cells. This finding demonstrates that phosphorylation of ERK1/2 is one of the downstream signalling mechanisms for some of the bradykinin effects via B<sub>2</sub>R in the aortic tissues in B<sub>2</sub><sup>tg</sup>.

#### 4.5. Sex-specific difference in response to bradykinin

Although there isn't much knowledge on the sex-specific vascular effects of bradykinin, one study showed a difference in pituitary B<sub>2</sub>R expression. The authors reported that the difference in B<sub>2</sub>R expression had an impact on prolactin secretion (371), suggesting that B<sub>2</sub>R signalling might have differential effects in males and females.

Aortic reactivity in response to bradykinin was studied in aortic rings from male and female mice. In B<sub>2</sub><sup>tg</sup>, bradykinin-induced vasorelaxation was more prominent in aortic rings of females than males, additionally in B<sub>2</sub><sup>n</sup>, rings of females showed lower bradykinin-induced vasoconstriction than those from males. These findings are consistent with results from omental tissue and subcutaneous fat vessels that showed more vasodilation to bradykinin in premenopausal women than men (372). Importantly, the measured B<sub>2</sub>R mRNA expression was comparable between males and females which refutes the speculations that the underlying cause in variability between genders in response to bradykinin stimulation is related to difference in B<sub>2</sub>R expression. Moreover, the *eNos* mRNA expression was comparable between males and females; however, this finding couldn't exclude post-translational changes that might have occurred. This sex-specific effect might be related to oestrogen effects which is known to increase the release of NO and decreasing ACE-induced degradation of bradykinin (373).

#### 4.6. Limitations and future recommendations

In the present study a unique mice model with endothelium-specific B<sub>2</sub>R overexpression was used to gain new insights about the effects of B<sub>2</sub>R on various cardiovascular and endothelial functions. To provide a comprehensive understanding of the endothelial B<sub>2</sub>R pathway, various techniques were employed, including echocardiography, FMD, tail-cuff method, vascular reactivity studies, and proteomic analysis. However, it is important to emphasize that the scope of this work was limited to studying the role of B<sub>2</sub>R in the basal conditions, rather than the pathophysiological ones. It would be useful to crossbreed the B<sub>2</sub><sup>tg</sup> mice with knockout models of various genes related to vascular functions or to induce pathological conditions such as myocardial infarction, LV hypertrophy, heart failure, or hypertension. These models would provide an opportunity to gain novel insights into the interactions among multiple pathways and may provide knowledge about potential benefits of B<sub>2</sub>R in CVDs.

It is worth mentioning that the accurate quantification of bradykinin levels is difficult due to the presence of various preanalytical variables that may compromise measurement accuracy (374). Therefore, bradykinin levels were not measured in this study. However, data from proteomic analysis may provide an indication that a change in bradykinin production was unlikely. To increase bradykinin levels in B<sub>2</sub><sup>tg</sup> mice and evaluate the

consequences of chronic B<sub>2</sub>R activation, a study using ACEI should be conducted. The present work focused on investigating the NOS and COX signalling, rather than the EDHF signalling, of the B<sub>2</sub>R pathway due to the difficulty in addressing the EDHF signalling. Investigating the EDHF signalling is challenging due to insufficient evidence about the safety and efficacy of EDHF inhibitors *in vivo*.

## Summary and Conclusions

This study investigated the role of endothelium-specific B<sub>2</sub>R on various cardiovascular functions using endothelium-specific B<sub>2</sub>R overexpression mice. The following conclusions were driven:

- Endothelium-specific B<sub>2</sub>R overexpression decreases systolic blood pressure and heart rate. The reduction in systolic blood pressure is potentially attributed to the decrease in heart rate.
- Endothelium-specific B<sub>2</sub>R overexpression does not affect systolic and diastolic functions but is associated with an increase in aortic flow velocity under basal conditions.
- Endothelium-specific B<sub>2</sub>R overexpression doesn't have a favourable effect on flow-mediated dilation under basal conditions.
- Difference in response to bradykinin between male and female mice in aortic reactivity studies suggests sex-specific effects in bradykinin signalling.
- Endothelium-specific B<sub>2</sub>R signalling is involved in various biological process related to endothelial functions such as angiogenesis, cell migration, ROS modulation, electron transport chain, and lipid metabolism in B<sub>2</sub><sup>tg</sup> mice. Further studies are required to elucidate the specific underlying mechanisms and mediators.
- Bradykinin-induced relaxation in aorta is eNOS-dependent.

Despite several differences observed in isolated tissues, *in vivo* only blood pressure and heart rate were significantly reduced. These data confirm that activation of endothelial B<sub>2</sub>R signalling, as accomplished by endothelium-specific overexpression of B<sub>2</sub>R, contributes to blood pressure regulation. Further studies should be carried out to determine whether the other changes in the cardiovascular system observed in B<sub>2</sub><sup>tg</sup> mice may have a positive impact on the progression of hypertension, coronary artery disease or heart failure.

## Summary

Cardiovascular diseases (CVDs) continue over many years now to be one of the leading causes of death worldwide. Exploring new pathways in pathogenesis of CVDs is necessary to guide the development of new therapeutic agents to decrease mortality and morbidity among patients with CVDs. Hypertension is a prominent risk factor for most CVDs.

Bradykinin is an endogenous peptide exerting vasodilation on blood vessels through acting on bradykinin type-II receptors (B<sub>2</sub>R). This vasodilatory effect is thought to be mediated by nitric oxide (NO), prostacyclin and endothelium derived hyperpolarizing factor (EDHF). Evidence about role of B<sub>2</sub>R in blood pressure control came from bradykinin administration *in vivo*, B<sub>2</sub>R knockout (B<sub>2</sub>R-KO) models and studies on Angiotensin-Converting Enzyme Inhibitors (ACEI) where bradykinin levels increased following ACEI administration. However, results from B<sub>2</sub>R-KO models weren't confirmatory and the B<sub>2</sub>R effects remains incompletely characterized.

Therefore, B<sub>2</sub>R signalling, particularly in endothelium, was thoroughly investigated in this work to get new insights about vascular and cardiac effects of B<sub>2</sub>R pathway, in addition to the underlying mediators for these effects. To achieve this, an endothelium-specific human B<sub>2</sub>R overexpression mice model (B<sub>2</sub><sup>tg</sup>) was used.

Vascular reactivity studies were done with the aim of testing the responsiveness to bradykinin of aortic tissues to illustrate its vasodilatory effects and to understand the underlying mechanisms. Hemodynamic measurements [systolic blood pressure (sBP) and heart rate (HR)] of B<sub>2</sub><sup>tg</sup> mice were measured by the tail-cuff method to investigate the systemic effects of B<sub>2</sub>R overexpression. A flow-mediated dilation (FMD) study was conducted to assess endothelial function in conduit blood vessels, to explore the proposed role of B<sub>2</sub>R as mechanosensors and their ability to induce vasodilation in response to increased blood flow. Cardiac systolic and diastolic functions under basal conditions were assessed by echocardiography. To gain new insights about novel proteins and biological processes related to B<sub>2</sub>R signalling, proteomic analysis was performed on aortic tissues.

Bradykinin-induced vasodilation was shown *ex vivo* in aortic rings of B<sub>2</sub><sup>tg</sup> mice confirming the overexpression of human B<sub>2</sub>R and validating the vasodilatory effect of bradykinin. This effect was dependent on the nitric oxide synthase enzyme (NOS). B<sub>2</sub>R overexpression affected the hemodynamics demonstrated as a decrease in sBP and HR in B<sub>2</sub><sup>tg</sup> mice. The decrease in sBP was not mediated by cyclooxygenase (COX)-derived products, or NOS. FMD data did not show a significant effect of endothelial B<sub>2</sub>R overexpression. Likewise, under basal conditions endothelium-specific B<sub>2</sub>R has no particular effects on systolic and diastolic functions, but an increase in aortic valve mean velocity was observed that warrant further investigations. In B<sub>2</sub><sup>tg</sup> mice, proteomic analysis revealed change in expression of proteins that are related to reactive oxygen species metabolic process, electron transport chain, cellular lipid metabolic process, cell migration, and angiogenesis. Furthermore, several proteins e.g. CD44, hyaluronidase 1 and uncoupling protein 1 that are most likely related to endothelial B<sub>2</sub>R signalling, were newly reported.

These findings increase the current knowledge on the role of B<sub>2</sub>R signalling in blood pressure regulation and provide new aspects about vascular and cardiac effects of the endothelial B<sub>2</sub>R under basal conditions. Using

different methods in this study, the vasodilatory effect of bradykinin and the role of B<sub>2</sub>R in vascular reactivity was investigated at various levels, from molecular signalling pathways to systemic cardiovascular responses. Finally, this work provides new questions regarding the role of B<sub>2</sub>R in aortic valve functions and reported new proteins which might be regulated by B<sub>2</sub>R pathway.

## References

1. <https://www.who.int/news-room/fact-sheets/detail/the-top-10-causes-of-death>
2. Williams B, Mancia G, Spiering W, et al. 2018 ESC/ESH Guidelines for the management of arterial hypertension: The Task Force for the management of arterial hypertension of the European Society of Cardiology and the European Society of Hypertension: The Task Force for the management of arterial hypertension of the European Society of Cardiology and the European Society of Hypertension. *Journal of hypertension*. 2018;36(10):1953-2041.
3. Michael E. Hall JEH. 5 - Pathogenesis of Hypertension. In: George L. Bakris MJS, editor. *Hypertension: A Companion to Braunwald's Heart Disease (Third Edition)* ed: Elsevier; 2018. p. 33-51.
4. Ma J, Li Y, Yang X, et al. Signaling pathways in vascular function and hypertension: molecular mechanisms and therapeutic interventions. *Signal Transduct Target Ther*. 2023;8(1):168.
5. Zhang Z, Zhao L, Zhou X, et al. Role of inflammation, immunity, and oxidative stress in hypertension: New insights and potential therapeutic targets. *Front Immunol*. 2022;13:1098725.
6. Mancia G, Kreutz R, Brunström M, et al. 2023 ESH Guidelines for the management of arterial hypertension The Task Force for the management of arterial hypertension of the European Society of Hypertension: Endorsed by the International Society of Hypertension (ISH) and the European Renal Association (ERA). *Journal of hypertension*. 2023;41(12):1874-2071.
7. Ma J, Chen X. Advances in pathogenesis and treatment of essential hypertension. *Front Cardiovasc Med*. 2022;9:1003852.
8. Xu S, Ilyas I, Little PJ, et al. Endothelial Dysfunction in Atherosclerotic Cardiovascular Diseases and Beyond: From Mechanism to Pharmacotherapies. *Pharmacol Rev*. 2021;73(3):924-67.
9. de Oliveira MG, Nadruz W, Jr., Mónica FZ. Endothelial and vascular smooth muscle dysfunction in hypertension. *Biochem Pharmacol*. 2022;205:115263.
10. Triggle CR, Samuel SM, Ravishankar S, et al. The endothelium: influencing vascular smooth muscle in many ways. *Can J Physiol Pharmacol*. 2012;90(6):713-38.
11. Rocha ESM, Beraldo WT, Rosenfeld G. Bradykinin, a hypotensive and smooth muscle stimulating factor released from plasma globulin by snake venoms and by trypsin. *Am J Physiol*. 1949;156(2):261-73.
12. Campbell DJ. The kallikrein-kinin system in humans. *Clin Exp Pharmacol Physiol*. 2001;28(12):1060-5.
13. Nzeako UC, Frigas E, Tremaine WJ. Hereditary angioedema: a broad review for clinicians. *Arch Intern Med*. 2001;161(20):2417-29.
14. Marcondes S, Antunes E. The plasma and tissue kininogen-kallikrein-kinin system: role in the cardiovascular system. *Curr Med Chem Cardiovasc Hematol Agents*. 2005;3(1):33-44.

15. Blaes N, Girolami JP. Targeting the 'Janus face' of the B2-bradykinin receptor. *Expert Opin Ther Targets*. 2013;17(10):1145-66.
16. Saameli K, Eskes TK. Bradykinin and cardiovascular system: estimation of half-life. *Am J Physiol*. 1962;203:261-5.
17. Pinheiro AS, Silbak S, Schmaier AH. Bradykinin - An elusive peptide in measuring and understanding. *Res Pract Thromb Haemost*. 2022;6(2):e12673.
18. Duncan AM, Kladis A, Jennings GL, et al. Kinins in humans. *Am J Physiol Regul Integr Comp Physiol*. 2000;278(4):R897-904.
19. Leeb-Lundberg LM, Marceau F, Müller-Esterl W, et al. International union of pharmacology. XLV. Classification of the kinin receptor family: from molecular mechanisms to pathophysiological consequences. *Pharmacol Rev*. 2005;57(1):27-77.
20. Koumbadinga GA, Désormeaux A, Adam A, et al. Effect of interferon- $\gamma$  on inflammatory cytokine-induced bradykinin B1 receptor expression in human vascular cells. *Eur J Pharmacol*. 2010;647(1-3):117-25.
21. Zhang Y, Adner M, Cardell LO. Up-regulation of bradykinin receptors in a murine in-vitro model of chronic airway inflammation. *Eur J Pharmacol*. 2004;489(1-2):117-26.
22. Tschöpe C, Heringer-Walther S, Koch M, et al. Upregulation of bradykinin B1-receptor expression after myocardial infarction. *Br J Pharmacol*. 2000;129(8):1537-8.
23. Kammerer S, Braun A, Arnold N, et al. The human bradykinin B2 receptor gene: full length cDNA, genomic organization and identification of the regulatory region. *Biochem Biophys Res Commun*. 1995;211(1):226-33.
24. Jarnagin K, Bhakta S, Zuppan P, et al. Mutations in the B2 bradykinin receptor reveal a different pattern of contacts for peptidic agonists and peptidic antagonists. *The Journal of biological chemistry*. 1996;271(45):28277-86.
25. <https://www.uniprot.org/uniprotkb/P30411/entry>
26. Marceau F, Bachelard H, Bouthillier J, et al. Bradykinin receptors: Agonists, antagonists, expression, signaling, and adaptation to sustained stimulation. *Int Immunopharmacol*. 2020;82:106305.
27. Bareis DL, Manganiello VC, Hirata F, et al. Bradykinin stimulates phospholipid methylation, calcium influx, prostaglandin formation, and cAMP accumulation in human fibroblasts. *Proc Natl Acad Sci USA*. 1983;80(9):2514-8.
28. Yi J, Bertels Z, Del Rosario JS, et al. Bradykinin receptor expression and bradykinin-mediated sensitization of human sensory neurons. *Pain*. 2024;165(1):202-15.
29. Marketou ME, Kontaraki J, Zacharis E, et al. Differential gene expression of bradykinin receptors 1 and 2 in peripheral monocytes from patients with essential hypertension. *J Hum Hypertens*. 2014;28(7):450-5.

30. Minshall RD, Nakamura F, Becker RP, et al. Characterization of bradykinin B2 receptors in adult myocardium and neonatal rat cardiomyocytes. *Circ Res.* 1995;76(5):773-80.
31. Blaukat A, Pizard A, Breit A, et al. Determination of bradykinin B2 receptor in vivo phosphorylation sites and their role in receptor function. *The Journal of biological chemistry.* 2001;276(44):40431-40.
32. Gambardella J, Sorriento D, Bova M, et al. Role of Endothelial G Protein-Coupled Receptor Kinase 2 in Angioedema. *Hypertension.* 2020;76(5):1625-36.
33. Shen JK, Zhang HT. Function and structure of bradykinin receptor 2 for drug discovery. *Acta Pharmacol Sin.* 2023;44(3):489-98.
34. Poulos TL. Soluble guanylate cyclase. *Curr Opin Struct Biol.* 2006;16(6):736-43.
35. Busse R, Edwards G, Félétou M, et al. EDHF: bringing the concepts together. *Trends Pharmacol Sci.* 2002;23(8):374-80.
36. Aliwarga T, Evangelista EA, Sotoodehnia N, et al. Regulation of CYP2J2 and EET Levels in Cardiac Disease and Diabetes. *Int J Mol Sci.* 2018;19(7).
37. Zeng C, Liu J, Zheng X, et al. Prostaglandin and prostaglandin receptors: present and future promising therapeutic targets for pulmonary arterial hypertension. *Respir Res.* 2023;24(1):263.
38. Hellsten Y, Nyberg M, Jensen LG, et al. Vasodilator interactions in skeletal muscle blood flow regulation. *J Physiol.* 2012;590(24):6297-305.
39. Brown NJ, Gainer JV, Murphey LJ, et al. Bradykinin stimulates tissue plasminogen activator release from human forearm vasculature through B(2) receptor-dependent, NO synthase-independent, and cyclooxygenase-independent pathway. *Circulation.* 2000;102(18):2190-6.
40. Rahman AM, Murrow JR, Ozkor MA, et al. Endothelium-derived hyperpolarizing factor mediates bradykinin-stimulated tissue plasminogen activator release in humans. *J Vasc Res.* 2014;51(3):200-8.
41. Giannarelli C, Viridis A, De Negri F, et al. Effect of sulfaphenazole on tissue plasminogen activator release in normotensive subjects and hypertensive patients. *Circulation.* 2009;119(12):1625-33.
42. Kuhr F, Lowry J, Zhang Y, et al. Differential regulation of inducible and endothelial nitric oxide synthase by kinin B1 and B2 receptors. *Neuropeptides.* 2010;44(2):145-54.
43. Rex DAB, Deepak K, Vaid N, et al. A modular map of Bradykinin-mediated inflammatory signaling network. *J Cell Commun Signal.* 2022;16(2):301-10.
44. Moraes MS, Costa PE, Batista WL, et al. Endothelium-derived nitric oxide (NO) activates the NO-epidermal growth factor receptor-mediated signaling pathway in bradykinin-stimulated angiogenesis. *Arch Biochem Biophys.* 2014;558:14-27.
45. Terzuoli E, Corti F, Nannelli G, et al. Bradykinin B2 Receptor Contributes to Inflammatory Responses in Human Endothelial Cells by the Transactivation of the Fibroblast Growth Factor Receptor FGFR-1. *Int J Mol Sci.* 2018;19(9).

46. Gryglewski RJ, Uracz W, Chłopicki S, et al. Bradykinin as a major endogenous regulator of endothelial function. *Pediatr Pathol Mol Med*. 2002;21(3):279-90.
47. Regoli D, Gobeil F. Kallikrein-kinin system as the dominant mechanism to counteract hyperactive renin-angiotensin system. *Can J Physiol Pharmacol*. 2017;95(10):1117-24.
48. Rubin LE, Levi R. Protective role of bradykinin in cardiac anaphylaxis. Coronary-vasodilating and antiarrhythmic activities mediated by autocrine/paracrine mechanisms. *Circ Res*. 1995;76(3):434-40.
49. Blais PA, Côté J, Morin J, et al. Hypotensive effects of hemopressin and bradykinin in rabbits, rats and mice. A comparative study. *Peptides*. 2005;26(8):1317-22.
50. Holte HR, Bjørnstad-Ostensen A, Berg T. The role of endogenous bradykinin in blood pressure homeostasis in spontaneously hypertensive rats. *Br J Pharmacol*. 1996;118(8):1925-30.
51. Duka A, Duka I, Gao G, et al. Role of bradykinin B1 and B2 receptors in normal blood pressure regulation. *Am J Physiol Endocrinol Metab*. 2006;291(2):E268-74.
52. Rhaleb NE, Yang XP, Carretero OA. The kallikrein-kinin system as a regulator of cardiovascular and renal function. *Compr Physiol*. 2011;1(2):971-93.
53. Barros CC, Schadock I, Sihn G, et al. Chronic Overexpression of Bradykinin in Kidney Causes Polyuria and Cardiac Hypertrophy. *Front Med (Lausanne)*. 2018;5:338.
54. Madeddu P, Anania V, Parpaglia PP, et al. Effects of Hoe 140, a bradykinin B2-receptor antagonist, on renal function in conscious normotensive rats. *Br J Pharmacol*. 1992;106(2):380-6.
55. Mamenko M, Zaika O, Pochynyuk O. Direct regulation of ENaC by bradykinin in the distal nephron. Implications for renal sodium handling. *Curr Opin Nephrol Hypertens*. 2014;23(2):122-9.
56. Zhang DD, Gao ZX, Vio CP, et al. Bradykinin Stimulates Renal Na(+) and K(+) Excretion by Inhibiting the K(+) Channel (Kir4.1) in the Distal Convuluted Tubule. *Hypertension*. 2018;72(2):361-9.
57. Marchetti J, Imbert-Teboul M, Alhenc-Gelas F, et al. Kallikrein along the rabbit microdissected nephron: a micromethod for its measurement. Effect of adrenalectomy and DOCA treatment. *Pflugers Arch*. 1984;401(1):27-33.
58. Bądzyńska B, Baranowska I, Gawryś O, et al. Evidence against a crucial role of renal medullary perfusion in blood pressure control of hypertensive rats. *J Physiol*. 2019;597(1):211-23.
59. Bądzyńska B, Sadowski J. Differential action of bradykinin on intrarenal regional perfusion in the rat: waning effect in the cortex and major impact in the medulla. *J Physiol*. 2009;587(Pt 15):3943-53.
60. Pasquié JL, Herizi A, Jover B, et al. Chronic bradykinin infusion and receptor blockade in angiotensin II hypertension in rats. *Hypertension*. 1999;33(3):830-4.
61. Hamid S, Rhaleb IA, Kassem KM, et al. Role of Kinins in Hypertension and Heart Failure. *Pharmaceuticals (Basel)*. 2020;13(11).

62. Groves P, Kurz S, Just H, et al. Role of endogenous bradykinin in human coronary vasomotor control. *Circulation*. 1995;92(12):3424-30.
63. Given MB, Greenberg SS, Giles TD. Coronary vasodilator responses to bradykinin in euglycemic and diabetic rats. *Am J Hypertens*. 2001;14(5 Pt 1):446-54.
64. Dora KA, Lin J, Borysova L, et al. Signaling and structures underpinning conducted vasodilation in human and porcine intramyocardial coronary arteries. *Front Cardiovasc Med*. 2022;9:980628.
65. Tschöpe C, Heringer-Walther S, Walther T. Regulation of the kinin receptors after induction of myocardial infarction: a mini-review. *Braz J Med Biol Res*. 2000;33(6):701-8.
66. Westermann D, Schultheiss HP, Tschöpe C. New perspective on the tissue kallikrein-kinin system in myocardial infarction: role of angiogenesis and cardiac regeneration. *Int Immunopharmacol*. 2008;8(2):148-54.
67. Lu L, Li DX, Chen W, et al. Bradykinin-(1-9) mitigates autophagy through upregulating PI3K/Akt in rats with myocardial infarction. *Biochem Biophys Res Commun*. 2023;660:35-42.
68. Wu C, Zhou XX, Li JZ, et al. Pretreatment of cardiac progenitor cells with bradykinin attenuates H<sub>2</sub>O<sub>2</sub>-induced cell apoptosis and improves cardiac function in rats by regulating autophagy. *Stem Cell Res Ther*. 2021;12(1):437.
69. Kuoppala A, Shiota N, Lindstedt KA, et al. Expression of bradykinin receptors in the left ventricles of rats with pressure overload hypertrophy and heart failure. *Journal of hypertension*. 2003;21(9):1729-36.
70. Kuoppala A, Shiota N, Kokkonen JO, et al. Down-regulation of cardioprotective bradykinin type-2 receptors in the left ventricle of patients with end-stage heart failure. *J Am Coll Cardiol*. 2002;40(1):119-25.
71. Tonduangu D, Hittinger L, Ghaleh B, et al. Chronic infusion of bradykinin delays the progression of heart failure and preserves vascular endothelium-mediated vasodilation in conscious dogs. *Circulation*. 2004;109(1):114-9.
72. Smith RS, Jr., Gao L, Chao L, et al. Tissue kallikrein and kinin infusion promotes neovascularization in limb ischemia. *Biol Chem*. 2008;389(6):725-30.
73. Desposito D, Potier L, Chollet C, et al. Kinin receptor agonism restores hindlimb postischemic neovascularization capacity in diabetic mice. *J Pharmacol Exp Ther*. 2015;352(2):218-26.
74. Fu C, Cao Y, Yao Y, et al. Expression of B2 Receptor on Circulating CD34-Positive Cells and Outcomes of Myocardial Infarction. *Dis Markers*. 2019;2019:7816438.
75. Kränkel N, Katare RG, Siragusa M, et al. Role of kinin B2 receptor signaling in the recruitment of circulating progenitor cells with neovascularization potential. *Circ Res*. 2008;103(11):1335-43.
76. Khosravani F, Suvorava T, Dao VT, et al. Stability of murine bradykinin type 2 receptor despite treatment with NO, bradykinin, icatibant, or C1-INH. *Allergy*. 2015;70(3):285-94.
77. Jin L, Chao L, Chao J. Potassium supplement upregulates the expression of renal kallikrein and bradykinin B2 receptor in SHR. *Am J Physiol*. 1999;276(3):F476-84.

78. Liesmaa I, Kokkonen JO, Kovanen PT, et al. Lovastatin induces the expression of bradykinin type 2 receptors in cultured human coronary artery endothelial cells. *J Mol Cell Cardiol.* 2007;43(5):593-600.
79. Rodrigues ES, Silva RF, Martin RP, et al. Evidence that kinin B2 receptor expression is upregulated by endothelial overexpression of B1 receptors. *Peptides.* 2013;42:1-7.
80. Liesmaa I, Leskinen HK, Kokkonen JO, et al. Hypoxia-induced expression of bradykinin type-2 receptors in endothelial cells triggers NO production, cell migration, and angiogenesis. *J Cell Physiol.* 2009;221(2):359-66.
81. Kintsurashvili E, Duka I, Gavras I, et al. Effects of ANG II on bradykinin receptor gene expression in cardiomyocytes and vascular smooth muscle cells. *Am J Physiol Heart Circ Physiol.* 2001;281(4):H1778-83.
82. Othman R, Cagnone G, Joyal JS, et al. Kinins and Their Receptors as Potential Therapeutic Targets in Retinal Pathologies. *Cells.* 2021;10(8).
83. Chen Y, Yu Y, Sun S, et al. Bradykinin promotes migration and invasion of hepatocellular carcinoma cells through TRPM7 and MMP2. *Exp Cell Res.* 2016;349(1):68-76.
84. Thomas SM, Bhola NE, Zhang Q, et al. Cross-talk between G protein-coupled receptor and epidermal growth factor receptor signaling pathways contributes to growth and invasion of head and neck squamous cell carcinoma. *Cancer Res.* 2006;66(24):11831-9.
85. Zhang W, Bhola N, Kalyankrishna S, et al. Kinin b2 receptor mediates induction of cyclooxygenase-2 and is overexpressed in head and neck squamous cell carcinomas. *Mol Cancer Res.* 2008;6(12):1946-56.
86. Wang W, Zhou Y, Wei R, et al. Bradykinin promotes proliferation, migration, and invasion of cervical cancer cells through STAT3 signaling pathways. *Oncol Rep.* 2019;42(6):2521-7.
87. Zhou Y, Wang W, Wei R, et al. Serum bradykinin levels as a diagnostic marker in cervical cancer with a potential mechanism to promote VEGF expression via BDKRB2. *Int J Oncol.* 2019;55(1):131-41.
88. Yu HS, Wang SW, Chang AC, et al. Bradykinin promotes vascular endothelial growth factor expression and increases angiogenesis in human prostate cancer cells. *Biochem Pharmacol.* 2014;87(2):243-53.
89. Zhao J, Dong QZ, Zhong F, et al. NMI promotes hepatocellular carcinoma progression via BDKRB2 and MAPK/ERK pathway. *Oncotarget.* 2017;8(7):12174-85.
90. Hahn J, Greve J, Bas M, et al. Bradykinin-Mediated Angioedema Induced by Commonly Used Cardiovascular Drugs. 2023;2(3):708-27.
91. Smolinska S, Antolín-Amérigo D, Popescu FD. Bradykinin Metabolism and Drug-Induced Angioedema. *Int J Mol Sci.* 2023;24(14).
92. McDonagh TA, Metra M, Adamo M, et al. 2021 ESC Guidelines for the diagnosis and treatment of acute and chronic heart failure. *Eur Heart J.* 2021;42(36):3599-726.
93. Zhang Y, He D, Zhang W, et al. ACE Inhibitor Benefit to Kidney and Cardiovascular Outcomes for Patients with Non-Dialysis Chronic Kidney Disease Stages 3-5: A Network Meta-Analysis of Randomised Clinical Trials. *Drugs.* 2020;80(8):797-811.

94. Kleindorfer DO, Towfighi A, Chaturvedi S, et al. 2021 Guideline for the Prevention of Stroke in Patients With Stroke and Transient Ischemic Attack: A Guideline From the American Heart Association/American Stroke Association. *Stroke*. 2021;52(7):e364-e467.
95. Cutrell S, Alhomoud IS, Mehta A, et al. ACE-Inhibitors in Hypertension: A Historical Perspective and Current Insights. *Curr Hypertens Rep*. 2023;25(9):243-50.
96. Taddei S, Bortolotto L. Unraveling the Pivotal Role of Bradykinin in ACE Inhibitor Activity. *Am J Cardiovasc Drugs*. 2016;16(5):309-21.
97. Marceau F, Rivard GE, Gauthier JM, et al. Measurement of Bradykinin Formation and Degradation in Blood Plasma: Relevance for Acquired Angioedema Associated With Angiotensin Converting Enzyme Inhibition and for Hereditary Angioedema Due to Factor XII or Plasminogen Gene Variants. *Front Med (Lausanne)*. 2020;7:358.
98. Ancion A, Tridetti J, Nguyen Trung ML, et al. A Review of the Role of Bradykinin and Nitric Oxide in the Cardioprotective Action of Angiotensin-Converting Enzyme Inhibitors: Focus on Perindopril. *Cardiol Ther*. 2019;8(2):179-91.
99. Gainer JV, Morrow JD, Loveland A, et al. Effect of bradykinin-receptor blockade on the response to angiotensin-converting-enzyme inhibitor in normotensive and hypertensive subjects. *N Engl J Med*. 1998;339(18):1285-92.
100. Silva PS, Fontana V, Luizon MR, et al. eNOS and BDKRB2 genotypes affect the antihypertensive responses to enalapril. *Eur J Clin Pharmacol*. 2013;69(2):167-77.
101. Ceconi C, Fox KM, Remme WJ, et al. ACE inhibition with perindopril and endothelial function. Results of a substudy of the EUROPA study: PERTINENT. *Cardiovasc Res*. 2007;73(1):237-46.
102. Silvestre JS, Bergaya S, Tamarat R, et al. Proangiogenic effect of angiotensin-converting enzyme inhibition is mediated by the bradykinin B(2) receptor pathway. *Circ Res*. 2001;89(8):678-83.
103. Ebrahimian TG, Tamarat R, Clergue M, et al. Dual effect of angiotensin-converting enzyme inhibition on angiogenesis in type 1 diabetic mice. *Arterioscler Thromb Vasc Biol*. 2005;25(1):65-70.
104. Li P, Kondo T, Numaguchi Y, et al. Role of bradykinin, nitric oxide, and angiotensin II type 2 receptor in imidapril-induced angiogenesis. *Hypertension*. 2008;51(2):252-8.
105. Yang XP, Liu YH, Mehta D, et al. Diminished cardioprotective response to inhibition of angiotensin-converting enzyme and angiotensin II type 1 receptor in B(2) kinin receptor gene knockout mice. *Circ Res*. 2001;88(10):1072-9.
106. Duka A, Kintsurashvili E, Duka I, et al. Angiotensin-converting enzyme inhibition after experimental myocardial infarct: role of the kinin B1 and B2 receptors. *Hypertension*. 2008;51(5):1352-7.
107. Fujii M, Wada A, Tsutamoto T, et al. Bradykinin improves left ventricular diastolic function under long-term angiotensin-converting enzyme inhibition in heart failure. *Hypertension*. 2002;39(5):952-7.

108. Cargnoni A, Comini L, Bernocchi P, et al. Role of bradykinin and eNOS in the anti-ischaemic effect of trandolapril. *Br J Pharmacol*. 2001;133(1):145-53.
109. Buléon M, Allard J, Jaafar A, et al. Pharmacological blockade of B2-kinin receptor reduces renal protective effect of angiotensin-converting enzyme inhibition in db/db mice model. *Am J Physiol Renal Physiol*. 2008;294(5):F1249-56.
110. Messerli FH, Bangalore S, Bavishi C, et al. Angiotensin-Converting Enzyme Inhibitors in Hypertension: To Use or Not to Use? *J Am Coll Cardiol*. 2018;71(13):1474-82.
111. Liu YH, Yang XP, Sharov VG, et al. Effects of angiotensin-converting enzyme inhibitors and angiotensin II type 1 receptor antagonists in rats with heart failure. Role of kinins and angiotensin II type 2 receptors. *J Clin Invest*. 1997;99(8):1926-35.
112. Sgarra L, Leo V, Addabbo F, et al. Intermittent losartan administration triggers cardiac post-conditioning in isolated rat hearts: role of BK2 receptors. *PLoS One*. 2014;9(2):e88542.
113. Bonde MM, Olsen KB, Erikstrup N, et al. The angiotensin II type 1 receptor antagonist Losartan binds and activates bradykinin B2 receptor signaling. *Regul Pept*. 2011;167(1):21-5.
114. Campbell DJ, Krum H, Esler MD. Losartan increases bradykinin levels in hypertensive humans. *Circulation*. 2005;111(3):315-20.
115. Bozkurt B, Nair AP, Misra A, et al. Neprilysin Inhibitors in Heart Failure: The Science, Mechanism of Action, Clinical Studies, and Unanswered Questions. *JACC Basic Transl Sci*. 2023;8(1):88-105.
116. Li K, Kratzmann V, Dai M, et al. Angiotensin receptor-neprilysin inhibitor improves coronary collateral perfusion. *Front Cardiovasc Med*. 2022;9:981333.
117. Amorim MA, Jentsch Matias de Oliveira JR, Souza Oliveira VH, et al. Role of nitric oxide, bradykinin B(2) receptor, and TRPV1 in the airway alterations caused by simvastatin in rats. *Eur J Pharmacol*. 2021;912:174591.
118. Zhang XS, Ren JH, Lu JP, et al. Atorvastatin protects against angiotensin II-induced injury and dysfunction in human umbilical vein endothelial cells through bradykinin 2 receptors. *J Cardiovasc Pharmacol*. 2010;56(2):171-6.
119. Emerich DF, Dean RL, Osborn C, et al. The development of the bradykinin agonist labradimil as a means to increase the permeability of the blood-brain barrier: from concept to clinical evaluation. *Clin Pharmacokinet*. 2001;40(2):105-23.
120. Elliott PJ, Hayward NJ, Dean RL, et al. Dissociation of blood-brain barrier permeability and the hypotensive effects of the bradykinin B2 agonist, RMP-7. *Immunopharmacology*. 1996;33(1-3):205-8.
121. Sarin H, Kanevsky AS, Fung SH, et al. Metabolically stable bradykinin B2 receptor agonists enhance transvascular drug delivery into malignant brain tumors by increasing drug half-life. *J Transl Med*. 2009;7:33.
122. Savard M, Labonté J, Dubuc C, et al. Further pharmacological evaluation of a novel synthetic peptide bradykinin B2 receptor agonist. *Biol Chem*. 2013;394(3):353-60.

123. Maurer M, Magerl M, Betschel S, et al. The international WAO/EAACI guideline for the management of hereditary angioedema-The 2021 revision and update. *Allergy*. 2022;77(7):1961-90.
124. Leach JK, Spencer K, Mascelli M, et al. Pharmacokinetics of single and repeat doses of icatibant. *Clin Pharmacol Drug Dev*. 2015;4(2):105-11.
125. Gamboa JL, Mambungu CA, Clagett AR, et al. Bradykinin B(2) receptor blockade and intradialytic hypotension. *BMC Nephrol*. 2023;24(1):134.
126. Bailey M, Linden D, Guo-Parke H, et al. Vascular risk factors for COVID-19 ARDS: endothelium, contact-kinin system. *Front Med (Lausanne)*. 2023;10:1208866.
127. Fang C, Schmaier AH. Novel anti-thrombotic mechanisms mediated by Mas receptor as result of balanced activities between the kallikrein/kinin and the renin-angiotensin systems. *Pharmacol Res*. 2020;160:105096.
128. Lara LS, Bourgeois CR, El-Dahr SS, et al. Bradykinin/B(2) receptor activation regulates renin in M-1 cells via protein kinase C and nitric oxide. *Physiol Rep*. 2017;5(7).
129. Yosipiv IV, Dipp S, El-Dahr SS. Targeted disruption of the bradykinin B(2) receptor gene in mice alters the ontogeny of the renin-angiotensin system. *Am J Physiol Renal Physiol*. 2001;281(5):F795-801.
130. Qwitterer U, AbdAlla S. Pathological AT1R-B2R Protein Aggregation and Preeclampsia. *Cells*. 2021;10(10).
131. Qwitterer U, Fu X, Pohl A, et al. Beta-Arrestin1 Prevents Preeclampsia by Downregulation of Mechanosensitive AT1-B2 Receptor Heteromers. *Cell*. 2019;176(1-2):318-33.e19.
132. Isbell DC, Voros S, Yang Z, et al. Interaction between bradykinin subtype 2 and angiotensin II type 2 receptors during post-MI left ventricular remodeling. *Am J Physiol Heart Circ Physiol*. 2007;293(6):H3372-8.
133. Tsutsumi Y, Matsubara H, Masaki H, et al. Angiotensin II type 2 receptor overexpression activates the vascular kinin system and causes vasodilation. *J Clin Invest*. 1999;104(7):925-35.
134. Abadir PM, Periasamy A, Carey RM, et al. Angiotensin II type 2 receptor-bradykinin B2 receptor functional heterodimerization. *Hypertension*. 2006;48(2):316-22.
135. Cerrato BD, Carretero OA, Janic B, et al. Heteromerization Between the Bradykinin B2 Receptor and the Angiotensin-(1-7) Mas Receptor: Functional Consequences. *Hypertension*. 2016;68(4):1039-48.
136. Braun A, Kammerer S, Maier E, et al. Polymorphisms in the gene for the human B2-bradykinin receptor. New tools in assessing a genetic risk for bradykinin-associated diseases. *Immunopharmacology*. 1996;33(1-3):32-5.
137. Lung CC, Chan EK, Zuraw BL. Analysis of an exon 1 polymorphism of the B2 bradykinin receptor gene and its transcript in normal subjects and patients with C1 inhibitor deficiency. *J Allergy Clin Immunol*. 1997;99(1 Pt 1):134-46.

138. Pretorius MM, Gainer JV, Van Guilder GP, et al. The bradykinin type 2 receptor BE1 polymorphism and ethnicity influence systolic blood pressure and vascular resistance. *Clin Pharmacol Ther.* 2008;83(1):122-9.
139. Souza LV, de Almeida SS, De Meneck F, et al. Polymorphism of the bradykinin type 2 receptor gene modulates blood pressure profile and microvascular function in prepubescent children. *Peptides.* 2021;137:170491.
140. Brull D, Dhamrait S, Myerson S, et al. Bradykinin B2BKR receptor polymorphism and left-ventricular growth response. *Lancet.* 2001;358(9288):1155-6.
141. Hallberg P, Lind L, Michaëlsson K, et al. B2 bradykinin receptor (B2BKR) polymorphism and change in left ventricular mass in response to antihypertensive treatment: results from the Swedish Irbesartan Left Ventricular Hypertrophy Investigation versus Atenolol (SILVHIA) trial. *Journal of hypertension.* 2003;21(3):621-4.
142. Van Guilder GP, Pretorius M, Luther JM, et al. Bradykinin type 2 receptor BE1 genotype influences bradykinin-dependent vasodilation during angiotensin-converting enzyme inhibition. *Hypertension.* 2008;51(2):454-9.
143. Niu W, Qi Y, Gao P, et al. A meta-analysis of the bradykinin B2 receptor gene --58C/T polymorphism with hypertension. *Clin Chim Acta.* 2010;411(5-6):324-8.
144. Li YY, Zhang H, Xu J, et al. Bradykinin  $\beta$ 2 receptor -58T/C gene polymorphism and essential hypertension: a meta-analysis. *PLoS One.* 2012;7(8):e43068.
145. Luo K, Yang P, Xu G. Risk of bradykinin B2 receptor -58T/C gene polymorphism on hypertension: A meta-analysis. *Nephrology (Carlton).* 2016;21(8):655-62.
146. Borkowski JA, Ransom RW, Seabrook GR, et al. Targeted disruption of a B2 bradykinin receptor gene in mice eliminates bradykinin action in smooth muscle and neurons. *The Journal of biological chemistry.* 1995;270(23):13706-10.
147. Alfie ME, Yang XP, Hess F, et al. Salt-sensitive hypertension in bradykinin B2 receptor knockout mice. *Biochem Biophys Res Commun.* 1996;224(3):625-30.
148. Madeddu P, Varoni MV, Palomba D, et al. Cardiovascular phenotype of a mouse strain with disruption of bradykinin B2-receptor gene. *Circulation.* 1997;96(10):3570-8.
149. Madeddu P, Milia AF, Salis MB, et al. Renovascular hypertension in bradykinin B2-receptor knockout mice. *Hypertension.* 1998;32(3):503-9.
150. Madeddu P, Emanuelli C, Gaspa L, et al. Role of the bradykinin B2 receptor in the maturation of blood pressure phenotype: lesson from transgenic and knockout mice. *Immunopharmacology.* 1999;44(1-2):9-13.
151. Emanuelli C, Maestri R, Corradi D, et al. Dilated and failing cardiomyopathy in bradykinin B(2) receptor knockout mice. *Circulation.* 1999;100(23):2359-65.

152. Milia AF, Gross V, Plehm R, et al. Normal blood pressure and renal function in mice lacking the bradykinin B(2) receptor. *Hypertension*. 2001;37(6):1473-9.
153. Cervenka L, Harrison-Bernard LM, Dipp S, et al. Early onset salt-sensitive hypertension in bradykinin B(2) receptor null mice. *Hypertension*. 1999;34(2):176-80.
154. Maestri R, Milia AF, Salis MB, et al. Cardiac hypertrophy and microvascular deficit in kinin B2 receptor knockout mice. *Hypertension*. 2003;41(5):1151-5.
155. Schanstra JP, Duchene J, Praddaude F, et al. Decreased renal NO excretion and reduced glomerular tuft area in mice lacking the bradykinin B2 receptor. *Am J Physiol Heart Circ Physiol*. 2003;284(6):H1904-8.
156. Roman-Campos D, Duarte HL, Gomes ER, et al. Investigation of the cardiomyocyte dysfunction in bradykinin type 2 receptor knockout mice. *Life Sci*. 2010;87(23-26):715-23.
157. Delemasure S, Blaes N, Richard C, et al. Antioxidant/oxidant status and cardiac function in bradykinin B(1)- and B(2)-receptor null mice. *Physiol Res*. 2013;62(5):511-7.
158. Fang C, Stavrou E, Schmaier AA, et al. Angiotensin 1-7 and Mas decrease thrombosis in Bdkrb2<sup>-/-</sup> mice by increasing NO and prostacyclin to reduce platelet spreading and glycoprotein VI activation. *Blood*. 2013;121(15):3023-32.
159. Cayla C, Todiras M, Iliescu R, et al. Mice deficient for both kinin receptors are normotensive and protected from endotoxin-induced hypotension. *Faseb j*. 2007;21(8):1689-98.
160. Kakoki M, McGarrah RW, Kim HS, et al. Bradykinin B1 and B2 receptors both have protective roles in renal ischemia/reperfusion injury. *Proc Natl Acad Sci U S A*. 2007;104(18):7576-81.
161. Wende AR, Soto J, Olsen CD, et al. Loss of bradykinin signaling does not accelerate the development of cardiac dysfunction in type 1 diabetic akita mice. *Endocrinology*. 2010;151(8):3536-42.
162. Meneton P, Bloch-Faure M, Hagege AA, et al. Cardiovascular abnormalities with normal blood pressure in tissue kallikrein-deficient mice. *Proc Natl Acad Sci U S A*. 2001;98(5):2634-9.
163. Trabold F, Pons S, Hagege AA, et al. Cardiovascular phenotypes of kinin B2 receptor- and tissue kallikrein-deficient mice. *Hypertension*. 2002;40(1):90-5.
164. Kopkan L, Husková Z, Jíchová Š, et al. Conditional knockout of collecting duct bradykinin B2 receptors exacerbates angiotensin II-induced hypertension during high salt intake. *Clin Exp Hypertens*. 2016;38(1):1-9.
165. Ohnaka Y, Tsukamoto S, Iwai Y, et al. Bradykinin deficiency causes high blood pressure in mice. *Biochem Biophys Res Commun*. 2023;681:73-9.
166. Silva JA, Jr., Araujo RC, Baltatu O, et al. Reduced cardiac hypertrophy and altered blood pressure control in transgenic rats with the human tissue kallikrein gene. *Faseb j*. 2000;14(13):1858-60.
167. Wang DZ, Chao L, Chao J. Hypotension in transgenic mice overexpressing human bradykinin B2 receptor. *Hypertension*. 1997;29(1 Pt 2):488-93.

168. Percie du Sert N, Ahluwalia A, Alam S, et al. Reporting animal research: Explanation and elaboration for the ARRIVE guidelines 2.0. *PLoS Biol.* 2020;18(7):e3000411.
169. Introduction to Gene Expression: Getting Started Guide [Available from: <https://www.thermofisher.com/> last accessed 31.05.2023.
170. Schmittgen TD, Livak KJ. Analyzing real-time PCR data by the comparative C(T) method. *Nat Protoc.* 2008;3(6):1101-8.
171. Bradford MM. A rapid and sensitive method for the quantitation of microgram quantities of protein utilizing the principle of protein-dye binding. *Anal Biochem.* 1976;72:248-54.
172. Bass JJ, Wilkinson DJ, Rankin D, et al. An overview of technical considerations for Western blotting applications to physiological research. *Scand J Med Sci Sports.* 2017;27(1):4-25.
173. Renart J, Reiser J, Stark GR. Transfer of proteins from gels to diazobenzyloxymethyl-paper and detection with antisera: a method for studying antibody specificity and antigen structure. *Proc Natl Acad Sci U S A.* 1979;76(7):3116-20.
174. Towbin H, Staehelin T, Gordon J. Electrophoretic transfer of proteins from polyacrylamide gels to nitrocellulose sheets: procedure and some applications. *Proc Natl Acad Sci U S A.* 1979;76(9):4350-4.
175. Burnette WN. "Western blotting": electrophoretic transfer of proteins from sodium dodecyl sulfate--polyacrylamide gels to unmodified nitrocellulose and radiographic detection with antibody and radioiodinated protein A. *Anal Biochem.* 1981;112(2):195-203.
176. Aslam B, Basit M, Nisar MA, et al. Proteomics: Technologies and Their Applications. *J Chromatogr Sci.* 2017;55(2):182-96.
177. Duong VA, Lee H. Bottom-Up Proteomics: Advancements in Sample Preparation. *Int J Mol Sci.* 2023;24(6).
178. Li B, Ming Y, Liu Y, et al. Recent Developments in Pharmacological Effect, Mechanism and Application Prospect of Diazoniumdiolates. *Front Pharmacol.* 2020;11:923.
179. Krege JH, Hodgins JB, Hagaman JR, et al. A noninvasive computerized tail-cuff system for measuring blood pressure in mice. *Hypertension.* 1995;25(5):1111-5.
180. Gao S, Ho D, Vatner DE, et al. Echocardiography in Mice. *Curr Protoc Mouse Biol.* 2011;1:71-83.
181. Zacchigna S, Paldino A, Falcão-Pires I, et al. Towards standardization of echocardiography for the evaluation of left ventricular function in adult rodents: a position paper of the ESC Working Group on Myocardial Function. *Cardiovasc Res.* 2021;117(1):43-59.
182. Hahn RT, Abraham T, Adams MS, et al. Guidelines for performing a comprehensive transesophageal echocardiographic examination: recommendations from the American Society of Echocardiography and the Society of Cardiovascular Anesthesiologists. *J Am Soc Echocardiogr.* 2013;26(9):921-64.

183. Celermajer DS, Sorensen KE, Gooch VM, et al. Non-invasive detection of endothelial dysfunction in children and adults at risk of atherosclerosis. *Lancet*. 1992;340(8828):1111-5.
184. Thijssen DHJ, Bruno RM, van Mil A, et al. Expert consensus and evidence-based recommendations for the assessment of flow-mediated dilation in humans. *Eur Heart J*. 2019;40(30):2534-47.
185. Schuler D, Sansone R, Freudenberger T, et al. Measurement of endothelium-dependent vasodilation in mice--brief report. *Arterioscler Thromb Vasc Biol*. 2014;34(12):2651-7.
186. Anton EL, Fernandes D, Assreuy J, et al. Bradykinin increases BP in endotoxemic rat: functional and biochemical evidence of angiotensin II AT(1) /bradykinin B(2) receptor heterodimerization. *Br J Pharmacol*. 2019;176(14):2608-26.
187. Billet S, Aguilar F, Baudry C, et al. Role of angiotensin II AT1 receptor activation in cardiovascular diseases. *Kidney Int*. 2008;74(11):1379-84.
188. Benicky J, Hafko R, Sanchez-Lemus E, et al. Six commercially available angiotensin II AT1 receptor antibodies are non-specific. *Cell Mol Neurobiol*. 2012;32(8):1353-65.
189. Abd Alla J, Reeck K, Langer A, et al. Calreticulin enhances B2 bradykinin receptor maturation and heterodimerization. *Biochem Biophys Res Commun*. 2009;387(1):186-90.
190. (<https://www.uniprot.org/uniprotkb/P32299/entry>)
191. Pesquero JB, Lindsey CJ, Zeh K, et al. Molecular structure and expression of rat bradykinin B2 receptor gene. Evidence for alternative splicing. *The Journal of biological chemistry*. 1994;269(43):26920-5.
192. Liu Q, Fang L, Wu C. Alternative Splicing and Isoforms: From Mechanisms to Diseases. *Genes (Basel)*. 2022;13(3).
193. Suvorava T, Metry S, Pick S, et al. Alterations in endothelial nitric oxide synthase activity and their relevance to blood pressure. *Biochem Pharmacol*. 2022;205:115256.
194. Lu N, Malemud CJ. Extracellular Signal-Regulated Kinase: A Regulator of Cell Growth, Inflammation, Chondrocyte and Bone Cell Receptor-Mediated Gene Expression. *Int J Mol Sci*. 2019;20(15).
195. Bisha M, Dao VT, Gholamreza-Fahimi E, et al. The role of bradykinin receptor type 2 in spontaneous extravasation in mice skin: implications for non-allergic angio-oedema. *Br J Pharmacol*. 2018;175(10):1607-20.
196. <https://resources.jax.org/white-papers/whitepaper-gsp-2>
197. Müller AM, Hermanns MI, Skrzynski C, et al. Expression of the endothelial markers PECAM-1, vWf, and CD34 in vivo and in vitro. *Exp Mol Pathol*. 2002;72(3):221-9.
198. Merkulov S, Zhang WM, Komar AA, et al. Deletion of murine kininogen gene 1 (mKng1) causes loss of plasma kininogen and delays thrombosis. *Blood*. 2008;111(3):1274-81.
199. García-Llorca A, Carta F, Supuran CT, et al. Carbonic anhydrase, its inhibitors and vascular function. *Frontiers in molecular biosciences*. 2024;11:1338528.

200. Huang da W, Sherman BT, Lempicki RA. Bioinformatics enrichment tools: paths toward the comprehensive functional analysis of large gene lists. *Nucleic Acids Res.* 2009;37(1):1-13.
201. Huang da W, Sherman BT, Lempicki RA. Systematic and integrative analysis of large gene lists using DAVID bioinformatics resources. *Nat Protoc.* 2009;4(1):44-57.
202. Qu K, Yan F, Qin X, et al. Mitochondrial dysfunction in vascular endothelial cells and its role in atherosclerosis. *Frontiers in physiology.* 2022;13:1084604.
203. Sousa JS, D'Imprima E, Vonck J. Mitochondrial Respiratory Chain Complexes. *Subcell Biochem.* 2018;87:167-227.
204. Houten SM, Violante S, Ventura FV, et al. The Biochemistry and Physiology of Mitochondrial Fatty Acid  $\beta$ -Oxidation and Its Genetic Disorders. *Annual review of physiology.* 2016;78:23-44.
205. Fukai T, Ushio-Fukai M. Superoxide dismutases: role in redox signaling, vascular function, and diseases. *Antioxidants & redox signaling.* 2011;15(6):1583-606.
206. Ikeda K, Yamada T. UCP1 Dependent and Independent Thermogenesis in Brown and Beige Adipocytes. *Frontiers in endocrinology.* 2020;11:498.
207. Simpson MA. Concurrent expression of hyaluronan biosynthetic and processing enzymes promotes growth and vascularization of prostate tumors in mice. *Am J Pathol.* 2006;169(1):247-57.
208. Jaskuła K, Sacharczuk M, Gaciong Z, et al. Cardiovascular Effects Mediated by HMMR and CD44. *Mediators Inflamm.* 2021;2021:4977209.
209. Suvorava T, Pick S, Kojda G. Selective impairment of blood pressure reduction by endothelial nitric oxide synthase dimer destabilization in mice. *Journal of hypertension.* 2017;35(1):76-88.
210. Marchalant Y, Brownjohn PW, Bonnet A, et al. Validating Antibodies to the Cannabinoid CB2 Receptor: Antibody Sensitivity Is Not Evidence of Antibody Specificity. *J Histochem Cytochem.* 2014;62(6):395-404.
211. Beermann S, Seifert R, Neumann D. Commercially available antibodies against human and murine histamine H<sub>4</sub>-receptor lack specificity. *Naunyn Schmiedebergs Arch Pharmacol.* 2012;385(2):125-35.
212. Hafko R, Villapol S, Nostramo R, et al. Commercially available angiotensin II At<sub>2</sub> receptor antibodies are nonspecific. *PLoS One.* 2013;8(7):e69234.
213. Lee K, Kim YJ, Choi LM, et al. Human salivary gland cells express bradykinin receptors that modulate the expression of proinflammatory cytokines. *Eur J Oral Sci.* 2017;125(1):18-27.
214. Bélanger S, Bovenzi V, Côté J, et al. Structure-activity relationships of novel peptide agonists of the human bradykinin B2 receptor. *Peptides.* 2009;30(4):777-87.
215. Wu Y, Fu C, Li B, et al. Bradykinin Protects Human Endothelial Progenitor Cells from High-Glucose-Induced Senescence through B2 Receptor-Mediated Activation of the Akt/eNOS Signalling Pathway. *J Diabetes Res.* 2021;2021:6626627.

216. Kramarenko, II, Bunni MA, Morinelli TA, et al. Identification of functional bradykinin B(2) receptors endogenously expressed in HEK293 cells. *Biochem Pharmacol.* 2009;77(2):269-76.
217. Mesquita TRR, Campos-Mota GP, Lemos VS, et al. Vascular Kinin B(1) and B(2) Receptors Determine Endothelial Dysfunction through Neuronal Nitric Oxide Synthase. *Frontiers in physiology.* 2017;8:228.
218. Chataigneau T, Félétou M, Huang PL, et al. Acetylcholine-induced relaxation in blood vessels from endothelial nitric oxide synthase knockout mice. *Br J Pharmacol.* 1999;126(1):219-26.
219. Veronez CL, Maghsodi S, Todiras M, et al. Endothelial B2-receptor overexpression as an alternative animal model for hereditary angioedema. *Allergy.* 2019;74(10):1998-2002.
220. Wu H, Roks AJ, Leijten FP, et al. Genetic variation and gender determine bradykinin type 1 receptor responses in human tissue: implications for the ACE-inhibitor-induced effects in patients with coronary artery disease. *Clin Sci (Lond).* 2014;126(6):441-9.
221. Bas M, Kirchhartz N, Hochfeld J, et al. Potential role of vasomotor effects of fibrinogen in bradykinin-induced angioedema. *J Allergy Clin Immunol.* 2008;121(4):969-75.e2.
222. Gomes MB, Affonso FS, Cailleaux S, et al. Glucose levels observed in daily clinical practice induce endothelial dysfunction in the rabbit macro- and microcirculation. *Fundam Clin Pharmacol.* 2004;18(3):339-46.
223. Siltari A, Korpela R, Vapaatalo H. Bradykinin -induced vasodilatation: Role of age, ACE1-inhibitory peptide, mas- and bradykinin receptors. *Peptides.* 2016;85:46-55.
224. Pannirselvam M, Ding H, Anderson TJ, et al. Pharmacological characteristics of endothelium-derived hyperpolarizing factor-mediated relaxation of small mesenteric arteries from db/db mice. *Eur J Pharmacol.* 2006;551(1-3):98-107.
225. Felipe SA, Rodrigues ES, Martin RP, et al. Functional expression of kinin B1 and B2 receptors in mouse abdominal aorta. *Braz J Med Biol Res.* 2007;40(5):649-55.
226. Rodrigues ES, Martin RP, Felipe SA, et al. Cross talk between kinin and angiotensin II receptors in mouse abdominal aorta. *Biol Chem.* 2009;390(9):907-13.
227. Lui AH, McManus BM, Laher I. Endothelial and myogenic regulation of coronary artery tone in the mouse. *Eur J Pharmacol.* 2000;410(1):25-31.
228. Wölkart G, Kollau A, Russwurm M, et al. Varied effects of tobacco smoke and e-cigarette vapor suggest that nicotine does not affect endothelium-dependent relaxation and nitric oxide signaling. *Sci Rep.* 2023;13(1):15833.
229. Blum-Johnston C, Thorpe RB, Wee C, et al. Long-term hypoxia uncouples Ca(2+) and eNOS in bradykinin-mediated pulmonary arterial relaxation. *Am J Physiol Regul Integr Comp Physiol.* 2018;314(6):R870-r82.

230. Bopp C, Auger C, Diemunsch P, et al. The effect of urapidil, an alpha-1 adrenoceptor antagonist and a 5-HT<sub>1A</sub> agonist, on the vascular tone of the porcine coronary and pulmonary arteries, the rat aorta and the human pulmonary artery. *Eur J Pharmacol*. 2016;779:53-8.
231. Schneider JC, El Kebir D, Chéreau C, et al. Involvement of Na<sup>(+)</sup>/Ca<sup>(2+)</sup> exchanger in endothelial NO production and endothelium-dependent relaxation. *Am J Physiol Heart Circ Physiol*. 2002;283(2):H837-44.
232. Rodríguez-Mañas L, El-Assar M, Vallejo S, et al. Endothelial dysfunction in aged humans is related with oxidative stress and vascular inflammation. *Aging Cell*. 2009;8(3):226-38.
233. Nurmi L, Heikkilä HM, Vapaatalo H, et al. Downregulation of Bradykinin type 2 receptor expression in cardiac endothelial cells during senescence. *J Vasc Res*. 2012;49(1):13-23.
234. Feng W, Xu X, Zhao G, et al. Increased Age-Related Cardiac Dysfunction in Bradykinin B<sub>2</sub> Receptor-Deficient Mice. *J Gerontol A Biol Sci Med Sci*. 2016;71(2):178-87.
235. Kintsurashvili E, Duka A, Ignjacev I, et al. Age-related changes of bradykinin B<sub>1</sub> and B<sub>2</sub> receptors in rat heart. *Am J Physiol Heart Circ Physiol*. 2005;289(1):H202-5.
236. Bönner G, Preis S, Schunk U, et al. Hemodynamic effects of bradykinin on systemic and pulmonary circulation in healthy and hypertensive humans. *J Cardiovasc Pharmacol*. 1990;15 Suppl 6:S46-56.
237. Silver LM. *Mouse Genetics Concepts and Applications*: Oxford University Press; 1995.
238. Ji H, Pai AV, West CA, et al. Loss of Resistance to Angiotensin II-Induced Hypertension in the Jackson Laboratory Recombination-Activating Gene Null Mouse on the C57BL/6J Background. *Hypertension*. 2017;69(6):1121-7.
239. Wang D, Yoshida H, Song Q, et al. Enhanced renal function in bradykinin B<sub>(2)</sub> receptor transgenic mice. *Am J Physiol Renal Physiol*. 2000;278(3):F484-91.
240. Quaschnig T, Koçak S, Bauer C, et al. Increase in nitric oxide bioavailability improves endothelial function in endothelin-1 transgenic mice. *Nephrol Dial Transplant*. 2003;18(3):479-83.
241. Quaschnig T, Voss F, Relle K, et al. Lack of endothelial nitric oxide synthase promotes endothelin-induced hypertension: lessons from endothelin-1 transgenic/endothelial nitric oxide synthase knockout mice. *J Am Soc Nephrol*. 2007;18(3):730-40.
242. Tsuprykov O, Chaykovska L, Kretschmer A, et al. Endothelin-1 Overexpression Improves Renal Function in eNOS Knockout Mice. *Cell Physiol Biochem*. 2015;37(4):1474-90.
243. Gödecke A, Schrader J. Adaptive mechanisms of the cardiovascular system in transgenic mice--lessons from eNOS and myoglobin knockout mice. *Basic Res Cardiol*. 2000;95(6):492-8.
244. [https://www.criver.com/sites/default/files/resources/doc\\_a/RM-CS-how-to-refresh-your-mutant-or-transgenic-mouse-strains.pdf](https://www.criver.com/sites/default/files/resources/doc_a/RM-CS-how-to-refresh-your-mutant-or-transgenic-mouse-strains.pdf)
245. Kurtz TW, Griffin KA, Bidani AK, et al. Recommendations for blood pressure measurement in humans and experimental animals: part 2: blood pressure measurement in experimental animals: a statement for

professionals from the Subcommittee of Professional and Public Education of the American Heart Association Council on High Blood Pressure Research. *Arterioscler Thromb Vasc Biol.* 2005;25(3):e22-33.

246. Harrison DG, Bader M, Lerman LO, et al. Tail-Cuff Versus Radiotelemetry to Measure Blood Pressure in Mice and Rats. *Hypertension.* 2024;81(1):3-5.

247. Keidar S, Attias J, Coleman R, et al. Attenuation of atherosclerosis in apolipoprotein E-deficient mice by ramipril is dissociated from its antihypertensive effect and from potentiation of bradykinin. *J Cardiovasc Pharmacol.* 2000;35(1):64-72.

248. Wirth K, Hock FJ, Albus U, et al. Hoe 140 a new potent and long acting bradykinin-antagonist: in vivo studies. *Br J Pharmacol.* 1991;102(3):774-7.

249. Xiao F, Jiang H, Li Z, et al. Reduced hepatic bradykinin degradation accounts for cold-induced BAT thermogenesis and WAT browning in male mice. *Nat Commun.* 2023;14(1):2523.

250. Scotland RS, Madhani M, Chauhan S, et al. Investigation of vascular responses in endothelial nitric oxide synthase/cyclooxygenase-1 double-knockout mice: key role for endothelium-derived hyperpolarizing factor in the regulation of blood pressure in vivo. *Circulation.* 2005;111(6):796-803.

251. Athirakul K, Kim HS, Audoly LP, et al. Deficiency of COX-1 causes natriuresis and enhanced sensitivity to ACE inhibition. *Kidney Int.* 2001;60(6):2324-9.

252. Kawada N, Solis G, Ivey N, et al. Cyclooxygenase-1-deficient mice have high sleep-to-wake blood pressure ratios and renal vasoconstriction. *Hypertension.* 2005;45(6):1131-8.

253. Seta F, Chung AD, Turner PV, et al. Renal and cardiovascular characterization of COX-2 knockdown mice. *Am J Physiol Regul Integr Comp Physiol.* 2009;296(6):R1751-60.

254. Dinchuk JE, Car BD, Focht RJ, et al. Renal abnormalities and an altered inflammatory response in mice lacking cyclooxygenase II. *Nature.* 1995;378(6555):406-9.

255. Norwood VF, Morham SG, Smithies O. Postnatal development and progression of renal dysplasia in cyclooxygenase-2 null mice. *Kidney Int.* 2000;58(6):2291-300.

256. Morham SG, Langenbach R, Loftin CD, et al. Prostaglandin synthase 2 gene disruption causes severe renal pathology in the mouse. *Cell.* 1995;83(3):473-82.

257. Yang T, Huang YG, Ye W, et al. Influence of genetic background and gender on hypertension and renal failure in COX-2-deficient mice. *Am J Physiol Renal Physiol.* 2005;288(6):F1125-32.

258. Mitchell JA, Shala F, Pires MEL, et al. Endothelial cyclooxygenase-1 paradoxically drives local vasoconstriction and atherogenesis despite underpinning prostacyclin generation. *Sci Adv.* 2021;7(12).

259. Hinz B, Dormann H, Brune K. More pronounced inhibition of cyclooxygenase 2, increase in blood pressure, and reduction of heart rate by treatment with diclofenac compared with celecoxib and rofecoxib. *Arthritis Rheum.* 2006;54(1):282-91.

260. Krum H, Swergold G, Gammaitoni A, et al. Blood pressure and cardiovascular outcomes in patients taking nonsteroidal antiinflammatory drugs. *Cardiovasc Ther.* 2012;30(6):342-50.
261. Krum H, Swergold G, Curtis SP, et al. Factors associated with blood pressure changes in patients receiving diclofenac or etoricoxib: results from the MEDAL study. *Journal of hypertension.* 2009;27(4):886-93.
262. Shesely EG, Maeda N, Kim HS, et al. Elevated blood pressures in mice lacking endothelial nitric oxide synthase. *Proc Natl Acad Sci U S A.* 1996;93(23):13176-81.
263. Yadav VR, Teng B, Mustafa SJ. Enhanced A(1) adenosine receptor-induced vascular contractions in mesenteric artery and aorta of in L-NAME mouse model of hypertension. *Eur J Pharmacol.* 2019;842:111-7.
264. Paulis L, Zicha J, Kunes J, et al. Regression of L-NAME-induced hypertension: the role of nitric oxide and endothelium-derived constricting factor. *Hypertens Res.* 2008;31(4):793-803.
265. van Haperen R, de Waard M, van Deel E, et al. Reduction of blood pressure, plasma cholesterol, and atherosclerosis by elevated endothelial nitric oxide. *The Journal of biological chemistry.* 2002;277(50):48803-7.
266. Kojda G, Laursen JB, Ramasamy S, et al. Protein expression, vascular reactivity and soluble guanylate cyclase activity in mice lacking the endothelial cell nitric oxide synthase: contributions of NOS isoforms to blood pressure and heart rate control. *Cardiovasc Res.* 1999;42(1):206-13.
267. Musialek P, Lei M, Brown HF, et al. Nitric oxide can increase heart rate by stimulating the hyperpolarization-activated inward current, I(f). *Circ Res.* 1997;81(1):60-8.
268. Gholamreza-Fahimi E, Bisha M, Hahn J, et al. Cyclooxygenase activity in bradykinin-induced dermal extravasation. A study in mice and humans. *Biomed Pharmacother.* 2020;123:109797.
269. Krybus M, Sieradzki M, Fahimi E, et al. Contribution of cyclooxygenase-1-dependent prostacyclin synthesis to bradykinin-induced dermal extravasation. *Biomed Pharmacother.* 2022;148:112786.
270. Félétou M, Huang Y, Vanhoutte PM. Endothelium-mediated control of vascular tone: COX-1 and COX-2 products. *Br J Pharmacol.* 2011;164(3):894-912.
271. Eskandari D, Zou D, Grote L, et al. Acetazolamide Reduces Blood Pressure and Sleep-Disordered Breathing in Patients With Hypertension and Obstructive Sleep Apnea: A Randomized Controlled Trial. *J Clin Sleep Med.* 2018;14(3):309-17.
272. Pickkers P, Hughes AD, Russel FG, et al. In vivo evidence for K(Ca) channel opening properties of acetazolamide in the human vasculature. *Br J Pharmacol.* 2001;132(2):443-50.
273. Parati G, Revera M, Giuliano A, et al. Effects of acetazolamide on central blood pressure, peripheral blood pressure, and arterial distensibility at acute high altitude exposure. *Eur Heart J.* 2013;34(10):759-66.
274. Zhao X, Ho D, Gao S, et al. Arterial Pressure Monitoring in Mice. *Curr Protoc Mouse Biol.* 2011;1:105-22.
275. Janssen BJ, De Celle T, Debets JJ, et al. Effects of anesthetics on systemic hemodynamics in mice. *Am J Physiol Heart Circ Physiol.* 2004;287(4):H1618-24.

276. Erkens R, Kramer CM, Lückstädt W, et al. Left ventricular diastolic dysfunction in Nrf2 knock out mice is associated with cardiac hypertrophy, decreased expression of SERCA2a, and preserved endothelial function. *Free Radic Biol Med*. 2015;89:906-17.
277. Black MA, Cable NT, Thijssen DH, et al. Importance of measuring the time course of flow-mediated dilatation in humans. *Hypertension*. 2008;51(2):203-10.
278. Green DJ, Dawson EA, Groenewoud HM, et al. Is flow-mediated dilation nitric oxide mediated?: A meta-analysis. *Hypertension*. 2014;63(2):376-82.
279. Kooijman M, Thijssen DH, de Groot PC, et al. Flow-mediated dilatation in the superficial femoral artery is nitric oxide mediated in humans. *J Physiol*. 2008;586(4):1137-45.
280. Bellien J, Iacob M, Eltchaninoff H, et al. AT1 receptor blockade prevents the decrease in conduit artery flow-mediated dilatation during NOS inhibition in humans. *Clin Sci (Lond)*. 2007;112(7):393-401.
281. Fischer D, Landmesser U, Spiekermann S, et al. Cytochrome P450 2C9 is involved in flow-dependent vasodilation of peripheral conduit arteries in healthy subjects and in patients with chronic heart failure. *Eur J Heart Fail*. 2007;9(8):770-5.
282. Joannides R, Haefeli WE, Linder L, et al. Nitric oxide is responsible for flow-dependent dilatation of human peripheral conduit arteries in vivo. *Circulation*. 1995;91(5):1314-9.
283. Hu Y, Chen M, Wang M, et al. Flow-mediated vasodilation through mechanosensitive G protein-coupled receptors in endothelial cells. *Trends Cardiovasc Med*. 2022;32(2):61-70.
284. Dela Paz NG, Melchior B, Frangos JA. Shear stress induces  $G\alpha(q/11)$  activation independently of G protein-coupled receptor activation in endothelial cells. *Am J Physiol Cell Physiol*. 2017;312(4):C428-c37.
285. Chachisvilis M, Zhang YL, Frangos JA. G protein-coupled receptors sense fluid shear stress in endothelial cells. *Proc Natl Acad Sci U S A*. 2006;103(42):15463-8.
286. Gryglewski RJ, Chłopicki S, Uraz W, et al. Significance of endothelial prostacyclin and nitric oxide in peripheral and pulmonary circulation. *Med Sci Monit*. 2001;7(1):1-16.
287. Liuba P, Batra S, Pesonen E, et al. Bradykinin preconditions postischemic arterial endothelial function in humans. *J Card Surg*. 2005;20(5):420-4.
288. Matsuo S, Matsumoto T, Takashima H, et al. The relationship between flow-mediated brachial artery vasodilation and coronary vasomotor responses to bradykinin: comparison with those to acetylcholine. *J Cardiovasc Pharmacol*. 2004;44(2):164-70.
289. Tarutani Y, Matsumoto T, Takashima H, et al. Brachial artery flow-mediated vasodilation is correlated with coronary vasomotor and fibrinolytic responses induced by bradykinin. *Hypertens Res*. 2005;28(1):59-66.
290. Emanuelli C, Minasi A, Zacheo A, et al. Local delivery of human tissue kallikrein gene accelerates spontaneous angiogenesis in mouse model of hindlimb ischemia. *Circulation*. 2001;103(1):125-32.

291. Li J, Song F, Chen R, et al. Bradykinin-pretreated Human cardiac-specific c-kit(+) Cells Enhance Exosomal miR-3059-5p and Promote Angiogenesis Against Hindlimb Ischemia in mice. *Stem Cell Rev Rep*. 2023.
292. Rosenberry R, Nelson MD. Reactive hyperemia: a review of methods, mechanisms, and considerations. *Am J Physiol Regul Integr Comp Physiol*. 2020;318(3):R605-r18.
293. Schneckmann R, Suvorava T, Hundhausen C, et al. Endothelial Hyaluronan Synthase 3 Augments Postischemic Arteriogenesis Through CD44/eNOS Signaling. *Arterioscler Thromb Vasc Biol*. 2021;41(10):2551-62.
294. Riccioppo Neto F, Corrado AP, Rocha e Silva M. Apnea, bradycardia, hypotension and muscular contraction induced by intracarotid injection of bradykinin. *J Pharmacol Exp Ther*. 1974;190(2):316-26.
295. Soukhova-O'Hare GK, Zhang JW, Gozal D, et al. Bradykinin B2 receptors mediate pulmonary sympathetic afferents induced reflexes in rabbits. *Life Sci*. 2006;78(17):1990-7.
296. Prostran M, Samardžić R, Todorović Z, et al. The potentiation of cardiodepressant and hypotensive effects of bradykinin by enalapril and captopril both in vitro and in vivo. *Gen Pharmacol*. 1991;22(6):995-1000.
297. Driamov SV, Bellahcene M, Butz S, et al. Bradykinin is a mediator, but unlikely a trigger, of antiarrhythmic effects of ischemic preconditioning. *J Cardiovasc Electrophysiol*. 2007;18(1):93-9.
298. Madeddu P, Salis MB, Emanuelli C. Altered baroreflex control of heart rate in bradykinin B2-receptor knockout mice. *Immunopharmacology*. 1999;45(1-3):21-7.
299. Perego F, De Maria B, Bova M, et al. Analysis of Heart-Rate Variability during Angioedema Attacks in Patients with Hereditary C1-Inhibitor Deficiency. *Int J Environ Res Public Health*. 2021;18(6).
300. Izrailtyan I, Kresh JY. Bradykinin modulation of isolated rabbit heart function is mediated by intrinsic cardiac neurons. *Cardiovasc Res*. 1997;33(3):641-9.
301. Brailoiu E, McGuire M, Shuler SA, et al. Modulation of cardiac vagal tone by bradykinin acting on nucleus ambiguus. *Neuroscience*. 2017;365:23-32.
302. Ribuot C, Godin D, Couture R, et al. In vivo B2-receptor-mediated negative chronotropic effect of bradykinin in canine sinus node. *Am J Physiol*. 1993;265(3 Pt 2):H876-9.
303. Emanuelli C, Madeddu P. Effect of early blockade of bradykinin B2-receptors on the blood pressure phenotype of normotensive and spontaneously hypertensive rats. *Pharmacol Res*. 1997;35(6):522-6.
304. Carini F, Guelfi M, Lecci A, et al. Cardiovascular effects of peptide kinin B2 receptor antagonists in rats. *Can J Physiol Pharmacol*. 2002;80(4):310-22.
305. Braun C, Ade M, Unger T, et al. Effects of bradykinin and icatibant on renal hemodynamics in conscious spontaneously hypertensive and normotensive rats. *J Cardiovasc Pharmacol*. 1997;30(4):446-54.
306. LeFebvre J, Shintani A, Gebretsadik T, et al. Bradykinin B(2) receptor does not contribute to blood pressure lowering during AT(1) receptor blockade. *J Pharmacol Exp Ther*. 2007;320(3):1261-7.

307. Lee JS, Morrow D, Andresen MC, et al. Isoflurane depresses baroreflex control of heart rate in decerebrate rats. *Anesthesiology*. 2002;96(5):1214-22.
308. Marketou M, Kintsurashvili E, Papanicolaou KN, et al. Cardioprotective effects of a selective B(2) receptor agonist of bradykinin post-acute myocardial infarct. *Am J Hypertens*. 2010;23(5):562-8.
309. Yin H, Chao J, Bader M, et al. Differential role of kinin B1 and B2 receptors in ischemia-induced apoptosis and ventricular remodeling. *Peptides*. 2007;28(7):1383-9.
310. Ito H, Hayashi I, Izumi T, et al. Bradykinin inhibits development of myocardial infarction through B2 receptor signalling by increment of regional blood flow around the ischaemic lesions in rats. *Br J Pharmacol*. 2003;138(1):225-33.
311. Wollert KC, Studer R, Doerfer K, et al. Differential effects of kinins on cardiomyocyte hypertrophy and interstitial collagen matrix in the surviving myocardium after myocardial infarction in the rat. *Circulation*. 1997;95(7):1910-7.
312. Stauss HM, Zhu YC, Redlich T, et al. Angiotensin-converting enzyme inhibition in infarct-induced heart failure in rats: bradykinin versus angiotensin II. *J Cardiovasc Risk*. 1994;1(3):255-62.
313. Tei C, Nishimura RA, Seward JB, et al. Noninvasive Doppler-derived myocardial performance index: correlation with simultaneous measurements of cardiac catheterization measurements. *J Am Soc Echocardiogr*. 1997;10(2):169-78.
314. Marshall AG, Neikirk K, Vue Z, et al. Cardiovascular hemodynamics in mice with tumor necrosis factor receptor-associated factor 2 mediated cytoprotection in the heart. *Front Cardiovasc Med*. 2023;10:1064640.
315. Alhakak AS, Teerlink JR, Lindenfeld J, et al. The significance of left ventricular ejection time in heart failure with reduced ejection fraction. *Eur J Heart Fail*. 2021;23(4):541-51.
316. Goody PR, Hosen MR, Christmann D, et al. Aortic Valve Stenosis: From Basic Mechanisms to Novel Therapeutic Targets. *Arterioscler Thromb Vasc Biol*. 2020;40(4):885-900.
317. Biberthaler P, Mendler N, Ettner U, et al. Endothelial prostacyclin (PGI-2) production of human and porcine valve allografts related to ischemic history. *Eur J Cardiothorac Surg*. 1998;14(5):503-7.
318. Feng XJ, Van Hove CE, Walter PJ, et al. Effects of storage temperature and fetal calf serum on the endothelium of porcine aortic valves. *J Thorac Cardiovasc Surg*. 1996;111(1):218-30.
319. Helske S, Lindstedt KA, Laine M, et al. Induction of local angiotensin II-producing systems in stenotic aortic valves. *J Am Coll Cardiol*. 2004;44(9):1859-66.
320. Helske S, Laine M, Kupari M, et al. Increased expression of profibrotic neutral endopeptidase and bradykinin type 1 receptors in stenotic aortic valves. *Eur Heart J*. 2007;28(15):1894-903.
321. Niepmann ST, Willemsen N, Boucher AS, et al. Toll-like receptor-3 contributes to the development of aortic valve stenosis. *Basic Res Cardiol*. 2023;118(1):6.

322. Niepmann ST, Steffen E, Zietzer A, et al. Graded murine wire-induced aortic valve stenosis model mimics human functional and morphological disease phenotype. *Clin Res Cardiol*. 2019;108(8):847-56.
323. Honda S, Miyamoto T, Watanabe T, et al. A novel mouse model of aortic valve stenosis induced by direct wire injury. *Arterioscler Thromb Vasc Biol*. 2014;34(2):270-8.
324. Peltonen T, Ohukainen P, Ruskoaho H, et al. Targeting vasoactive peptides for managing calcific aortic valve disease. *Ann Med*. 2017;49(1):63-74.
325. <https://www.jax.org/news-and-insights/jax-blog/2017/November/when-are-mice-considered-old#:~:text=Mice%20Oranging%20from%2018%20%2D%2024,all%20biomarkers%20in%20all%20animals>.
326. Lee G, Chikwe J, Milojevic M, et al. ESC/EACTS vs. ACC/AHA guidelines for the management of severe aortic stenosis. *Eur Heart J*. 2023;44(10):796-812.
327. Alvandi Z, Bischoff J. Endothelial-Mesenchymal Transition in Cardiovascular Disease. *Arterioscler Thromb Vasc Biol*. 2021;41(9):2357-69.
328. Ishihara K, Kamata M, Hayashi I, et al. Roles of bradykinin in vascular permeability and angiogenesis in solid tumor. *Int Immunopharmacol*. 2002;2(4):499-509.
329. Wang G, Sun J, Liu G, et al. Bradykinin Promotes Cell Proliferation, Migration, Invasion, and Tumor Growth of Gastric Cancer Through ERK Signaling Pathway. *J Cell Biochem*. 2017;118(12):4444-53.
330. Li G, Che H, Wu WY, et al. Bradykinin-mediated Ca(2+) signalling regulates cell growth and mobility in human cardiac c-Kit(+) progenitor cells. *J Cell Mol Med*. 2018;22(10):4688-99.
331. Tan JX, Wang XY, Li HY, et al. HYAL1 overexpression is correlated with the malignant behavior of human breast cancer. *Int J Cancer*. 2011;128(6):1303-15.
332. Trochon V, Mabilat C, Bertrand P, et al. Evidence of involvement of CD44 in endothelial cell proliferation, migration and angiogenesis in vitro. *Int J Cancer*. 1996;66(5):664-8.
333. Krettek A, Sjöberg S. CD44 - a new cardiovascular drug target or merely an innocent bystander? *Cardiovasc Hematol Disord Drug Targets*. 2009;9(4):293-302.
334. Mount PF, Lane N, Venkatesan S, et al. Bradykinin stimulates endothelial cell fatty acid oxidation by CaMKK-dependent activation of AMPK. *Atherosclerosis*. 2008;200(1):28-36.
335. Xiong J, Kawagishi H, Yan Y, et al. A Metabolic Basis for Endothelial-to-Mesenchymal Transition. *Mol Cell*. 2018;69(4):689-98.e7.
336. Hariri MA, Jaffa MA, Saoud R, et al. Vascular Cells Proteome Associated with Bradykinin and Leptin Inflammation and Oxidative Stress Signals. *Antioxidants (Basel)*. 2020;9(12).
337. Dong R, Xu X, Li G, et al. Bradykinin inhibits oxidative stress-induced cardiomyocytes senescence via regulating redox state. *PLoS One*. 2013;8(10):e77034.

338. Mesquita TRR, Miguel-Dos-Santos R, Jesus ICG, et al. Ablation of B(1)- and B(2)-kinin receptors causes cardiac dysfunction through redox-nitroso unbalance. *Life Sci.* 2019;228:121-7.
339. Perhal A, Wolf S, Jamous YF, et al. Increased Reactive Oxygen Species Generation Contributes to the Atherogenic Activity of the B2 Bradykinin Receptor. *Front Med (Lausanne).* 2019;6:32.
340. AbdAlla S, Lothar H, Quitterer U. AT1-receptor heterodimers show enhanced G-protein activation and altered receptor sequestration. *Nature.* 2000;407(6800):94-8.
341. Quitterer U, AbdAlla S. Vasopressor meets vasodepressor: The AT1-B2 receptor heterodimer. *Biochem Pharmacol.* 2014;88(3):284-90.
342. Wambi-Kiéssé CO, Katusic ZS. Inhibition of copper/zinc superoxide dismutase impairs NO.-mediated endothelium-dependent relaxations. *Am J Physiol.* 1999;276(3):H1043-8.
343. Nolfi-Donagan D, Braganza A, Shiva S. Mitochondrial electron transport chain: Oxidative phosphorylation, oxidant production, and methods of measurement. *Redox Biol.* 2020;37:101674.
344. Liu Y, Huang Y, Xu C, et al. Mitochondrial Dysfunction and Therapeutic Perspectives in Cardiovascular Diseases. *Int J Mol Sci.* 2022;23(24).
345. Ranjbarvaziri S, Kooiker KB, Ellenberger M, et al. Altered Cardiac Energetics and Mitochondrial Dysfunction in Hypertrophic Cardiomyopathy. *Circulation.* 2021;144(21):1714-31.
346. Donnadieu E, Bourguignon LY. Ca<sup>2+</sup> signaling in endothelial cells stimulated by bradykinin: Ca<sup>2+</sup> measurement in the mitochondria and the cytosol by confocal microscopy. *Cell Calcium.* 1996;20(1):53-61.
347. Chiang WC, Chen YM, Lin SL, et al. Bradykinin enhances reactive oxygen species generation, mitochondrial injury, and cell death induced by ATP depletion--a role of the phospholipase C-Ca(2+) pathway. *Free Radic Biol Med.* 2007;43(5):702-10.
348. Park SS, Zhao H, Mueller RA, et al. Bradykinin prevents reperfusion injury by targeting mitochondrial permeability transition pore through glycogen synthase kinase 3beta. *J Mol Cell Cardiol.* 2006;40(5):708-16.
349. Reis FC, Haro AS, Bacurau AV, et al. Deletion of Kinin B2 Receptor Alters Muscle Metabolism and Exercise Performance. *PLoS One.* 2015;10(8):e0134844.
350. Venema RC. Post-translational mechanisms of endothelial nitric oxide synthase regulation by bradykinin. *Int Immunopharmacol.* 2002;2(13-14):1755-62.
351. Murthy S, Koval OM, Ramiro Diaz JM, et al. Endothelial CaMKII as a regulator of eNOS activity and NO-mediated vasoreactivity. *PLoS One.* 2017;12(10):e0186311.
352. Fleming I, Fisslthaler B, Dimmeler S, et al. Phosphorylation of Thr(495) regulates Ca(2+)/calmodulin-dependent endothelial nitric oxide synthase activity. *Circ Res.* 2001;88(11):E68-75.
353. Förstermann U, Sessa WC. Nitric oxide synthases: regulation and function. *Eur Heart J.* 2012;33(7):829-37, 37a-37d.

354. Yu Y, Xu LS, Wu Y, et al. The antihypertensive effect of MK on spontaneously hypertensive rats through the AMPK/Akt/eNOS/NO and ERK1/2/Cx43 signaling pathways. *Hypertens Res*. 2021;44(7):781-90.
355. Harris MB, Ju H, Venema VJ, et al. Reciprocal phosphorylation and regulation of endothelial nitric-oxide synthase in response to bradykinin stimulation. *The Journal of biological chemistry*. 2001;276(19):16587-91.
356. Biwer LA, Taddeo EP, Kenwood BM, et al. Two functionally distinct pools of eNOS in endothelium are facilitated by myoendothelial junction lipid composition. *Biochim Biophys Acta*. 2016;1861(7):671-9.
357. Schrage WG, Dietz NM, Eisenach JH, et al. Agonist-dependent variability of contributions of nitric oxide and prostaglandins in human skeletal muscle. *J Appl Physiol (1985)*. 2005;98(4):1251-7.
358. Lauer T, Kleinbongard P, Preik M, et al. Direct biochemical evidence for eNOS stimulation by bradykinin in the human forearm vasculature. *Basic Res Cardiol*. 2003;98(2):84-9.
359. Pretorius M, Brown NJ. Endogenous nitric oxide contributes to bradykinin-stimulated glucose uptake but attenuates vascular tissue-type plasminogen activator release. *J Pharmacol Exp Ther*. 2010;332(1):291-7.
360. Ren Y, Garvin J, Carretero OA. Mechanism involved in bradykinin-induced efferent arteriole dilation. *Kidney Int*. 2002;62(2):544-9.
361. Fisslthaler B, Popp R, Kiss L, et al. Cytochrome P450 2C is an EDHF synthase in coronary arteries. *Nature*. 1999;401(6752):493-7.
362. Heaps CL, Bray JF, McIntosh AL, et al. Endothelial nitric oxide synthase protein distribution and nitric oxide production in endothelial cells along the coronary vascular tree. *Microvasc Res*. 2019;122:34-40.
363. Vaziri ND, Ding Y, Ni Z, et al. Bradykinin down-regulates, whereas arginine analogs up-regulates, endothelial nitric-oxide synthase expression in coronary endothelial cells. *J Pharmacol Exp Ther*. 2005;313(1):121-6.
364. Heuser SK, LoBue A, Li J, et al. Downregulation of eNOS and preserved endothelial function in endothelial-specific arginase 1-deficient mice. *Nitric Oxide*. 2022;125-126:69-77.
365. Suvorava T, Stegbauer J, Thieme M, et al. Sustained hypertension despite endothelial-specific eNOS rescue in eNOS-deficient mice. *Biochem Biophys Res Commun*. 2015;458(3):576-83.
366. Yang CM, Lin MI, Hsieh HL, et al. Bradykinin-induced p42/p44 MAPK phosphorylation and cell proliferation via Src, EGF receptors, and PI3-K/Akt in vascular smooth muscle cells. *J Cell Physiol*. 2005;203(3):538-46.
367. Ji B, Shang L, Wang C, et al. Roles for heterodimerization of APJ and B2R in promoting cell proliferation via ERK1/2-eNOS signaling pathway. *Cell Signal*. 2020;73:109671.
368. Dagher OK, Jaffa MA, Habib A, et al. Heteromerization fingerprints between bradykinin B2 and thromboxane TP receptors in native cells. *PLoS One*. 2019;14(5):e0216908.

369. Yu Y, Wu XQ, Su FF, et al. Maximakinin reduced intracellular Ca<sup>2+</sup> level in vascular smooth muscle cells through AMPK/ERK1/2 signaling pathways. *Hypertens Res.* 2023;46(8):1949-60.
370. Misra A, Feng Z, Zhang J, et al. Using In Vivo and Tissue and Cell Explant Approaches to Study the Morphogenesis and Pathogenesis of the Embryonic and Perinatal Aorta. *J Vis Exp.* 2017(127).
371. Abeledo-Machado A, Peña-Zanoni M, Bornancini D, et al. Sex-specific Regulation of Prolactin Secretion by Pituitary Bradykinin Receptors. *Endocrinology.* 2022;163(9).
372. Sato A, Miura H, Liu Y, et al. Effect of gender on endothelium-dependent dilation to bradykinin in human adipose microvessels. *Am J Physiol Heart Circ Physiol.* 2002;283(3):H845-52.
373. Kulkarni M, Travers JB, Rohan C. High Estrogen States in Hereditary Angioedema: a Spectrum. *Clin Rev Allergy Immunol.* 2021;60(3):396-403.
374. Gangnus T, Burckhardt BB. Reliable measurement of plasma kinin peptides: Importance of preanalytical variables. *Res Pract Thromb Haemost.* 2022;6(1):e12646.
375. Emanuelli C, Salis MB, Chao J, et al. Adenovirus-mediated human tissue kallikrein gene delivery inhibits neointima formation induced by interruption of blood flow in mice. *Arterioscler Thromb Vasc Biol.* 2000;20(6):1459-66.
376. Tschöpe C, Walther T, Königer J, et al. Prevention of cardiac fibrosis and left ventricular dysfunction in diabetic cardiomyopathy in rats by transgenic expression of the human tissue kallikrein gene. *Faseb j.* 2004;18(7):828-35.
377. Koch M, Spillmann F, Dendorfer A, et al. Cardiac function and remodeling is attenuated in transgenic rats expressing the human kallikrein-1 gene after myocardial infarction. *Eur J Pharmacol.* 2006;550(1-3):143-8.
378. Hu D, Dong R, Yang Y, et al. Human kallikrein overexpression alleviates cardiac aging by alternatively regulating macrophage polarization in aged rats. *Faseb j.* 2019;33(7):8436-52.

**Appendix 1:** Model description, main findings, publication year and references of genetically modified models of kallikrein-kinin system.

Model description	Main findings	Publication year and reference.
<b><i>Knockout models</i></b>		
<b>B<sub>2</sub>R-KO mice</b> on a 129/J genetic background.	-The blood pressure response to bradykinin was completely abolished in B <sub>2</sub> R-KO. The hypertensive response to high sodium intake increased in B <sub>2</sub> R-KO mice but not to angiotensin II.  -Increased heart weight.	1996, (147)
<b>B<sub>2</sub>R-KO mice</b> on a 129Sv/J mice background.	-B <sub>2</sub> R-KO mice showed elevated sBP, increased blood pressure sensitivity to salt and angiotensin II. No effect to B <sub>2</sub> R stimulation but increased sensitivity to B <sub>1</sub> R stimulation. Lower sensitivity to NOS inhibition.  -Increased heart weight.	1997, (148)
<b>B<sub>2</sub>R-KO mice</b> on a 129Sv/J mice background.	-Under basal conditions, sBP and heart rate (HR) were higher in B <sub>2</sub> R-KO mice.  -B <sub>2</sub> R-KO mice showed accelerated renovascular hypertension.	1998, (149)
<b>B<sub>2</sub>R-KO mice</b> on a 129Sv/J mice background.	In heterozygous B <sub>2</sub> R-KO mice, sBP was like WT mice until 5 months old, then it raised to the elevated levels of knockout mice at 7 months of age.	1999, (150)
<b>B<sub>2</sub>R-KO mice</b> on a 129/J mice background.	-sBP of B <sub>2</sub> R-KO mice was normal at 50 days of age and gradually increased, reaching a plateau at 6 months.  -In heterozygous B <sub>2</sub> R mice, sBP elevation was elevated after 6 months of age.  -Intra-arterial measurements confirmed the elevated blood pressure at 360 days.  -Tachycardia was observed in B <sub>2</sub> R-KO and heterozygous mice since the early phases of life through adulthood.  -LV end-diastolic pressure increased in B <sub>2</sub> R-KO at 180 days and increased even more at 360 days.	1999, (151)
<b>B<sub>2</sub>R-KO mice</b> on C57BL/6 mice background.	-B <sub>2</sub> R-KO mice on high salt diet showed elevated sBP at 2,3, and 4 months of age.  -MAP was elevated when measured at 4 months of age.	1999, (153)
<b>B<sub>2</sub>R-KO mice</b> on a 129Sv/J mice background.	B <sub>2</sub> R-KO mice showed normal blood pressure, HR, and renal functions on normal or high salt diet.	2001, (152)

Model description	Main findings	Publication year and reference.
<b>B<sub>2</sub>R-KO mice</b> on a 129Sv/J mice background.	-B <sub>2</sub> R-KO mice showed comparable blood pressure and cardiac function to WT mice. -After induction of myocardial infarction, development of heart failure and remodelling were also comparable between B <sub>2</sub> R-KO and WT mice.	2001, (105)
<b>B<sub>2</sub>R-KO mice</b> on a 129Sv/J mice background.	-B <sub>2</sub> R-KO mice showed comparable blood pressure to WT mice at baseline and after infusion of Ang-II. -B <sub>1</sub> R expression levels was higher in B <sub>2</sub> R-KO mice at baseline and after infusion of Ang-II.	2001, (81)
<b>Tissue kallikrein-deficient mice</b>	-Decrease in LV functions. -Decrease in flow-Induced dilatation in isolated perfused carotid arteries. -Normal systolic blood pressure and heart rate.	2001, (162)
Comparative study of female <b>B<sub>2</sub>R-KO mice</b> and <b>tissue kallikrein-deficient mice</b> on C57BL/6 genetic background.	-B <sub>2</sub> R-KO and tissue kallikrein-deficient mice showed comparable sBP and dBP to WT mice. -Only B <sub>2</sub> R-KO showed lower heart rate, renal and coronary blood flow than WT. -Cardiac functions were comparable to WT mice. -B <sub>2</sub> R-KO showed higher increase of blood pressure to angiotensin II and norepinephrine injections. -Response to bradykinin was absent in B <sub>2</sub> R-KO but was totally preserved in tissue kallikrein-deficient mice. -Increase in renal renin mRNA in B <sub>2</sub> R-KO mice.	2002, (163)
<b>B<sub>2</sub>R-KO mice</b> on C57BL/6 background.	-B <sub>2</sub> R-KO mice showed higher sBP than WT mice through 6 to 12 months of age. -B <sub>2</sub> R-KO mice showed higher HR than WT mice at 8 and 12 months of age. -At 12 months of age, B <sub>2</sub> R-KO mice showed mild impairment in cardiac structure and functions.	2003, (154)
<b>B<sub>2</sub>R-KO mice</b> on C57BL/6J background	-Blood pressure, HR, renal plasma flow, glomerular filtration rate, and renal vascular resistance were comparable between WT and B <sub>2</sub> R-KO mice.	2003, (155)

Model description	Main findings	Publication year and reference.
Double <b>knockout of B<sub>1</sub>R and B<sub>2</sub>R</b> mice on C57BL/6J background	<p>-B<sub>1</sub>R/B<sub>2</sub>R double knockout mice have similar blood pressure to WT mice and lower HR.</p> <p>-Normal heart function even at mice of 15-18 months of age.</p> <p>-Showed lower decrease in blood pressure in response to bacterial lipopolysaccharide injection.</p>	2007, (159)
<b>B<sub>2</sub>R-KO</b> mice and double <b>knockout of B<sub>1</sub>R and B<sub>2</sub>R</b> mice on C57BL/6J background	Blood pressure was comparable among WT, B <sub>2</sub> R-KO, and B <sub>1</sub> R/B <sub>2</sub> R double knockout mice.	2007,(160)
Double <b>knockout of B<sub>1</sub>R and B<sub>2</sub>R</b> on C57BL/6J background	Loss of both B <sub>1</sub> R and B <sub>2</sub> R did not further deteriorate the cardiac dysfunction in mice model with type-1 diabetes.	2010, (161)
<b>B<sub>2</sub>R-KO mice</b> on C57BL/6J background.	<i>Ex vivo</i> studies on B <sub>2</sub> R-KO mice showed impairment in cardiomyocytes functions.	2010,(156)
<b>B<sub>2</sub>R-KO mice</b> on C57BL/6J background.	B <sub>2</sub> R-KO mice showed normal cardiac functions.	2013, (157)
Conditional <b>knockout of collecting duct B<sub>2</sub>R</b> .	-Mice lacking collecting duct B <sub>2</sub> R showed higher increase in blood pressure than WT mice only after intake of 8% salt diet and angiotensin II infusion.	2016, (164)
Mice in which <b>B<sub>2</sub>R gene has been specifically deleted from the endothelium</b> (B <sub>2</sub> <sup>flox/flox</sup> .Tie2 <sup>Cre</sup> )	<p>-Normal blood pressure readings compared to the WT.</p> <p>-Lower body temperature (by about 1.5 °C) compared to WT mice.</p>	2020, unpublished observation documented in (61)
Mice in which CRISPR/Cas9 method to delete <b>kininogen1 and kininogen2</b> genes.	Both mice models had about 50% reductions in plasma low molecular weight kininogen, significantly elevated systolic blood pressure and normal heart rate compared to WT mice.	2023, (165)
<b><u>Overexpression models</u></b>		
Transgenic mice with <b>human B<sub>2</sub> receptor overexpression</b> under the control of the Rous sarcoma virus long terminal repeat promoter.	<p>-Transgenic mice showed significant reductions in systolic blood pressure.</p> <p>-Intra-aortic injections of bradykinin resulted in decrease in mean blood pressure in both transgenic and control mice with more pronounced decrease in transgenic mice.</p>	1997, (167)
Transgenic mice with <b>human B<sub>2</sub> receptor overexpression</b> under the control of the Rous sarcoma virus long terminal repeat promoter.	-Enhanced renal function through activation of NO-cGMP and cAMP signal transduction pathways.	2000, (239)

Model description	Main findings	Publication year and reference.
Adenovirus-mediated <b>human tissue kallikrein gene</b> delivery in B <sub>2</sub> R-KO mice on J129Sv background and B <sub>2</sub> R overexpression mice on C57BL/6 background.	-Adenovirus-mediated human tissue kallikrein gene reduced neointima formation which is responsible for artery restenosis after angioplasty.  -The protective action of Adenovirus-mediated human tissue kallikrein gene on neointima formation was reduced in B <sub>2</sub> R-KO mice and amplified in transgenic mice overexpressing human B <sub>2</sub> R.	2000, (375)
Transgenic rat harboring the <b>human tissue kallikrein gene</b> under the control of the zinc-inducible metallothionein promoter.	-Transgenic rats had a lower MAP in comparison with control rats.  -Upon induction of cardiac hypertrophy with isoproterenol, transgenic rats showed less fibrosis and hypertrophy.	2000, (166)
Transgenic rat harboring the <b>human tissue kallikrein gene</b> under the control of the zinc-inducible metallothionein promoter.	Transgenic rats conferred extra protection against LV contractile dysfunction and extracellular matrix remodelling in comparison to WT rats after induction of diabetic cardiomyopathy by streptozotocin.	2004, (376)
Transgenic rat harboring the <b>human tissue kallikrein gene</b> under the control of the zinc-inducible metallothionein promoter	Transgenic rats showed better LV function and less LV remodelling than WT rats after induction of myocardial infarction.	2006, (377)
<b>Endothelium-specific human B<sub>2</sub>R overexpression</b> mice. Tie-2 promoter was used to specifically target the construct to the vascular endothelium.	Transgenic mice showed lower sBP than negative littermates.	2018, (195)
<b>Transgenic rats with overexpression of bradykinin in the proximal convoluted tubules in kidney.</b> Kidney androgen regulated protein promoter was used to direct the expression of the construct specifically in proximal tubules.	Transgenic rats showed: -increase in sBP and HR. -no change in MAP. -increase in LV mass, cardiac output, and decrease in renal artery blood flow. -decrease in plasma renin and increase in plasma angiotensinogen. -increase in B <sub>2</sub> R mRNA expression in outer cortex of kidney.	2018, (53)
<b>Human kallikrein overexpression</b> rats.	Human kallikrein overexpression protected against aging-induced cardiac dysfunction.	2019, (378)
<b>Endothelium-specific overexpression of B<sub>2</sub>R in rats.</b> Vascular endothelial cadherin promoter was used to specifically target the construct to the vascular endothelium.	No data about cardiovascular characterization.	2019, (219)

Abbreviations: B<sub>2</sub>R-KO: bradykinin type-II receptor knockout, B<sub>2</sub>R: bradykinin type-II receptor, B<sub>1</sub>R: bradykinin type-I receptor, WT: wild-type, NO: nitric oxide, NOS: nitric oxide synthase, sBP: systolic blood pressure, HR: heart rate, MAP: mean arterial pressure, dBP: diastolic blood pressure, mRNA: messenger ribonucleic acid, cAMP: Cyclic adenosine monophosphate, cGMP: Cyclic guanosine monophosphate, LV: left ventricular.

**Appendix 2:** Proteins that were significantly changed in B<sub>2</sub><sup>tg</sup> mice, uniprot accession, description, symbol, abundance ratio, Log<sub>2</sub> (abundance ratio), and adjusted P-value are described for every protein.

Uniprot Accession	Description	Symbol	Abundance Ratio: (B <sub>2</sub> <sup>tg</sup> )/(wild-type)	Log <sub>2</sub> (abundance ratio)	Adjusted P-value
Q9JK42	[Pyruvate dehydrogenase (acetyl-transferring)] kinase isozyme 2, mitochondrial	PDK2	0.64	-0.65	4.31E-02
Q9DAK9	14 kDa phosphohistidine phosphatase	PHPT1	2.03	1.02	1.84E-02
G3X9M0	28S ribosomal protein S29, mitochondrial	DAP3	0.55	-0.87	3.04E-02
Q61733	28S ribosomal protein S31, mitochondrial	MRPS31	0.45	-1.15	2.03E-03
Q6P3A8	2-oxoisovalerate dehydrogenase subunit beta, mitochondrial	BCKDHB	0.53	-0.91	1.85E-03
Q3UK02	39S ribosomal protein L9, mitochondrial	MRPL9	0.44	-1.19	4.20E-02
Q91WT7	3-alpha-hydroxysteroid dehydrogenase type 1	AKR1C14	2.42	1.27	3.62E-02
Q91VT4	3-oxoacyl-[acyl-carrier-protein] reductase	CBR4	0.61	-0.71	1.80E-02
P62281	40S ribosomal protein S11	RPS11	1.56	0.64	2.19E-02
A0A140LIF0	5-demethoxyubiquinone hydroxylase, mitochondrial	COQ7	0.41	-1.29	3.16E-05
P62830	60S ribosomal protein L23	RPL23	1.89	0.92	9.26E-05
A0A1W2P7X0	ABRA C-terminal-like protein (Fragment)	ABRACL	0.44	-1.20	3.57E-06
Q14DH7	Acyl-CoA synthetase short-chain family member 3, mitochondrial	ACSS3	0.60	-0.75	8.31E-03
Q8VHQ9	Acyl-coenzyme A thioesterase 11	ACOT11	0.50	-1.00	4.84E-04
Q9CQR4	Acyl-coenzyme A thioesterase 13	ACOT13	0.56	-0.83	7.94E-03
J3QP56	Acyl-protein thioesterase 1	LYPLA1	0.54	-0.89	3.49E-03
A2BDX3	Adenylyltransferase and sulfurtransferase MOCS3	MOCS3	1.61	0.68	4.35E-03
Q9CQW2	ADP-ribosylation factor-like protein 8B	ARL8B	0.54	-0.89	1.32E-03
Q91VB8	Alpha globin 1	HBA-A1	0.59	-0.75	4.33E-02
A0A0G2JE03	Anaphase-promoting complex subunit 5	ANAPC5	0.36	-1.49	1.61E-02
P14824	Annexin A6	ANXA6	0.60	-0.75	3.82E-02
Q06185	ATP synthase subunit e, mitochondrial	ATP5ME	1.80	0.85	2.04E-03
P97450	ATP synthase-coupling factor 6, mitochondrial	ATP5PF	2.47	1.30	1.45E-03
Q6P542	ATP-binding cassette sub-family F member 1	ABCF1	0.45	-1.14	2.19E-06
K3W4Q8	Basigin	BSG	0.57	-0.81	1.67E-02
Q61335	B-cell receptor-associated protein 31	BCAP31	1.53	0.61	3.61E-02
A8DUK4	Beta-globin	HBB-BS	0.55	-0.85	1.36E-02
Q9DBL7	Bifunctional coenzyme A synthase	COASY	0.56	-0.83	2.19E-03

Uniprot Accession	Description	Symbol	Abundance Ratio: (B <sub>2</sub> <sup>tg</sup> )/(wild-type)	Log <sub>2</sub> (abundance ratio)	Adjusted P-value
Q6GQS1	Calcium-binding mitochondrial carrier protein SCaMC-3	SLC25A23	2.05	1.04	1.89E-05
A0A0G2JFI6	Calponin-3 (Fragment)	CNN3	0.27	-1.91	5.66E-04
P31324	cAMP-dependent protein kinase type II-beta regulatory subunit	PRKAR2B	0.54	-0.89	3.23E-03
P13634	Carbonic anhydrase 1	CA1	0.42	-1.26	4.65E-07
P00920	Carbonic anhydrase 2	CA2	0.49	-1.04	2.44E-04
P52825	Carnitine O-palmitoyltransferase 2, mitochondrial	CPT2	0.59	-0.76	4.11E-02
A2APM3	CD44 antigen	CD44	2.91	1.54	5.66E-04
Q91WS0	CDGSH iron-sulfur domain-containing protein 1	CISD1	0.61	-0.72	4.31E-02
Q924Z4	Ceramide synthase 2	CERS2	1.77	0.82	2.73E-02
Q6IRU5	Clathrin light chain B	CLTB	3.07	1.62	1.16E-06
P60824	Cold-inducible RNA-binding protein	CIRBP	0.54	-0.90	2.18E-02
A0A087WS16	Collagen, type VI, alpha 3	COL6A3	1.51	0.60	4.41E-02
Q3U898	COP9 signalosome complex subunit 9	COPS9	0.18	-2.45	8.97E-08
P63254	Cysteine-rich protein 1	CRIP1	0.58	-0.78	5.63E-03
Q9CPX8	Cytochrome b-c1 complex subunit 10	UQCR11	0.34	-1.57	3.16E-04
Q9CR68	Cytochrome b-c1 complex subunit Rieske, mitochondrial	UQCRC1	0.50	-1.01	1.42E-03
P43024	Cytochrome c oxidase subunit 6A1, mitochondrial	COX6A1	0.51	-0.96	1.01E-04
P56392	Cytochrome c oxidase subunit 7A1, mitochondrial	COX7A1	0.42	-1.26	4.14E-07
O35459	Delta(3,5)-Delta(2,4)-dienoyl-CoA isomerase, mitochondrial	ECH1	0.57	-0.82	1.96E-02
O08749	Dihydrolipoyl dehydrogenase, mitochondrial	DLD	0.54	-0.89	8.23E-03
D3YUZ8	Disks large homolog 2	DLG2	0.41	-1.27	2.29E-02
Q9D0M5	Dynein light chain 2, cytoplasmic	DYNLL2	0.46	-1.12	2.69E-04
F8WJ93	Echinoderm microtubule-associated protein-like 4	EML4	0.60	-0.73	2.07E-02
Q921G7	Electron transfer flavoprotein-ubiquinone oxidoreductase, mitochondrial	ETFDH	0.56	-0.83	1.89E-02
A0A0R4J2D2	Extracellular sulfatase Sulf-1	SULF1	0.46	-1.11	2.01E-02
P11404	Fatty acid-binding protein, heart	FABP3	0.56	-0.83	1.80E-02
F6SJM7	Fucose mutarotase (Fragment)	FUOM	0.17	-2.59	1.03E-08
Q8R3R8	Gamma-aminobutyric acid receptor-associated protein-like 1	GABARAPL1	0.15	-2.77	1.65E-08
Q7TMG8	Glioblastoma amplified sequence	NIPSNAP2	0.63	-0.67	4.51E-02
Q64516	Glycerol kinase	GK	0.63	-0.66	3.30E-02
P13707	Glycerol-3-phosphate dehydrogenase [NAD(+)], cytoplasmic	GPD1	0.53	-0.91	6.36E-03
Q9ET01	Glycogen phosphorylase, liver form	PYGL	0.60	-0.74	4.97E-02
P02089	Hemoglobin subunit beta-2	HBB-B2	0.48	-1.05	2.72E-05

Uniprot Accession	Description	Symbol	Abundance Ratio: (B <sub>2</sub> <sup>tg</sup> )/(wild-type)	Log <sub>2</sub> (abundance ratio)	Adjusted P-value
Q9JMG7	Hepatoma-derived growth factor-related protein 3	HDGFL3	1.50	0.59	2.68E-02
O08528	Hexokinase-2	HK2	0.57	-0.80	2.40E-02
A2AWS5	Histone deacetylase	HDAC5	2.31	1.21	2.99E-03
P10922	Histone H1.0	H1-0	1.91	0.94	1.29E-03
P15864	Histone H1.2	H1-2	1.71	0.77	1.59E-03
P43274	Histone H1.4	H1-4	1.92	0.94	7.35E-04
P43276	Histone H1.5	H1-5	1.94	0.95	6.50E-03
Q8BFU2	Histone H2A type 3	H2AC25	3.44	1.78	2.67E-14
D3YXU8	Hyaluronidase	HYAL1	4.35	2.12	5.76E-05
Q61425	Hydroxyacyl-coenzyme A dehydrogenase, mitochondrial	HADH	0.44	-1.18	7.53E-05
Q2TPA8	Hydroxysteroid dehydrogenase-like protein 2	HSDL2	0.57	-0.82	1.12E-02
P01837	Immunoglobulin kappa constant	IGKC	1.53	0.61	1.90E-02
A0A0B4J1H8	Immunoglobulin kappa variable 1-133 (Fragment)	IGKV1-133	2.27	1.18	4.96E-02
Q91UZ5	Inositol monophosphatase 2	IMPA2	0.34	-1.56	1.23E-05
P85094	Isochorismatase domain-containing protein 2A	ISOC2A	0.39	-1.36	1.89E-06
P58044	Isopentenyl-diphosphate Delta-isomerase 1	IDI1	0.50	-1.01	8.90E-03
Q3UV17	Keratin, type II cytoskeletal 2 oral	KRT76	1.98	0.98	5.90E-06
O89017	Legumain	LGMN	0.47	-1.08	1.77E-03
E9QP62	LIM and senescent cell antigen-like-containing domain protein	LIMS1	0.56	-0.83	5.68E-03
A0A1L1SRE8	Low-density lipoprotein receptor	LDLR	0.33	-1.59	6.47E-03
Q62190	Macrophage-stimulating protein receptor	MST1R	6.48	2.70	4.83E-07
A0A1Y7VJZ2	Maleylacetoacetate isomerase	GSTZ1	0.59	-0.76	2.20E-02
Q9D115	Methylmalonyl-CoA epimerase, mitochondrial	MCEE	0.58	-0.78	2.41E-02
Q8R404	MICOS complex subunit MIC13	MICOS13	0.57	-0.81	6.53E-03
Q9CQ20	Mid1-interacting protein 1	MID1IP1	0.28	-1.82	8.52E-04
P12242	Mitochondrial brown fat uncoupling protein 1	UCP1	0.44	-1.20	5.73E-05
Q9Z2Z6	Mitochondrial carnitine/acylcarnitine carrier protein	SLC25A20	0.52	-0.93	4.56E-03
Q9D6M3	Mitochondrial glutamate carrier 1	SLC25A22	0.62	-0.69	2.11E-02
Q5HZ19	Mitochondrial nicotinamide adenine dinucleotide transporter SLC25A51	SLC25A51	0.29	-1.79	7.60E-07
P63030	Mitochondrial pyruvate carrier 1	MPC1	0.55	-0.87	1.07E-02
Q9DAM5	Mitochondrial thiamine pyrophosphate carrier	SLC25A19	0.50	-1.00	2.42E-02
Q9CXT8	Mitochondrial-processing peptidase subunit beta	PMPCB	0.58	-0.80	3.74E-02
Q99LC3	NADH dehydrogenase [ubiquinone] 1 alpha subcomplex subunit 10, mitochondrial	NDUFA10	0.59	-0.76	3.78E-02

Uniprot Accession	Description	Symbol	Abundance Ratio: (B <sub>2</sub> <sup>tg</sup> )/(wild-type)	Log <sub>2</sub> (abundance ratio)	Adjusted P-value
Q9D8B4	NADH dehydrogenase [ubiquinone] 1 alpha subcomplex subunit 11	NDUFA11	0.59	-0.76	4.27E-02
Q9CPU2	NADH dehydrogenase [ubiquinone] 1 beta subcomplex subunit 2, mitochondrial	NDUFB2	0.52	-0.94	1.13E-03
Q3UIU2	NADH dehydrogenase [ubiquinone] 1 beta subcomplex subunit 6	NDUFB6	0.61	-0.72	2.23E-02
Q9CR61	NADH dehydrogenase [ubiquinone] 1 beta subcomplex subunit 7	NDUFB7	0.56	-0.84	1.60E-03
Q91WD5	NADH dehydrogenase [ubiquinone] iron-sulfur protein 2, mitochondrial	NDUFS2	0.57	-0.81	2.31E-02
Q9CXZ1	NADH dehydrogenase [ubiquinone] iron-sulfur protein 4, mitochondrial	NDUFS4	0.59	-0.76	3.40E-02
P03911	NADH-ubiquinone oxidoreductase chain 4	MTND4	0.51	-0.97	5.47E-03
P03921	NADH-ubiquinone oxidoreductase chain 5	MTND5	0.32	-1.64	4.64E-12
Q9QZ23	NFU1 iron-sulfur cluster scaffold homolog, mitochondrial	NFU1	0.60	-0.74	4.20E-02
Q9D0J8	Parathymosin	PTMS	1.68	0.75	1.77E-02
Q8BJ56	Patatin-like phospholipase domain-containing protein 2	PNPLA2	0.46	-1.12	6.22E-05
Q99KR7	Peptidyl-prolyl cis-trans isomerase F, mitochondrial	PPIF	0.55	-0.87	1.36E-02
Q8R2Y8	Peptidyl-tRNA hydrolase 2, mitochondrial	PTRH2	0.48	-1.06	1.09E-03
Q9R0M4	Podocalyxin	PODXL	0.45	-1.15	2.03E-03
Q99NF7	Ppm1b protein	PPM1B	3.33	1.74	3.55E-04
Q9JIG8	PRA1 family protein 2	PRAF2	1.77	0.82	1.60E-02
Q61823	Programmed cell death protein 4	PDCD4	0.42	-1.25	2.39E-02
Q9D1T5	Proline-rich protein 15	PRR15	0.23	-2.14	6.63E-06
Q8BWM0	Prostaglandin E synthase 2	PTGES2	0.61	-0.71	1.66E-02
Q8BGC4	Prostaglandin reductase-3	PTGR3	0.62	-0.68	4.51E-02
A0A0A6YW06	Protein enabled homolog	ENAH	0.34	-1.57	4.00E-08
Q3TDD9	Protein phosphatase 1 regulatory subunit 21	PPP1R21	0.19	-2.41	1.72E-06
Q61074	Protein phosphatase 1G	PPM1G	1.84	0.88	2.98E-03
Q91V77	Protein S100	S100A1	0.43	-1.20	1.67E-07
P50543	Protein S100-A11	S100A11	0.48	-1.05	7.23E-05
Q9QVP9	Protein-tyrosine kinase 2-beta	PTK2B	0.40	-1.34	2.66E-05
P60603	Reactive oxygen species modulator 1	ROMO1	0.45	-1.17	6.71E-04
Q9DCV4	Regulator of microtubule dynamics protein 1	RMDN1	0.59	-0.76	2.35E-02
A0A0R4J0S3	Reticulon-4-interacting protein 1, mitochondrial	RTN4IP1	0.58	-0.78	3.30E-02

Uniprot Accession	Description	Symbol	Abundance Ratio: (B <sub>2</sub> <sup>tg</sup> )/(wild-type)	Log <sub>2</sub> (abundance ratio)	Adjusted P-value
Q9DD06	Retinoic acid receptor responder protein 2	RARRES2	3.54	1.82	7.28E-04
Q9Z0J1	Reversion-inducing cysteine-rich protein with Kazal motifs	RECK	0.49	-1.03	2.29E-03
Q9CQE8	RNA transcription, translation and transport factor protein	RTRAF	1.67	0.74	4.41E-02
O88632	Semaphorin-3F	SEMA3F	0.34	-1.56	1.91E-03
O35326	Serine/arginine-rich splicing factor 5	SRSF5	1.94	0.96	2.62E-02
Q62086	Serum paraoxonase/arylesterase 2	PON2	0.51	-0.97	7.96E-03
Q9D8T7	SRA stem-loop-interacting RNA-binding protein, mitochondrial	SLIRP	0.48	-1.07	1.38E-02
Q9CXV1	Succinate dehydrogenase [ubiquinone] cytochrome b small subunit, mitochondrial	SDHD	0.53	-0.92	3.26E-02
Q8K2B3	Succinate dehydrogenase [ubiquinone] flavoprotein subunit, mitochondrial	SDHA	0.60	-0.74	4.86E-02
P09671	Superoxide dismutase [Mn], mitochondrial	SOD2	0.59	-0.76	4.14E-02
A0A087WQSO	Tensin 1	TNS1	1.94	0.96	4.10E-02
A0A1L1SUX8	Thy-1 antigen (Fragment)	THY1	1.58	0.66	1.25E-02
P20065	Thymosin beta-4	TMSB4X	2.54	1.34	2.57E-08
Q62264	Thyroid hormone-inducible hepatic protein	THRSP	0.61	-0.71	2.32E-02
Q9D289	Trafficking protein particle complex subunit 6B	TRAPPC6B	0.43	-1.20	4.97E-02
Q9DBB8	Trans-1,2-dihydrobenzene-1,2-diol dehydrogenase	DHDH	0.54	-0.88	9.47E-04
F6V6T4	Transmembrane emp24 domain-containing protein 2 (Fragment)	TMED2	0.43	-1.22	1.45E-04
Q78IS1	Transmembrane emp24 domain-containing protein 3	TMED3	0.43	-1.23	2.02E-06
D3Z0I8	Transmembrane protein 109 (Fragment)	TMEM109	1.71	0.77	4.30E-02
Q9CQN6	Transmembrane protein 14C	TMEM14C	0.38	-1.38	7.74E-06
Q99LG2	Transportin-2	TNPO2	0.37	-1.45	1.54E-02
D3Z3Z5	Tumor necrosis factor alpha-induced protein 8	TNFAIP8	0.28	-1.82	1.89E-04
Q8VE95	UPF0598 protein C8orf82 homolog	NA	0.49	-1.04	6.00E-04
P50544	Very long-chain specific acyl-CoA dehydrogenase, mitochondrial	ACADVL	0.54	-0.90	7.61E-03
F2Z471	Voltage-dependent anion-selective channel protein 1	VDAC1	1.53	0.61	2.38E-02

NA: not available

## Publications

### Original publications

Suvorava T\*, **Metry S\***, Pick S, Kojda G. Alterations in endothelial nitric oxide synthase activity and their relevance to blood pressure. *Biochem Pharmacol.* 2022 Nov;205:115256. doi: 10.1016/j.bcp.2022.115256.

\*Equal contribution

Contribution: literature research, manuscript writing, and figure design.

### Posters

**Metry S**, Suvorava T, Kojda G. Bradycardic effect of endothelial-specific bradykinin type-II receptors overexpression in mice: impact on blood pressure. Poster presentation in: ESC Congress 2023, 25–28 August 2023 Amsterdam, Netherlands. Published in: *European Heart Journal*, Volume 44, Issue Supplement\_2, November 2023, ehad655.3222, <https://doi.org/10.1093/eurheartj/ehad655.3222>

**Metry S**, Krybus M, Kocgirli O, Suvorava T, Kojda G. Differential signalling of endothelial B2 receptors in small blood vessels and aorta. Digital poster presentation in: 88th Annual Meeting of the German Society for Experimental and Clinical Pharmacology and Toxicology (DGPT), 7 March – 10 March 2022, Digital. Published in: *Naunyn-Schmiedeberg's Arch Pharmacol.* DOI 10.1007/s00210-022-02205-7 (2022) 395 (Suppl 1): S1–S80. page S42, Poster 199.

## Acknowledgments

For all I am grateful to my Lord Jesus, who gave me the strength to complete this dissertation and surrounded me with people who supported me throughout the entire process.

My deep gratitude and appreciation go to Prof. Dr. Georg Kojda for accepting me as a PhD student in his research group and giving me the opportunity to work under his supervision. His continuous guidance and insightful scientific knowledge helped me a lot throughout the experimental work and the writing of the thesis. Additionally, his encouragement to attend conferences greatly contributed to my professional development. I am deeply indebted to him for nourishing my scientific knowledge and fostering my personal growth.

My gratitude extends to Prof. Dr. Stephanie Lärer for her acceptance to review my dissertation and her sincere support and consideration.

My heartfelt gratitude goes to PD Dr. Tatsiana Suvorava, who taught me numerous techniques, engaged in extensive scientific discussions, continuously followed up on planning, and provided deep scientific insights into research. Above all, her constant motivation, sincere consideration, and unforgettable coffee breaks.

I am grateful for the financial support of the German Egyptian Research Long-Term Scholarship (GERLS) program (Funding ID: 57403037) that covers my stay in Germany, funded by the Egyptian Ministry of Higher Education and Scientific Research (MHESR) and the German Academic Exchange Service (DAAD). This support certainly contributed to the completion of this work. My gratitude to Mrs. Iman Al-Rashdan for her immense efforts in many organizational matters during the scholarship time. Additionally, I am thankful to the Completion of Studies Scholarship of Heinrich-Heine university Düsseldorf STIPET scholarship (from German Academic Exchange Service). I am grateful for the facilities and supplies provided by the Institute of Pharmacology at University Hospital Düsseldorf, under the direction of Prof. Dr. Jens Fischer.

Many thanks to the technical assistants Martina, Peggy, Beate, Kerstin, and Kirsten, who always had open ears for any technical questions and thanks to Petra Pieres for her continuous efforts in the organizational matters.

Thanks to my colleagues, Dr. Oktay Kocgirli and Dr. Michael Krybus for guidance in demonstrating techniques, scientific discussions, continuous encouragement and creating a nice environment in the laboratory. Thanks to Cansu Aközbek for her sincere support and sharing scientific knowledge during the last period of my PhD studies. Thanks to Heba Zabri for offering many scientific tips for the experimental work and her heartfelt support.

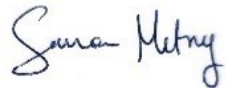
My sincere friends— Diana, Noran, Salma, Luzhou, Mona Ghazy, and Mona Mahmoud—have been there for me during both joyful and challenging moments. They have made this journey smoother with their genuine support and generosity in sharing scientific knowledge. They have taught me that friends are a significant grace in life.

My heartfelt gratitude extends to my lovely mother, kind father, and dear brother Kirolos. I owe every success in my life to their presence beside me; I could not be who I am without them.

Lastly, full appreciation goes to the souls of the mice that were sacrificed during this study for the sake of research and human welfare.

## Declaration of authorship

I declare under oath that I have produced my thesis independently and without any undue assistance from third parties considering the "Principles for the Safeguarding of Good Scientific Practice" at Heinrich Heine University Düsseldorf. The presented dissertation has not been submitted to another faculty. So far, I have not attempted to earn a doctoral degree (neither successfully nor unsuccessfully).

A handwritten signature in black ink that reads "Sara Metry". The signature is written in a cursive style with a large initial 'S'.

Sara Metry

Düsseldorf, 04.07.2024